THE EFFECT OF PUNCH CONTRACTION, SPRINGBACK AND COMPACTION TOOLING DESIGN ON THE CUTTING EDGE OF POSITIVE WC-Co COMPACTS

Denis Ovcina

A dissertation submitted to the Faculty of Engineering and the Built Environment, University of the Witwatersrand, Johannesburg, in fulfillment of the requirements for the degree of Master of Science in Engineering

Johannesburg, 2010

DECLARATION

I declare that this research report is my own unaided work. It is being submitted for the degree of Master of Science in Engineering to the University of the Witwatersrand, Johannesburg. It has not been submitted before for any degree or examination at any other University. All experimental data was obtained at Pilot Tools (PTY) Ltd while employed by the company.

……………………………..
(Signature of Candidate)

………….. day of ……………. Year …………

Abstract

In the current work the effects of machine-tool deflections, component unloading, and component-tool interactions on the dimensions of positive WC-Co compacts were determined on the basis of various tests performed using different compact geometries, compaction materials, tool designs and press decompression settings. Specifically the machine-tool deflection was defined and examined in terms of the punch-ram system contraction along the vertical axis of the press, component unloading in terms of axial, radial and volumetric compact springback, and component-tool interaction in terms of contact between the ejecting compacts and the die-wall. A new tool design was introduced to study the springback behaviour of compacts and compared against the conventional tooling design which makes use of a tight-fitting upper punch and die combination. As a result of the new tool design, positive compacts that were formed had near perfectly sharp cutting edges. Contraction experiments allowed for the determination of the contraction profile along several points of the machine-tool system especially contraction of the upper punch-ram. This quantity was found to be independent of tool geometry; a significant result which allows for the prediction of contraction behaviour and therefore increased control over the final pressing position of a variety of other production punches. Natural springback behaviour of positive compacts was studied on the basis of the determined contraction measurements and the newly introduced tool design which allowed for the formation and ejection of compacts free from die-wall contact and associated frictional influences. Axial and radial springback, as well as their fractional counterparts, could be expressed in terms of the same functions of the pressing force, dependant only on the hold-down setting (geometric and material factors being accounted for and embodied in the pressing force parameter). This new result simplifies the prediction of linear springback and its effect on the net shape of production items. Volumetric springback was found to be independent of compact shape which can then be used to make general predictions regarding the effect of three-dimensional springback on the total net shape of compacts in production. Both relative and volumetric springback were also found to be independent of the compaction material and hold-down setting.

Acknowledgements

I would like to thank Dr. Natasha Sacks for her invaluable encouragement, guidance and support throughout this work, without which I would not have been able to develop an understanding of the subject.

I would also like to thank Pilot Tools (PTY) Ltd. for the time and resources necessary for the completion of this work.

Finally, I would like to thank the Centre of Excellence in Strong Materials for providing the necessary financial assistance.

Table of Contents

List of Figures

List of Tables

1 Introduction

Hardmetals today are produced industrially by the powder metallurgy route which involves mixing, milling and spraying of the starting powders, pressing of the powders into a “green” compact and consolidating the compact into a hardmetal blank via a sintering process. In this industry over 50 % of the cost is spent on geometric shaping such as pressing, grinding, and edge honing. Therefore to increase company competitiveness by minimizing the costs of such production processes, it becomes essential to move toward producing parts that are as near-net-shape as possible. Thus sophisticated shaping methods which offer the possibility of producing tailored application specific shapes at low cost are used whenever possible in order to reduce production cost while maintaining or improving the product quality.

When die-compaction is chosen as a preferred method of producing near net shapes – a process suitable for high volume production due to the relatively short press cycle times – special demands on the shaping process in terms of the factors that affect the component accuracy must be considered before any attempt is made at producing. Owing to the coaxial pressing principle some of these factors can be extremely difficult to control. However a holistic evaluation of all of these factors is essential in the unified approach to net shape manufacture. In cold die compaction, plastic flow of the material, component - tool interaction, machine - tool deflection, and component unloading are regarded as the main contributors to the net shape accuracy.

In the current work it was only feasible to deal with some of these factors and the effect of their associated phenomena on the near net shape of positive insert compacts. These phenomena are in the case of machine-tool deflection defined as punch-ram system contraction, in the case of component unloading as springback, and in the case of component-tool interaction as compact – die wall interaction. A description of each of these factors is presented in Chapter 2.

For indexable cutting inserts, net shapes are defined by tolerance classes specified in the ISO standard 1832 [1]. These tolerance classes and the corresponding dimensions are normally defined based on geometric factors such as the over all insert shape, insert thickness, the diameter of the inner circle of the insert, and the radius of the insert corners. After the pressing and sintering processes, up to three finishing operations such as top and bottom grinding, periphery grinding, and edge honing may typically be used in order to get as near to these tolerances as possible. Besides geometric tolerances, other work standards need to be met for the cutting edge configuration which plays a decisive role in the performance of indexable inserts in machining operations. The cutting edge radii requirements are typically in the micron range putting additional demands on the sharpness of the cutting edges that can be achieved in the pressing process. Thus the evaluation of the compaction process factors – punch-ram contraction, springback and compact - die wall interaction – in the context of their effect on the geometric accuracy and the cutting edge quality of positive inserts was chosen as the main goal and the basis for the current work. A step closer to the understanding of these processes is a step closer to the net shape.

2 Factors influencing the compaction process

In this chapter the factors which influence the compaction process and which formed the basis of the dissertation, are described. This reader is provided the reader with sufficient background information to understand the work done in the project.

2.1 Positive insert definition

In the hardmetal industry a cutting insert can have one of two geometries as defined by the insert wedge angle. A wedge angle of 90º represents a negative insert and a wedge angle smaller than this represents a positive insert. When observed from the profile a negative insert has parallel sides and a positive insert has non-parallel sides. This naturally makes the cutting edges of positive inserts much sharper than those of negative inserts. Thus although negative inserts have more cutting edges – since both top and bottom edges can be used in cutting – and from this perspective can machine more parts, positive inserts have a distinct advantage when machining long and slender parts, thin wall parts, and other parts subject to bending and chatter [2]. Typical wedge angles values for some of the more common geometries defined in the ISO 1832 are 83º, 79º, and 75º or 7º, 11º, and 15º respectively, if measured with respect to the vertical (refer to Figure 1). In the current work several distinct geometries each with a 7º wedge angle were chosen for the purposes of carrying out the experimental work.

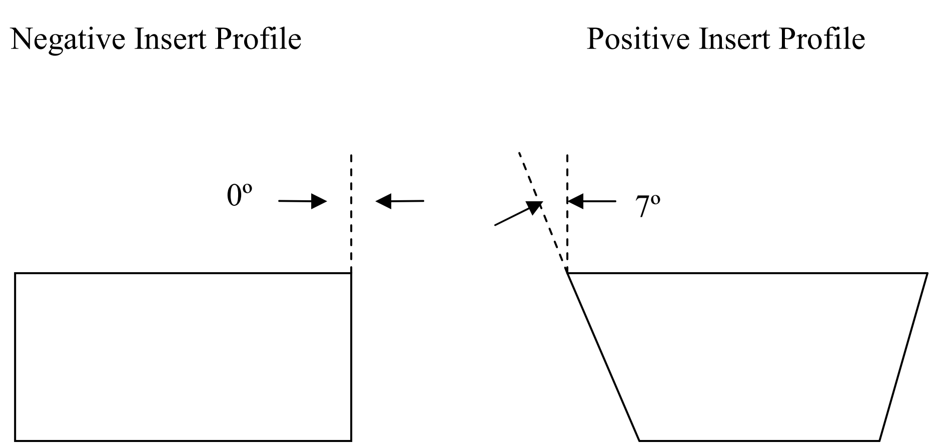

Figure 1: Differentiation between the negative and positive insert profiles.

2.2 Brief description of the Pressing cycle

Parts with a wedge angle less than 90º as described above require a die with a tapered cross-section and top and bottom punches with different cross sectional areas. A figure of a setup commonly used in coaxial industrial presses involving such a tool is shown below (refer to Figure 2). The same setup was used in the current work although several different tools were tested with the same setup.

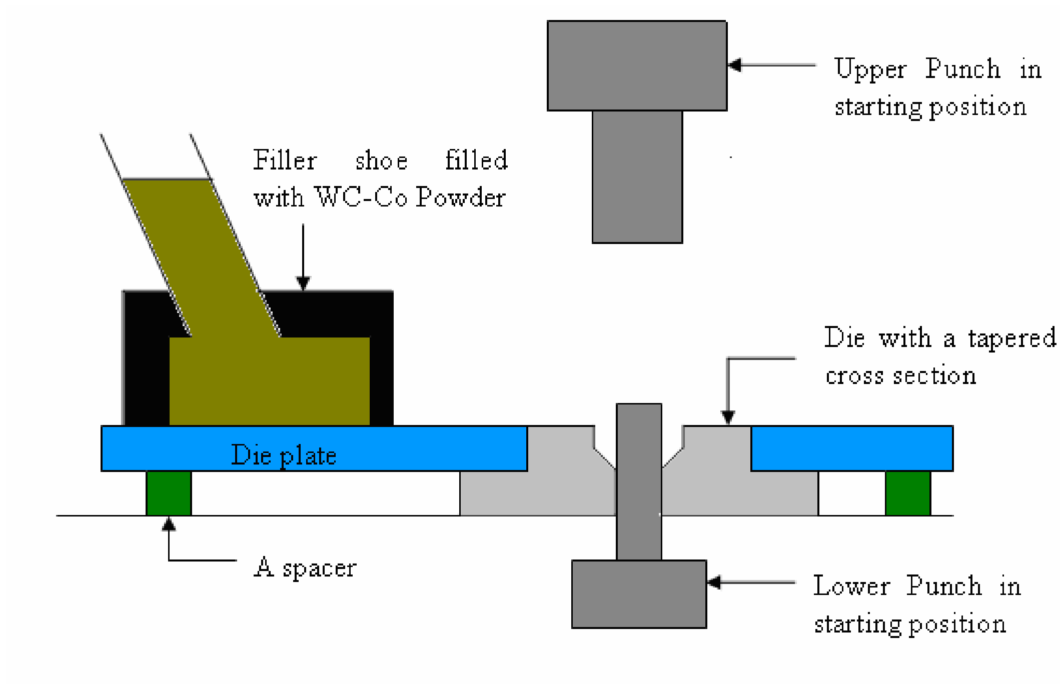

Figure 2: A tooling setup involving a positive tool with a die tapered cross section.

The motion of the two punches is governed by two independently controlled rams to which the punches can be fixed via suitably chosen adapters. The punches are perfectly aligned with the die which is fixed to an immovable middle adapter plate of the press. The die contains a cavity which can be used to form the component via the compaction process. The sides of the die form the sides of the component while the top and bottom punches form the top and bottom surfaces of the component. A filler shoe capable of forward and backward motion is able to dispense the powder into the die cavity. Sometimes depending on the complexity of the component it is possible for the setup to include a core pin inside the lower punch which can be used to produce a corresponding hole on the component. In some cases, especially with modern presses, it is also possible to produce a cross-hole on the component via an independently controlled cross-pin.

Having described a typical press setup, a specific sequence of the punch and filler motions as defined by a suitable punch travel arrangement and the associated compaction processes can be described as follows.

1. Tools are in the starting position (refer to Figure 2)

2. Lower punch descends to the filling position leaving space for the powder to fill the die cavity.

3. The shoe moves forward covering the die cavity and releasing powder into it until it is completely filled. The shoe is normally vibrated over the die cavity to ensure a homogeneous fill. In some cases the filling process can begin before the lower

punch has moved to the final filling position. This is called suction filling and can be used to reduce the amount of air that is entrapped in the powder fill.

4. After the retraction of the shoe the upper punch descends toward the die cavity and penetrates the powder level commencing the loading part of the pressing cycle which is sometimes also referred to as densification.

5. The loading process is performed according to the chosen punch travel arrangement which is normally done in a way that ensures a uniform density distribution. Several works have been written on the links between green compact density distribution and the sintered compact dimensions and the generally accepted view is that uniform density distribution in green compacts results in minimal distortions of the parts after sintering [3-6]. Thus the main controlling parameter of sintered compact distortion is the loading process.

   For example, the best possible density distributions for positive inserts according to Rodiger [7] are achieved by a final pressing operation of the upper punch called top pressing. While the best possible density distribution for negative inserts is achievable via a fully coaxial loading process in which equal amounts of powder are displaced by the top and bottom punches as they move to their final pressing positions. This type of double action pressing is the main advantage of the newer CNC hydraulic industrial presses over the older mechanical presses which utilize a technique called floating die or die-withdrawal in which only the upper ram is able to move [8].

6. The next stage is the decompression phase which begins by the slow movement of either or both punches away from their end pressing position the result of which is the removal of the pressing force from the compact. During the initial loading stage the compact essentially behaves like a plastic body but as density increases the elastic compression component grows due to the bracketing and hooking of the powder particles resulting in the springback effect upon removal of the pressing force [7]. Springback refers to the change and specifically the increase in the compact dimensions that happens during this part of the cycle as well as the ejection phase. The stresses associated with these dimensional changes in conjunction with the compact - die-wall interaction and associated frictional forces, can have a major effect on cracking and geometric accuracy of the part.

7. The last stage of the unloading process is the ejection. The upper punch is retracted and the compact is ejected by the upward movement of the lower punch until the original starting position is achieved. The upper punch can either be fully retracted before the lower punch begins the ejection movement or it can be partially retracted to a point where a certain force remains on the compact. This is referred to as the hold-down force. In this case the top punch normally remains in contact with the component until the part is completely ejected from the die. Thereafter the upper punch is completely retracted and returns to the starting position signalling the end of the pressing cycle. The correct selection of the hold-

down can be used as an effective means of springback control and since a significant part of compact expansion due to springback occurs during ejection – specifically during the emergence of the compact from the die – hold-down plays a critical role in crack prevention and the control of geometric accuracy [7]. Due to the critical nature of this compaction process parameter, the effect of hold down on the positive insert geometry was investigated as a part of this work.

2.3 Punch-ram contraction

During the loading process, the high pressure needed to shape the powder and promote it to higher packing densities results in the contraction of the punches as well as the mechanical components of the press in the axial or pressing direction [9, 10]. The deformation is the inevitable consequence of the elastic properties of nearly all rigid bodies and its magnitude is determined by the well known Hooke’s law. The effect of this phenomenon on the loading process is the deviation of the end pressing positions of the punches from the intended pressing positions and therefore a deviation in the geometric dimensions of the pressed compact form that of the net shape.

In the context of positive insert compaction the effect of contraction on punch positioning during the loading process is significantly more important for the upper punch than the lower punch. This is due to the fact that only the upper edges of positive inserts are used in the cutting operations. Thus particular attention was given to the accurate determination of the upper punch-ram contraction and the effect thereof on the resulting compact edge configuration. Further to this an accurate evaluation of the extent of punch contraction and thus the determination of actual punch positions in the die during the loading process will lead to fewer tool breakage incidents which in positive insert compaction normally arise as a result of the upper punch colliding with the die. A schematic representation of punch-contraction is shown below.

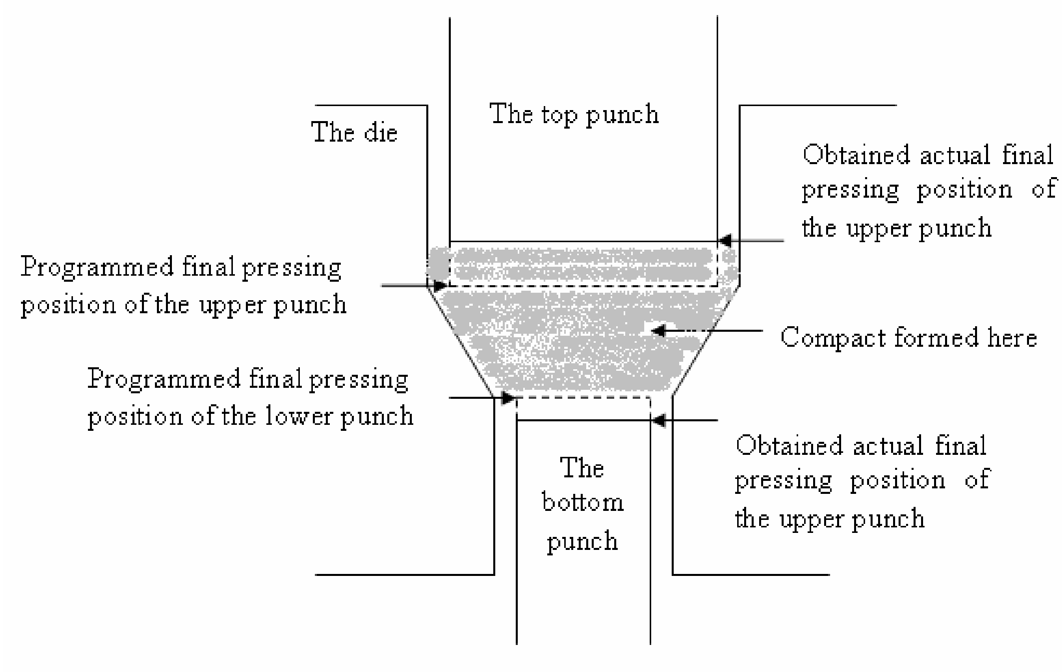

Figure 3: A schematic representation of the effect of contraction of top and bottom punches on the compact dimensions. The formed compact has larger dimensions than intended. The wide gap between the punch and die wall is there just for purposes of clarity. In reality this gap for a tight-fitting tool is only 0.005 mm – 0.010 mm per side and is hardly visible to the naked eye.

2.4 Springback

Springback refers to the expansion of the component which occurs during the unloading stage of the pressing cycle. During decompression inside a conventional tight-fitting die, the hydrostatic pressure component caused by the exceeded yield point of the compacted granules during loading typically causes the expansion of the compact in the axial direction upon removal of the pressing force. This is sometimes referred to as in-die springback [11]. In addition there is also a radial component to springback which normally becomes more apparent once the component has been fully ejected from the die. The end result is that the component dimensions after ejection exceed the die dimensions. During ejection the component can also experience further axial springback depending on the selection of the ejection process criteria such as the hold-down force, mentioned previously. The extent to which the ejected compact dimensions exceed those defined by the final pressing position of the punches is sometimes referred to as out-of-die springback and represents the deviation of the actual part from the net shape. In the current work, only the effect of out-of-die springback on the net shape is measured using three different compact geometries, two different tool designs and two different compaction materials. A schematic representation of springback in two stages – during decompression (in-die) and after ejection (out-of-die) is shown below.

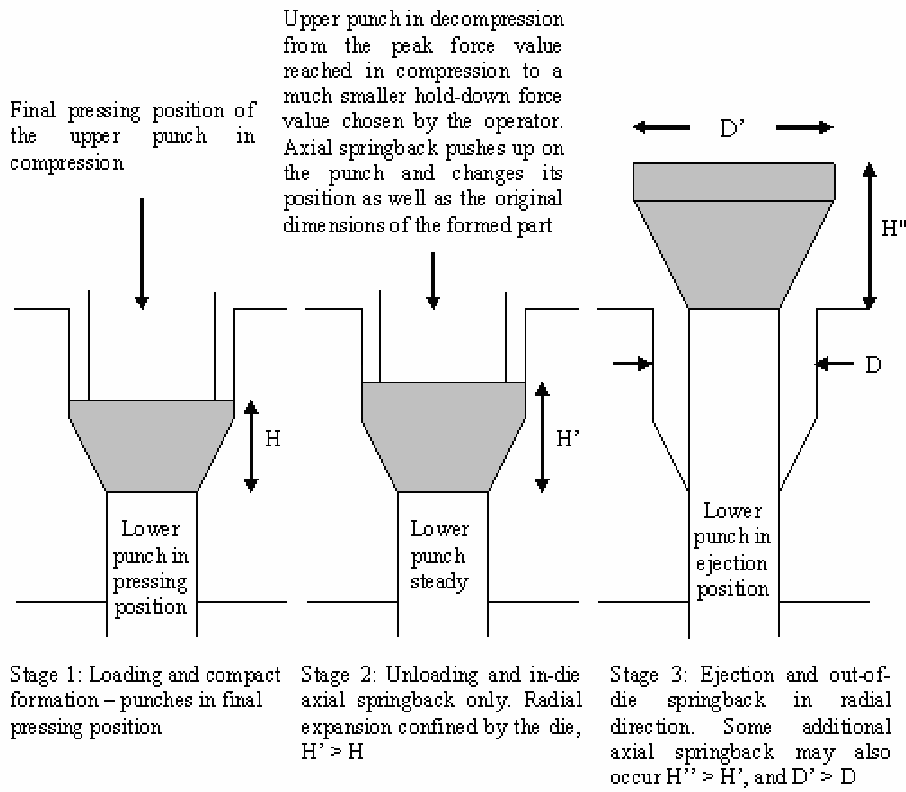

Figure 4: A representation of the unloading cycle in a tight-fitting die and a schematic representation of in-die and out-of-die springback. Some dimensions have been exaggerated for clarity.

2.5 Compact – die-wall interaction

The interaction between compact and the die wall in the current work refers specifically to the unloading stage of the pressing cycle i.e. during decompression and ejection of the part from the die. In a tight-fitting die the compact is at all times in contact with the die-wall and this inevitably leads to die-wall friction or ejection friction as it is sometimes referred to [12]. Radial springback and die-wall friction are closely linked in the sense that large radial expansions can result in large shearing stresses during ejection which in turn can lead to compact failure in terms of severe cracks and laminations [12, 13]. Conversely ejection friction can lead to reduced axial and radial expansions due to the dissipation of springback energy by friction [15]. In the case of positive inserts, contact between the upper edges of the compact and die wall during ejection can lead to scuffed and deformed cutting edges [7]. As a part of this work the combined effect of springback and ejection friction on the net shape of tight-fit positive compacts and the standalone effect of springback on the net shape of free compacts are evaluated on the basis of two slightly different tool designs. One of them is a conventional design which makes use of a tight-fit upper punch and die, and the other, a new design, is simply the opposite of that and makes use of a loose fit between the upper punch and die. This loose gap between the upper punch and die is referred to as the springback allowance (SBA) and allows the compact to springback freely without making contact with the die wall. Hence in this case ejection friction can be circumvented and the effect of pure springback could be investigated. Compacts formed in this way are from this point on referred to as free or SBA compacts in the text.

2.6 Crack formation and the influence of Hold-Down

The appearance of cracks on compacts can be the result of excessive compact expansion during unloading or high friction experienced between the compact surfaces and the die-wall. In negative compacts, crack formation generally starts with the unloading of pressure from the top surface of the compact during decompression or ejection of the compact from the die. During force removal the top surface of the compact expands axially while the compact edges are hindered by friction between the die wall and the compact sides. The resulting tensile stresses in this area can produce cracks if these stresses exceed the mechanical strength of the material in this region. This cracking mechanism is commonly referred to as “endcapping”. Another common crack formation mechanism is related to the part of the ejection process immediately when the compact begins to emerge from the die. The radial expansion of the compact at this point and the associated tensile stresses that result can cause the appearance of laminar cracks or laminations, if again the magnitude of these stresses exceeds the mechanical strength of the compact. Both crack formation mechanisms are explained comprehensively by Albaro [11].

Proper selection of hold-down is a very effective way to deal with such defects [7]. Hold-down can to some extent control the extent of axial and radial compact expansions until the part has been fully ejected and therefore liberated from the constrictions of the die-cavity and the influences of wall friction during ejection. In the current work the effect of hold down on the springback of positive compacts and therefore the deviation of pressed parts from the net shape as a result of springback was evaluated on the basis of the SBA tool design. The effects were evaluated using two different types of compaction materials or powders.

2.7 Project Aim

In view of the factors discussed above the following has been identified as the main project aim:

- To improve the understanding of the various processes encountered in die-compaction of hardmetal powder that influence the net shape of positive inserts; those being related to machine-tool deflections, component unloading, and component-tool interaction.

The improvement of the understanding of these factors will eventually lead not only to the improvement of the near net shaping of positive compacts but fewer incidents of tool breakage and reduced setup times in the production of positive inserts.

3 Literature Review

3.1 Measurement of Characteristic Insert Dimensions

The measurement of certain characteristic insert dimensions may be done using a variety of methods. Some of the methods mentioned in this section have been used by published authors, while the rest are reviewed as possible measurement methods.

The Novagraph from Novatest shown in Figure 5 is PC-controlled equipment that can be used to measure insert radii, angles and sizes in very quick time either in production or final inspection. However since the measurements are made by direct mechanical contact between the measurement probe and the compact it is normally used for measuring sintered compact dimensions. Accuracy of measurement of the green compact dimensions with such equipment might have depended on the hardness or the green strength of the compact in the region where the measurement would be made. It is questionable whether such equipment would have yielded accurate results for compact edge radii or lip sizes which are discussed in the following section. The use of this equipment for the measurement of compact edges was not found anywhere in literature.

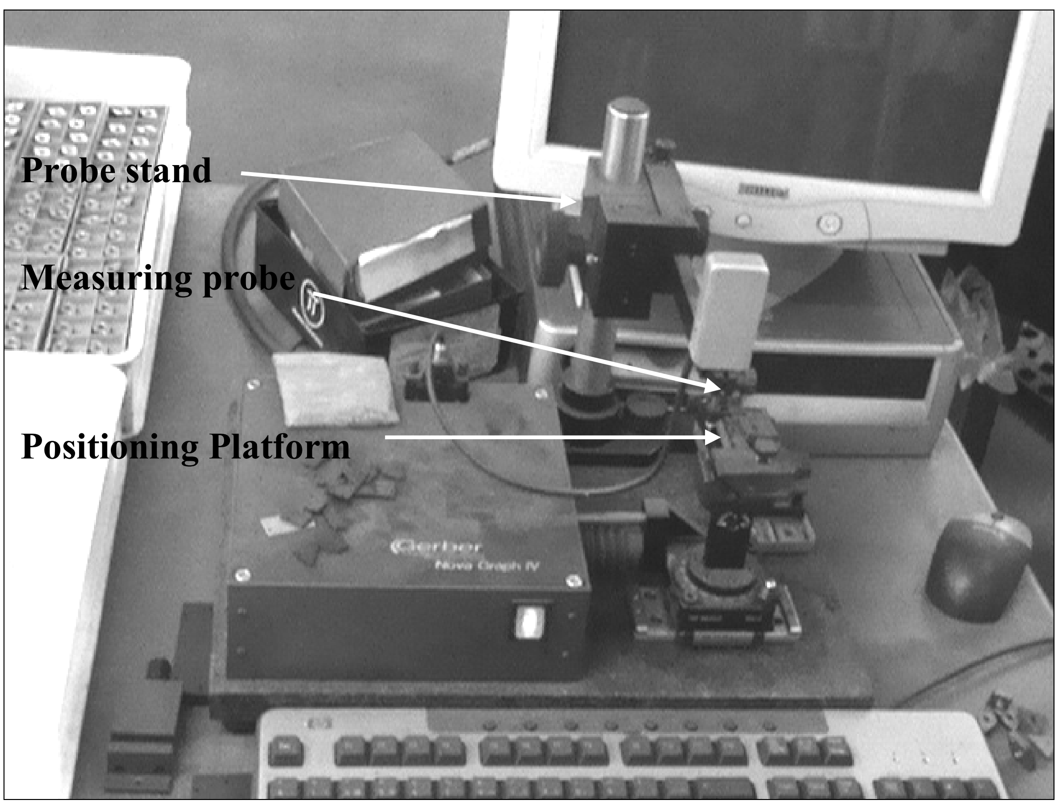

Figure 5: Novagraph measuring equipment from Novatest.

Another possibility for the measurement of compact edge features such as the lip dimension is the shadow graph shown in Figure 6 depicting a projection of a positive insert profile on a screen. The digital readouts on the right give the amount of translation of the onscreen crosshairs which can be moved from one point of the shadow to another in order to make a measurement. This device is normally used to measure insert angles but can also be used to measure linear dimension in the horizontal and vertical directions. However accurate measurements using this equipment are often hindered by focusing difficulties and shadow effects. The use of this equipment for the measurement of compact edge condition was not found in literature.

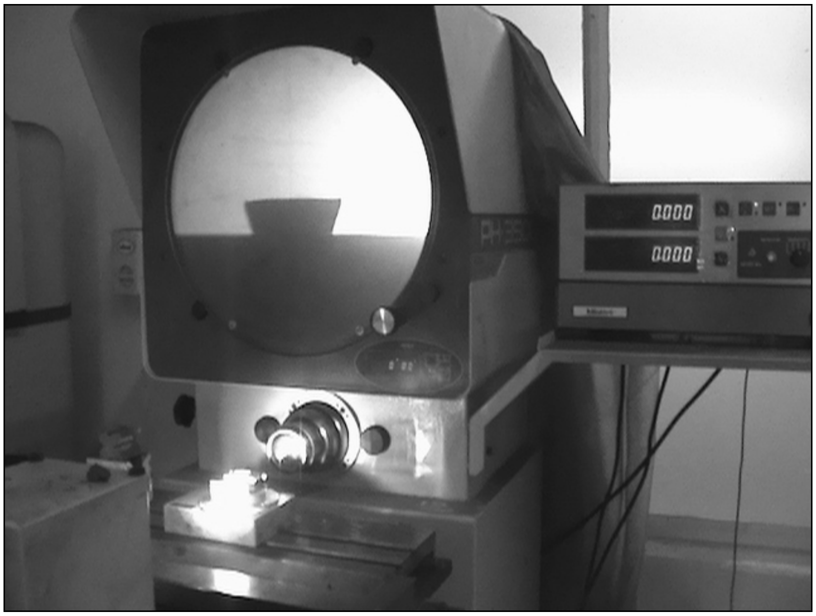

Figure 6: A projection of a positive insert profile using a shadow graph.

Weckenmann and Nalkntic [15] discuss precision measurement of cutting tools using two matched optical 3D sensors with minimal user influence. The method relies on the capabilities of optical sensors and numeric evaluation procedures which according to the authors should allow for accurate measurement of complete 3D shapes of new or worn cutting tools. This approach was intended for evaluations of wear characteristics and their dimensions which are dependant on various machining process parameters but could possibly be adapted for measurement of green insert characteristics. In addition to being practical, the method allows for highly repeatable measurements which according to Weckenmann and Nalkntic [15] correlate well with other methods. The equipment comprises of the measuring system equipped with the optical sensors, a fringe protection system, a white light interferometer, and a positioning system as shown in Figure 7.

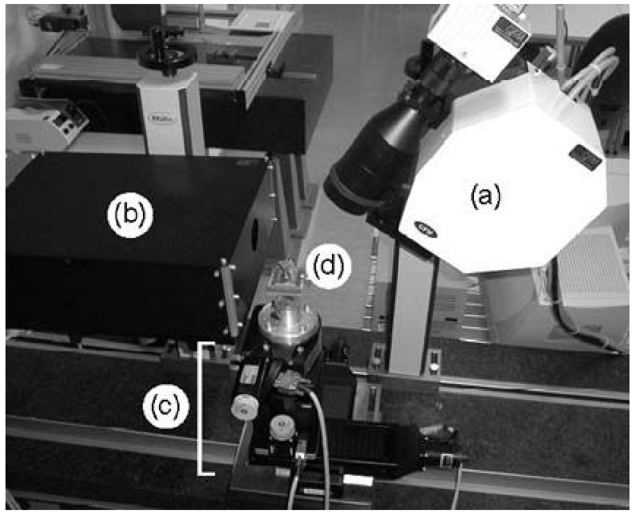

Figure 7: 3D optical sensor setup for measuring of insert dimensions (d) involving a fringe protector (a), interferometer (b) and positioning system (c) [15].

3.2 Punch-Ram Contraction

The influence of press stiffness on the dimensional accuracy of work pieces was first described in several classical books on metal forming by Doege and co-workers [9, 10] at the Technical University of Hanover which led to the DIN 55189 standard. Special conditions of process engineering at the time together with the demand for economical use of metalworking presses resulted in eccentric loads with additional horizontal forces and bending moments leading to reduced values of exactness of forming tools and presses. In several research projects at the University of Hanover, between 1978 and 1988, statistical studies of metalworking presses were carried out and experimental values for the horizontal machine characteristics such as tilting and displacement of the upper ram were measured to be in mm-range prompting further research into increasing the accuracy and exactness of machine tools. Although no consideration was given to measurement of lateral stiffness by Doege [9, 10], as in later work by Arentoft *et al* [16] and Chodnikiewicz [17], this initial work paved the way to understanding the importance of press deflections in precision forming.

Arentoft *et al* [16] described the press by six load/deflection curves and two assumed rotation points about which small deflections can be assumed to rotate, while Chodnikiewicz [17] first introduced the flexibility matrix of action and reaction vectors which could be used to model the flexibility of simple presses. In more recent studies, other authors such as Ou and Armstrong [18] used linear load deflection relationships to derive a similar stiffness matrix for a screw press implementing these deflections successfully in forging simulations of airfoil sections using FE analysis.

In their work on the generation of automated compaction diagrams – which are a useful tool in characterization of granular powders with respect to granule deformation and the reduction of inter-granule pore volume – Mort *et al* [19] used a baseline subtraction method to compensate for the elastic deformation in the testing apparatus. The authors collected baseline data by compressing an empty die and subtracting it from the net crosshead translation during loading. The difference between the crosshead position of an actual pressing cycle with powder and the baseline crosshead position for the empty die represented the thickness of the compacted pellet before the release of elastic springback in the pellet. Furthermore, the authors were able to collect springback data by calculating the difference between the thickness of the ejected pellet and the baseline-corrected crosshead position at the maximum load. The pellets were agglomerates of spray dried alumina powder and organic compounds which made up approximately 4.5 % of the material.

In earlier works, Shapiro [20] and Matsumoto [21] performed similar studies on the generation of automated compaction diagrams. Shapiro [20] assumed that the crosshead position was equal to pellet thickness at low pressures and made corrections to high pressure data by measuring the combined elastic recovery as a function of load for a series of pre-compacted pellets. Matsumoto's [21] unload-subtraction method made use of a computer-interfaced testing machine which was able to collect the cross-head translation data over the entire load-unload cycle, thereby enabling the calculation of the elastic deformations from the difference between the load and unload curves for each cycle. Other authors such as Rosochowski and Balendra [22] have applied elastic FE analysis in order to evaluate both tool deflection and component springback under a defined component-tool interface force contour. Superposition of tool deflection and component springback enabled estimation of the final component form and thus the development of a compensation procedure for designing die cavities for more accurate net shape forming.

In an online measurement procedure Antikainen and Yliruusi [23] were able to determine the deformation of the eccentric tablet machine from measuring the displacement of the lower punch during maximum compression force, which was set up so as not to move during the compaction cycle. The authors controlled the loading force by changing the mass of powder in the die. By determining the paths of the upper punch displacements with time at five different compression forces and then plotting the maximum upper punch displacements against the corresponding compression forces, the authors were able to derive an exponential relationship between the upper punch-tablet deformation and the compression force.

$$\text{Deformation }(F) = S_{df}\,\{1 - \exp(-\lambda F)\} \qquad \ldots (1)$$

Where:

S_{df} is the theoretical maximum limit for deformation, λ the deformation speed as the compression force increases, and F the upper punch pressing force. The test materials used by the authors were lactose monohydrate, two grades of microcrystalline cellulose, maize starch and dicalcium phosphate dihydrate.

Despite improvements in the accuracy and exactness of industrial tablet and hardmetal presses, some degree of flexibility is unavoidable and the above studies highlight the compensation procedures developed by various authors in the pursuit of net shaping. Although the contraction measurement method used in the current work was developed independently from the above methods, it bears methodological similarities with some of these; particularly the work of Mort, Sabia, Niesz and Riman where the collection of baseline data by compression of an empty die and subtraction of this data from the net crosshead translation is similar to the current approach of baseline data collection by external loading of the punches and subtraction of this data from the net contraction of the complete punch-ram system.

3.3 Springback

The subject of springback has been widely studied in literature, from theoretical modelling based on finite elements to experimental work based on empirical research. The experimental work ranges from research in expansion characteristics of spray-dried ceramics to elastic relaxations of starch based pharmaceuticals. However, no springback analysis of WC-Co positive inserts could be found in literature.

Carneim and Messing [24] investigated the effects of binder content and binder plasticity on axial loading and unloading of PVA (poly vinyl alcohol) containing spray dried ceramic powder. Pellets were compacted by single action uniaxial pressing in a universal mechanical testing machine with compaction taking place at a stroke rate of 0.5 mm/min in a cylindrical steel die lubricated with zinc stearate. Stress-strain data was collected during compression via a PC-interface and as done by Matsumoto [21] the deflections of the die and testing apparatus were corrected for by subtracting the stress-strain characteristics of a blank compaction run from the sample data. In order to evaluate the dimensional change of pellets after ejection, they were placed in a thermo-mechanical analyzer which could be used to make very small measurements of strain.

The authors observed that compact expansion after ejection occurred mainly in the axial direction and that the total dimensional change was dominated by instantaneous springback due to the stored energy of the pellets and not the time-dependent viscoelastic character of the organic pellet binder. Increasing the size of the sample pellets resulted in less instantaneous springback as well as time-dependant relaxation. This was explained by a limited region of expansion at the surface layer of the pellet thickness. Sample size was shown to have a significant effect on compaction of powder in general. In the larger samples the influence of die-wall friction on bulk compaction of powder was reduced because the surface area to volume ratio in larger samples was less than in smaller samples.

Nam *et al* [25] used laser dilatometry with X-ray computed tomography (XRCT) to investigate the effect of environmental influences on the springback and internal density gradients of spray-dried agglomerates of alumina. Laser dilatometry was used to measure the external dimensions of the compacts while XRCT was used to measure the internal density distribution. By combining the data relating dimensional change and density gradients they observed that radial expansion in the low density zone is always larger than that of the high density zone for all the powders tested regardless of the way they were prepared.

Nam *et al* [25] found this to be a result of severely deformed high density zone agglomerates compared with the agglomerates in the low density zone which are predominantly round and more "springlike" in character. As a result, the instantaneous radial springback in the high density zone was diminished compared to that of the low density zone where ''spring constants'' of the nearly undeformed agglomerates was largely preserved. Their results run counter to previous work on the subject by Thompson [26] that showed greater residual stresses in the high density zone often result in greater expansion. The authors also confirmed that the concentration of the binder is the primary cause of non-uniform densification and differential springback.

In work on compaction behaviour of spray-dried silicon carbide powders, Liu and Fu [27] tested the elastic recovery of spray-dried silicon carbide powder – prepared with an organic phase consisting of a binder (acrylate-based polymeric material) and plasticizer (PEG) – at three different temperatures with one being above the glass transition temperature of the organic phase. For the two temperatures below the glass transition temperature, approximately 2 % springback was observed after the removal of a 100MPa pressing force. Through this work authors highlighted the importance of the elastic nature and recovery of the organic phase which may under certain conditions cause cracking and laminations within pressed bodies in the SiC industrial operations.

In a study on the stress relaxation of compacts produced from viscoelastic materials based on the underlying assumption that the increase in tablet volume is an expression of stress relaxation and stored energy of the tablet [28], van der Voort Maarschalk *et al* [29] showed that springback of starch based tablets experience a counteracting force determined by particle bonding, as quantified by the Ryshkewitch-Duckworth [30] relation and the friction of the tablet with the die-wall, as quantified by the ejection pressure.

The authors were able to determine that the materials that exhibit low friction and bonding capacity such as pre-gelatinized starch and microcrystalline cellulose will create porous structures while materials with high resistance against expansion are prevented from the creation of a porous structure but the relief of stored energy might result in laminations or capping. Furthermore, logarithmic relationships between compact densities and compaction pressures were derived for the tablets based on the collected data at several different compression speeds.

In more recent work on the elastic relaxation of starch tablets during ejection Anuar and Briscoe [14] investigated the existence of possible inter-relationships between the ejection force and the tablet elastic relaxation in the axial direction and found that continuously measured ejection forces are generally inversely proportional to the variations in the ejected tablet heights. Since the ejection force is a result of radial springback and die-wall friction, this implies an existence of an intimate and possibly inverse dependency between die-wall frictional work and tablet stored elastic energy. The possibility of such links might exist in compacts produced from hardmetal powder despite typically small organic binder contents and thus relatively limited viscous components of such powders.

Through the use of novel non-contact laser measuring devices the authors were also able to make continuous measurements of tablet relaxations throughout the entire ejection motion and were thus able to infer the existence of periodic diametrical expansions–contractions of the emerging tablets, the amplitudes of which were believed to be dependant on the corresponding stored elastic energy of circumferential area in contact with the die walls.

In a paper on the mathematical treatment of secondary yielding – a result of component unloading by punch removal and die contraction – Rosochowski and Balendra [22] were able to show that the main factors affecting secondary yielding are the flow stress of the workpiece material and the elastic properties of both the workpiece and the die. The authors based their analysis on the unloading of a cylindrical component from a closed die for which they calculated that the change in the component stress-state due to elastic unloading can lead to the breaching of the yield criterion on the opposite side of the Von Misses [31] cylinder thus leading to some plastic flow of the component caused by the contracting die. Furthermore the authors calculated that the secondary yielding occurred only if during compression the punch pressure exceeds a certain threshold pressure, a function of the yield stress of the component material and the elastic properties of the workpiece and the die.

In a finite element study by Wu *et al* [32], compaction of idealized homogeneous and composite 2D powders was simulated under carefully controlled conditions. The idealized compacts were constructed using rods of aluminium and hardened steel, with special attention paid to the material behaviour of the rods, the die boundary conditions, the periodic packing arrangement and springback during ejection from the die. Two significant contributions of springback upon load removal were studied namely, particle compressibility and void reopening upon load removal. The authors found that at low compaction pressures (below 100MPa) most of the springback was related to void re-opening while at higher pressures compressibility effects dominated. Springback stemming from void reopening was observed to produce up to 0.5 % volume change.

In further modelling work, through discrete element methods (DEM), Martin [33] proposed an analytical equation for the extent of springback in closed-die and isostatic conditions which coincided well with simulation results. The author was able to show that springback depends on the material parameters of the powder (elastic and plastic), on the relative density attained during compaction and on the process route (isostatic versus closed die compaction). Thus although springback is often treated as an elastic problem, it is in fact also dependant on de-cohesion of the material particles at the contact level during unloading as well as the elasticity.

Finally, several studies in other related fields such as high-velocity compaction [34, 35] and metal stamping [36] have also shown numerous compact flaws and anisotropic part dimensions which can occur as a result of an improper understanding and control of this process parameter.

3.4 Die-Wall Friction

In the current work, die-wall friction was not studied by direct quantitative means, and only its general effect on the net shape of positive inserts was determined by a comparison of the ejected compact dimensions pressed using two different tool designs. More direct means of friction measurement and the consequent evaluations of compact quality are summarized below. Measurement of ejection force as a function of time is available on most modern hydraulic presses such as the MP250 Fette and TPA15HS Dorst.

Kikuta and Kitamori [13] were able to develop a hydraulic press apparatus for measuring ejection forces under varying radial loads in the compaction of lactose tablets. In the series of measurements of ejection forces, a linear relationship between ejection and radial forces was obtained using Coulomb's equation from which the coefficient of friction and adhesive force could be determined from the slope and intercept of the straight line respectively.

$$F = \mu W + C \qquad \text{. . . (2)}$$

The authors found that a linear relationship between the radial and ejection forces could be obtained and therefore Coulomb's equation for the friction between two bodies could be applied to the boundary of a tablet and die-wall. Using the linear relationship between the radial and ejection force it was shown that when the tablet in the die is allowed to stand for a certain time, the measured ejection force was lower then in ordinary ejection from the die due to the reduced adhesive force between the tablet and the die wall. In addition, the authors tested the effect of ejection speed on the relation between the ejection and radial stresses and found that the adhesive force was larger at higher ejection speeds.

Briscoe and Rough [37] investigated the effect of wall friction on the ejection of pressed ceramic parts and found that maximum ejection stress depends directly on the applied compaction stress, aspect ratio of the part, and the state of die wall lubrication. Ejection stress was found to increase with the increase in applied compaction load. Greater applied compaction loads resulted in higher radial and frictional stresses at the die walls which had to be overcome in order to eject the compact. They showed that as the aspect ratio of the part increases the ejection stresses increase due to a subsequent increase in the compact die-wall contact area. Die-wall lubrication significantly decreases ejection stresses due to the reduction in the frictional forces at the compact - die-wall interface. Finally, varying the ejection speed had little effect on ejection stress profiles in lubricated dies while larger "stick-slip" fluctuations were observed at slower ejection speeds in unlubricated dies. The origins of the stick-slip behaviour seemed to be associated with stress relaxation phenomena at higher levels of traction in unlubricated systems.

In order to perform the necessary experimental work, the authors used a commercial universal testing machine, to generate applied compaction stresses of up to 70MPa. Force transducers, attached to the upper and lower punches were used to make simultaneous measurements of the applied and transmitted stresses. A displacement transducer attached to the upper punch was used to measure upper punch displacements while the lower punch was stationary. In order to eject the test pieces from the die, the lower punch would be removed and a force applied to the upper punch. Ejection stress was recorded continuously as a function of upper punch displacement. Radial and axial dimensions of the ejected pieces were then measured using a digital micrometer with an accuracy of ±0.001 mm.

In a study of wall friction measurement and compaction characteristics of bentonite powders by Tien *et al* [12], a new method for measuring wall friction during powder compaction and ejection was presented. In conventional or indirect measurement methods which have been widely used in the field of powder metallurgy, two load cells are employed as in Briscoe and Rough's [37] setup. The two cells measure the applied and transmitted force from which die-wall friction can be determined as follows:

$$F\ (\text{die-wall}) = F\ (\text{applied}) - F\ (\text{transmitted}) \qquad \ldots (3)$$

The new method adopts a ring-type load cell (referred to as washer-type or donut-type by some manufacturers) installed under the die in order to measure wall friction directly. In this arrangement since the base of the die transmits the friction between the powder and the die-wall during compaction, the force measured by the ring-type load cell is exactly equal to the wall friction.

The proposed measuring method was validated by comparing the readings of the ejection force recorded by both the upper load cell and the ring-type load cell. The direct method compared favourably to the indirect measurement method based on the accuracy in the wall friction and compact density measurements. Ejection profiles of compacted bentonite powder using this method were similar to the results published by Briscoe and Rough [37].

Huang and Hwang [38] investigated the effect of mixing an additional lubricant, EBS (ethylene bis-stearamide), on the apparent density, flow rate, green density, green strength and "pressability" of spray dried molybdenum powder compacts pressed using a floating die press. The authors found that additives such as EBS and others commonly used in metal powder compaction [39-43] lower ejection forces significantly. When the powder was sprayed with as little as 0.1 % EBS the ejection energy decreased markedly from that of unmodified spray dried powder and when the amount of EBS was greater than 0.2 %, the lubrication provided could attain results close to those of using direct die-wall lubrication. The authors concluded that when flow properties, dimensional control, and low ejection force are a major concern, small amounts of EBS, between 0.1 % and 0.2 %, should be added to improve press productivity, tool life and dimensional stability.

4 Experimental Methods

All rigid bodies are to some extent elastic and change their dimensions slightly by being pulled, pushed, compressed or twisted. Compaction tools as well as the upper and lower ram systems of the hydraulic press to which they are attached are rigid bodies and similarly undergo dimensional changes during the compaction process. In the punch-ram contraction experiments that are described in this chapter only the dimensional changes due to the compressive action along the vertical axis were examined. In powder compaction the compressive stress arises from compression of the powder to form the required green shape but in these experiments contraction was examined independently of compaction and compressive forces developed without the use of powder.

The compact itself is a rigid body and experiences some dimensional strain during the ‘pressure release’ and ‘ejection’ phases of the compaction cycle. This dimensional change is a natural consequence of compression of loose powder into a solid green body. During relaxation the dimensional change of the compact in the horizontal direction is known to be significantly larger than that of the punch during compression (due to the difference in elastic moduli between solid carbide and soft carbide) thus both vertical and horizontal changes in the compact dimensions were studied.

This chapter explains the experimental methods developed in order to determine the effect of punch-ram contraction and compact relaxation on the final green insert dimensions, and the various compaction parameters which may influence punch-ram contraction and compact relaxation.

4.1 Methods for measuring ram and punch contraction

4.1.1 Equipment used

1. MP250 hydraulic CNC press.
   3 x test tools and their corresponding flat upper and lower punches. The three chosen geometries are amongst the most commonly encountered tool geometries in production, namely square, round and triangular tools. The tool length measurements as measured using a Zeiss machine are reported in Appendix A (Tables A2 and A3)[1].
2. A large steel plate with reasonably flat surfaces.
3. A relatively small flat carbide disc which was chosen because it has a higher Young’s modulus than the steel plate (450-600GPa compared to 200GPa for steel [44]) and therefore deforms less than steel. This was necessary in order to increase the accuracy of the experimental procedure since the deformation of any platform is difficult to measure accurately using a finger clock, particularly when the deformations are large.
4. A finger clock with an accuracy of ± 0.001 mm attached to a clock stand with a magnetic base for clamping.

[1] Accurate tool lengths are required for the automatic punch referencing procedure of the MP250 press, made possible by the tool database module of the press software.

4.1.2 General overview of procedure

Four distinct types of measurements were performed on each of the three test tools. The same measurements were performed on 'tight-fit' and 'SBA' punches. SBA punches are 'tight-fit' punches that have been modified by grinding the periphery of the original tight-fit punch to within the required SBA tolerance (discussed in more detail later). With the aid of these measurements it was possible to determine the contraction behaviour of individual elements that make up the punch-ram system as a whole and thus determine a contraction profile, as such, of the complete punch-ram system.

4.1.2.1 Contraction behaviour of upper and lower punch-ram systems

The axial contraction of both the upper and lower punch-ram systems as a function of force was determined in order to assess how the total contraction of the two systems affect the overall ejected compact height since the upper and lower punches form the upper and lower surfaces respectively of the compact. For this experiment the contraction measurements were recorded using the measuring system[2] of the press. The lower and upper punch were brought into contact and pressed slowly against each other (refer to Figure 8) developing pressing forces between 0 kN and 100 kN. The pressing action was performed by the upper ram while the press maintained a perfectly steady or fixed position of the lower ram so that the total compression of the upper and lower punch-ram system was calculated from the readings displayed on the screen of the actual upper ram axis position before and after the pressing action was initiated. The resulting force and contraction readings were captured from the press screen and analyzed.

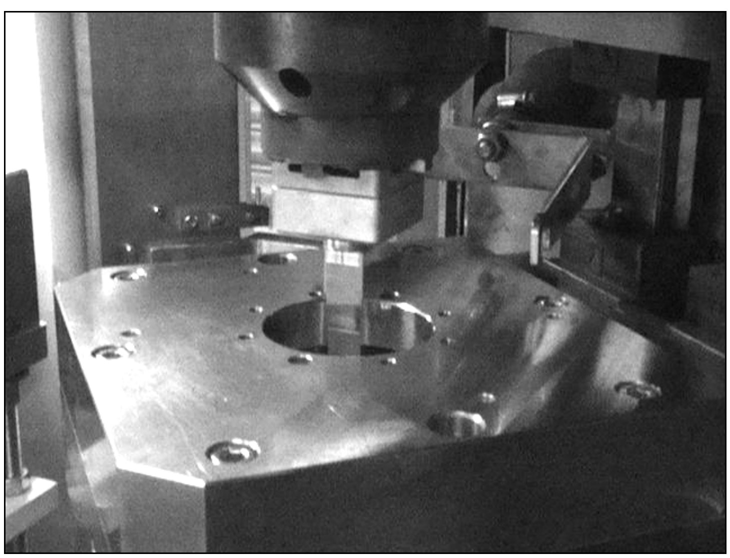

Figure 8: Upper and lower punch in close contact during the experiment for the determination of contraction of upper and lower punch-ram system.

[2] This is the SSI Endat measuring system from Fette, which is affixed to the rail guides in line with the upper ram adapter plate.

4.1.2.2 Contraction behaviour of the upper punch-ram system

As stated previously the contraction of the upper punch-ram system affects the upper dimensions of the compact. This is particularly true in the case of tight-fit components where the contraction of the upper punch directly affects the lip size. Thus it is important to determine the contraction behaviour with force of this system separate from the lower punch-ram system.

To determine the upper punch-ram contraction behaviour with force, the large steel plate was placed on the middle adapter plate of the press – where a die would normally be clamped – and the carbide disc placed on top of it. The upper punch is brought slowly into contact with the carbide disc using the 'move individual axes mode' of the press until contact is made between the two. Thereafter, further small downward movements of the upper ram are made resulting in the evolution of forces between 0 kN and 100 kN with the actual axis position of the upper ram being displayed on the press screen at each pressing force. True contraction behaviour of the upper punch-ram system must also take into account the deformation of the carbide disc. This is done by making simultaneous disc deformation measurements using a finger clock which is placed on the disc in close vicinity of the punch as shown in figure 9.

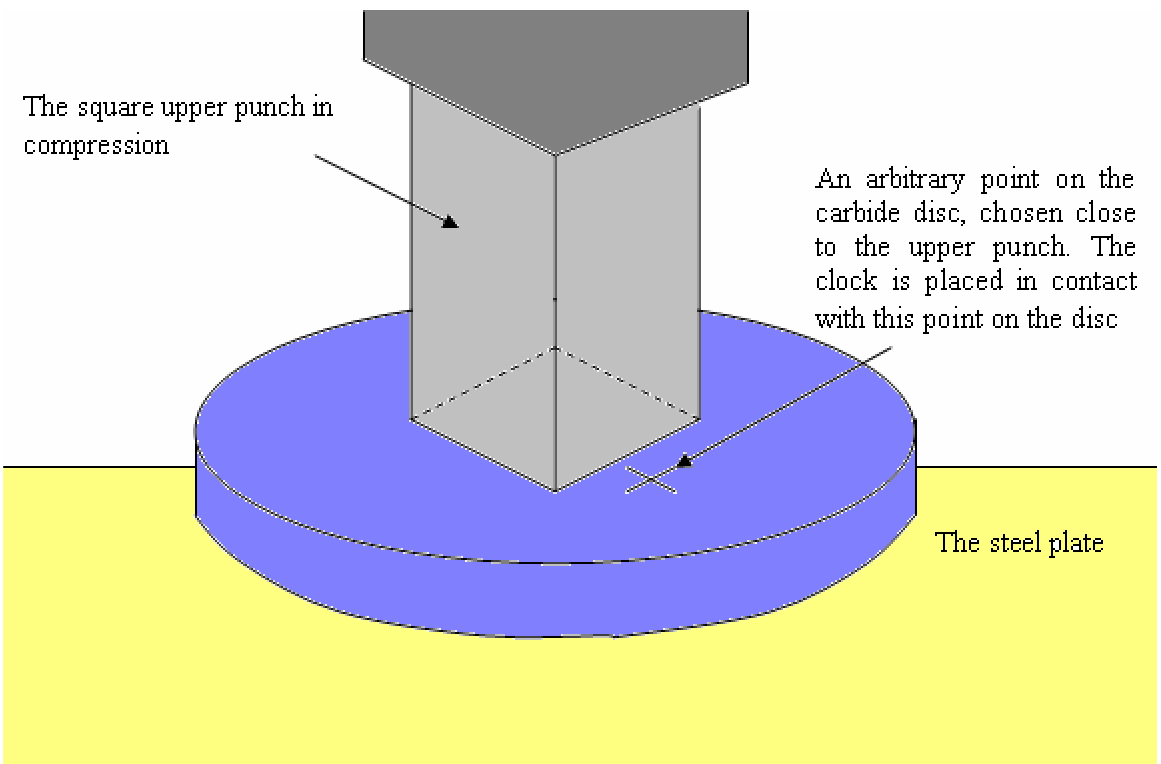

Figure 9: An arbitrarily chosen point for the measurement of disc deformation. The point is in close vicinity of the punch where the deformation is greatest.

The contraction behaviour of the upper punch-ram system was determined by subtracting the clock reading from the axis position reading at each increment and plotting the results against the displayed force.

4.1.2.3 Contraction behaviour of the upper ram

The same procedure as above was followed except that the clock was placed in contact with the upper ram chuck. This is the part of the upper ram to which the upper punch is clamped. By subtracting the clock readings – which indicate the movement of this, the lowest point of the ram - from the upper ram axis position readings – which indicate the movement of the highest point on the ram where the transducer is connected to the Endat measuring system – the contraction of only the upper ram structure can be obtained at each value of the pressing force. From this result the contraction behaviour of the upper punch as a whole could be determined in the following way:

If,

$$\Delta L_{\text{Upper Punch-Ram}} = C_{\text{Upper Punch-Ram.}} \times F \qquad \text{. . . (4)}$$

And,

$$\Delta L_{\text{Upper Ram}} = C_{\text{Upper Ram}} \times F \qquad \text{. . . (5)}$$

Then,

$$\Delta L_{\text{Upper Punch}} = \Delta L_{\text{Upper Punch-Ram}} - \Delta L_{\text{Upper Ram}} = (C_{\text{Upper Punch-Ram}} - C_{\text{Upper Ram}}) \times F \qquad \text{. . . (6)}$$

4.1.2.4 Contraction behaviour of the punch shaft

In essentially the same procedure as above the finger clock is placed in contact with the punch base. By subtracting the clock readings – which in this case indicate the movement of the punch base - from the upper ram axis position readings – which indicate the movement of the point on the ram to which the measuring system is attached – the contraction of the punch shaft can be determined using identical calculation methods to above.

If,

$$\Delta L_{\text{Upper Punch-Ram}} = C_{\text{Upper Punch-Ram.}} \times F \qquad \text{. . . (4)}$$

And,

$$\Delta L_{\text{Upper Ram + Upper Punch Base}} = C_{\text{Upper Ram + Upper Punch Base}} \times F \qquad \text{. . . (7)}$$

Then,

$\Delta L_{\text{Upper Punch Shaft}} = \Delta L_{\text{Upper Punch-Ram}} - \Delta L_{\text{Upper Ram + Upper Punch Base}} = (C_{\text{Upper Punch-Ram}} - C_{\text{Upper Ram + Upper Punch Base}}) \times F$

. . . (8)

A comparison of punch shaft contraction for the three different tools tested allowed for a qualitative determination of the effect of brazing on the overall contraction.

4.2 Methods for measuring relaxation or springback induced dimensional changes in compacts

4.2.1 Equipment used

1. MP250 hydraulic CNC press.
2. Three test tools (square, round and triangular) made from two different powder grades (A and B). The compositions are in Appendix B (Table A4).The experiments were done using tight-fit and SBA tools and the corresponding pressed compacts.
3. Lip measuring setup which includes a Mitutoyo microscope and a holder for positioning the insert at approximately a 45 degree angle for optimum illumination of the lip (Figure 10). A small magnet was used to position the inserts on the holder[3].

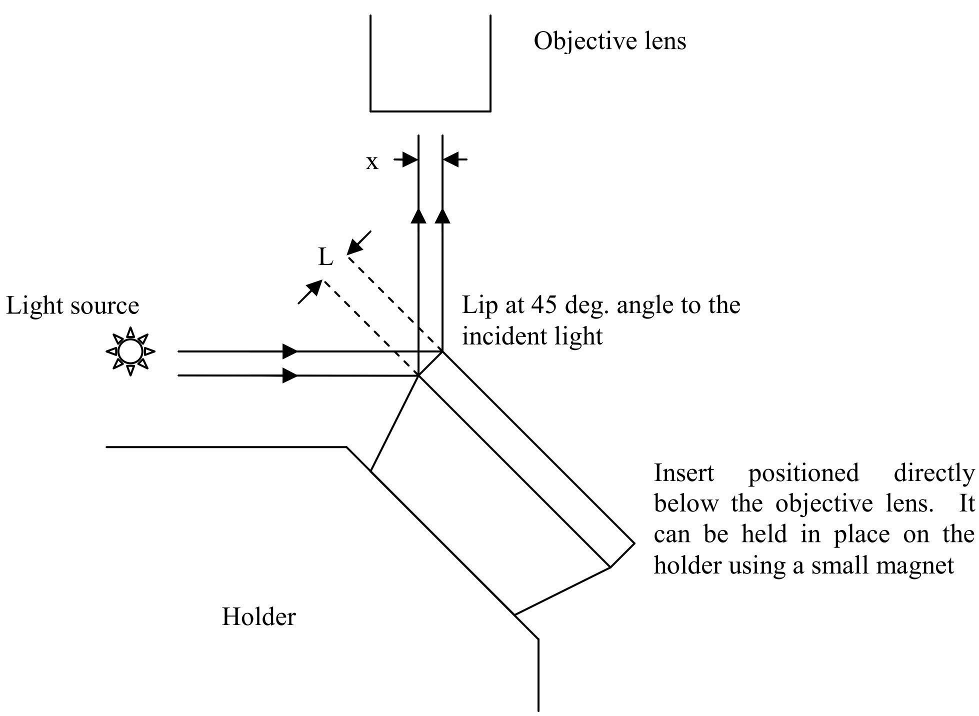

Figure 10: A diagram of the experimental setup used to measure lip size, where $L = \sqrt{2}\,x$ and x is the measured reading.

[3] Compacts were found to be magnetic in the green state.

4. Vernier callipers for measuring the height of the compacts to within ±0.010 mm accuracy. Vertical dimensional changes due to compact relaxation could be determined on the basis of these measurements.

5. IC[4] micrometer for measuring the IC or the diametrical dimension of compacts within ±0.010 mm accuracy. The IC measurement is a good way to measure the horizontal change in compact dimensions due to relaxation, on the basis that it can be measured for all three tool geometries (figure 11).

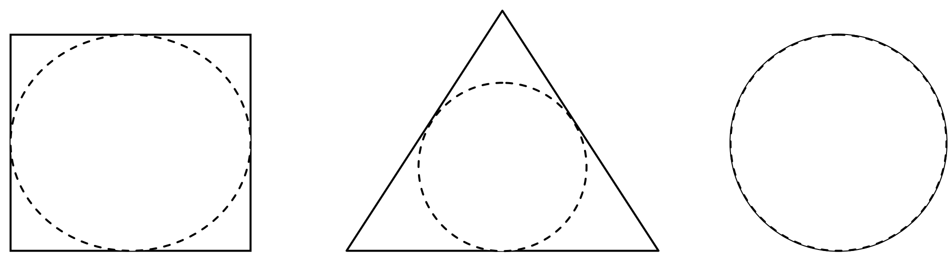

Figure 11: All three geometries contain an inscribe circle. These three compact geometries correspond to the three chosen tools.

The Mitutoyo microscope was used to measure the IC dimensions of the square and round SBA components as these edges were found to be too soft to be measured using the micrometer.

6. The compact mass was measured on one of the press scales with an accuracy of ±0.001g.

7. Two fine-bristle paint brushes for deburring of pressed compacts prior to measurement. A burr is a form of uncompacted powder found at the edges of the formed compacts as result of loose powder escaping in the spaces between the punch and the die wall during pressing. Schematically it can be represented as shown in figure 12 where both burrs on a tight-fit and an SBA compact are shown.

[4] IC refers to the diameter of the inscribed circle.

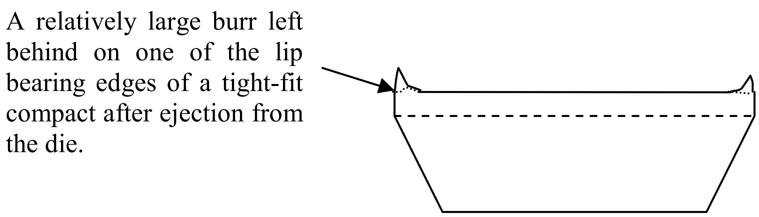

a) A tight-fit compact with a burr.

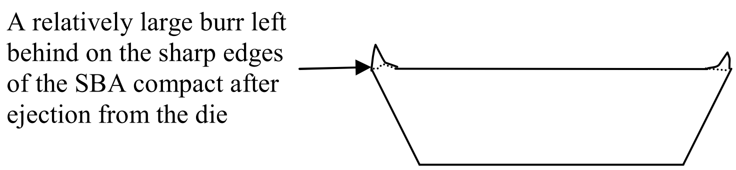

b) A SBA compact with a burr.

Figure 12: a schematic representation of a burr a) on a tight-fit compact and b) on a SBA compact.

4.2.2 General overview of procedure

Tight-fit test pieces of all three geometries were pressed using the same parameters. The programmed final pressing positions of the upper and lower punches were kept constant while the pressing force was varied. The pressing force was varied by varying the mass of each of the pressed components. The mass in turn was varied by a filling position parameter in the press software which controls the position of the lower ram during powder filling. When the hopper shoe containing powder is over the die cavity, the lower ram is in the programmed position below the die and shoe as indicated in Fig. 16. Lowering this position allows more powder to enter the die resulting in heavier compacts and greater pressing forces; that is if the programmed end pressing positions of the punches remain unchanged.

The pressing force was varied in the range that allowed the chosen punch travel schedule to be maintained. The schedule that was chosen is one of equal powder displacement by the top and bottom punches which ensures a roughly even density distribution throughout the green compact. This schedule is generally used commercially. The range of pressing forces also depends on the tool shrinkage[5]. The tool shrinkage of all three test tools was 24%. Given these constraints, the range of pressing forces that could be achieved in the

[5] In general the larger the shrinkage the smaller the pressing force.

experiment was between 5 kN and 35 kN for all three tools. Several tests pieces were pressed covering this range and critical dimensions measured as shown in figure 24[6].

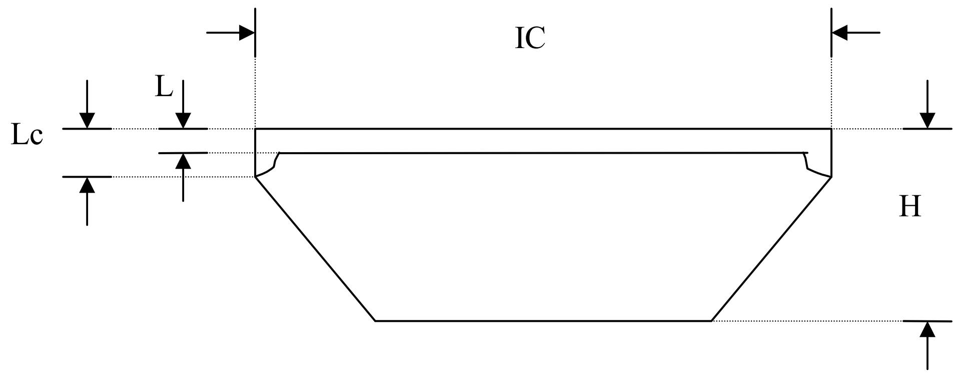

Figure 13: Tight-fit compact key dimensions.

The SBA test pieces were pressed in a similar manner with minor differences. The main difference was that the final pressing position could be safely increased with the SBA punch i.e. penetration depth (SBA) > penetration depth (tight-fit). This is a natural consequence of having ground the punch from its original tight-fit dimensions; it allows the punch to penetrate the die further without colliding with the positive faces of the die (refer to section 4.3). The end result was that the SBA compacts had a slightly different shape from that of the tight-fit compacts as shown schematically in Fig. 14 with critical dimensions that were measured.

A second difference is that the SBA compacts could be pressed without the use of pneumatic download. All tight-fit compacts have to be pressed using the pneumatic download to avoid cracks induced by tensile and frictional stresses present in the die wall. SBA compacts are never in contact with the die wall and hence do not experience friction and tensile stresses

[6] Only one side of the compact was chosen for the measurement of lip size and the measurements were performed on the same side for each tests piece in order to preserve consistency of results. Similarly, corner lip measurements were performed on the same corner for each test piece. Corner lip measurements were obviously not possible on the round compacts.

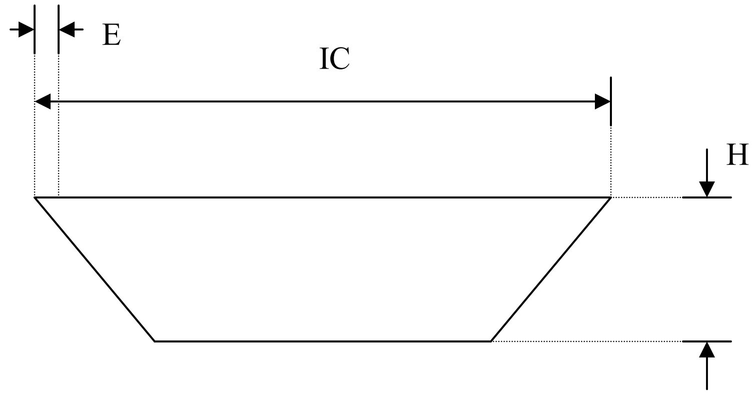

Figure 14: SBA compact key dimensions.

4.2.2.1 Lip measuring setup for tight-fit compacts

In order to measure the lip dimension accurately the experimental setup shown in figure 10 was developed for this project. One advantage of this method is that it is non-destructive and does not cause damage to the green component. The holder ensures that the compacts can be positioned so that the lip is always at a 45 degree angle to the incident light and the objective lens ensuring maximum illumination and visibility. Measurements of the corner lip dimension were also made using this setup. The compacts were simply rotated on the holder until the compact corner faced the incident light and the reflection became visible in the eye piece.

4.3 Modification of tight-fitting tools into SBA tools

In order to study the springback or relaxation behaviour of compacts independent of friction and to improve certain negative characteristics found on tight-fit compacts thought to be caused by friction, such as the expansion of corner lip size, a new method of pressing involving a change in tool design and manufacture was developed in the course of this project.

This modification involved the introduction of a compact relaxation gap between the upper punch and the die, referred to as the ‘springback allowance’. The transformation could be done in two of the following ways: by re-sparking the tight-fit dies and essentially making the die cavities of each tool larger, or by grinding the periphery of upper tight-fitting punches making them smaller. The second option was chosen as grinding is a significantly easier, less expensive and less time consuming option.

The sizes of the tool gaps were originally estimated based on radial springback measurements of tight-fit compacts and other considerations which are discussed later. The idea was to introduce a gap large enough so that after radial springback the compacts would be free to eject without making contact with the die walls or any loose powder that may be stuck to them. A gap of approximately 0.100 mm was created for each tool. On the basis of these chosen gaps, practical and meaningful results could be obtained as discussed in later sections. The two tools designs are shown in figures 15 and 16 below.

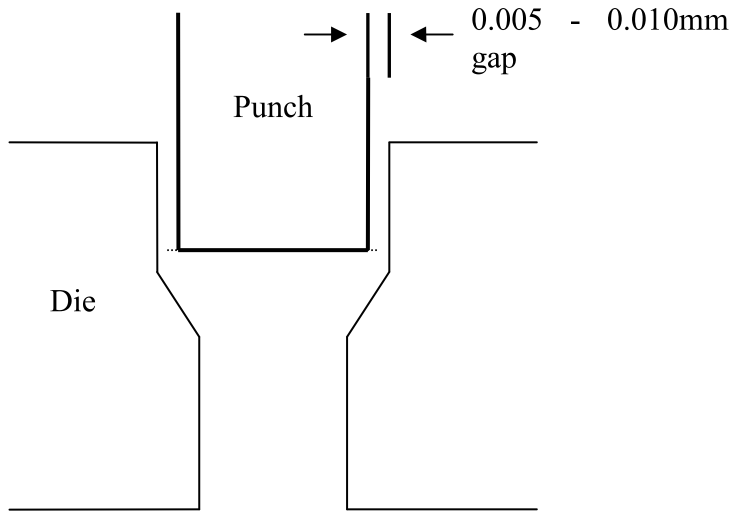

Figure 15: A diagram of the conventional tight-fit tooling design with a relatively small clearance of 0.005 mm to 0.010 mm between the upper punch and die.

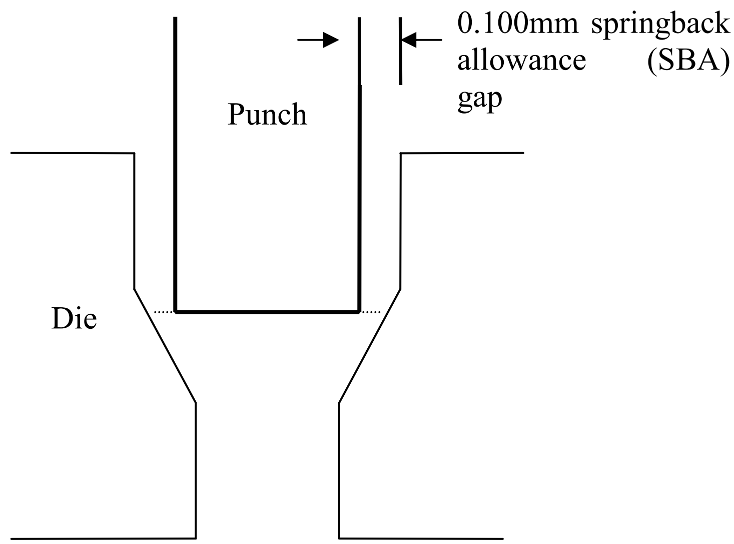

Figure 16: A diagram of the new SBA design developed during this work with a relatively large clearance of approximately 0.100 mm between the upper punch and die.

It is clear from the diagrams that in the SBA design the punch can penetrate the die to a deeper level without colliding with the die. The final pressing position can be increased considerably beyond the ‘leadin’ and come very close to the positive faces of the die, leading to the formation of slightly differently shaped compacts shown schematically in figure 14.

4.4 Edge width measurements

This dimension is a direct consequence of the compact edge formation in a SBA die and an accurate measurement of this dimension can theoretically be used to determine the actual punch position in the die during pressing. Such a result would be very useful in practice since the penetration depth could safely be increased in order to improve the quality of the compact edges for example, while maintaining a relatively low probability of incurring tool damage due to a collision between the upper punch and die. The edge width was measured using the Mitutoyo Microscope by placing the compact flat on the microscope viewing platform and measuring the compact edge from the top

4.5 De-burring methods

In commercial practice burrs are normally removed from the compact edges prior to sintering by light brushing using a suitably soft brush or another medium. If the burrs are not removed they may lead to early service failures and/or distortion of the cutting edges. Therefore a proper de-burring technique is essential for the successful production of inserts. Although the focus of this work was on green compacts and not sintered alloys, it was necessary to de-burr the pressed test pieces since the burrs can affect dimensional measurements, especially the lip size and compact height. When a burr is present the lip appears larger than it actually is. Two paint brushes were used in the experiment for this purpose. The types of burrs found and the factors influencing burr size and characteristics are discussed in detail in Chapter 7.

5 Result analysis and calculation methods

5.1 Introduction

From the measurements of the linear compact dimensions the one-dimensional springback behaviour in the axial and radial directions and the three dimensional springback behaviour of compacts referred to as volumetric springback were determined. The compact volume equations used for this purpose were developed based on right pyramidal frustum formulae for the volumes of pyramids with square, circular and triangular bases.

5.2 Analysis procedures for tight-fit compact data

The analytical methods described below were used for all compact geometries and grades of powder except where indicated otherwise.

5.2.1 Change in lip size with pressing force

The change in lip size with pressing force due to the effects of contraction, springback and compact die-wall interaction could be determined by plotting the measured lip size values against the recorded pressing force values. The best fit equation could be plotted against the measured data and the value of the y-axis intercept determined[7]. The intercept could then be subtracted from the best fit equation in order to determine the behaviour of the change in lip size as a function of force. Thus for example, if the best fit equation for the variation of lip size with force was found to be quadratic:

$$L(F) = aF^2 + bF + c \qquad \text{. . . (9)}$$

Then,

$$\Delta L(F) = aF^2 + bF \qquad \text{. . . (10)}$$

would have represented the variation in the change in lip-size with force. It can be seen that the quadratic and the linear coefficients of the L(F) vs. F equation fully describe the change in lip size $\Delta L(F)$ with force.

[7] The y-axis intercept gives the lip size at 0kN, which theoretically should equal the difference between the programmed penetration depth and the leadin which was in all cases was chosen at 0.100mm. However practically, it was found that the obtained intercepts were often slightly different from the expected value and the reasons for this could very well be related to tool referencing inaccuracies or presences of small burrs on the compacts despite the efforts to accurately reference the tools (using accurate offline tool measurements and the tool database of the press) and free the compacts from the burr as discussed in section 4.5.

5.2.2 Determination of axial lip springback as a function of force

In order to determine the change in compact dimensions due to springback as influenced by die-wall friction, the dimensional change in lip size due to contraction must be subtracted from the total change in lip size as follows:

$$\Delta L(F) - (C_{\text{Upper Punch-Ram}} \times F) = \Delta L(F)_{\text{springback}} \qquad \ldots (11)$$

Where,

- $\Delta L(F)$ represents the total change in lip size at force F calculated by the method described in 5.2.1
- $C_{\text{Upper Punch-Ram}}$ is the contraction constant of the upper punch-ram system as determined by the method described in 4.1.2.2.
- $\Delta L(F)_{\text{springback}}$ is the change in lip size due to springback under the influence of die-wall friction.

The effect of contraction on the lip size is to increase it, and is thus subtracted from the total lip size in the above equation in order to be left with only the springback contribution.

5.2.3 Determination of relative or fractional axial springback of the lip dimension

The determination of relative or fractional springback allows an examination of the amount of springback observed for a particular dimension relative to the initial or starting size of that dimension. For example, if springback is found to be naturally larger for larger dimensions and in proportion to the size of the dimension, then one would expect to find that the relative springback of L, H, or IC is the same regardless of the dimension.

In the case of the lip dimension, the percentage springback was calculated as follows:

$$\Delta L(F)_{\text{relative springback}} = \{\Delta L(F)_{\text{springback}} / L_o(F)\} \times 100 \qquad \ldots (12)$$

Where,

- $\Delta L(F)_{\text{springback}}$ is the change in lip size at force F due to springback under the influence of die-wall friction
- L_o is the size of the lip in the final pressing position of the upper punch, after contraction but before decompression and springback, i.e.

$$L_o(F) = L(F) - \Delta L(F)_{\text{springback}} = L(F) - \Delta L(F) + (C_{\text{Upper Punch-Ram}} \times F) \qquad \ldots (13)$$

5.2.4 Change in height with pressing force

A change in the total compact height as a result of contraction, springback, and friction can be determined by plotting the measured compact height as a function of pressing force and obtaining the best fit equation from which the constant term may be omitted. The constant term should match the expected height of the component at 0 kN of pressing force perfectly well negating any tool referencing errors and compact burrs.

5.2.5 Determination of the total axial springback

In order to determine the total axial change in the compact dimensions due to springback and the effect of friction, the total change in compact dimensions due to the upper and lower punch-ram systems must be subtracted from the total change in height of the compact. This is done because the contraction in the lower and upper punch-ram systems has an increasing effect on the total compact height. Therefore:

$$\Delta H(F) - (C_{\text{Upper + Lower Punch-Ram}} \times F) = \Delta H(F)_{\text{springback}} \qquad \ldots (14)$$

Where,

- $\Delta H(F)$ represents the total change in compact height at force F, calculated by the method described in 5.2.3
- $C_{\text{Upper + Lower Punch-Ram}}$ is the contraction constant of the upper and lower punch-ram systems as determined in 4.1.2.1
- $\Delta H(F)_{\text{springback}}$ is the change in compact height due to springback under the influence of friction at the lip die-wall interface

5.2.6 Determination of relative or fractional axial springback of the total height

The relative axial springback for the total height of a compact can be calculated as follows:

$$\Delta H(F)_{\text{relative springback}} = \{\Delta H(F)_{\text{springback}} / H_o(F)\} \times 100 \qquad \ldots (15)$$

Where,

$\Delta H(F)_{\text{springback}}$ is the change in height due to springback under the influence of friction,

and

$$H_o(F) = H(F) - \Delta H(F)_{\text{springback}} = H(F) - \Delta H(F) + (C_{\text{Upper + Lower Punch-Ram}} \times F) \qquad \ldots (16)$$

5.2.7 Change in horizontal compact dimensions with pressing force

The change in the horizontal compact dimensions with pressing force due to the effects of radial springback under the influence of die-wall friction can be determined by plotting the measured IC values against the recorded pressing force values. The best fit equation can be plotted against the measured data and the value of the y-axis intercept subtracted from the best fit equation in order to determine the behaviour of the change in horizontal compact dimensions as a function of pressing force. At 0 kN pressing force, the compact IC represented by the constant term of the best fit equation should match the horizontal die dimension if the curve is an accurate representation of the actual behaviour.

5.2.8 Determination of radial springback

Radial springback of tight-fit compacts is affected only by friction and possibly slight extension of the die in the radial direction during pressing. The latter effect as well as that of secondary yielding are however likely to be comparatively insignificant due to the relatively high modulus of elasticity of carbide from which the die is manufactured and the relatively large size and shape of the die. Punch contraction in tight-fit compaction only affects the vertical dimensions of compacts. Thus, radial springback is equal to the change in horizontal compact dimensions i.e.

$$IC(F) - IC_o(F) = IC(F) - IC(F{=}0\text{ kN}) = \Delta IC(F) = \Delta IC(F)_{\text{springback}} \qquad \ldots (17)$$

5.2.9 Determination of the relative or fractional radial springback

Percentage radial springback is calculated as follows:

$$\Delta IC(F)_{\text{relative springback}} = \{\Delta IC(F)_{\text{springback}} / IC_o\} \times 100 \qquad \ldots (18)$$

Where,

- $\Delta IC(F)_{\text{springback}}$ is the amount of radial springback as influenced by die-wall friction at force F calculated in 5.2.8.

- IC_o is the compact IC at 0 kN of pressing force which in tight-fit compacts is a constant term independent of the pressing force.

5.2.10 Axial to radial springback ratio

As a measure of comparison between the axial and radial springback behaviours, a ratio of axial to radial springback could be plotted as a function of force according to:

$$\Delta H(F)_{\text{springback}} / \Delta IC(F)_{\text{springback}} \text{ vs. } F \qquad \ldots (19)$$

Where,

$\Delta H(F)_{springback}$ and $\Delta IC(F)_{springback}$ are as calculated in 5.2.5 and 5.2.8 respectively.

5.2.11 Relative springback ratio

In order to compare the axial and radial springback as measured relative to the initial compact dimensions, a ratio of the relative axial springback to the relative radial springback can be plotted as a function of pressing force according to:

$$\Delta H(F)_{relative\ springback} / \Delta IC(F)_{relative\ springback} \text{ vs. } F \qquad \ldots (20)$$

Where,

$\Delta H(F)_{relative\ springback}$ and $\Delta IC(F)_{relative\ springback}$ are as calculated in 5.2.6 and 5.2.9 respectively.

5.2.12 Variation of volumetric springback with pressing force

The elastic nature of the pressed compacts can be compared on the basis of volumetric springback which takes into account the changes in all three spatial dimensions and is thus a more complete measure of springback albeit not that practical. Volumetric springback is calculated as follows:

$$\Delta V(F)_{springback} = V(F) - V_o(F) \qquad \ldots (21)$$

Where V(F) is the volume of the ejected compact pressed at force F, and $V_o(F)$ the volume of the compact before in-die springback, pressed at force F.

The equations used for V(F) and $V_o(F)$ for the square, round and triangular compact geometries were based on the right pyramidal frustum formulae for pyramids with square, round and triangular bases according to:

$$V\square = 1/3 \times [H(F) - L(F)] \times [IC(F)^2 + IC(F)\times IC_{bottom} + IC^2_{bottom}] + IC(F)^2\times L(F) \qquad \ldots (22)$$
$$V\circ = \pi/3 \times [H(F) - L(F)] \times [IC(F)^2 + IC(F)\times IC_{bottom} + IC^2_{bottom}] + \pi(IC(F)/2)^2\times L(F) \qquad \ldots (23)$$
$$V\Delta = 1/(6\tan^2 30^\circ) \times [H(F) - L(F)] \times [IC(F)^2 + IC(F)\times IC_{bottom} + IC^2_{bottom}] + (IC(F)/2)^2\times L(F) \ldots (24)$$

Where,

$IC_{bottom}\ \square = 10.562$ mm
$IC_{bottom}\ \circ = 11.149$ mm
$IC_{bottom}\ \Delta = 10.557$ mm

were obtained from the offline measurements of the corresponding compact dies.

The measurement of the IC of the bottom die edge made for a good approximation of the compact IC_{bottom} since the adopted pressing schedule ensures that most of the springback occurs in the upper parts of the compact as opposed to the lower. Specifically, during decompression the lower punch is stationary while the upper punch moves slightly away from the compact allowing the relaxation of the upper compact dimensions but not the lower. Whatever springback energy is left in the compact after ejection it is unlikely to have a significant effect on the IC of the lower compact surface.

Similarly, $V_o(F)$ equations can be defined as:

$$V_o\square = 1/3 \times [H_o(F) - L_o(F)] \times [IC_o(F)^2 + IC_o(F)\times IC_{bottom} + IC^2_{bottom}] + IC_o(F)^2\times L_o(F) \quad ...(25)$$
$$V_o\circ = \pi/3 \times [H_o(F) - L_o(F)] \times [IC_o(F)^2 + IC_o(F)\times IC_{bottom} + IC^2_{bottom}] + \pi(IC_o(F)/2)^2\times L_o(F) \quad ...(26)$$
$$V_o\Delta = 1/(6\tan^2 30^o)\times[H_o(F) - L_o(F)]\times[IC_o(F)^2 + IC_o(F)\times IC_{bottom} + IC^2_{bottom}] + (IC_o(F)/2)^2\times L_o(F) \quad ..(27)$$

Where $H_o(F)$, $L_o(F)$, and $IC_o(F)$ are as defined previously.

5.2.13 Relative volumetric springback

The percentage volumetric springback as a function of pressing force was calculated as follows:

$$\Delta V(F)_{relative\ springback} = \Delta V(F)_{springback} / V_o(F) \times 100 \quad ...(28)$$

5.2.14 Variation of green density with pressure

Green density can be calculated from measurements of the compact mass and the above mentioned volume formulae as:

$$\rho(F) = M/V(F) \quad ...(29)$$

Compaction pressure can be calculated from the recorded pressing forces and the known upper punch surface areas using the formula:

$$P(F) = F/A \quad ...(30)$$

The results are reported in Appendix D (Tables 50, 57, 64, 71, and 78).

5.3 Analysis procedures for SBA compacts

The procedures discussed below were used for all the compact geometries and grades of powder used in the experiments. The procedures described below are in essence identical to those described for the tight-fit compacts. The major differences are in the procedure used to calculate radial springback and that L vs. F profiles could not be established for SBA compacts as discussed below.

5.3.1 Lip size measurements and determination of axial lip springback

In SBA compacts the lip was observed only at exceptionally high pressing forces as discussed in later sections. At typical pressing forces and penetration depths sufficiently close to the die face the edges of SBA compacts were sharp and did not have a lip. Thus, L(F) vs. F profiles for these compacts could not be established. Axial springback could only be determined for the overall vertical dimension i.e. the compact height.

5.3.2 Height measurements and the determination of total axial springback

The determination of axial springback behaviour followed the same procedure described in sections 5.2.4, 5.2.5, and 5.2.6. However, at typical pressing forces it could be assumed that SBA compacts were free from die-wall contact and for all practical purposes did not experience any friction during ejection from the die[8]. Thus the term $\Delta H(F)_{springback}$ in this chapter denotes free springback; that is springback free from frictional effects and die-wall contact.

5.3.3 IC measurements and the determination of radial springback

Radial springback is calculated in a similar way to section 5.2.8 except that in this case:

$$IC_o(F) \neq IC(F = 0 \text{ kN}) \qquad \text{. . . (31)}$$

Unlike in tight-fit compacts, in SBA compacts the $IC_o(F)$ quantity changed slightly with each new pressing force depending on the final pressing position of the upper punch and therefore the amount of contraction experienced by the upper punch-ram system in compaction. SBA compact formation is discussed in more detail later on but for now it is important to note that $IC_o(F)$ could be expressed in terms of the upper punch-ram contraction as follows:

$$IC_o(F) = IC(F = 0 \text{ kN}) + 2(\tan 7^{\circ})(\Delta L_{\text{Upper Punch-Ram}}) \qquad \text{. . . (32)}$$

The following diagram is helpful in understanding how the relationship was derived.

[8] Any friction that these compacts might have experienced at typical pressing forces would be a result of non-compacted or loose powder in the gaps between the upper punch and the die against which the compact may rub during ejection. However, this is unlikely to have a significant effect on the end component dimensions and axial springback of these parts can for all practical purposes be considered friction free.

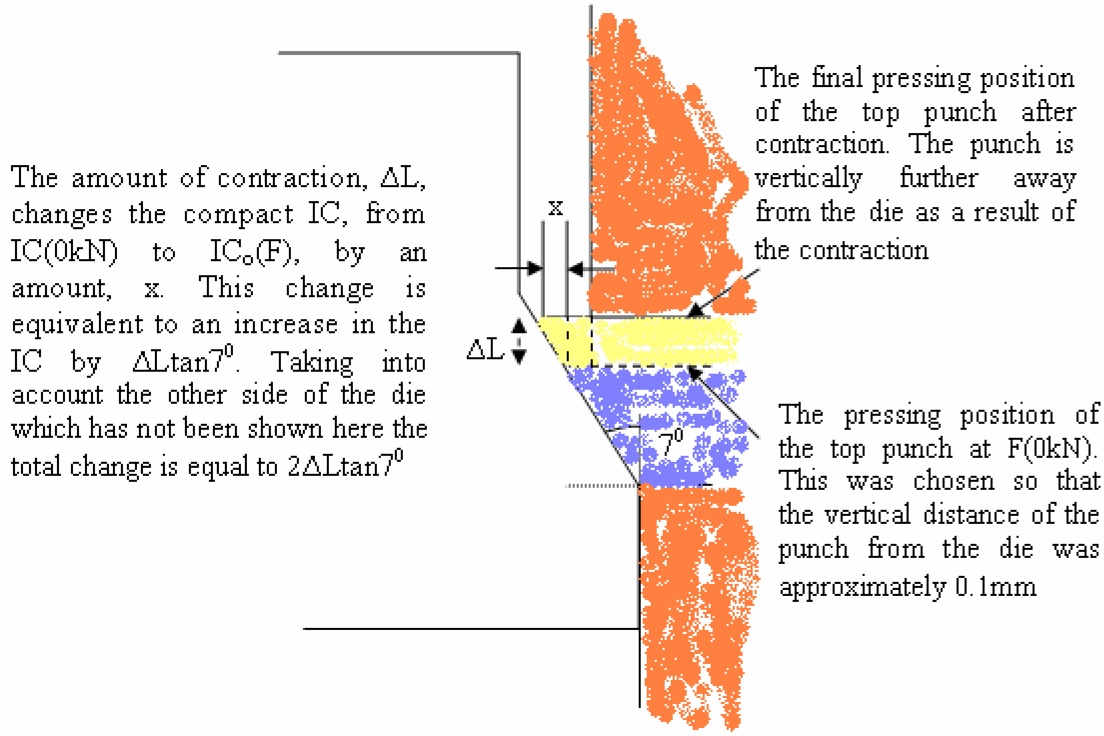

Figure 17: The effect of punch contraction on the final pressing position of the upper punch and therefore the IC dimension of the compact before in-die springback.

Therefore:

$$\begin{aligned}\Delta IC(F)_{springback} &= IC(F) - IC_o(F) \\ &= IC(F) - [IC(F = 0\text{ kN}) + 2(\tan 7^o)(\Delta L_{\text{Upper Punch-Ram}})] \\ &= IC(F) - IC(F = 0\text{ kN}) - 2(\tan 7^o)(C_{\text{Upper Punch-Ram}} \times F) \\ &= \Delta IC(F) - 2(\tan 7^o)(C_{\text{Upper Punch-Ram}} \times F) \qquad \ldots (33)\end{aligned}$$

The relative radial springback was calculated as in section 5.2.9 (refer to equation 18).

5.3.4 The variation of the springback and the relative springback ratio

The same method described in sections 5.2.10 and 5.2.11 was used. Equations 19 and 20 were plotted using SBA data.

5.3.5 Determination of volumetric springback

The identical procedure in section 5.2.12 was followed. Equations 21 to 27 could be used to determine the radial springback of SBA compacts. In equations 22 to 27, L was set equal to zero as the lip dimension was not observed on these compacts except at exceptionally high pressing forces[9]. Thus equations 22 to 27 could effectively be reduced to the following equivalent equations used for the calculation of volume of SBA compacts:

$$V\square = 1/3 \times H(F) \times [IC(F)^2 + IC(F)\times IC_{bottom} + IC^2_{bottom}] \quad ...(34)$$
$$V\circ = \pi/3 \times H(F) \times [IC(F)^2 + IC(F)\times IC_{bottom} + IC^2_{bottom}] \quad ...(35)$$
$$V\Delta = 1/(6\tan^2 30^o) \times H(F) \times [IC(F)^2 + IC(F)\times IC_{bottom} + IC^2_{bottom}] \quad ...(36)$$

and,

$$V_o\square = 1/3 \times H_o(F) \times [IC_o(F)^2 + IC_o(F)\times IC_{bottom} + IC^2_{bottom}] \quad ...(37)$$
$$V_o\circ = \pi/3 \times H_o(F) \times [IC_o(F)^2 + IC_o(F)\times IC_{bottom} + IC^2_{bottom}] \quad ...(38)$$
$$V_o\Delta = 1/(6\tan^2 30^o) \times H_o(F) \times [IC_o(F)^2 + IC_o(F)\times IC_{bottom} + IC^2_{bottom}] \quad ...(39)$$

Where $H_o(F)$ and $IC_o(F)$ are as described in sections 5.2.6 (equation 16) and 5.3.3 (equation 32) respectively.

The percentage volumetric springback was calculated the same as section 5.2.13.

5.3.6 Determination of green density as a function of pressure

The same method described in section 5.2.14 was used. Equations 29 and 30 were used to calculate green density and pressure sets of data were plotted against each other in order to determine the density vs. pressure profile.

[9] An explanation for the formation of lip on SBA compacts at very high pressing forces is offered in Chapter 7.

6 Results

6.1 Contraction measurements

The contraction measurements for the relevant punch-ram and punch-base systems are given in this section for tight-fit square tool compacts. Similar measurements were made for tight-fit round and triangular tools as well as SBA square, round and triangular tools. Data for these tools is listed in Appendix C.

6.1.1 Upper and lower punch-ram system contraction

As described in section 4.1.2.1, the combined contraction of the upper and lower punch ram systems is given directly by the upper ram measuring system reading which is listed in Table 1 as a function of pressing force. Since the upper ram axis is denoted by the letter A on the press display screen, the measuring system reading for the upper ram axis will be denoted by the letter A(mm) as shown in Table 1 below.

Table 1: Upper and lower punch-ram system contraction data for the square tight-fit tool.

No.	Upper ram measuring system reading A(mm) ± 0.003 mm	Pressing Force F(kN) ± 0.5 kN
1	0.000	0.0
2	0.009	3.5
3	0.019	6.1
4	0.028	9.0
5	0.048	14.9
6	0.058	18.2
7	0.078	24.4
8	0.098	31.2
9	0.116	37.3
10	0.134	43.6
11	0.153	50.6

6.1.2 Upper punch-ram system contraction

As described in section 4.1.2.2, the upper punch-ram system contraction is given by the difference between the upper ram measuring system reading and the plate deformation readings as listed in Table 2. The maximum error in the upper punch-ram system contraction is the sum of errors of the measuring system reading and the plate deformation clock reading.

Table 2: Upper punch-ram system contraction data for the square tight-fit tool.

No.	Upper ram measuring system reading A(mm) ± 0.003 mm	Plate deformation clock reading C(mm) ± 0.002 mm	Upper punch- ram system contraction ΔL(mm) ± 0.005 mm	Pressing Force F(kN) ± 0.5 kN
1	0.000	0.000	0.000	0.0
2	0.011	0.002	0.009	4.2
3	0.021	0.005	0.016	7.0
4	0.032	0.008	0.024	10.1
5	0.042	0.011	0.031	13.6
6	0.063	0.014	0.049	21.2
7	0.074	0.015	0.059	25.8
8	0.096	0.017	0.079	35.7
9	0.106	0.018	0.089	40.8
10	0.117	0.018	0.099	45.9
11	0.128	0.018	0.110	50.6

6.1.3 Upper ram contraction

As described in section 4.1.2.3, the upper ram system contraction is given by the difference between the upper ram measuring system reading and the upper ram chuck position as listed in Table 3. The maximum error in the upper ram contraction is the sum of errors of the measuring system reading and the chuck movement clock reading.

Table 3: Upper ram contraction data for the square tight-fit tool.

No.	Upper ram measuring system reading A(mm) ± 0.003 mm	Chuck position clock reading C(mm) ± 0.002 mm	Upper ram system contraction ΔL(mm) ± 0.005 mm	Pressing Force F(kN) ± 0.5 kN
1	0.000	0.000	0.000	0.0
2	0.009	0.006	0.003	3.8
3	0.020	0.015	0.005	7.1
4	0.031	0.023	0.008	10.2
5	0.043	0.033	0.010	15.0
6	0.055	0.040	0.015	19.7
7	0.066	0.047	0.019	24.4
8	0.078	0.056	0.022	30.3
9	0.089	0.062	0.027	35.1
10	0.109	0.075	0.034	45.0
11	0.120	0.083	0.037	50.5

6.1.4 Contraction of the upper ram and punch base system

The contraction of the upper ram and punch base system is given by the difference between the upper ram measuring system reading and the punch base position (refer to Table 4). The maximum error in the upper ram and punch base system contraction is the sum of errors of the measuring system reading and the punch base movement clock readings.

Table 4: Upper ram and punch base system contraction data for the square tight-fit tool.

No.	Upper ram measuring system reading A(mm) ± 0.003 mm	Punch base clock reading C(mm) ± 0.002mm	Upper ram and punch base contraction ΔL(mm) ± 0.005 mm	Pressing Force F(kN) ± 0.5 kN
1	0.000	0.000	0.000	0.0
2	0.011	0.006	0.005	4.2
3	0.024	0.015	0.009	8.0
4	0.037	0.023	0.014	12.7
5	0.050	0.030	0.020	17.4
6	0.061	0.037	0.024	22.6
7	0.075	0.044	0.031	28.6
8	0.085	0.050	0.035	33.8
9	0.099	0.059	0.040	39.9
10	0.113	0.066	0.047	46.7
11	0.124	0.072	0.052	52.3

6.2 Tight-fit compact measured and calculated data

To preserve 1:1 punch travel ratios the maximum filling heights for each powder grade and tool geometry differed. The selected filling heights have corresponding pressing forces which in turn led to a variation in pressed compact properties. Data based on the variation of filling height, pressing force and resulting pressed compact properties was generated for tight-fit compacts using Grade A and Grade B powders for all three compact geometries (square, round, triangular). Examples of the generated data are given in this section for the square tools produced using Grade A powder. Data for all the tested compacts can be found in Appendix D.

6.2.1 Measured data

In order to preserve a 1:1 punch travel ratio the maximum filling height that could be chosen was 13.19 mm as seen in Table 25. At this filling height the corresponding pressing force was 29.5 kN. Thus this experiment was limited to a range of pressing forces between 0 kN and 29.5 kN.

Table 5: Recorded and measured data for the square tight-fit compact using Grade A powder.

No.	Filling height F_h(mm)	Pressing Force F(kN) ± 0.1 kN	Mass M(g) ± 0.001g	Lip L(mm) ± 0.01mm	Corner Lip L_c(mm) ± 0.01 mm	Height H(mm) ± 0.01mm	IC(mm) ± 0.01mm
1	10.50	6.6	4.622	0.196	0.246	5.46	11.90
2	11.00	8.4	4.787	0.210	0.264	5.48	11.90
3	11.50	11.5	4.978	0.231	0.313	5.50	11.91
4	12.00	15.2	5.156	0.253	0.340	5.52	11.91
5	12.25	17.6	5.253	0.271	0.347	5.54	11.91
6	12.50	20.6	5.351	0.290	0.364	5.55	11.92
7	12.75	23.1	5.430	0.309	0.387	5.57	11.92
8	13.00	26.3	5.515	0.323	0.398	5.58	11.92
9	13.19	29.5	5.594	0.329	0.418	5.59	11.92

6.2.2 Calculated data

The data listed in Tables 6 to 11 was calculated using the equations described in section 5.2.

Table 6: Change in lip size with pressing force.

No.	$\Delta L(F)$ ± 0.01 mm	$\Delta L(F)_{contraction}$ ± 0.005 mm	$\Delta L(F)_{springback}$ ± 0.015 mm	$\Delta L(F)_{relative\ springback}$ (%)
1	0.057	0.015	0.042	27.4
2	0.071	0.019	0.052	33.3
3	0.094	0.025	0.069	42.4
4	0.119	0.033	0.086	51.6
5	0.135	0.039	0.096	54.6
6	0.152	0.045	0.107	58.4
7	0.166	0.051	0.115	59.3
8	0.181	0.057	0.124	62.0
9	0.195	0.064	0.131	65.9

Table 7: Change in height with pressing force.

No.	$\Delta H(F)$ $\pm$ 0.01 mm	$\Delta H(F)_{contraction}$ $\pm$ 0.005 mm	$\Delta H(F)_{springback}$ $\pm$ 0.015 mm	$\Delta H(F)_{relative\ springback}$ (%)
1	0.057	0.020	0.037	0.68
2	0.071	0.025	0.046	0.84
3	0.094	0.035	0.059	1.08
4	0.119	0.047	0.072	1.31
5	0.133	0.055	0.078	1.44
6	0.149	0.064	0.085	1.56
7	0.161	0.071	0.090	1.64
8	0.175	0.082	0.093	1.70
9	0.186	0.091	0.095	1.72

Table 8: Change in IC with pressing force.

No.	$\Delta IC(F)$ $\pm$ 0.01 mm	$\Delta IC(F)_{springback}$ $\pm$ 0.01 mm	$\Delta IC(F)_{relative\ springback}$ (%)
1	0.017	0.017	0.14
2	0.017	0.017	0.14
3	0.027	0.027	0.23
4	0.027	0.027	0.23
5	0.027	0.027	0.23
6	0.037	0.037	0.31
7	0.037	0.037	0.31
8	0.037	0.037	0.31
9	0.037	0.037	0.31

Table 9: Change in the springback and the relative springback ratio with pressing force.

No.	$\Delta H(F)_{springback}$ $/\Delta IC(F)_{springback}$	$\Delta H(F)_{relative\ springback}$ $/\Delta IC(F)_{relative\ springback}$
1	2.18	4.77
2	2.68	5.85
3	2.17	4.74
4	2.65	5.78
5	2.90	6.32
6	2.31	5.01
7	2.42	5.25
8	2.52	5.46
9	2.56	5.54

Table 10: Change in volumetric and relative volumetric springback with pressing force.

No.	$\Delta V(F)$ (cm^3)	$\Delta V(F)_{contraction}$ (cm^3)	$\Delta V(F)_{springback}$ (cm^3)	$\Delta V(F)_{relative\ springback}$ (%)
1	0.009	0.003	0.006	0.90
2	0.011	0.003	0.008	1.11
3	0.015	0.005	0.010	1.43
4	0.019	0.007	0.012	1.75
5	0.021	0.008	0.013	1.92
6	0.023	0.008	0.015	2.10
7	0.025	0.009	0.016	2.20
8	0.027	0.011	0.016	2.30
9	0.029	0.013	0.016	2.35

Table 11: Change in green density and with pressure.

No.	Pressure (kN/cm^2)	Green density (g/cm^3)
1	4.79	6.67
2	6.09	6.89
3	8.34	7.12
4	11.0	7.35
5	12.8	7.46
6	14.9	7.57
7	16.8	7.65
8	19.1	7.76
9	21.4	7.85

6.3 SBA compacts measured and calculated data

Two pressing schedules were used namely, with and without download in order to examine the effect of this press setting on the springback behaviour of compacts. Data was generated for SBA compacts using Grade A and Grade B powders for all three compact geometries (square, round, triangular). Examples of the generated data are given in this section for the square tools produced using Grade A powder. Data for all the tested compacts can be found in Appendix E.

6.3.1 Measured data with hold-down

Due to a greater penetration depth with SBA tools, a much larger filling height could be chosen while still preserving a 1:1 punch travel ratio. The maximum filling height that could be chosen was 14.0 mm. This corresponded to a pressing force of 124.3 kN. Thus a much wider range of pressing forces could be explored with SBA tools. However typical pressing forces in insert production at Pilot Tools rarely exceed 30 kN. In Table 12 lip and corner lip dimensions appear only at extremely high pressing forces. Thus lip size versus pressing force analysis was omitted. There is an additional set of measurements which was not present in tight-fit data; the edge width, E (mm).

Table 12: Recorded and measured data for the square SBA compact using grade A powder with hold-down.

No.	Filling height F_h (mm)	Pressing Force F(kN) ± 0.1 kN	Mass M(g) ± 0.001 g	Lip L(mm) ± 0.01mm	Corner Lip L_c(mm) ± 0.01mm	Edge width ± 0.01mm	Height H(mm) ± 0.01mm	IC(mm) ± 0.01mm
1	9.25	8.5	4.104	0.000	0.000	0.020	4.67	11.738
2	9.50	10.4	4.193	0.000	0.000	0.021	4.68	11.737
3	10.00	15.4	4.379	0.000	0.000	0.023	4.70	11.743
4	10.25	18.7	4.470	0.000	0.000	0.024	4.72	11.746
5	10.50	22.4	4.561	0.000	0.000	0.023	4.74	11.756
6	10.75	26.8	4.657	0.000	0.000	0.024	4.75	11.763
7	11.00	31.0	4.741	0.000	0.000	0.026	4.77	11.769
8	11.50	41.9	4.922	0.000	0.000	0.025	4.80	11.780
9	12.00	54.6	5.100	0.000	0.000	0.027	4.85	11.792
10	13.00	86.3	5.464	0.000	0.000	0.025	4.96	11.836
11	14.00	124.3	5.840	0.106	0.209	0.027	5.07	11.879

6.3.2 Calculated data with hold-down

The data listed in Tables 13 to 17 was calculated using the equations described in section 5.3.

Table 13: Change in height with pressing force.

No.	$\Delta H(F)$ ± 0.01 mm	$\Delta H(F)_{contraction}$ ± 0.005 mm	$\Delta H(F)_{springback}$ ± 0.015 mm	$\Delta H(F)_{relative\ springback}$ (%)
1	0.036	0.024	0.012	0.26
2	0.044	0.030	0.015	0.32
3	0.065	0.044	0.022	0.46
4	0.079	0.053	0.026	0.55
5	0.094	0.064	0.030	0.64
6	0.111	0.076	0.035	0.75
7	0.128	0.088	0.040	0.84
8	0.169	0.119	0.050	1.06
9	0.216	0.155	0.061	1.26
10	0.321	0.245	0.076	1.55
11	0.427	0.353	0.074	1.49

Table 14: Change in IC with pressing force.

No.	$\Delta IC(F)$ ± 0.01 mm	$\Delta IC(F)_{contraction}$ ± 0.01 mm	$\Delta IC(F)_{springback}$ ± 0.02 mm	$\Delta IC(F)_{relative\ springback}$ (%)
1	0.011	0.004	0.007	0.06
2	0.014	0.005	0.009	0.08
3	0.021	0.007	0.013	0.11
4	0.025	0.009	0.016	0.14
5	0.030	0.011	0.019	0.16
6	0.035	0.013	0.023	0.19
7	0.041	0.015	0.026	0.22
8	0.055	0.020	0.035	0.30
9	0.071	0.026	0.045	0.38
10	0.110	0.041	0.069	0.59
11	0.156	0.059	0.096	0.82

Table 15: Change in the springback and relative springback ratio with pressing force.

No.	$\Delta H(F)_{springback} / \Delta IC(F)_{springback}$	$\Delta H(F)_{relative\ springback} / \Delta IC(F)_{relative\ springback}$
1	1.68	4.24
2	1.67	4.20
3	1.63	4.10
4	1.61	4.02
5	1.58	3.95
6	1.55	3.86
7	1.52	3.77
8	1.44	3.56
9	1.34	3.29
10	1.09	2.63
11	0.77	1.82

Table 16: Change in volumetric and relative volumetric springback with pressing force.

No.	$\Delta V(F)$ (cm^3)	$\Delta V(F)_{contraction}$ (cm^3)	$\Delta V(F)_{springback}$ (cm^3)	$\Delta V(F)_{fractional\ springback}$ (%)
1	0.005	0.003	0.002	0.33
2	0.006	0.004	0.002	0.40
3	0.009	0.006	0.003	0.58
4	0.011	0.007	0.004	0.69
5	0.013	0.008	0.005	0.82
6	0.016	0.010	0.006	0.96
7	0.018	0.012	0.006	1.08
8	0.024	0.016	0.008	1.38
9	0.031	0.021	0.010	1.68
10	0.046	0.033	0.013	2.19
11	0.062	0.046	0.016	2.39

Table 17: Change in green density with pressure.

No.	Pressure (kN/cm^2)	Green density (g/cm^3)
1	6.26	7.06
2	7.66	7.20
3	11.3	7.48
4	13.8	7.60
5	16.5	7.72
6	19.7	7.86
7	22.8	7.96
8	30.9	8.21
9	40.2	8.41
10	63.6	8.77
11	91.6	9.12

6.3.3 Measured data without hold-down

The maximum filling height that could be achieved while preserving the 1:1 travel ratio was 14.00 mm however this compact had many cracks and defects caused probably by strong contact with the die wall and consequent increased friction during ejection[10]. Thus the maximum filling height that could be achieved without the compact disintegrating was 13.00 mm at a pressing force of 85.7 kN. Therefore the range of forces that could be explored in this experiment was less than in section 6.3.1 but nevertheless significantly larger compared to that of the tight-fit compacts. As seen previously lip and corner lip dimensions appeared only at extremely high pressing forces.

[10] Contact of SBA compacts with the die wall at high compaction pressures is explained in more detail in Chapter 7.

Table 18: Recorded and measured data for the square SBA compact using grade A powder without hold-down.

No.	Filling height F_h (mm)	Pressing Force F(kN) ± 0.1 kN	Mass M(g) ± 0.001g	Lip L(mm) ± 0.01mm	Corner Lip L_c(mm) ± 0.01mm	Edge width ± 0.01mm	Height H(mm) ± 0.01mm	IC(mm) ± 0.01mm
1	9.25	8.4	4.108	0.000	0.000	0.021	4.69	11.742
2	9.50	10.3	4.198	0.000	0.000	0.022	4.70	11.744
3	10.00	15.3	4.382	0.000	0.000	0.021	4.72	11.757
4	10.25	18.4	4.471	0.000	0.000	0.020	4.73	11.771
5	10.50	21.9	4.560	0.000	0.000	0.022	4.74	11.777
6	10.75	26.1	4.649	0.000	0.000	0.020	4.76	11.786
7	11.00	30.6	4.744	0.000	0.000	0.026	4.77	11.806
8	12.00	54.4	5.109	0.000	0.000	0.024	4.84	11.841
9	13.00	85.7	5.466	0.192	0.357	0.033	4.92	11.902

6.3.4 Calculated data without hold-down

The data listed in Tables 19 to 23 was calculated using the equations described in section 5.3.

Table 19: Change in height with pressing force.

No.	$\Delta H(F)$ ± 0.01 mm	$\Delta H(F)_{contraction}$ ± 0.005 mm	$\Delta H(F)_{springback}$ ± 0.015 mm	$\Delta H(F)_{relative\ springback}$ (%)
1	0.035	0.024	0.011	0.23
2	0.042	0.029	0.013	0.28
3	0.061	0.043	0.018	0.38
4	0.073	0.052	0.021	0.44
5	0.086	0.062	0.023	0.50
6	0.100	0.074	0.026	0.55
7	0.115	0.087	0.028	0.60
8	0.183	0.154	0.029	0.59
9	0.243	0.243	0.000	0.00

Table 20: Change in IC with pressing force.

No.	$\Delta IC(F)$ ± 0.01 mm	$\Delta IC(F)_{contraction}$ ± 0.01 mm	$\Delta IC(F)_{springback}$ ± 0.02 mm	$\Delta IC(F)_{relative\ springback}$ (%)
1	0.029	0.004	0.025	0.21
2	0.035	0.005	0.030	0.26
3	0.050	0.007	0.043	0.37
4	0.059	0.009	0.051	0.43
5	0.069	0.010	0.058	0.50
6	0.080	0.012	0.067	0.57
7	0.090	0.015	0.076	0.65
8	0.132	0.026	0.106	0.90
9	0.148	0.041	0.107	0.90

Table 21: Change in springback and relative springback ratio with pressing force.

No.	$\Delta H(F)_{springback}$ $/\Delta IC(F)_{springback}$	$\Delta H(F)_{relative\ springback}$ $/\Delta IC(F)_{relative\ springback}$
1	0.44	1.08
2	0.43	1.07
3	0.42	1.03
4	0.41	1.00
5	0.40	0.97
6	0.39	0.93
7	0.37	0.89
8	0.27	0.65
9	0.00	0.26

Table 22: Change in volumetric and relative volumetric springback with pressing force.

No.	$\Delta V(F)$ (cm^3)	$\Delta V(F)_{contraction}$ (cm^3)	$\Delta V(F)_{springback}$ (cm^3)	$\Delta V(F)_{relative\ springback}$ (%)
1	0.006	0.003	0.003	0.46
2	0.007	0.004	0.003	0.56
3	0.010	0.006	0.005	0.78
4	0.012	0.007	0.005	0.91
5	0.014	0.008	0.006	1.04
6	0.017	0.010	0.007	1.17
7	0.019	0.012	0.008	1.30
8	0.030	0.021	0.009	1.57
9	0.039	0.030	0.009	1.00

Table 23: Change in green density with pressure.

No.	Pressure (kN/cm^2)	Green density (g/cm^3)
1	6.19	7.04
2	7.59	7.17
3	11.3	7.45
4	13.6	7.57
5	16.1	7.70
6	19.2	7.81
7	22.5	7.94
8	40.1	8.40
9	63.1	8.75

6.4 Contraction results

Graphical representations of all the measured contraction data listed in section 6.1 may be found in Appendix F for tight-fit and SBA tools made in all three compact geometries (square, round, triangular). Examples of the graphs and associated equations are given in this section for the tight-fit, square tools.

6.4.1 Upper and lower punch-ram system contraction

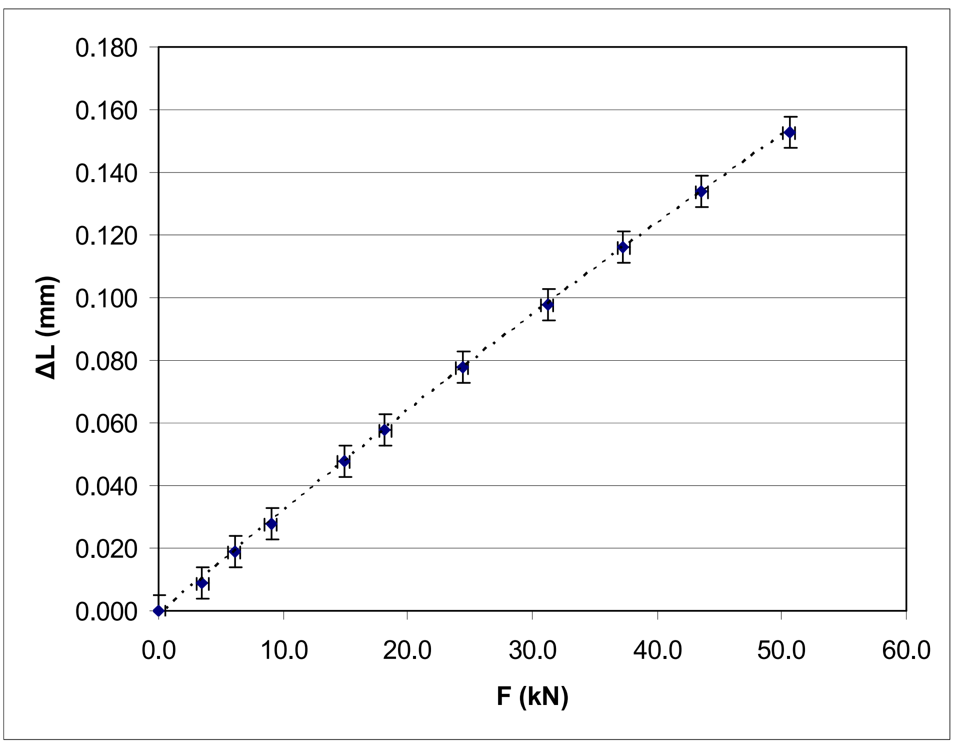

Figure 18: Change in upper and lower punch-ram system contraction with pressing force.

Best fit equation:

$\Delta L_{\text{Upper -Lower Punch-Ram}} = -6.737\times10^{-6}\, F^2 + 3.397\times10^{-3}\, F - 1.422\times10^{-3}\ (R^2 = 9.998\times10^{-1})$ . . . (40)

Best fit straight line equation with the intercept set to zero:

$\Delta L_{\text{Upper-Lower Punch-Ram}} = 3.090 \times10^{-3}\, F\ (R^2 = 9.988\times10^{-1})$ . . . (41)

Maximum difference between equations 43 and 44, at a typical pressing force of 25 kN, is 0.002 mm i.e. for all practical purposes negligible. Both equations above are excellent approximations of the actual data.

6.4.2 Upper punch-ram system contraction

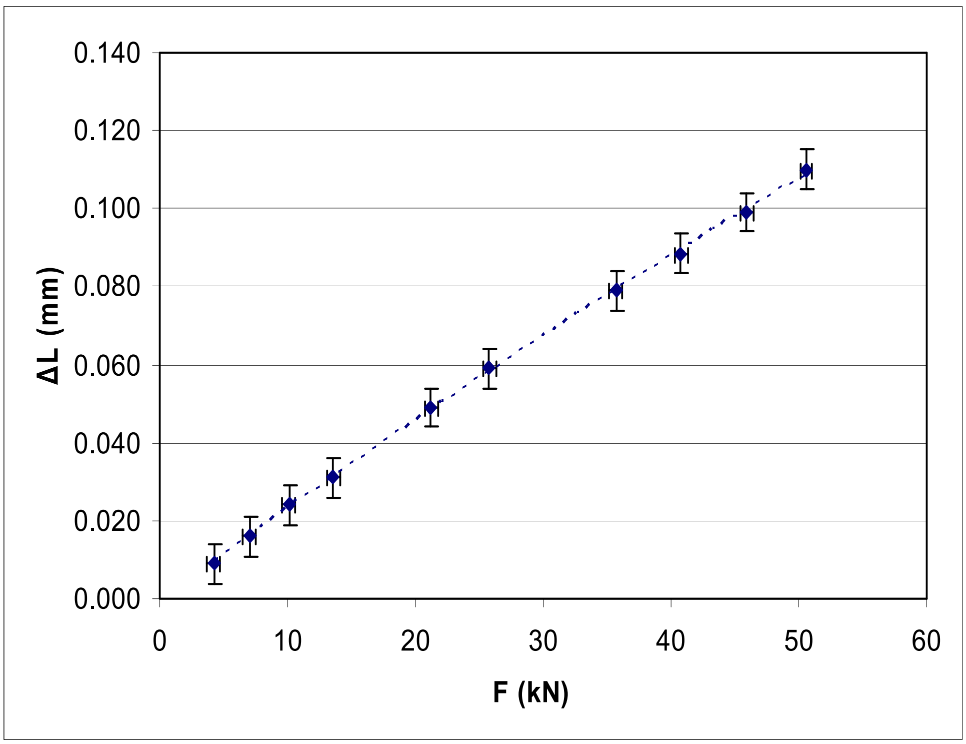

Figure 19: Change in upper punch-ram system contraction with pressing force.

Best fit equation:

$\Delta L_{\text{Upper Punch-Ram}} = -4.944\times10^{-6}\, F^2 + 2.411\times10^{-3}\, F - 5.019\times10^{-4}\ (R^2 = 9.996\times10^{-1})$ . . . (42)

Best fit straight line with zero intercept:

$\Delta L_{\text{Upper Punch-Ram}} = 2.195 \times10^{-3}\, F\ (R^2 = 9.981\times10^{-1})$ . . . (43)

Maximum difference between equations 42 and 43, at a typical pressing force of 25 kN, is approximately 0.002 mm thus equation 43 is thus an excellent approximation of equation 42.

6.4.3 Upper ram contraction

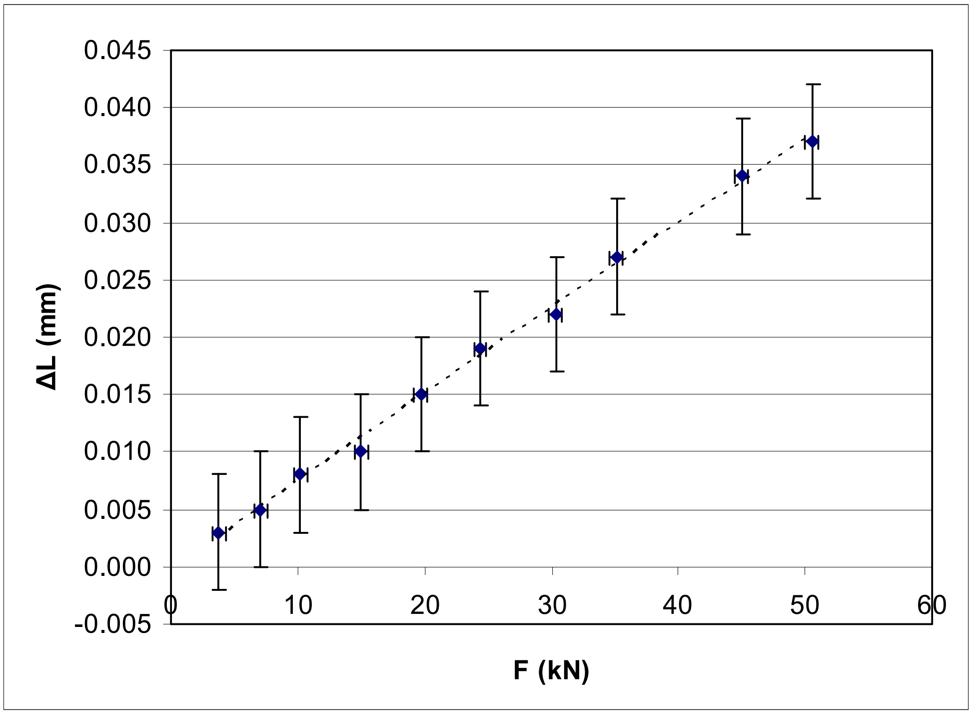

Figure 20: Change in upper ram contraction with pressing force.

Best fit equation:

$\Delta L_{\text{Upper Ram}} = -7.128\times10^{-7}\,F^2 + 7.852\times10^{-4}\,F - 3.427\times10^{-4}\,(R^2 = 9.970\times10^{-1})$ . . . (44)

Best fit straight line with zero intercept:

$\Delta L_{\text{Upper Ram}} = 7.471\times10^{-4}\,F\,(R^2 = 9.968\times10^{-1})$ . . . (45)

Maximum difference between equations 44 and 45, at a typical pressing force of 25 kN, is less than 0.001 mm thus equation 45 is an excellent approximation of equation 44.

6.4.4 Contraction of the upper ram and punch base system

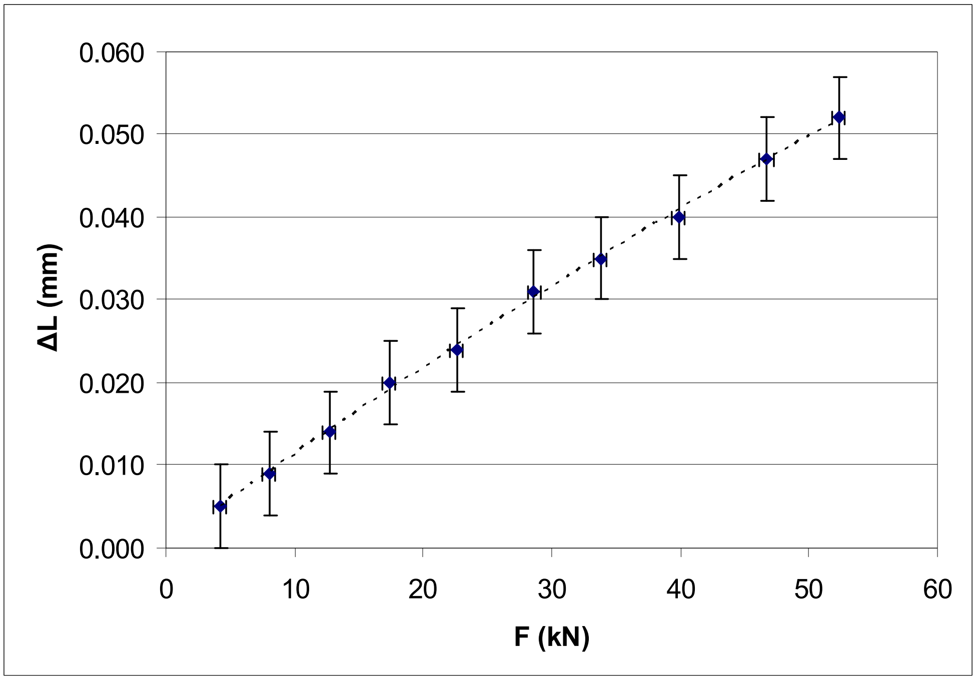

Figure 21: Change in upper ram and punch base system contraction with pressing force.

Best fit equation:

$$\Delta L_{\text{Upper ram and punch base}} = -2.718\times10^{-6}\,F^2 + 1.123\times10^{-3}\,F - 4.031\times10^{-4}\ (R^2 = 9.989\times10^{-1}) \quad \ldots (46)$$

Best fit straight line with zero intercept:

$$\Delta L_{\text{Upper ram and punch base}} = 1.023\times10^{-3}\,F\ (R^2 = 9.937\times10^{-1}) \quad \ldots (47)$$

Maximum difference between equations 46 and 47, at a typical pressing force of 25 kN, is less than 0.001 mm thus equation 47 is an excellent approximation of equation 46.

6.5 Springback results

Best fit equations representing the effect of springback were derived from the measured and calculated data listed in the tables in sections 6.2 and 6.3. The equations were derived for tight-fit and SBA compacts using Grade A and Grade B powders and all three compact geometries (square, round, triangular). The equations for all the compacts are listed in Appendix G. Examples of the derived equations are given below for the tight-fit, Grade A powder, square compacts.

$$\Delta L(F)_{\text{springback}} = -8.565\times10^{-5}F^2 + 6.955\times10^{-3}F\ (R^2 = 9.995\times10^{-1}) \quad \ldots (48)$$
$$\Delta L(F)_{\text{relative springback}} = -1.045\times10^{-1}F^2 + 5.056F - 1.638\ (R^2 = 9.994\times10^{-1}) \quad \ldots (49)$$

$$\Delta H(F)_{springback} = -1.046\times10^{-4}F^2 + 6.297\times10^{-3}F \ (R^2 = 9.996\times10^{-1}) \quad \ldots (50)$$
$$\Delta H(F)_{relative\ springback} = -1.941\times10^{-3}\ F^2 + 1.155\times10^{-1}F - 4.498\times10^{-3}\ (R^2 = 1.000) \quad \ldots (51)$$
$$\Delta IC(F)_{springback} = -4.295\times10^{-5}F^2 + 2.551\times10^{-3}F \ (R^2 = 8.973\times10^{-1}) \quad \ldots (52)$$
$$\Delta IC(F)_{relative\ springback} = -3.014\times10^{-4}F^2 + 1.890\times10^{-2}F - 2.310\times10^{-2} \ (R^2 = 9.128\times10^{-1}) \quad \ldots (53)$$
$$\Delta H(F)_{springback} / \Delta IC(F)_{springback} = 2.49 \pm 0.24 \quad \ldots (54)$$
$$\Delta H(F)_{relative\ springback} / \Delta IC(F)_{relative\ springback} = 5.41 \pm 0.53 \quad \ldots (55)$$
$$\Delta V(F)_{springback} = -1.682\times10^{-5}F^2 + 1.051\times10^{-3}F \ (R^2 = 9.990\times10^{-1}) \quad \ldots (56)$$
$$\Delta V(F)_{relative\ springback} = -2.472\times10^{-3}F^2 + 1.524\times10^{-1}F + 6.313\times10^{-3} \ (R^2 = 9.999\times10^{-1}) \quad \ldots (57)$$
$$\rho_g(P) = 7.769\times10^{-1}Ln(P) + 5.473 \ (R^2 = 9.995\times10^{-1}) \quad \ldots (58)$$

7 Discussion

7.1 Tight-fit tool results

7.1.1 Tool contraction behaviour

From the procedures described in section 4.1.2.2 it was possible to determine the contraction behaviour or profile along several points of the machine-tool system either by direct measurement or analytical methods. The contraction constants for the upper-lower punch-ram system, upper punch-ram system, upper ram only, and the upper ram and punch base system, were determined by direct measurement. Using these constants it was possible to determine the contraction constants for the contraction of the bottom punch-ram system, stand alone top punch, the punch shaft of the top punch, and the punch base, for each particular tool by analytical means. This analysis shows how the chosen experimental method can be used to give a relatively accurate estimation of the contraction behaviour of any part of the machine-tool system. Furthermore these results can be used to give an indication of the precision and accuracy of the experimental method.

In Chapter 6 it could be seen that the contraction behaviour of virtually any part of the machine tool systems over a sufficiently wide range of pressing forces exhibits some deviation from perfectly elastic behaviour and could best be described by quadratically varying functions of the pressing force[11]. However the quadratic coefficients were for practical purposes small enough so that the equations could be approximated by straight lines. The measured effective elasticity constants for the square tight-fit tool were:

1 3.1×10^{-3} mm/kN for the complete upper-lower punch-ram system
2 2.2×10^{-3} mm/kN for the upper punch-ram system
3 0.8×10^{-3} mm/kN for the upper ram only, and
4 1.0×10^{-3} mm/kN for the upper ram and punch base system

Thus the calculated contraction constants for the square tight-fit tool were:

5 8.9×10^{-3} mm/kN for the bottom punch-ram system
6 1.4×10^{-3} mm/kN for the stand alone top punch
7 1.2×10^{-3} mm/kN the punch shaft of the top punch, and
8 0.3×10^{-3} mm/kN for the punch base

Similarly, the four measured constants for the round tight-fit tool were:

1 3.4×10^{-3} mm/kN for the complete upper-lower punch-ram system
2 2.3×10^{-3} mm/kN for the upper punch-ram system
3 0.8×10^{-3} mm/kN for the upper ram only, and
4 0.9×10^{-3} mm/kN for the upper ram and punch base system

[11] Although the contraction behaviour of some parts of the machine tool system was best described by straight line equations, the overwhelming majority of the results was slightly quadratic in nature.

The calculated contraction constants round tight-fit tool were:

5 1.2×10^{-3} mm/kN for the bottom punch-ram system
6 1.4×10^{-3} mm/kN for the stand alone top punch
7 1.3×10^{-3} mm/kN the punch shaft of the top punch, and
8 0.1×10^{-3} mm/kN for the punch base

Finally, the four measured constants for the triangular tight-fit tool were:

1 3.1×10^{-3} mm/kN for the complete upper-lower punch-ram system
2 1.8×10^{-3} mm/kN for the upper punch-ram system
3 0.7×10^{-3} mm/kN for the upper ram only, and
4 1.0×10^{-3} mm/kN for the upper ram and punch base system

The calculated contraction constants triangular tight-fit tool were:

5 1.3×10^{-3} mm/kN for the bottom punch-ram system
6 1.2×10^{-3} mm/kN for the stand alone top punch
7 0.8×10^{-3} mm/kN the punch shaft of the top punch, and
8 0.3×10^{-3} mm/kN for the punch base

Examination of the constants determined by measurement shows that the average value for the contraction of the upper ram only is approximately 0.8×10^{-3} mm/kN $\pm$ 0.4×10^{-4} mm/kN. The relatively small standard error of the mean implies that this value can for all practical purposes be used as a relatively accurate approximation of the actual true value for this quantity. Examination of the analytically determined constants shows that the average value for the upper punch contraction constants is approximately 1.4×10^{-3} mm/kN with a relatively small standard error of 1.0×10^{-4} mm/kN. This means that for all practical purposes a variety of different punches can be treated as having the same contraction behaviour. As described in section 4.1.2.2 an important quantity for influencing the quality of the green cutting edge is the contraction of the upper punch-ram system. The above findings suggest that a single, universal value for this quantity may be used for a variety of other similar tools in production. This universal value calculated as the average of the measured upper punch-ram constants above, is 2.1×10^{-3} mm/kN $\pm$ 1.3×10^{-4} mm/kN.

The above result means that at a typical pressing force of 25 kN, approximately 0.053 mm ± 0.003 mm of contraction can be expected for a variety of similar but different punches that may be used in production. This information allows more accurate control over the final pressing position of the upper punch during the press setup procedure. For instance, if the intended final pressing position is 3.80 mm below die level, the penetration depth parameter that should be programmed in the press software in order to achieve this, should be approximately 3.85 mm. Even if the collision point between the upper punch and die is 3.85 mm below die level, the above value can still be programmed for the PD parameter safely in the knowledge that the collision will not occur and the punch will not be damaged. These calculations were repeated with the SBA tools and the results were found to compare favorably with those described above and are discussed in section 7.2.1. Similar calculation were not performed for the lower punch-ram system since the accuracy of the final pressing position of the lower punch in positive pressing does not affect the quality of the upper compact edges as mentioned in section 4.1.2.2.

Examination of the punch shaft contraction constants shows a larger deviation of the calculated values from the average of 1.1×10^{-3} mm/kN. This is seen by the relatively large standard error of 1.4×10^{-4} mm/kN associated with this value. The greater deviation is likely to be a normal result of the variation of the 'punch length to area ratio (L/A)' (a quantity which is directly proportional to the contraction constant according to Hooke's law) as well as the inconsistencies in the brazing thickness between the carbide tip and the steel portion of the shaft from one punch to another. These factors however have a much smaller effect on the larger upper punch-ram system and thus the standard error associated with this quantity was seen to be much smaller.

7.1.2 General observations in springback behaviour

For all compacts irrespective of geometry or compaction material, all linear dimensions showed some deviation in springback behaviour from that expected for fully elastic bodies. As with the results for contraction the observed behaviour could best be described by quadratically varying functions of the change in compact dimensions with pressing force[12]. Thus the rate of increase in the linear dimensions of the examined compacts decreased as the pressing force was increased. This deviation, although more pronounced in tight-fit compacts, was present also in the SBA compacts as discussed in section 7.2.2, and thus represents a non-elastic element that seems to be a natural characteristic of all the carbide compacts and tools that were examined in this work.

In addition, it was found that in all tight-fit compacts, irrespective of their geometry or material, the greatest springback was observed in the lip dimension. Furthermore, in the case of Grade A, it was found that axial springback was greater than radial springback. This information can be summarized by the following equation.

$$\Delta L(F)_{springback} > \Delta H(F)_{springback} > \Delta IC(F)_{springback} \qquad \text{. . . (59)}$$

This result is illustrated in Figure 22 for the springback behaviour of different linear dimensions of the examined compact geometries. Although the greatest amount of springback experienced by Grade B compacts also occurred in the lip dimension, no consistent trend could be found in the behaviour of absolute axial and radial springback. For instance, in the case of the square Grade B geometry, radial springback was greater than axial springback, while for the triangular Grade B geometry, axial springback was greater than radial springback indicating that the springback behaviour of Grade B compacts is geometry dependant. This can be seen in Figure 23.

[12] However, the quadratic coefficients of the springback equations were in most cases one order of magnitude greater than those observed for contraction as seen in Chapter 6.

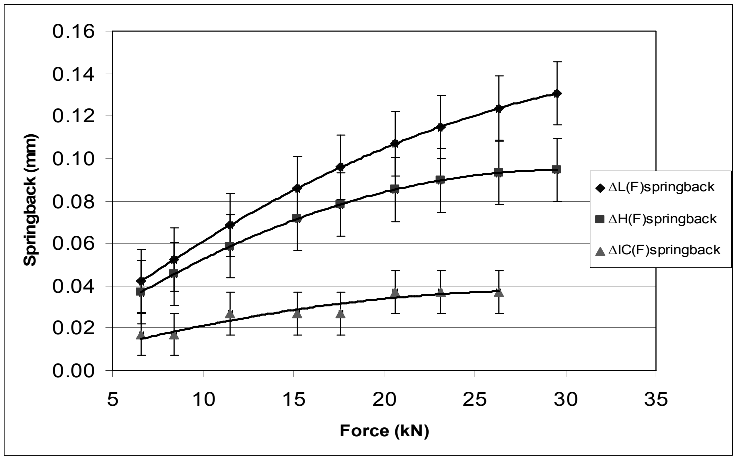

a) Square Grade A geometry

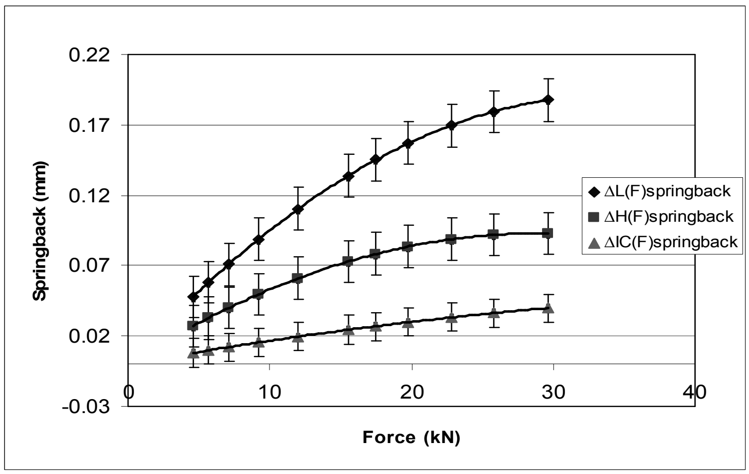

b) Round Grade A geometry

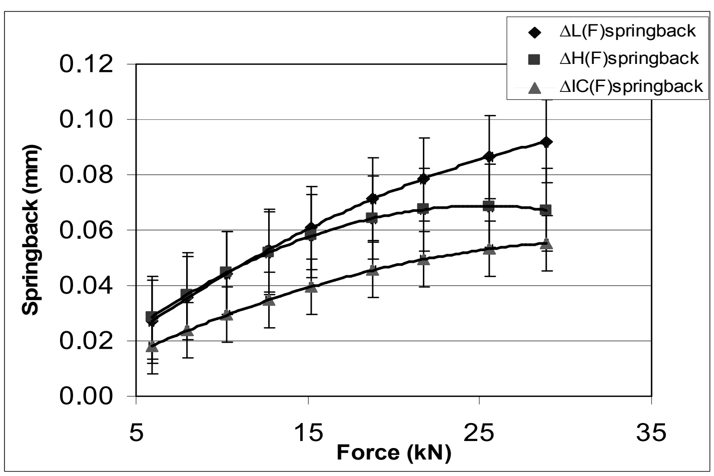

c) Triangular Grade A geometry

Figure 22: Springback behaviour of linear dimensions of the examined compact geometries using Grade A powder.

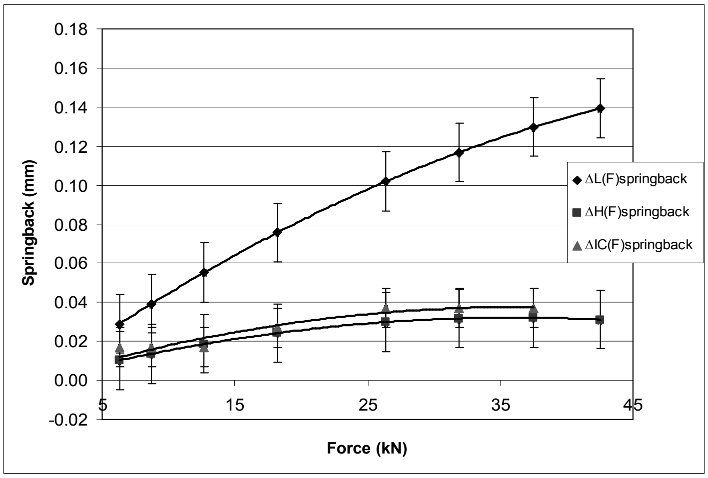

a) Square Grade B geometry

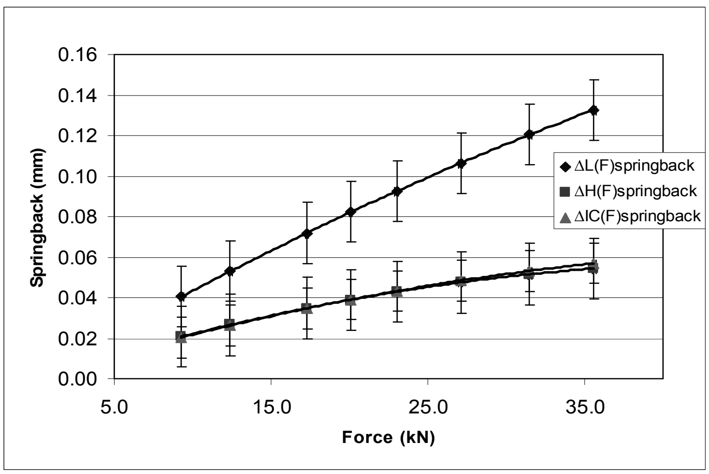

b) Round Grade B geometry

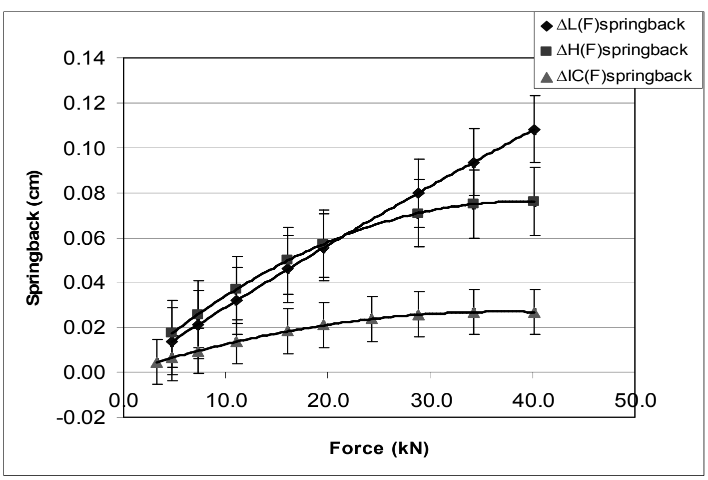

c) Triangular Grade B geometry

Figure 23: Springback behaviour of linear dimensions of the examined compact geometries using grade B powder.

7.1.3 Comparison between lip springback and axial springback

As mentioned previously, $\Delta L(F)_{springback} > \Delta H(F)_{springback}$ was found to be true regardless of the compact shape or compaction material. For example, at typical pressing force of 25 kN, lip springback of Grade A compacts exceeded the total axial springback by approximately 23 % for the square geometry, 49 % for the round geometry, and 20 % for the triangular geometry as calculated by the following equation:

$$(\Delta L(F)_{springback} - \Delta H(F)_{springback})/\Delta L(F)_{springback} \times 100 \qquad \ldots (60)$$

In the case of Grade B compacts, the absolute lip springback exceeded the total axial springback by approximately 72 % for the square geometry, 55 % for the round geometry, and 6 % for the triangular geometry.

This means that the 'H - L' dimension of the compact was found to be a decreasing function of the pressing force. Since this dimension represents the part of the compact below the lip, the result implies differential axial springback behaviour of different compact regions. The axial springback of the lip dimensions is larger than that of the rest of the compact. This result is unexpected in view of the fact that the lip is the only part of the compact which is in contact with the die wall, and thus its rate of expansion was expected to be relatively low due to frictional dissipation of the springback energy at the compact – die-wall interface as shown by Anuar *et al* [14].

There are two possible explanations for this. One is that the decompression phase of the compaction cycle has a profound effect on compact springback. The decompression phase in these experiments was carried out in a typical manner; by a reduction in the applied pressing force of the upper ram while the lower ram position remained fixed. The reduction in the applied force of the upper ram - after having reached the final pressing position and therefore the peak pressing force - to the programmed pneumatic hold-down force, allowed for the expansion of the compact in the upward direction under the driving force of its own springback energy. Since this entire energy can only be released axially upwards – and not radially due to the confines of the tight-fit die – it is logical that the expansion of the upper compact regions was greater than that of the lower compact regions. This in combination with further radial expansion upon ejection from the die, due to any residual springback, can result in a decrease of the axial dimensions of the lower parts of the compact.

Another possibility is that the direct contact between the lip and die-wall during decompression and ejection of tight-fit compacts can result in an unexpected increase of the lip dimension. This contact is a natural result of tight-fit compaction and of the radial component of springback due to which the compact may exert significant radial pressures against the sides of the die during the ejection and decompression phases. If this contact is severe enough it may lead to smearing or scuffing type deformation of the lip which could have an increasing effect on its dimensions as shown in Figure 24. Finally, both of the above effects could be responsible for the observed springback behaviour of the vertical compact dimensions.

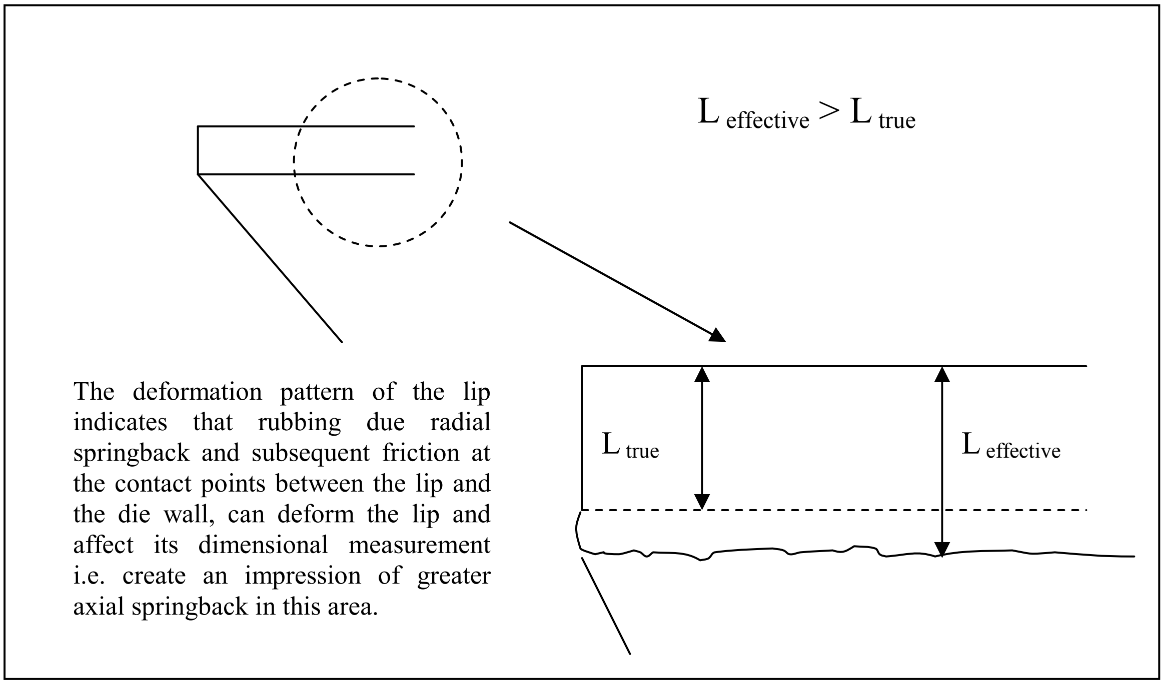

Figure 24: The effect of compact die-wall contact on lip size.

7.1.4 Comparison between axial and radial springback

As mentioned previously, for the square Grade A compacts, $\Delta H(F)_{springback} > \Delta IC(F)_{springback}$ was true over the entire range of pressing forces regardless of the compact geometry. At a typical pressing force of 25 kN, total axial springback of Grade A compacts exceeded the total radial springback by approximately 62 % for the square geometry, 61 % for the round geometry, and 24 % for the triangular geometry as calculated by the following equation:

$$(\Delta H(F)_{springback} - \Delta IC(F)_{springback})/\Delta H(F)_{springback} \times 100 \qquad \ldots (61)$$

One of the possible explanations for this follows from the above discussion. During decompression it is possible that a significant amount of springback occurs while the component is still in the die and since radial expansion is prevented by the confines of the die walls, springback can only take place in the axial direction. During ejection there is a loss of springback energy to friction so that after both phases, decompression and ejection, the energy that is available for out-of-die springback is given by the following equation:

U (out-of-die springback) = U (total springback energy) – U (in-die axial springback during decompression) – U (energy lost to friction during ejection) . . . (62)

Thus if a significant part of the total springback energy is used up in decompression and ejection from the die, it is unlikely that there will be much out-of-die energy left for the total radial springback to exceed the total axial springback. In addition, the out-of-die springback energy is shared between both axial and radial components upon removal of the hold-down force, as soon as the component has been fully ejected from the die i.e.

U (out-of-die springback) = U (out-of-die axial) + U (out-of-die radial) . . . (63)

Thus it is very unlikely that the two axial contributions can be exceeded by the sole out-of-die radial contribution.

The same results were not obtained with Grade B compacts for which the comparisons between axial and radial springback behaviours appeared to be geometry dependant. Possible explanations for this inconsistency are that the die-wall friction experienced by Grade B compacts during ejection had a non-linear effect on their springback, the experimental techniques used in the analysis did not allow for the required measurements to be made with the necessary sensitivity or accuracy, and/or the result of human measurement errors.

7.1.5 Comparison between relative axial and radial springback

For Grade A compacts, at 25 kN, relative axial springback for the square geometry was approximately 1.7 % while the relative radial springback for the same geometry was 0.26 %. For the round geometry, relative axial springback at 25 kN was 1.7 % while relative radial springback was 0.28 %, and for the triangular geometry, relative axial springback at the same force was 1.2 % while relative radial springback was 0.43 %. For Grade B compacts, at the same pressing force, relative axial and radial springback were 0.52 % and 0.20 % for the square geometries respectively, 0.81 % and 0.36 % for the round geometries respectively, and 1.20% and 0.20% for the triangular geometries respectively.

Therefore, regardless of the compact shape and material, total relative axial springback was found to be greater than its radial counterpart. Also, it can be seen that relative springback of either linear dimension was not more than 2 % in any of the cases which was similar to Liu and Fu's [27] result obtained with silicon carbide powder for PEG below the glass transition temperature. Furthermore, according to the above values, it can be concluded that relative axial springback at a typical pressing force of 25 kN, was significantly greater in the case of Grade A compacts than the Grade B compacts and thus appeared to be material dependant. This was especially true for the square and round geometries indicating a possible link between relative springback behaviour and compact aspect ratio which was larger for the square and round geometries. However this was not explored further in this work. The relative radial springback at this force was relatively similar for both materials and therefore appeared less sensitive to material properties.

7.1.6 Variation of the springback ratio with pressing force

The springback ratio of square Grade A compacts appeared to be independent of force with a constant value of 2.49 ± 0.24 representing a best fit of the actual experimental data. The springback ratios of both round and triangular geometries were found to decrease quadratically with force implying that the rate of increase of radial springback with force was greater than the rate of increase of axial springback with force for these two geometries. At 25 kN, $\Delta H/\Delta IC = 2.55$ for the round geometry while the result for the triangular geometry was 1.29. In all cases however, axial springback was found to be greater than the radial springback confirming previous findings.

The springback ratio of square Grade B compacts, like the square Grade A compacts, also appeared to be independent of force with a constant value of 0.85 ± 0.24 representing the best fit of the experimental data. The springback ratio of the round Grade B geometry, like that of the round Grade A geometry, was similarly found to be a decreasing quadratic function of the pressing force, being equal to 0.96 at 25 kN. However, the ratio for the Grade B triangular geometry seemed to be an increasing quadratic function of the pressing force and 2.72 was obtained at 25 kN pressing force.

These inconsistencies, as previously explained, are likely to be the result of possible non-linear frictional influences, inherent measurement method inaccuracies, or human measuring errors. In section 7.2.5 it will be shown that the free springback ratio behaviour with pressing force is a decreasing quadratic function of the pressing force indicating that that the rate of increase of radial springback with force is actually greater than the rate of increase of axial springback with force.

7.1.7 Variation of the relative springback ratio with pressing force

The relative springback ratio '$\Delta H(F)_{relative\ springback} / \Delta IC(F)_{relative\ springback}$' confirms the findings of the previous section, with relative axial springback exceeding the relative radial springback by at least a factor of two in all but one case. For the square Grade B geometry, relative axial springback was 1.82 times greater than the relative radial springback at the same force of 25 kN. For the round and triangular Grade B geometries relative axial springback was 2.2 and 5.43 times greater than relative radial springback respectively. Relative axial springback for Grade A geometries exceeded the relative radial springback by a factor of 5.41 for the square shape, 5.8 for the round shape, and 2.83 for the triangular shape.

7.1.8 Effect of geometry and compaction material on axial springback

Examination of Figure 25, in which the axial springback of all the tight-fit compacts has been plotted as a function of force, reveals firstly that axial springback of tight-fit compacts is geometry dependant and secondly that it is material dependant.

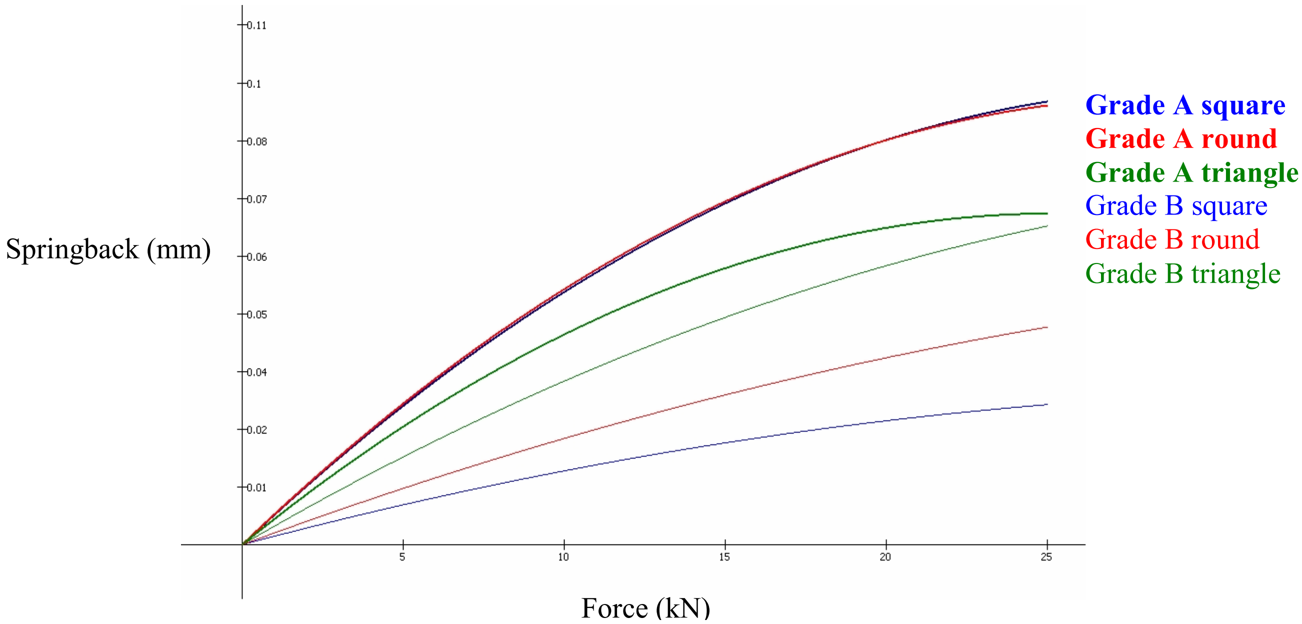

Figure 25: Change in axial springback with pressing force for all tight-fit Grade A and Grade B geometries.

As evidence for the first conclusion, the following trend can be seen throughout the range of the examined pressing forces for Grade A compacts:

$$\Delta H(F)_{\text{springback (square)}} \approx \Delta H(F)_{\text{springback (round)}} > \Delta H(F)_{\text{springback (triangle)}} \qquad \text{. . . (64)}$$

For Grade B compacts the following result can be deduced from the same graph:

$$\Delta H(F)_{\text{springback (triangle)}} > \Delta H(F)_{\text{springback (round)}} > \Delta H(F)_{\text{springback (square)}} \qquad \text{. . . (65)}$$

If axial springback behaviour of tight-fit compacts was geometry independent, axial springback would be the same regardless of the shape of the compact. As proof for the latter case, axial springback of Grade A compacts in all cases exceeds that of Grade B compacts as indicated by:

$$\Delta H(F)_{\text{springback (Grade A square)}} > \Delta H(F)_{\text{springback (Grade B square)}} \qquad \text{. . . (66)}$$

$$\Delta H(F)_{\text{springback (Grade A round)}} > \Delta H(F)_{\text{springback (Grade B round)}} \qquad \text{. . . (67)}$$

$$\Delta H(F)_{\text{ springback (Grade A round)}} > \Delta H(F)_{\text{ springback (Grade B round)}} \qquad \text{. . . (68)}$$

The fact that geometry dependence is inconsistent from one material to the other as seen from the comparison of Equation 64 with Equation 65, could be related to non-linear frictional effects, inherent method inaccuracies, or human measuring errors mentioned previously. The same conclusions hold in the case of relative axial springback as seen in Figure 26.

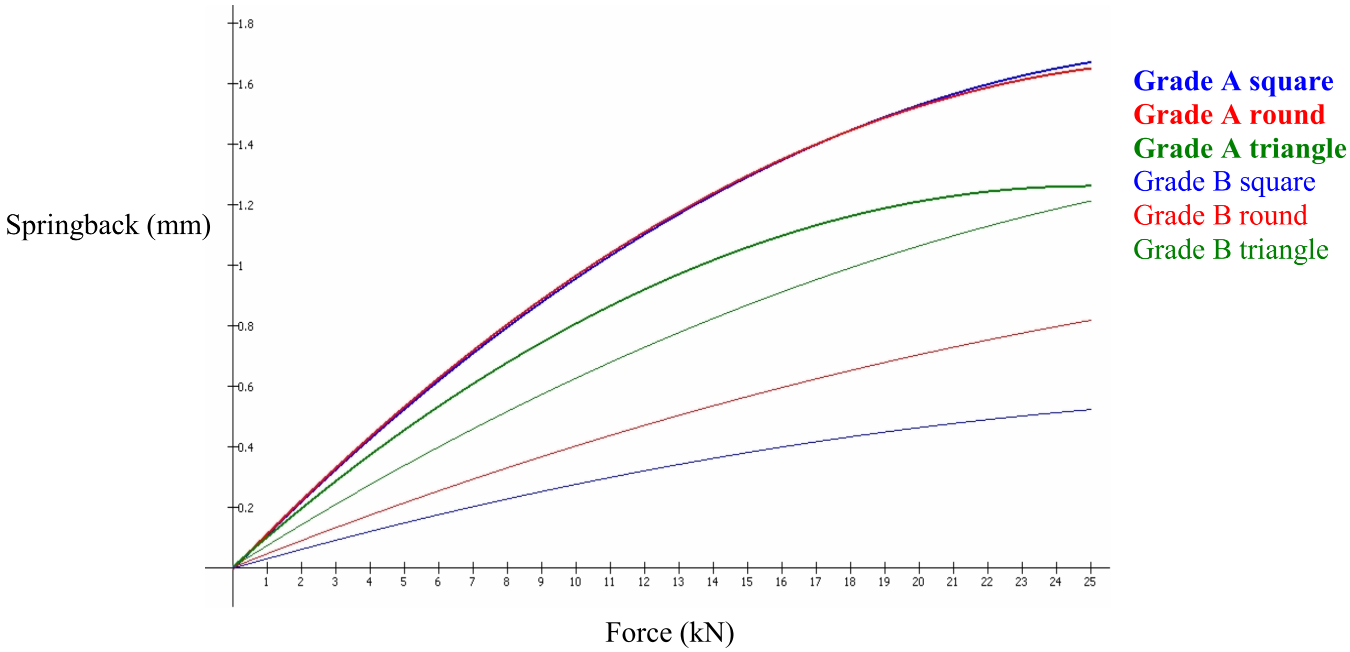

Figure 26: Change in relative axial springback with pressing force for all tight-fit Grade A and Grade B geometries.

Therefore material and geometric dependencies were true even when initial dimensions were accounted for.

7.1.9 Effect of geometry and compaction material on radial springback

Examination of Figure 27 leads to similar conclusions about radial springback. The relative differences between the obtained relationships are finite enough to draw the following conclusions. Radial springback in tight-fit compacts like axial springback is geometry dependant and material dependant. In the former case, geometry dependence can be seen from the following diametrical relationships that hold throughout the entire range of pressing forces.

For Grade A compacts:

$$\Delta IC(F)_{\text{springback (triangle)}} > \Delta IC(F)_{\text{springback (square)}} \approx \Delta IC(F)_{\text{springback (round)}} \quad \text{. . . (69)}$$

For Grade B compacts:

$$\Delta IC(F)_{\text{springback (round)}} > \Delta IC(F)_{\text{springback (square)}} > \Delta IC(F)_{\text{springback (triangle)}} \quad \text{. . . (70)}$$

In the latter case, the effect of changing the compaction material can be seen in the following relationships:

$$\Delta IC(F)_{\text{springback (Grade A square)}} \approx \Delta IC(F)_{\text{springback (Grade B square)}} \quad \text{. . . (71)}$$

$$\Delta IC(F)_{springback\ (Grade\ B\ round)} > \Delta IC(F)_{springback\ (Grade\ A\ round)} \quad ...(72)$$

$$\Delta IC(F)_{springback\ (Grade\ A\ triangle)} > \Delta IC(F)_{springback\ (Grade\ B\ triangle)} \quad ...(73)$$

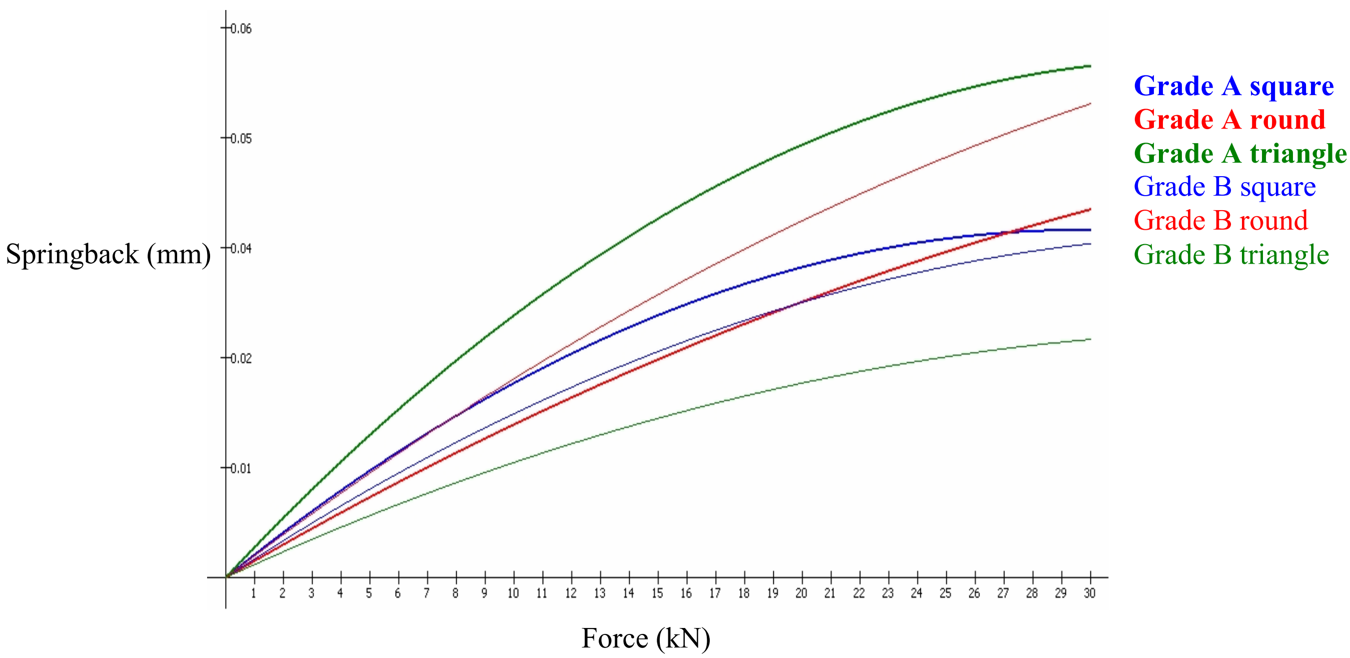

Figure 27: Change in radial springback with pressing force for all tight-fit Grade A and Grade B geometries.

Although the material dependence is relatively small in the case of the square geometry, it is much more pronounced in the round and particularly triangular geometries. In addition, the effect is different for the round and triangular geometries indicating that the effect of material on radial springback is itself geometry dependant. The same results are true of relative radial springback behaviour as seen in Figure 28. Thus material and geometric dependencies were true even when initial dimensions were accounted for.

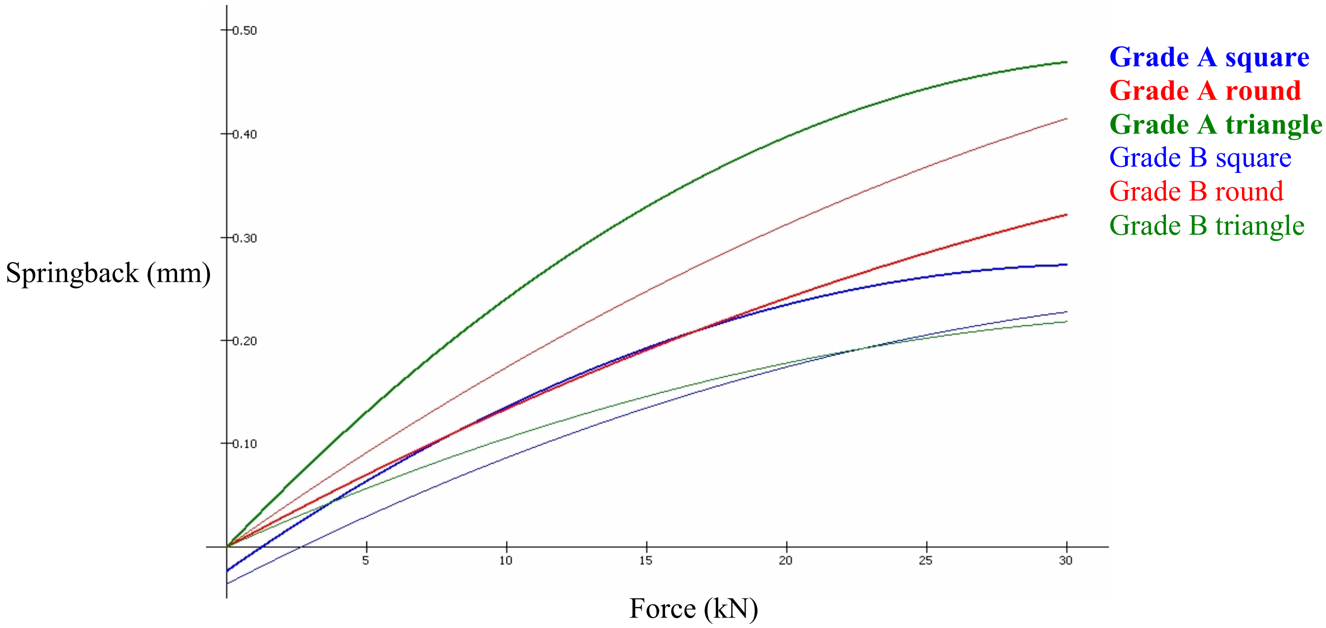

Figure 28: Change in relative radial springback with pressing force for all tight-fit Grade A and Grade B geometries.

7.1.10 Effect of geometry and compaction material on volumetric springback

The volumetric springback of Grade A compacts was largest in the case of the triangular geometry, with both square and round geometries exhibiting relatively similar behaviours. For instance, at 25 kN of pressing force, the volumetric springback was 0.023 cm^3 for the triangular geometry, 0.016 cm^3 for the square geometry, and 0.014 cm^3 for the round geometry. Thus the volumetric springback of the triangular geometry exceeded that of the square and round geometries by approximately 30 % and 39 % respectively, while the relative difference between the square and round geometries was only about 13% at this force. A possible link of proportionality between volumetric springback and the initial compact dimensions is discussed in section 7.2.

However, the results for the volumetric springback of Grade B compacts were not consistent with the above. Compared with Grade A there is a complete reversal in behaviour; the volumetric springback is largest in the case of the round geometry and smallest in the case of the triangular geometry. At a pressing force of 25 kN, the relative difference between the round and the square geometries was approximately 16 %, between the square and triangular geometries 28 %, and between the round and triangular geometries 40 %. The difference in geometry dependence between the two grades of materials could be a result of non-linear frictional effects during the unloading of the compacts from the dies, inherent inaccuracies in the experimental method, or human measuring error.

Overall the following conclusions could be drawn about the volumetric springback behaviour of tight-fit compacts.

1 Volumetric springback of tight-fit compacts appears to be material dependant, being larger in Grade A compacts than Grade B compacts at the same pressing forces.
2 It appears to be geometry dependant and proportional to the starting compact dimensions in the case of Grade A and inversely proportional to the starting compact dimensions in the case of Grade B geometries.

7.1.11 Effect of geometry and compaction material on the relative volumetric springback

Throughout the range of pressing forces tested, the relative volumetric springback of the different Grade A geometries was similar and for all practical purposes independent of compact shape. At 25 kN, the relative volumetric springback of the square geometry was approximately 2.3 %, while the same result for the round and triangular geometries was identical and equal to 2.3 %. This result implied that for tight-fit Grade A compacts, relative springback behaviour appeared to be geometry independent, and only a function of the pressing force. This in turn, meant that for Grade A compacts, the volumetric springback was directly proportional to the initial compact volume i.e. compact in-die volume just before springback, as defined by the die and punches in their final pressing positions.

For Grade B, a completely different behaviour was observed and the relative volumetric springback was found to be geometry dependent. Over the entire range of pressing forces, relative volumetric springback was largest in the case of round geometry compacts and smallest in the case of triangular geometry compacts. For example, at 25 kN, the relative volumetric springback was 1.4 % for the round geometry, 1.0 % for the square geometry, and 0.52 % for the triangular geometry. Thus the relative volumetric springback of the round Grade B geometry exceeded that of the square and triangular geometries by factors of 1.4 and 2.7 respectively, while the relative volumetric springback of the square Grade B geometry was about 2 times larger than that of the triangular Grade B geometry.

In conclusion, it can be said that relative volumetric springback of tight-fit compacts appeared to be material dependent; being greater for Grade A compacts than Grade B compacts at the same pressing forces. Furthermore, in Grade A compacts relative volumetric springback appears to be for all practical purposes geometry independent, while for Grade B compacts it appeared to be strongly geometry dependant. Again these inconsistencies could be attributed to the previously mentioned non-linear frictional influences and measurement related factors. In all cases, relative volumetric springback was not greater than 2.5 % of the starting compact volume which was significantly greater than the volume change of 0.5 % observed in idealized rods of aluminium and hardened steel rods by Wu *et al* [32].

7.1.12 Effect of geometry and compaction material on the change in green density with pressure

The variation of green density with pressure followed a logarithmic trend in all cases as was observed by van der Voort *et al* [29] in their work on the stress relaxation of compacts produced from viscoelastic materials. Furthermore, the variation appeared to be both geometry and material dependant. For Grade A compacts, at pressures corresponding to typical pressing forces of around 25 kN, the green density was approximately equal for the round and square geometries, while being the smallest in the case of the triangular geometry. At a pressure of 20 kN/cm^2, the green density of the square and round geometries was approximately 7.80 g/cm^3, while that of the triangular geometry was 7.03 g/cm^3. Thus the relative difference was approximately 11 %. This difference was more pronounced for the Grade B compacts. At the same pressure, the green density of the square, round and triangular Grade B geometries was 8.40 g/cm3, 8.37 g/cm^3 and 7.20 g/cm^3 respectively. This made the relative difference between the highest and the lowest green densities equal to approximately 17 %.

As a result, at the same compaction pressures, the smaller round and square compacts have higher green densities than the triangular compacts regardless of the compaction material while the green densities of Grade B compacts exceed those of Grade A compacts. The latter statement implies that in order to achieve the same levels of compaction densities in the Grade A as in Grade B material, higher pressing forces are required.

7.1.13 Effect of geometry and compaction material on the change in springback with green density

Linear as well as volumetric springback of all tight fit compacts that were tested varied exponentially with green density until a certain critical value was reached. Thereafter a rapid decrease and plateauing of the rate of expansion could be seen in all cases as shown in Figure 29. Although the green density values at which the breakdown occurred themselves appear to be geometry and material independent, the pressing forces at which they occurred, for all practical purposes appeared to be geometry independent. For the square, round and triangular Grade A geometries these values occurred at approximately 20.6 kN, 19.8 kN and 18.8 kN respectively. The corresponding green densities were 7.57 g/cm^3, 7.63 g/cm^3 and 6.57 g/cm^3 respectively. For the square and round Grade B geometries, these values occur at 26.4 kN and 27.1 kN respectively. Insufficient data was collected to determine this value accurately for the Grade B triangular geometry.

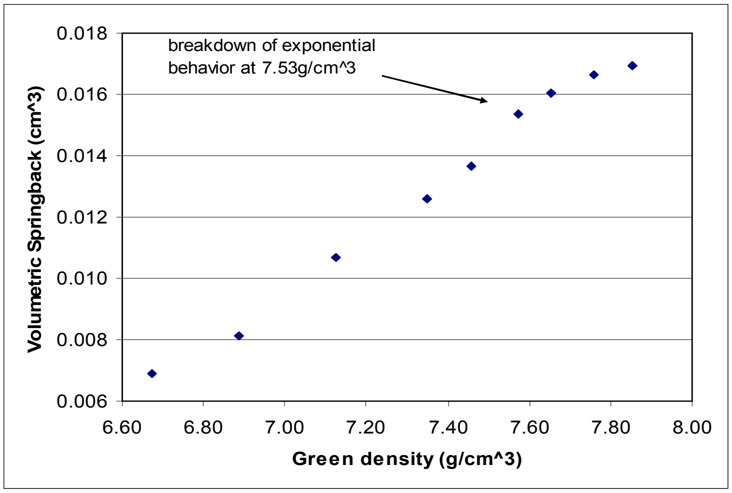

a) Square Grade A geometry

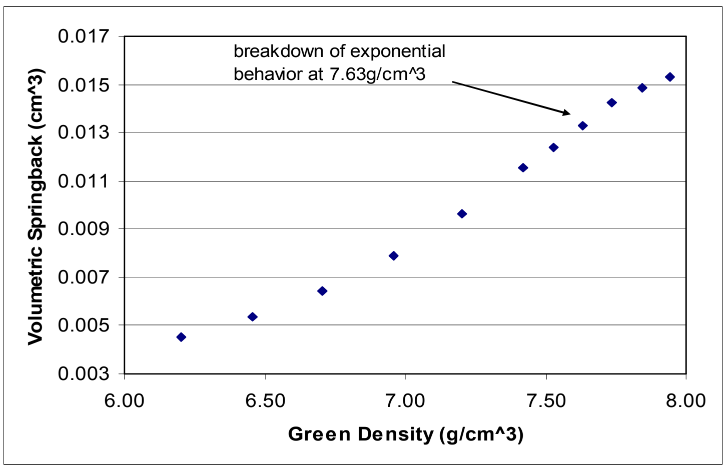

b) Round Grade A geometry

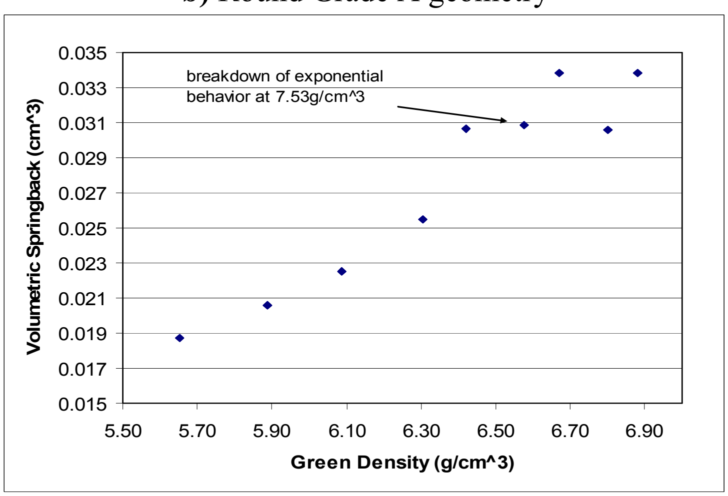

c) Triangular Grade A geometry

Figure 29: The variation of volumetric springback with green density in tight fit compacts.

7.1.14 Effect of compact–die-wall interaction on the corner lip of tight-fit compacts

In all cases, lip size was found to be significantly greater at the compact corners than along the straight edges. In Table 5 it can be seen that for the square Grade A geometry at approximately 25 kN, Lc was greater than L by approximately 23 % and 81 % for the triangular geometry. Similar results were found in Grade B data. The measurement could not be performed on the round inserts.

Previous sections findings (refer to section 7.1.13) in conjunction with the proposed theory of lip deformation by die-wall contact (refer to section 7.1.3), point toward an explanation of the corner lip expansion in terms of increased green densities in these areas of the compacts. Greater green densities, up to a certain critical value, result in greater springback, and increased radial springback behaviour at the compact corners can lead to greater radial pressures against the die walls, and hence stronger contact between the ejecting compact and die wall. The resulting deformation and enlargement of the lip appears to be sufficient enough to overcome the dissipation of springback by friction, and the result is an increased size of the lip in an area where radial springback and subsequent compact-die-wall contact are greater. Thus positive compact corners appear to be concentrators of green density and residual stresses that manifest themselves as inconsistencies in lip size which can lead to increased failure rates of inserts during machining operations. The enlargement of the lip at the corners of positive compacts is shown diagrammatically in Figure 30. Increased compaction densities in dimensional extremities of positive parts such as the compact corners have been investigated by other authors cf. B. Gale [45].

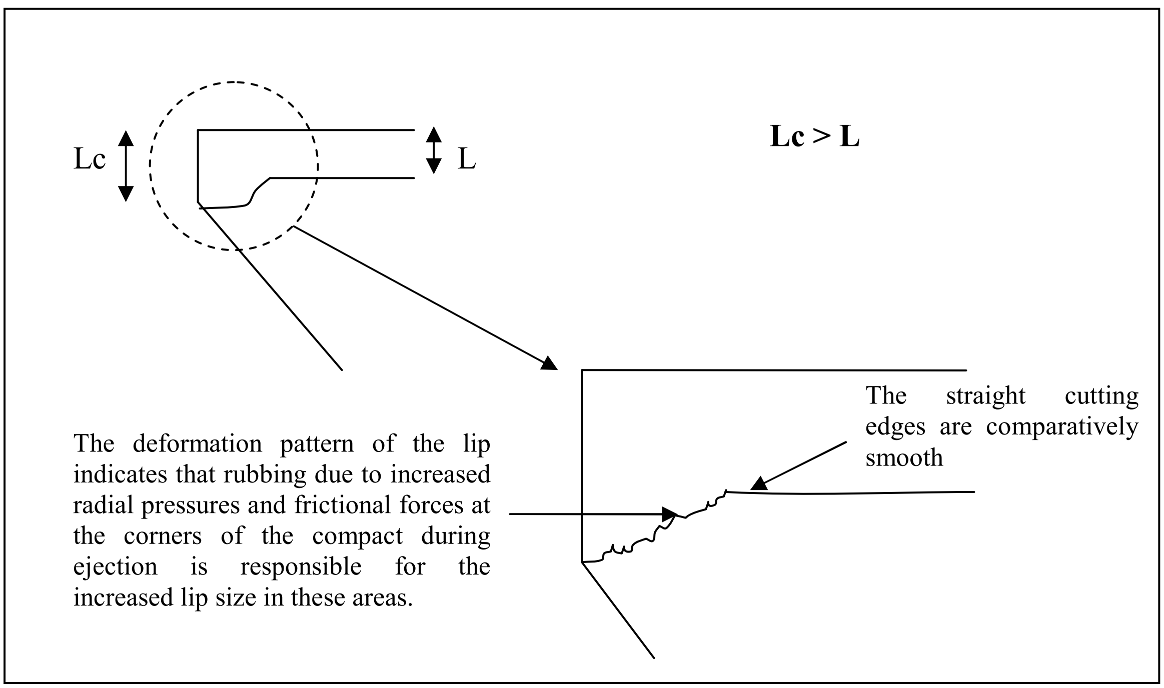

Figure 30: Enlargement of the lip at the corners of positive compacts.

7.1.15 SBA tool development

Modification of tight-fitting tools to SBA tools was done partly on the basis of the radial springback results and partly on consideration of other factors discussed below. At a typical pressing force of 25 kN, the following radial springback values were obtained for Grade A and Grade B compacts.

1 $\Delta IC(F)_{\text{springback (Grade A square)}} \approx 0.037$ mm
2 $\Delta IC(F)_{\text{springback (Grade A round)}} \approx 0.035$ mm
3 $\Delta IC(F)_{\text{springback (Grade A triangle)}} \approx 0.052$ mm
4 $\Delta IC(F)_{\text{springback (Grade B square)}} \approx 0.033$ mm
5 $\Delta IC(F)_{\text{springback (Grade B round)}} \approx 0.045$ mm
6 $\Delta IC(F)_{\text{springback (Grade B triangle)}} \approx 0.023$ mm

On the basis of previous discussion (refer to section 7.1.4) it is understood that these values are the result of only the radial component of the out-of-die springback which might be a representation of only a small portion of the total initial springback energy available in the compact. If a clearance or springback allowance is to be introduced, a larger portion of this initial energy might then be expected to occur in the radial direction while the compact is still in the die and undergoing decompression. Thus larger radial expansions would be expected than observed in SBA compacts than in tight-fit compacts and therefore much larger radial clearances than those suggested by the above values would be necessary to avoid any scuffing of the edges or contact between the compacts and the die walls. In order to further minimize such unwanted effects for the next part of the experiment it was necessary to understand that any "loose" or uncompacted powder in the die can also result in friction or other contact-related effects which can influence the accuracy of the results for pure springback behaviour. Finally, in order to study the expansion behaviour of free compacts at much higher pressing forces than those attained in the tight-fit experiments meant that the introduced clearance gaps would have to be substantially larger than the above values. Subsequently, a clearance of 0.100 mm was introduced to each of the tools by periphery grinding of the upper punches; an estimate which allowed for meaningful springback data to be collected as discussed in section 7.2.

7.1.16 Comparison between the effects of punch contraction and axial springback on the vertical compact dimensions

From the data listed in Tables 7, 53 and 67 it can be seen that for Grade A compacts the effects of punch contraction and axial springback on the vertical compact dimensions were approximately comparable. Calculated at 25 kN, the differences between the two effects were relatively small; approximately 11 % in favor of springback for the square geometry, 4.0 % in favor of springback for the round geometry, and 13 % in favor of contraction in the case of the triangular geometry. Since total axial springback of Grade B compacts was significantly smaller than that of Grade A compacts (refer to section 7.1.8), it is clear that the differences in the two effects for the case of Grade B material were significantly in favor of contraction; approximately 63 % for the square geometry, 43 % for the round geometry, and 20 % for the triangular geometry. Thus contraction and springback were found to be comparable in the case of tight-fit Grade A compacts but contraction was significantly larger than springback in the case of all Grade B geometries.

7.2 SBA results

7.2.1 Tool contraction

The contraction behaviour of SBA tools was summarized, as for the tight-fitting tools, by the effective elasticity constants of the machine-tool systems determined in Chapter 6.

For the square SBA tool, the measured constants are:

1 2.8×10^{-3} mm/kN for the complete upper-lower punch-ram system
2 1.9×10^{-3} mm/kN for the upper punch-ram system
3 0.9×10^{-3} mm/kN for the upper ram only, and
4 1.1×10^{-3} mm/kN for the upper ram and punch base system

Thus the calculated contraction constants for the square SBA tools are:

5 9.0×10^{-3} mm/kN for the bottom punch-ram system
6 1.0×10^{-3} mm/kN for the stand alone top punch
7 0.8×10^{-3} mm/kN the punch shaft of the top punch, and
8 0.2×10^{-3} mm/kN for the punch base

Similarly, the four measured constants for the round SBA tools are:

1 3.0×10^{-3} mm/kN for the complete upper-lower punch-ram system
2 2.0×10^{-3} mm/kN for the upper punch-ram system
3 0.8×10^{-3} mm/kN for the upper ram only, and
4 1.0×10^{-3} mm/kN for the upper ram and punch base system

The calculated contraction constants for the round SBA tools are:

5 1.0×10^{-3} mm/kN for the bottom punch-ram system
6 1.3×10^{-3} mm/kN for the stand alone top punch
7 1.0×10^{-3} mm/kN the punch shaft of the top punch, and
8 0.3×10^{-3} mm/kN for the punch base

Finally, the four measured constants for the triangular SBA tools are:

1 2.951×10^{-3} mm/kN for the complete upper-lower punch-ram system
2 1.846×10^{-3} mm/kN for the upper punch-ram system
3 0.8×10^{-3} mm/kN for the upper ram only, and
4 1.0×10^{-3} mm/kN for the upper ram and punch base system

The calculated contraction constants for the triangular SBA tools are:

5 1.1×10^{-3} mm/kN for the bottom punch-ram system
6 1.0×10^{-3} mm/kN for the stand alone top punch
7 0.9×10^{-3} mm/kN the punch shaft of the top punch, and
8 0.2×10^{-3} mm/kN for the punch base

If the average of the above values for the upper ram contraction is calculated, a value of 0.8×10^{-3} mm/kN is obtained with a relatively small standard error of 0.4×10^{-4} mm/kN. A comparison with the result obtained from the tight-fit tool analysis shows that the two values are in relatively close agreement with each other; their difference being similar in size to the standard error of either of the two individual measurements. Combining the tight-fit and SBA results for the contraction of the upper ram gives an average value of 0.8×10^{-3} mm/kN $\pm$ 0.3×10^{-4} mm/kN. Thus, it can be concluded that at a typical force of 25 kN, the upper ram structure only undergoes approximately 0.020 mm $\pm$ 0.001 mm of contraction.

The average contraction of the SBA punches was calculated at 1.1×10^{-3} mm/kN with a relatively small standard error of 0.8×10^{-4} mm/kN. A comparison against the tight-fitting results for which the same value was 1.3×10^{-3} mm/kN mm $\pm$ 1.0×10^{-4} mm/kN shows that these contractions are again relatively similar although this time, the difference between them was similar in size to the sum of individual standard errors of the two measurements. Combining the tight-fit and SBA sets of results gives an average value for the upper punch contraction only, of 1.2×10^{-3} mm/kN $\pm$ 0.8×10^{-4} mm/kN. Thus at a typical pressing force of 25 kN, a typical upper punch used in production will experience 0.031 mm $\pm$ 0.002 mm of contraction. In relative terms, this is significantly more than the contraction of upper ram calculated above.

The sources of the differences between the SBA and tight-fit results could have been the results of either measuring errors and/or inherent inaccuracies of the chosen experimental method. The definite presence of one or both is also evident in view of the smaller punch contraction constant of the SBA tools compared to the tight-fitting tools. This is unexpected because the contraction constant is inversely proportional to the cross-sectional punch area which was smaller in the case of the SBA tools. The smaller area was thus expected to result in a greater contraction and therefore larger contraction constants of the SBA punches as opposed to the tight-fitting punches. Since the standard errors in both the tight-fitting and the SBA results were similar, the inconsistency is most likely a result of the inherent inaccuracy in the experimental method which needs to be improved and refined should more accurate contraction results be required. For practical purposes and requirements of this project, the values obtained are sufficiently accurate.

The average contraction constant of the upper punch-ram system using the SBA tools was found to be 1.9×10^{-3} mm/kN$\pm$ 0.6×10^{-4} mm/kN. The standard deviation of the average is very small indicating high precision in this measurement. A comparison against the same value obtained using the tight-fitting tools which was 2.1×10^{-3} mm/kN $\pm$ 0.1×10^{-3} mm/kN shows that the two values show a small difference of 0.004 mm at a typical pressing force of 25 kN. This confirms the previous findings that a single, universal contraction constant can be used to approximate the effect of contraction on the compact dimensions for a variety of punches. This value, calculated as the average of the SBA and tight-fit upper punch-ram contraction was 2.0×10^{-3} mm/kN ± 0.7×10^{-4} mm/kN. Thus at 25 kN, the upper punch-ram contraction, for any typical tool in production can be expected to be 0.051 mm ± 0.002 mm.

7.2.2 General observations in springback behaviour and comparison with tight-fit results

The linear dimensions of SBA compacts, like those of the tight-fit compacts, showed some deviation in springback behaviour from that expected for a fully elastic body. The plots of axial and radial springback could best be described by quadratically varying functions of the pressing force regardless of the geometry, the material, or the hold-down force setting used in decompression and ejection. However, in all cases, the springback behaviour was significantly more elastic than that of tight-fit compacts when considered over the same range of pressing forces i.e. 0 kN to approximately 30 kN. For instance, the SBA springback data for the square, round, and triangular Grade A geometries under the action of the same hold-down force used in the pressing of tight-fit compacts, could be described by straight-line equations to within excellent approximation as indicated by the regression coefficients bellow.

$$\Delta H(F)_{springback\ (square)} = 1.224\times10^{-3}F + 2.347\times10^{-3}\ \ (R^2 = 9.985\times10^{-1}) \quad ...(74)$$
$$\Delta IC(F)_{springback\ (square)} = 8.377\times10^{-4}F + 2.337\times10^{-4}\ \ (R^2 = 1.000) \quad ...(75)$$
$$\Delta H(F)_{springback\ (round)} = 1.242\times10^{-3}F + 3.898\times10^{-3}\ \ (R^2 = 9.984\times10^{-1}) \quad ...(76)$$
$$\Delta IC(F)_{springback\ (round)} = 9.628\times10^{-4}F + 2.597\times10^{-3}\ \ (R^2 = 9.988\times10^{-1}) \quad ...(77)$$
$$\Delta H(F)_{springback\ (triangle)} = 1.195\times10^{-3}F + 4.880\times10^{-3}\ \ (R^2 = 9.952\times10^{-1}) \quad ...(78)$$
$$\Delta IC(F)_{springback\ (triangle)} = 1.536\times10^{-3}F + 5.102\times10^{-4}\ \ (R^2 = 1.000) \quad ...(79)$$

This small deviation reveals a possible presence of a non-elastic element which seems to be a natural characteristic of all compacts. Such behaviour could be attributed to the effects of secondary yielding, viscoelastic properties of PEG, etc., as discussed by other authors (refer to Chapter 3). The main deviation from straight line springback behaviour occurred at much higher pressing forces in SBA compacts; particularly when the compact IC approached that of the die suggesting that contact and subsequent friction with the die wall have a definite effect on the springback behaviour.

A general trend in the SBA data was that the deviation from elastic behaviour was much more pronounced for axial springback than radial springback of SBA compacts (with the hold-down force present). This can be seen by examining and comparing the quadratic coefficients of equations 169 vs.171 (Grade A) and 187 vs. 189 (Grade B) for the square geometry, 205 vs. 207 (Grade A) and 223 vs. 225 (Grade B) for the round geometry, and 241 vs. 243 (Grade A) and 259 vs. 261 (Grade B) for the triangular geometry. Thus the action of the hold-down force during decompression and ejection increases the non-elastic springback tendencies of the axial component of springback more so than the radial component. This result was found to be true regardless of the compact geometry or compaction material. The underlying explanation for this behaviour is unknown.

7.2.3 Effect of hold-down force on the behaviour of axial and radial springback

Using the relationships established in Section 6.5 and calculating the axial and radial springback at a pressing force of 25 kN for each geometry, material type and hold-down force setting, it was possible to determine that the difference between axial and radial springback was strongly dependant on the hold-down force setting. In the case of Grade A compacts ejected under the action of a hold-down force, axial springback was found to be greater than radial springback in two out of the three cases. For example, the calculated differences at 25 kN were 36 % in the favor of axial springback for the square geometry and 30% in the favor of axial springback for the round geometry. With Grade A compacts pressed without the action of hold-down force, radial springback was greater than axial springback in all three cases. The calculated differences were approximately 62 %, 72 % and 65 % for the square, round and triangular geometries respectively.

Similar results were observed with Grade B compacts calculated at 25 kN pressing force. Grade B compacts ejected with the hold-down force exhibited greater axial expansions than radial expansions in all cases regardless of the compact geometry; approximately 28 %, 36 % and 39 % for the square, round and triangular shapes respectively. Without the hold-down force however, the free radial expansion was significantly greater than the free axial expansion as seen by the differences calculated at 25 kN for the round and triangular geometries which were approximately 76 % and 69 % respectively. Figure 31 shows this effect on the round geometry pressed in Grade B powder.

These results were unexpected because the hold-down force is applied axially on the compact and was thus expected to contain axial expansion and enhance radial expansion. Instead the application of the hold-down axial pressure during ejection resulted in a larger total axial springback than total radial springback. The completely free springback behaviour of compacts, uninfluenced by friction or hold-down, was such that the absolute radial springback was naturally greater than axial springback, a result which was independent of compact geometry or compaction material.

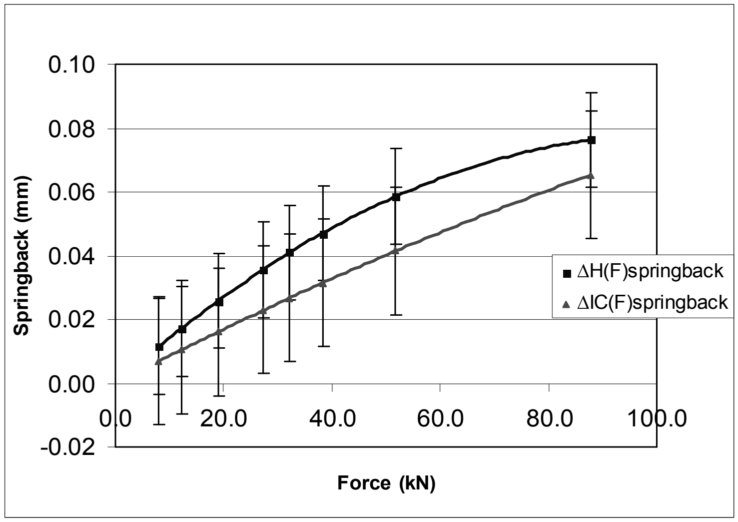

a) Round Grade B geometry with hold-down.

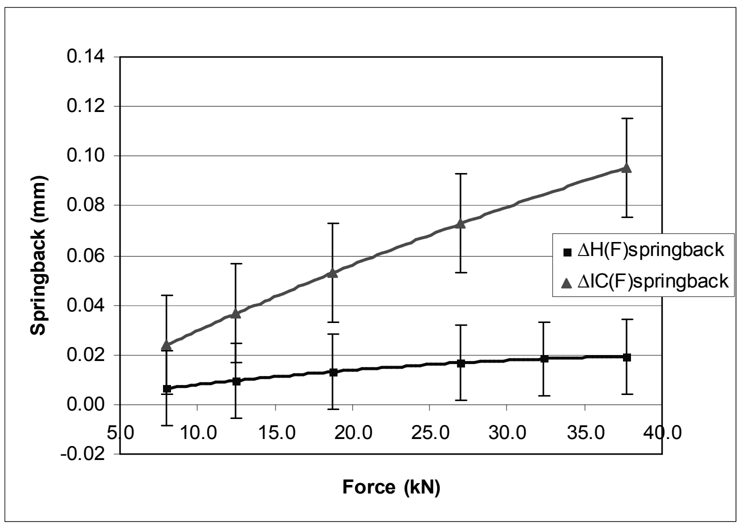

b) Round Grade B geometry without hold-down.

Figure 31: The effect of hold-down on axial and radial springback of SBA compacts.

7.2.4 Effect of hold-down force on the behaviour of relative axial and radial springback

For the square geometry Grade A compacts ejected under the action of a hold-down force, the relative axial and radial springback at 25 kN were approximately 0.68 % and 0.16 % respectively, for the round compact 0.73 % and 0.21 % respectively, and for the triangular compact 0.74 % and 0.32 % respectively. For square Grade A compacts ejected freely i.e. without the action of the hold-down force, the axial and radial springback at 25kN were approximately 0.53 % and 0.55 % respectively, for the round compact 0.37 % and 0.50 % respectively, and for the triangular compact 0.40 % and 0.46 % respectively. The same calculations for the Grade B compacts gave the following results. For the compacts ejected under the action of a hold-down force, the relative axial and radial springback for the square geometry at 25 kN were approximately 0.61 % and 0.18 % respectively, for the round geometry 0.69 % and 0.16 %, and 0.77 % and 0.18 % respectively for the triangular geometry. Without the hold-down force, these values were 1.33 % and 0.51 % respectively for the square Grade B geometry, 0.33 % and 0.55 % respectively for the round Grade B geometry, and 0.36 % and 0.45 % respectively for the triangular Grade B geometry.

Thus it is clear that when the hold-down force is applied during the ejection of the compacts from a SBA die the relative axial springback is in all cases significantly greater than the relative radial springback. Therefore this result is independent of the compact geometry or compaction material. However, without the hold-down force, in most cases the relative radial springback was slightly larger than its axial counterpart. The exception to this rule was only the result for the square Grade B compact for which the relative axial springback at 25 kN was an extraordinarily large value of approximately 1.33 %[13]. Thus the free springback behaviour as uninfluenced by hold-down, is such that the distributions of the axial and radial components relative to their starting dimensions are more or less equal and slightly in favour of radial expansion.

It can also be seen that the relative axial springback in compacts pressed without hold-down is smaller than the relative axial springback of compacts pressed with hold-down. The opposite was true of relative radial springback; the relative radial springback of compacts pressed without hold-down is greater than the relative radial springback of compacts pressed with hold-down. These results are consistent with the previous section's findings (refer to section 7.2.3) where the hold-down force was seen to have the same effect on the behaviour of absolute springback.

Finally, the comparison with the results obtained for the tight-fit compacts reveal one major difference in the relative springback behaviour between the two sets of compacts. Although the values of relative radial springback for the two sets of compacts calculated at 25 kN were comparable, the relative axial springback of tight-fitting compacts significantly exceeded that of SBA compacts. In fact this difference for the square and round Grade A geometries and the round and triangular Grade B geometries was more than two-fold in favour of tight-fit compacts. This might be further evidence that compacts ejected from tight-fitting dies are more prone to larger axial expansions.

7.2.5 Effect of hold-down on the variation of the springback ratio with pressing force

Unlike the results obtained for the tight-fitting compacts, all springback ratio curves for the SBA compacts were found to be decreasing quadratic functions of the pressing force. Thus non-linear frictional influences were the likely cause of the previously observed

[13] Given the trend of the rest of the data this is most likely a result of experimental error in measurement. This is further supported by an explicit calculation of the absolute axial springback of the square Grade B compact pressed without hold-down. When computed this gives a value of 0.063mm which is significantly greater than those of the round and triangular geometries which are approximately equal to 0.016mm and 0.017mm respectively.

inconsistencies in this result for the tight-fit compacts (refer to 7.1.6) and the true variation of the springback ratio with pressing force is that of a quadratically decreasing function.

Furthermore the calculated results are consistent with the observations made in the previous section (refer to section 7.2.4). For example, regardless of the grade of powder used in compaction, when the hold-down force was applied in the ejection of compacts, the springback ratio was in most cases greater than 1, implying that the absolute axial springback was greater than the absolute radial springback under these circumstances. Similarly when the hold-down force was removed the springback ratio was in most cases less than 1 implying that compacts naturally expand more in the radial direction as opposed to axial direction when allowed to springback freely.

The obtained values at 25 kN of pressing force were as follows. For Grade A compacts pressed with hold-down, the springback ratio for the square geometry was approximately 1.57, for the round geometry 1.30, and for the triangular geometry 0.90[14]. For the Grade A compacts pressed without hold-down, the springback ratios were approximately 0.38, 0.28, and 0.35 for the square, round, and triangular geometries respectively. For the Grade B compacts pressed with hold-down, the springback ratios were approximately 1.38, 1.57, and 1.64 for the square, round, and triangular geometry. For Grade B compacts pressed without hold-down, the springback ratios were approximately 1.05[15], 0.24, and 0.31 respectively.

Extending the analysis further and calculating the averages and corresponding standard errors of the above values shows, that axial springback for Grade A compacts pressed with hold-down is on average 1.26 ± 0.19 times greater than the absolute radial springback while the average springback ratio for Grade A compacts without hold down is equal to 0.34 ± 0.030. The same calculations for Grade B give an average springback ratio of 1.53 ± 0.078 for compacts pressed with hold-down and 0.28 ± 0.035 for compacts pressed without hold-down[16]. The relatively large standard error values associated with the calculated averages show that the absolute springback ratio is geometry dependant, while the differences between the calculated averages for the different grades of material show that the ratio is also somewhat material dependant.

7.2.6 Effect of hold-down on the variation of the relative springback ratio with pressing force

The relative springback ratio confirms the findings of the previous section, with relative axial springback exceeding the relative radial springback in all cases when the hold-down force was applied, and the relative radial springback exceeding the relative axial

[14] This value is less than one most probably due to an experimental error in measurement which has resulted in either smaller than expected axial springback or larger than expected radial springback.
[15] This value is larger than one most likely due to experimental error in the axial data measurement. This inaccuracy is also reflected in the unexpectedly large value of 1.33 obtained for the relative axial springback of the square Grade B compact pressed without hold-down (seen in the previous section).
[16] The springback ratio value of 1.05 for the square Grade B compact was left out of the calculation (refer to footnote 17 and 19).

springback in all cases when the hold-down force was not applied. When the hold-down force was active, the relative axial springback of Grade A geometries exceeded the relative radial springback by a factor of 4.25 for the square shape, 3.48 for the round shape, and 2.31 for the triangular shape at 25 kN of pressing force. Without the hold-down force, the relative springback ratio was approximately 0.96, 0.74, and 0.87 for the square, round, and triangular Grade A geometries. With the hold-down force active, the relative axial springback was 3.39, 4.31, and 4.28 times greater than the relative radial springback of the square, round, and triangular grade B geometries respectively. The springback ratios for Grade B compacts without hold-down were 0.60 and 0.80 for the round and triangular geometries respectively[17].

Extending the analysis further and calculating the averages and corresponding standard deviations of the above values shows, that the relative axial springback for Grade A compacts pressed with hold-down is on average 3.34 ± 0.56 times greater than the relative radial springback while the average relative springback ratio for Grade A compacts without hold down is equal to 0.86 ± 0.064. The same calculations for Grade B give an average relative springback ratio of 3.99 ± 0.30 for compacts pressed with hold-down and 0.70 ± 0.10 for compacts pressed without hold-down. The relatively large standard deviation values associated with the calculated averages show that the relative springback ratio is geometry dependant, while the differences between the calculated averages for the different grades of material show that the relative springback ratio is also to an extent material dependant.

7.2.7 Effect of geometry and compaction material on axial and relative axial springback under varying hold-down conditions

A comparison of equations 169, 178, 205, 214, 241, 250 for the axial springback of Grade A geometries and 171, 180, 207, 216, 243, 252 for the axial springback of Grade B geometries as well as examination of Figure 32 on which the absolute axial springback of all SBA compacts and grades is plotted reveals that for all practical purposes axial springback of these compacts is independent of geometry and compaction material but dependant on the hold-down force setting.

[17] The value for the square geometry is erroneous due to measurement inaccuracy as mentioned previously.

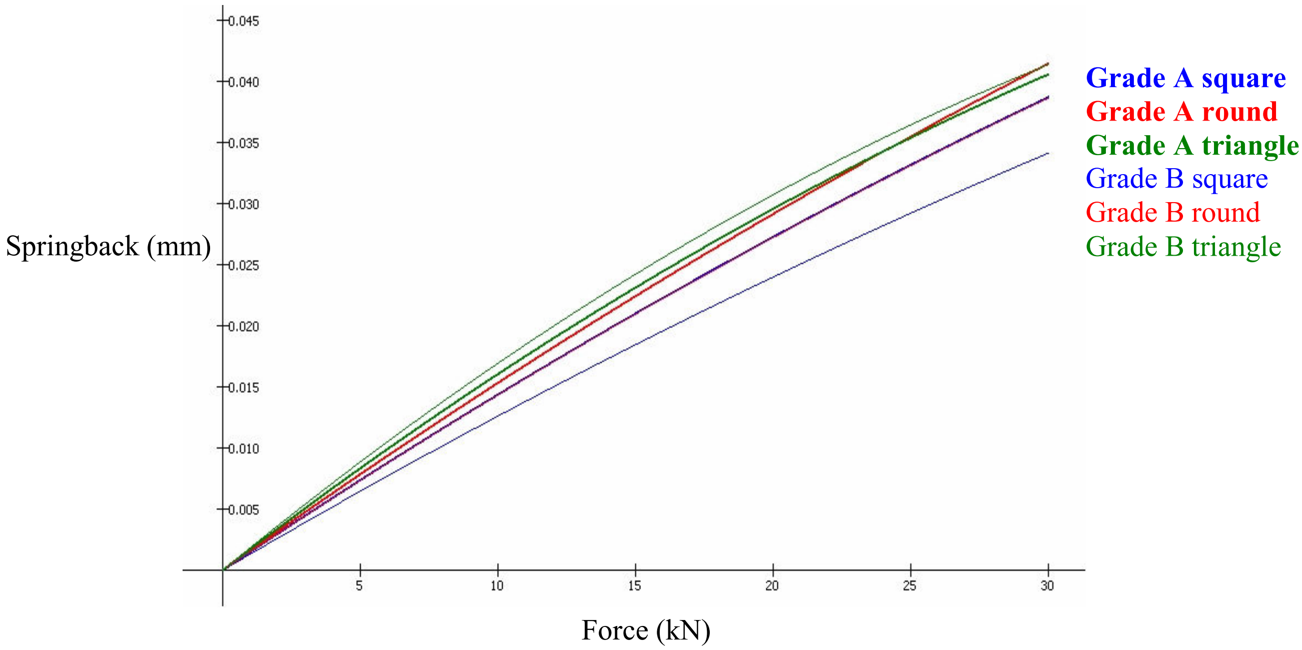

a) With hold-down

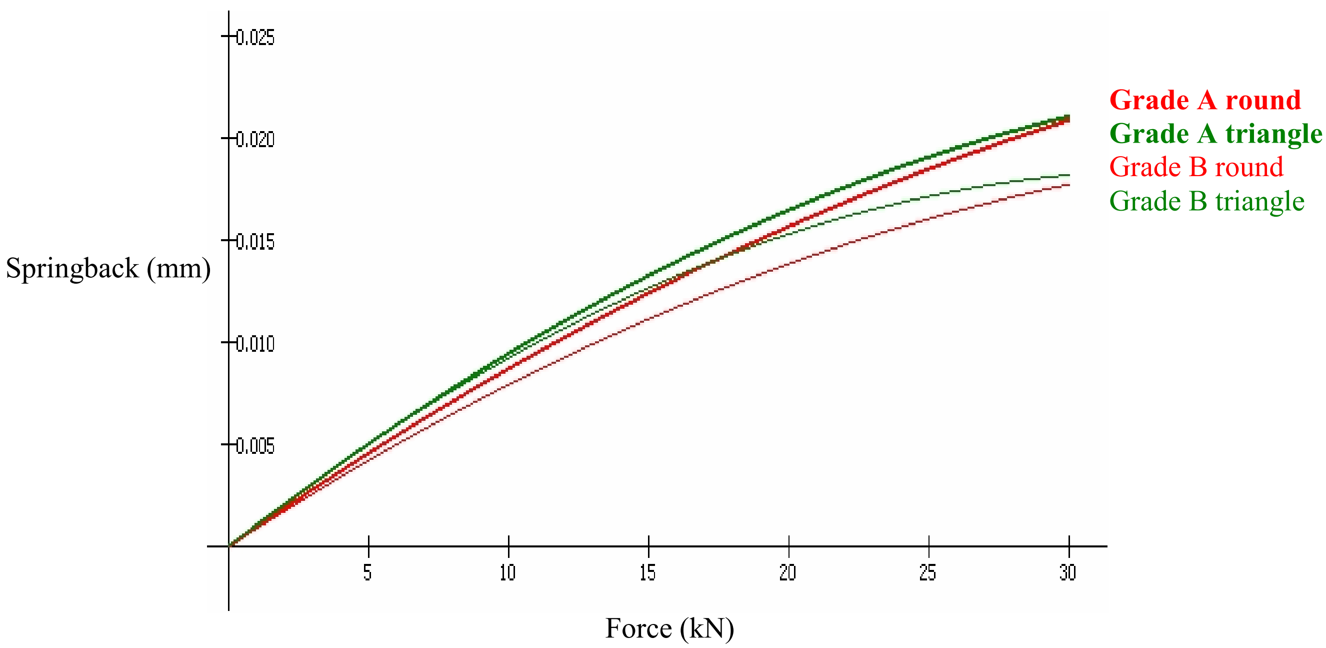

b) Without hold-down (square geometry excluded)

Figure 32: Change in axial springback with pressing force for SBA Grade A and Grade B geometries pressed a) with and b) without hold-down.

For example, at 25 kN the absolute axial springback of Grade A compacts ejected with hold-down was approximately 0.035 mm for the round and triangular geometries, and 0.033mm for the square geometry thus giving an average of 0.034 mm ± a standard error of 0.001 mm. Given that the error in each individual height measurement was 0.010 mm this result is extremely accurate and a value of 0.034 mm is a very good estimate of the actual axial springback for any of the wide range of shapes examined in this work. Thus this relationship can be represented mathematically as follows:

1 $\Delta H(25\ kN)_{springback\ (square)} \approx \Delta H(25\ kN)_{springback\ (round)} \approx \Delta H(25\ kN)_{springback\ (triangle)} \approx 0.034\ mm \pm 0.001\ mm.$

Without the pneumatic hold-down force however the absolute axial springback of Grade A compacts at 25 kN was 0.025 mm for the square geometry, 0.018 mm for the round geometry, and 0.019 mm for the triangular geometry yielding an average of 0.021 mm ± 0.002 mm.

2 $\Delta H(25\ kN)_{springback\ (square)} \approx \Delta H(25\ kN)_{springback\ (round)} \approx \Delta H(25\ kN)_{springback\ (triangle)} \approx 0.021\ mm \pm 0.002\ mm.$

Firstly it is clear that the free axial springback i.e. springback without the influence of hold-down, is smaller than the axial springback with hold-down thus implying that axial springback is dependent on this setting. Secondly, it is evident from the above that the free axial springback can with reasonable confidence be considered as geometry independent given that the standard error of the average is significantly smaller than the actual value of the average as well as the error in the individual measurement which in most cases was 0.010 mm. In this case a value of 0.021 mm represents a good estimate of the axial springback without hold-down for the range of geometries considered.

In a similar analysis to the above, axial springback of Grade B compacts pressed with and without hold-down can be shown to be geometry independent while being dependant on the hold-down condition. For example, at a typical pressing force of 25 kN the following values were obtained for the axial springback of Grade B geometries under the action of a hold-down pressure during ejection: 0.029 mm for the square geometry, 0.033 mm for the round geometry, and 0.036 mm for the triangular geometry. If an average of the above values is calculated, a mean of 0.033 mm and a small standard error of the mean of 0.002 mm are obtained indicating that for all practical purposes a single value can be used to approximate the axial springback of the examined Grade B compacts and that axial springback is thus geometry independent.

3 $\Delta H(25\ kN)_{springback\ (square)} \approx \Delta H(25\ kN)_{springback\ (round)} \approx \Delta H(25\ kN)_{springback\ (triangle)} \approx 0.033\ mm \pm 0.002\ mm.$

When the hold-down was removed, 0.016 mm and 0.017 mm were obtained for axial springback of the round and triangular Grade B geometries respectively. Thus axial springback without hold-down was again seen to be geometry independent.

4 $\Delta H(F)_{springback\ (round)} \approx \Delta H(F)_{springback\ (triangle)} \approx 0.017\ mm \pm 0.001\ mm$

A comparison of the averages with and without hold-down again shows the dependence of springback on hold-down.

Finally a comparison between the Grade A and Grade B results for axial springback shows a relatively small dependence of springback on compaction material type. This dependence is particularly small in the case with hold-down where the two calculated averages for Grade A and Grade B materials are almost identical. Without hold-down the obtained results were not as similar but for all practical purposes an average of the two values can be used to estimate the actual free springback for both compaction materials to within a reasonably good approximation i.e.

4 $\Delta H(F)_{\text{springback Grade A}} \approx \Delta H(F)_{\text{springback Grade B}} \approx 0.019 \text{ mm} \pm 0.002 \text{ mm}$

These results are in marked contrast to the results obtained for tight-fitting compacts where axial springback was found to be both geometry and material dependant[18]. Furthermore, a comparison with the previous results shows that the absolute axial springback of tight-fitting compacts is significantly greater than that of the SBA compacts. For instance the axial springback values obtained for the tight-fitting Grade A compacts at 25 kN were 0.091 mm for the square and round geometries.

The same conclusions hold in the case of relative axial springback with material and geometric independence being true even when initial dimensions were accounted for (refer to the equations in section 6.5 for the relative axial springback of Grade A and Grade B geometries pressed with and without hold-down). Here the average relative axial springback of Grade A geometries at 25 kN, was 0.72 % ± 0.017 % with hold-down and 0.43 % ± 0.052 % without hold-down. That of the Grade B geometries was 0.69 % ± 0.046 % with hold-down and 0.35 % ± 0.012 % without hold-down. The mean of the above averages allows for the determination of the value which can be used to estimate the relative axial springback of both materials. This value is 0.71 % ± 0.063 % for the case with hold-down and 0.39 % ± 0.064 % for the case without hold-down. The relative axial springback of tight-fit compacts was previously found to be powder and geometry dependant. In addition it is significantly greater than that of the SBA compacts. For instance the relative axial springback of the square and round Grade A tight-fitting geometries was approximately 1.66 %, more than two times greater than the above calculated average of 0.72 % for the relative axial springback of the Grade A SBA compacts.

7.2.8 Effect of geometry and compaction material on radial and relative radial springback under varying hold-down conditions

Similar conclusions to above can be reached for the absolute radial springback of SBA compacts. Radial springback seems particularly sensitive to the hold-down setting but not

[18] Hold-down dependence could not be investigated in the same fashion with tight-fitting compacts. These compacts would develop cracks and other defects if ejected without the use of hold-down force which would have made it difficult if not impossible to make accurate measurements of the required linear dimensions.

so on the geometry and material properties of the compacts. For all practical purposes, it can be concluded that radial springback of SBA compacts like its axial counterpart is dependant on the hold-down setting but independent of the compact geometry and the material used in compaction. This is evident from the following results which show the relevant calculated averages and the associated standard errors at 25 kN, as well as figure 33 on which all radial springback curves are plotted.

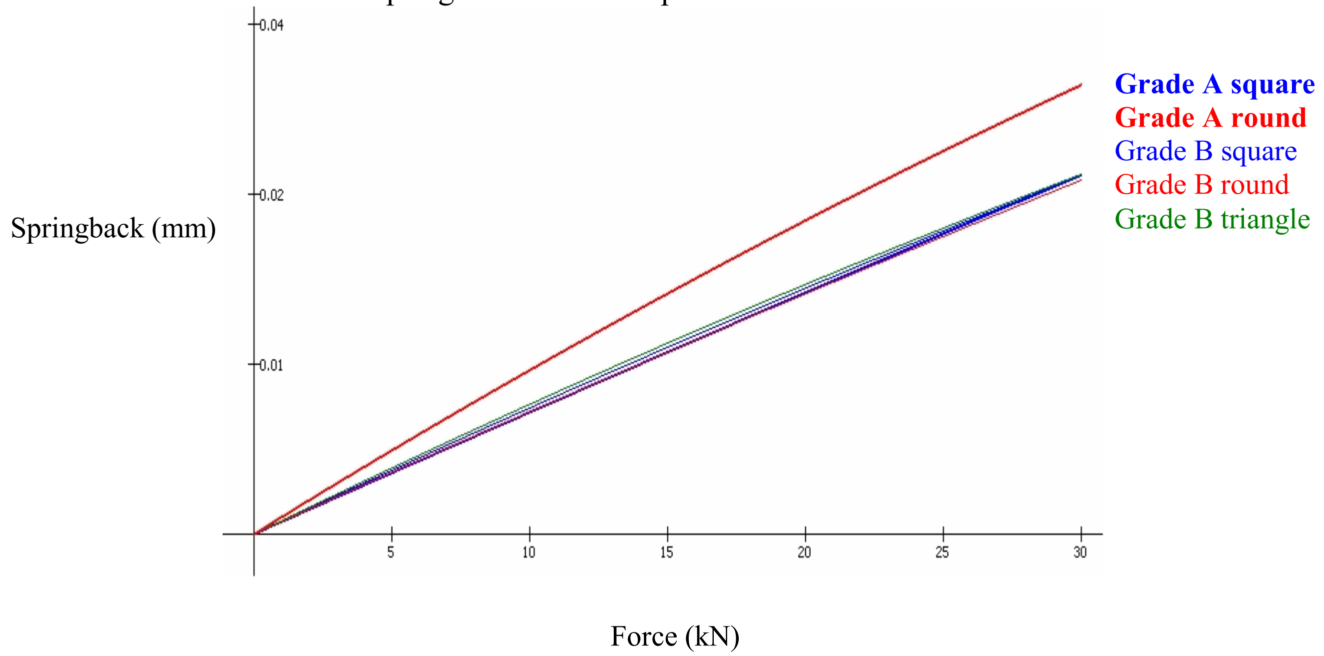

b) With hold-down (triangular compact excluded)

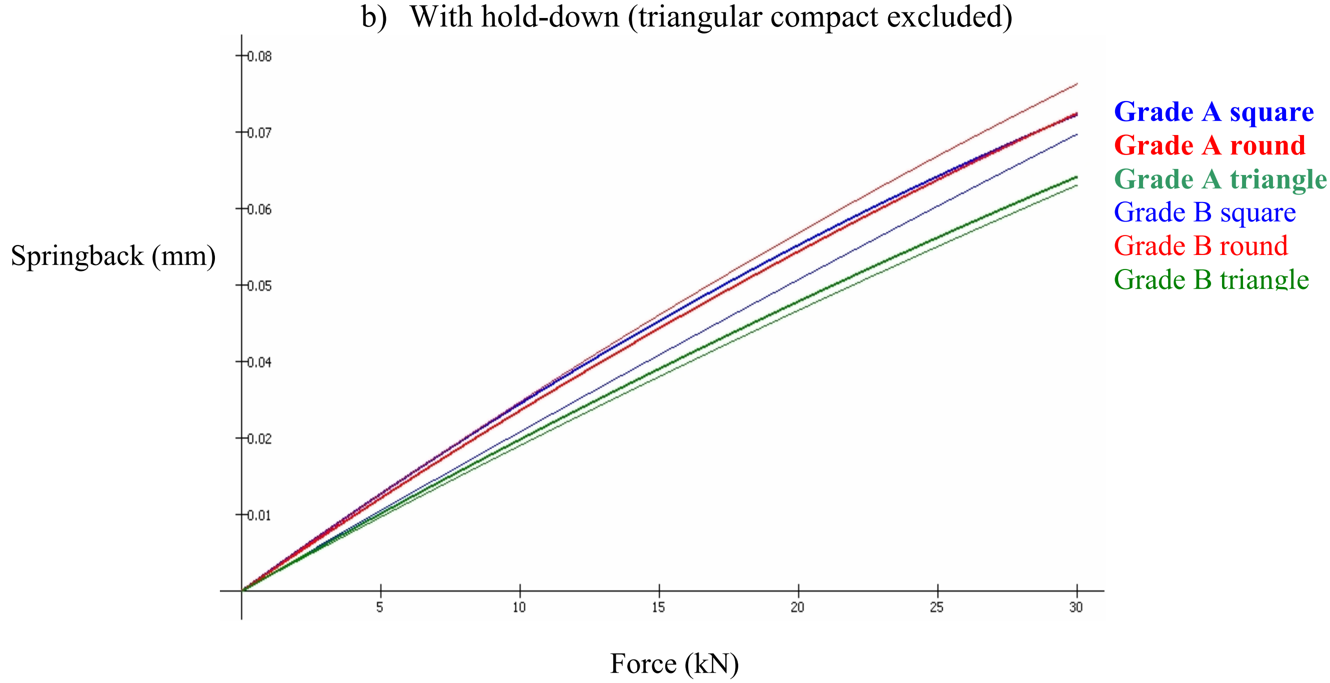

b) Without hold-down

Figure 33: Change in radial springback with pressing force for SBA Grade A and Grade B geometries pressed a) with and b) without hold-down.

Average radial springback of Grade A compacts ejected using hold-down was 0.024 mm ± 0.003 mm[19]. Average radial springback of Grade A compacts ejected without hold-down was 0.062 mm ± 0.003 mm. Same calculations for the radial springback of Grade B compacts with and without hold-down reveal an average value for all the geometries of 0.021mm ± 0.001mm in the former case and 0.061 mm ± 0.004 mm in the latter case. Thus the material independent averages are 0.023 mm ± 0.004 mm with hold-down and 0.062 mm ± 0.007 mm without hold-down. It can now be seen that while axial springback with hold-down was about 1.8 times greater than that without hold-down, radial springback with hold-down is about 2.7 times smaller than that without hold-down.

The analysis of relative radial springback values reveals similar findings. The average relative radial springback of Grade A compacts ejected using hold-down was 0.19 % ± 0.02 %. The average relative radial springback of Grade A compacts without hold-down was 0.50 % ± 0.02 %. Same calculations for the relative radial springback of Grade B compacts with and without hold-down reveals an average value of 0.17 % ± 0.01 % in the former case and 0.50 % ± 0.03 % in the latter case. Thus the material independent averages are 0.18 % ± 0.03 % with hold-down and 0.50 % ± 0.05 % without hold-down.

A comparison with the radial springback behaviour of the tight-fitting compacts reveals that although there were some differences in the magnitudes of the obtained values for the tight-fitting and SBA compacts – namely that the relative radial springback of tight-fit compacts was slightly greater than that of the SBA compacts (pressed with hold-down) – the results were much more similar than those for the axial springback of the tight-fitting and SBA compacts which were, as previously established, overwhelmingly in the favor of tight-fitting compacts. The similarity in magnitudes is particularly true when the comparison between the tight-fitting and SBA compacts is made on the basis of relative radial springback. Although as mentioned previously, the relative radial springback of tight-fitting compacts was found to be highly geometry and material dependant it is still possible to see that it is at least in the same size range as that for SBA compacts. In contrast both absolute axial and relative axial springback of tight-fitting compacts was significantly greater than that of SBA compacts serving as further proof that ejection from tight-fitting dies appears to enhance the axial component of springback.

Finally, the above calculated values of radial springback without hold-down at 25 kN indicate that the choice of 0.100 mm for the clearance gaps of SBA tools was a good estimate, and that the free radial springback behaviour could be observed without the effects of friction in the typical range of pressing forces, as was required for this part of the experiment.

---

[19] The radial springback for the triangular geometry was omitted from the calculation of the above average due to an evidently large human measuring error associated with this value. The radial springback value for the triangular geometry at 25kN was markedly larger than the rest of the radial springback values.

7.2.9 Effect of geometry and compaction material on volumetric and relative volumetric springback under varying hold-down conditions

The calculation of absolute volumetric springback values at 25 kN, with the aid of the previously established relationships of section 6.5 and the below figure (refer to Figure 34) reveal firstly that volumetric springback of SBA compacts is geometry dependant, secondly that it is for all practical purposes material independent, and finally that it is as expected, hold-down independent.

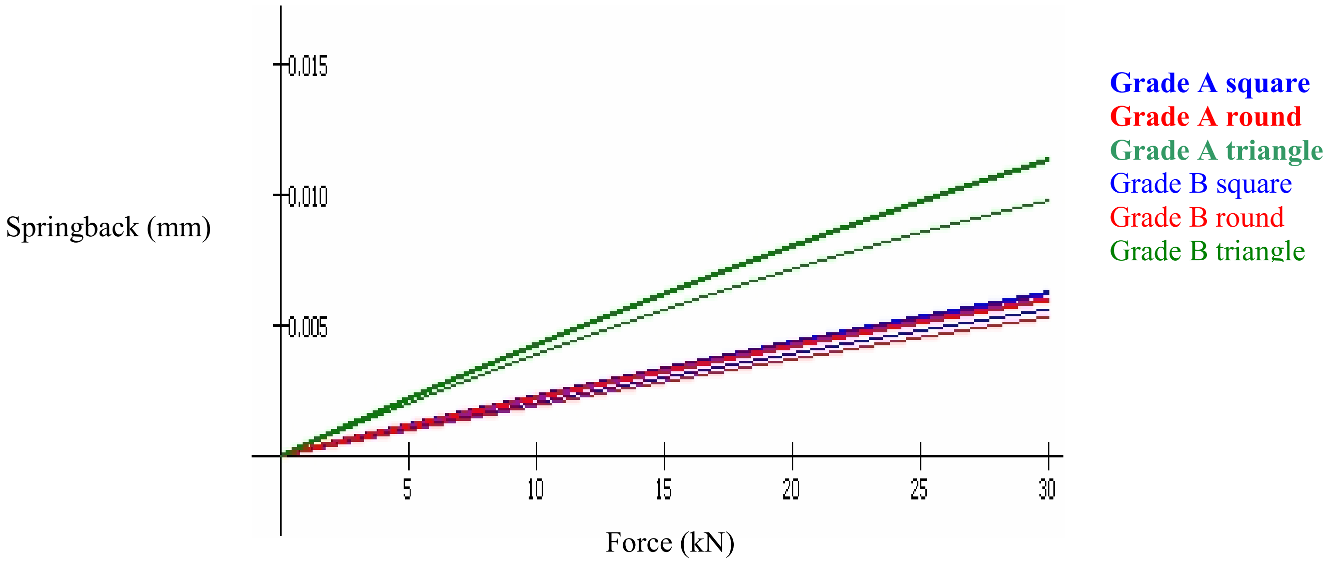

a) With hold-down

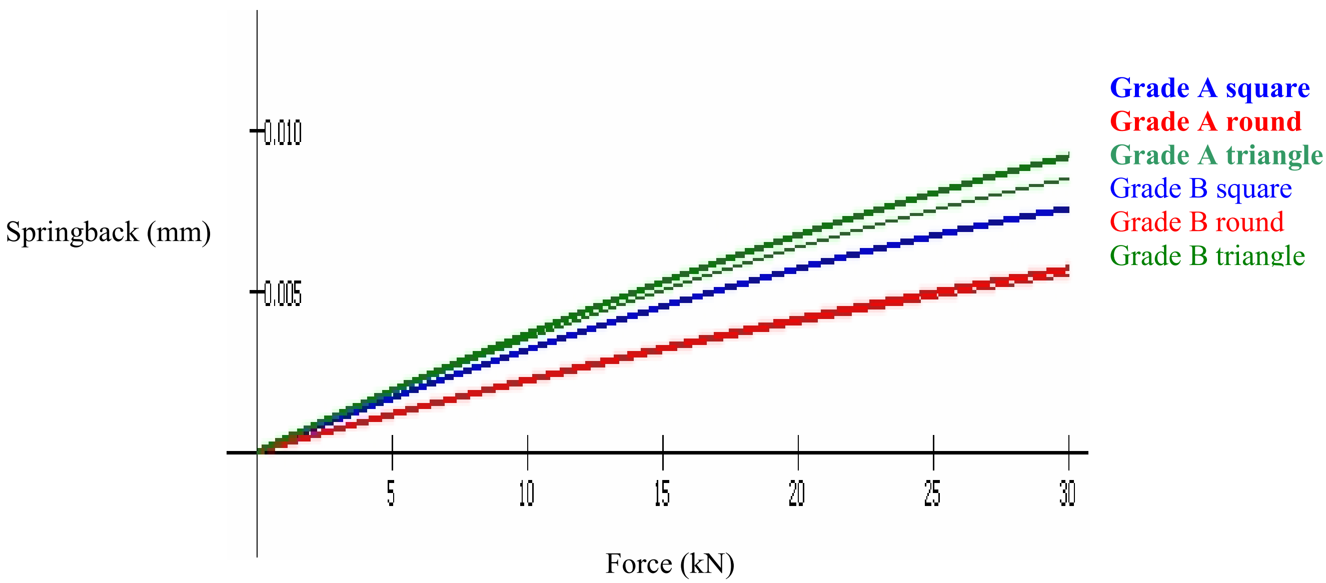

b) Without hold-down

Figure 34: Change in volumetric springback with pressing force for SBA Grade A and Grade B geometries pressed a) with and b) without hold-down.

The first conclusion is most easily reached by the comparison of the volumetric springback values without hold-down at 25 kN, for the three different geometries pressed with both Grade A and Grade B materials. The volumetric springback of Grade A compacts pressed without hold-down was 0.0066cm^3 for the square geometry, 0.0049cm^3 for the round geometry, and 0.0078cm^3 for the triangular geometry. Thus the volumetric springback of the triangular shape is approximately 15 % greater than that of the square shape which is in turn 26 % greater than that of the round shape. The difference between the triangular and the round shape is thus 37 %. A similar comparison for Grade B reveals that the volumetric springback of the triangular shape (calculated at 0.0074 cm^3) is 37 % greater than that of the round shape (calculated at 0.0047 cm^3), a nearly identical fraction to the above result with Grade A[20]. Thus in both cases volumetric springback is geometry dependant.

A cross comparison of the same values above for the Grade A and Grade B geometries allows the second conclusion to be made. The relative difference between the free (in this case meaning without hold-down) volumetric springback of the Grade A and Grade B round shapes is about 4.1 % while that of the triangular shape is 5.1 %. Thus free volumetric springback is to within excellent approximation, material independent.

The third conclusion is most easily reached from the comparison of volumetric springback values for Grade B geometries with and without hold-down. The results without hold-down at 25 kN were already stated above. With hold-down the volumetric springback of the triangular Grade B geometry was 0.0084cm^3 and 0.0045cm^3 for that of the round shape. Thus the relative difference between the results with and without hold-down expressed was only 11.9 % for the triangular shape and 4.3 % for the round shape. The same relative difference for the triangular and round Grade A geometries was 17.9 % and 2.0 % respectively. Thus although volumetric springback seems more sensitive to hold-down in the case of the triangular geometry than the round geometry for all practical purposes it can be described as hold-down independent, a result markedly different from the springback behaviour of the individual linear dimensions both of which were found to be highly dependant on the hold-down. Small geometry dependant differences observed above could be amongst other factors a result of formulas used to approximate volume calculations and/or the shearing movement of the top and bottom compact surfaces – driven by radial springback – under the load of the upper and lower punches during part removal with hold-down as described by Rodiger [7].

A comparison against the volumetric springback previously observed for tight-fit compacts shows that for most part the absolute volumetric springback of tight-fit compacts is significantly greater than that of the SBA compacts. This is particularly true in the case of Grade A compacts where in some cases the volumetric springback of tight-fit compacts was as much as three times greater than that of the SBA compacts. It means that the fraction of tight-fit compact springback which was dissipated by friction during ejection was not large enough to cause a drastic decrease in the springback of tight-fit

[20] Volumetric springback of the square Grade B shape was excessively large and was left out of the analysis on the account of inaccurate axial springback data of this geometry. This was mentioned in footnotes 17 and 19.

compacts below that of the friction-unaffected SBA compacts. The result however suggests due to the significantly larger starting dimensions of the tight-fitting compacts that the total volumetric springback may possibly be proportional to the initial compact dimensions, a possibility which was investigated below.

An analysis of relative volumetric springback reveals that relative volumetric springback is for all practical purposes independent of the compact geometry or shape (refer to figure 35), compaction material, and hold-down setting and that therefore it depends only on the pressing force into which all of the above are factored in. For instance, the relative volumetric springback of the Grade A compacts at 25 kN was 0.89 % for the square geometry, 0.98 % for the round geometry, and 1.1% for the triangular geometry giving an average of 0.99 % with a relatively small standard error of only 0.064 %. Without hold-down the calculated values for the Grade A compacts were 1.1 % for the square geometry, 0.95 % for the round geometry, and 0.91% for the triangular geometry, thus giving an average of 1.0 % with a relatively small standard error of 0.068 %. The relatively small standard error implies that relative volumetric springback of Grade A compacts is practically independent of geometry while the almost identical averages with and without hold-down imply its independence of the this setting. The grade B relative volumetric springback results were consistent with the above. The relative volumetric springback of Grade B compacts with hold-down was 0.81 % for the square geometry, 0.87 % for the round geometry, and 0.97 % for the triangular geometry yielding an average of 0.88 % ± 0.047 %, which on the basis of an even smaller standard error could also therefore be classified as geometry independent. The same is true of the Grade B result without hold-down, the average value of which was 0.89 % ± 0.029 %. The comparison of the Grade A and Grade B averages above shows a difference between them of 0.11 % – true of both results with hold-down and without – which is of the same order of magnitude as the above standard errors and allows for the relative volumetric springback to be classified as materially independent.

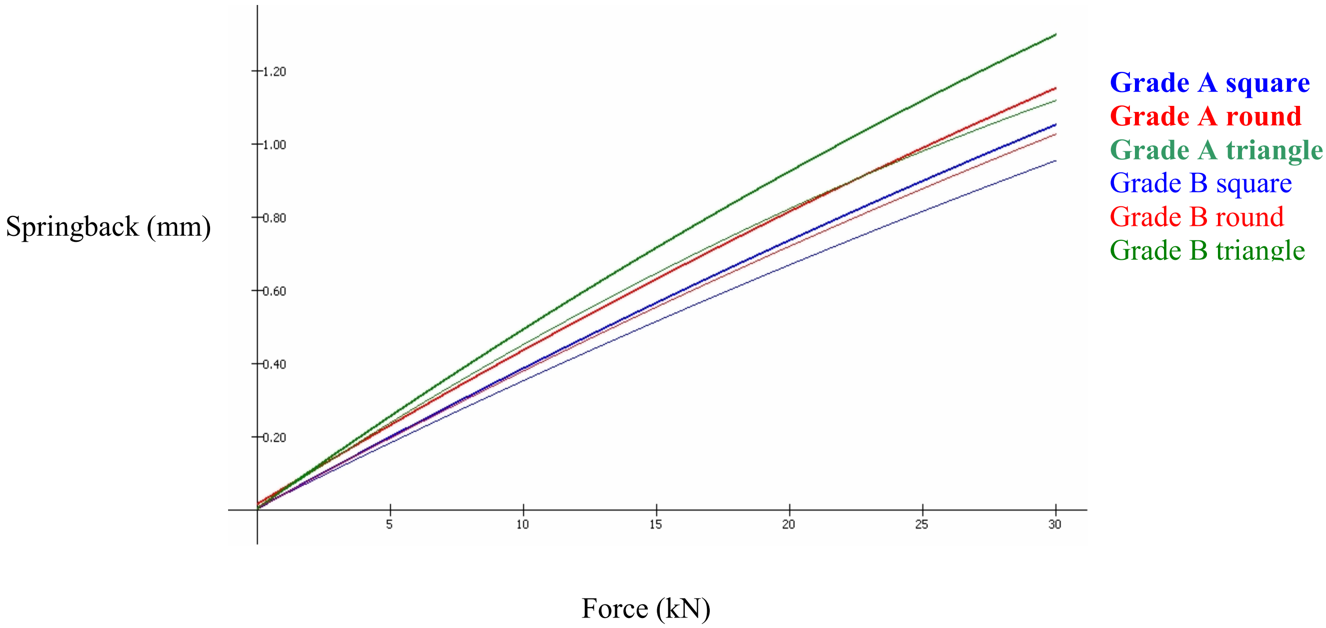

a) With hold-down

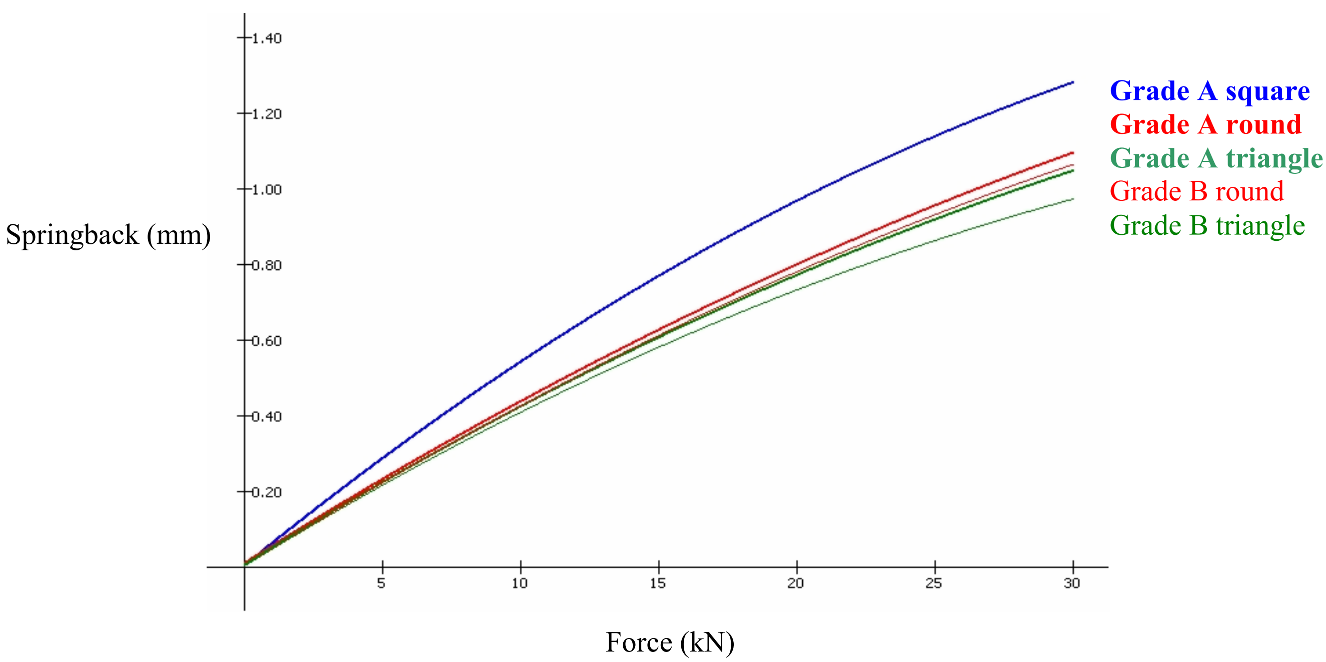

b) Without hold-down (Grade B square geometry excluded)

Figure 35 Change in relative volumetric springback with pressing force for SBA Grade A and Grade B geometries pressed a) with and b) without hold-down.

The geometric independence of the relative volumetric springback implies that the absolute volumetric springback in SBA compacts appears to be directly proportional to the initial size i.e. in-die volume of the compact just before springback. This explains why the absolute volumetric springback of the triangular geometry was larger than that of the other two geometries in the above analysis. However, the same conclusion cannot be extended to tight-fitting compacts for which the relative volumetric springback values were significantly larger than that of the SBA compacts.

7.2.10 Effect of geometry and material on the change in green density with pressure under varying hold-down conditions.

The variation of green density with pressure again followed a logarithmic trend in all cases. This was a common feature of both tight-fit and SBA compacts. Furthermore, the observed trends in the SBA data were very similar to the tight-fitting data. The green density appeared to be both geometry and somewhat material dependant regardless of the hold-down setting. As with tight-fit Grade A compacts, at pressures corresponding to typical pressing forces of around 25 kN, the green density values for the round and square SBA geometries were practically indistinguishable, while the green density of the triangular geometry was noticeably lower. For example, at a typical pressure of 20 kN/cm^2, green density of the square and round geometry was approximately 7.86 g/cm^3 (7.80 g/cm^3 in the case of tight-fit compacts), while that of the triangular geometry was 6.77 g/cm^3 (7.03 g/cm^3 in the tight-fit case). This gives a relative difference of approximately 14 % (10 % previously in the tight-fit case) implying a slight geometry dependence as before.

However, unlike the tight-fit findings where this relative difference was more pronounced in the Grade B compacts, practically the same relative difference was observed in the Grade B SBA compacts as in the Grade A SBA compacts. At the same typical pressure, green density of the square and round Grade B SBA geometries was approximately 8.57 g/cm^3 (8.40 g/cm^3 and 8.37 g/cm^3 previously) in both cases. The same for the triangular geometry was 7.43 g/cm^3 (7.20 g/cm^3 previously) making the relative difference between the round/square and triangular geometries equal to approximately 13 %. This is quite similar to the Grade A SBA result of 14 %. Therefore geometry dependence of green density was evident also in the Grade B SBA compacts. In addition, the slight material dependence mentioned previously is also clear from the above values. For example, the relative difference between the square (or round since they are the same) Grade A and Grade B SBA geometries is only 8.3 % while that for the triangular Grade A and Grade B geometry is only 8.9 %.

Thus the findings in the SBA are not too dissimilar from the tight-fit data; only the SBA results are a little more consistent owing probably to the significantly less pronounced frictional effects between the compacts and the die-wall. The same previous observations hold here too; the smaller round and square compacts have higher green densities than the triangular compacts regardless of the compaction material while the green densities of Grade B compacts exceed those of Grade A compacts at the same compaction pressures. The latter statement of the previous sentence implies that in order to achieve the same levels of compaction densities in Grade A as in Grade B, higher pressing forces are required.

7.2.11 Effect of geometry and compaction material on the change in springback with green density under varying hold-down conditions

Variation of springback with green density of SBA compacts was slightly different from that of tight-fit compacts. Both linear and volumetric springback of all SBA compacts exhibited quadratically increasing behaviour – and not exponential behaviour as seen previously – with green density until reaching a critical value. In addition, no clear trend was noticeable in the pressing force values corresponding to the breakdown points while in the tight-fit case these appeared to be geometry independent. Other than being geometry and material dependant, the critical values for the SBA compacts appeared to be highly sensitive to the hold-down condition as discussed below.

As seen in Figure 36 the following breakdown values were obtained for the SBA compacts. For the square, round and triangular Grade A geometries with hold-down, the breakdowns occurred at green densities of 8.77 g/cm^3, 8.78 g/cm^3, and 7.07 g/cm^3 respectively. The corresponding pressing forces were 86.3 kN, 72.6 kN, and 53.0 kN respectively. Without hold-down, the green densities for the three geometries were 7.94 g/cm^3, 8.40 g/cm^3, and 6.79 g/cm^3 respectively for which the corresponding forces were 30.6 kN, 46.9 kN, and 34.6 kN. These values highlight the significant geometry induced differences on the springback vs. green density data; particularly the sensitivity to hold-down, the presence of which appeared to delay the breakdown in the linearity of the data. Similar conclusions can be drawn from the Grade B results. For the square, round and triangular geometries with hold-down, the breakdowns occurred at green densities of 9.21 g/cm^3, 8.99 g/cm^3, and 7.45 g/cm^3 respectively. The corresponding pressing forces were 77.0 kN, 51.8 kN, and 45.9 kN respectively. Without hold down the green densities in the same order of geometries as above were 8.77 g/cm^3, 8.74 g/cm^3, and 7.23 g/cm^3 while the corresponding pressing forces were 44.3 kN, 37.7 kN, and 33.3 kN. A comparison with the Grade A values shows that they are for most part quite different indicating a strong material dependence of the breakdown points.

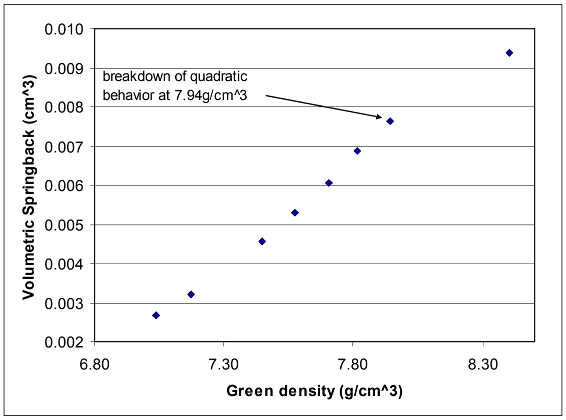

a) Square Grade A geometry

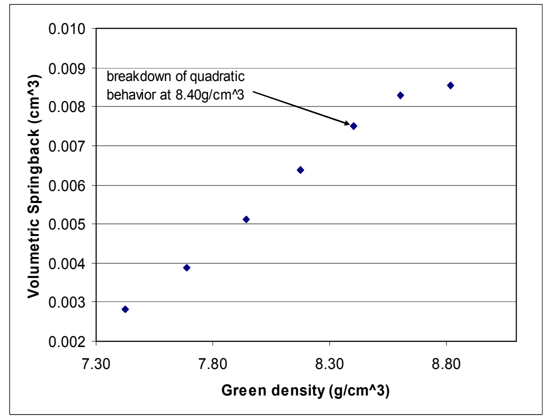

b) Round Grade A geometry

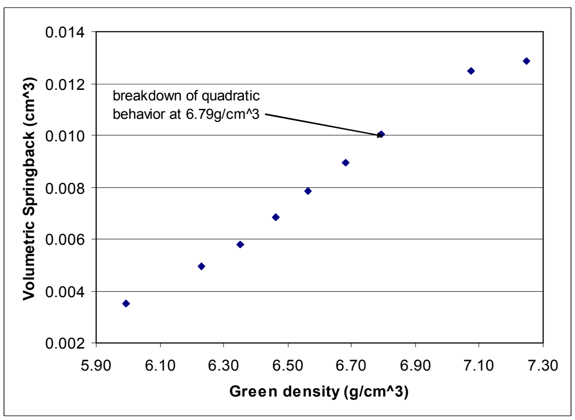

c) Triangular Grade A geometry

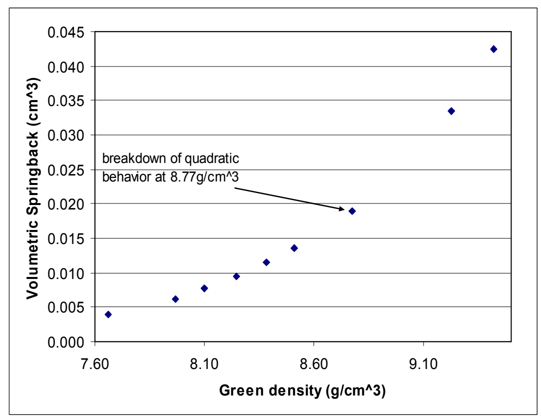

d) Square Grade B geometry

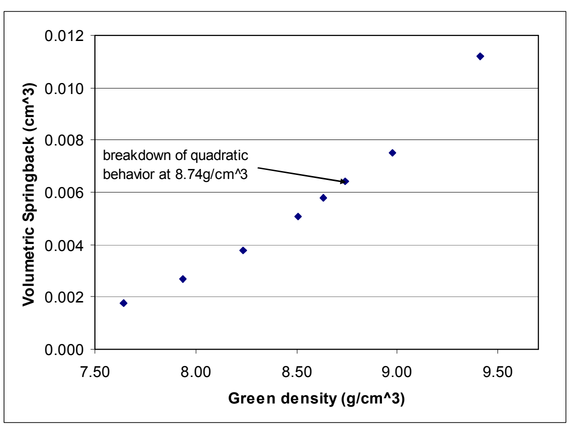

e) Round Grade B geometry

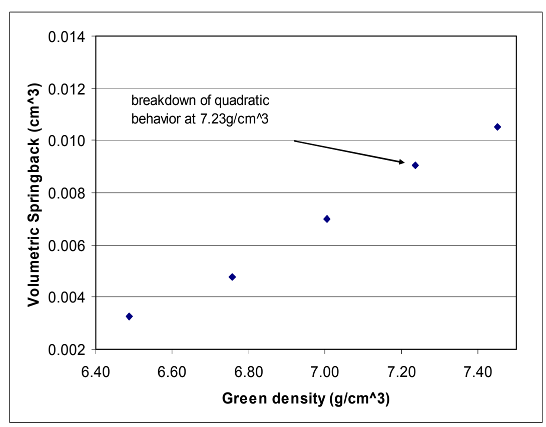

f) Triangular Grade B geometry

Figure 36 variation of volumetric springback with green density for Grade A and Grade B compacts without hold-down.

Thus true springback behaviour when analyzed as function of the green density, over quite a wide range of densities, is a quadratically increasing function until a breakdown point is reached. In tight-fitting compacts exponential behaviour may have been observed only as a result of a smaller force range having been considered. Indeed an exponential behaviour would have adequately described the SBA data too had the range of pressing forces been confined to between 0 kN and 30 kN for example.

7.2.12 Comparison between the effects of punch contraction and axial springback on vertical compact dimensions

Using equations 90, 102, and 108 the total effect of tool and machine contraction on the vertical dimensions of the compacts at 25 kN was calculated to be 0.071 mm, 0.076 mm, and 0.074 mm for the square, round, and triangular tools respectively. Comparing these values with the averages calculated in Section 7.2.7 shows that the effect of tool contraction on the vertical dimensions of SBA compacts is significantly greater than that of springback. The effect of contraction is on average about 2.2 times larger than springback with hold-down and 3.9 times larger than springback without hold-down.

7.2.13 Edge formation in SBA compacts

Near perfectly sharp edge condition as well as the presence of an additional measurable quantity or dimension in the SBA compacts suggests that these compacts are formed in an unexpectedly different new way to their tight-fit counterparts. The measurable quantity in question is the edge width or thickness as seen by looking at the compact directly from the top and it represents an area of the compact which appears to be formed purely by the presence of sufficiently large compaction pressures in the vicinity of the top punch while it is in the final pressing position and not by direct contact between the top punch and the material as is the case in tight-fit compacts. The compact edge is believed to be formed horizontally across in the area between the top punch and positive die face as indicated in Figure 37.

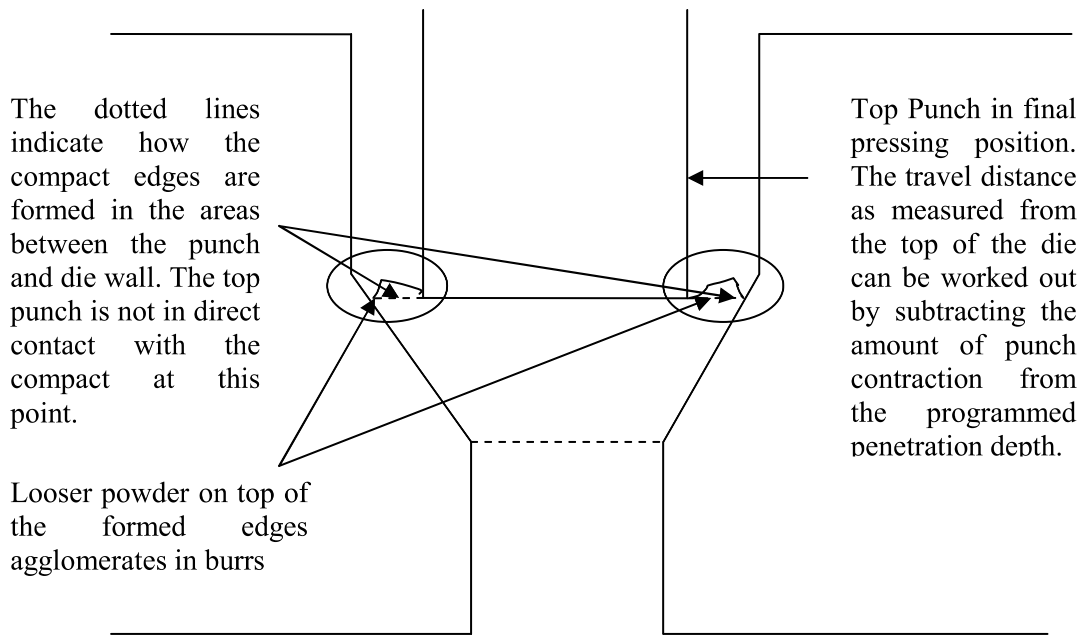

Figure 37: Two dimensional view of compact formation in an SBA die.

Adding the dimension of depth to the above figure, the formation of compact edges might better be represented in the following 3D see-through view of the die:

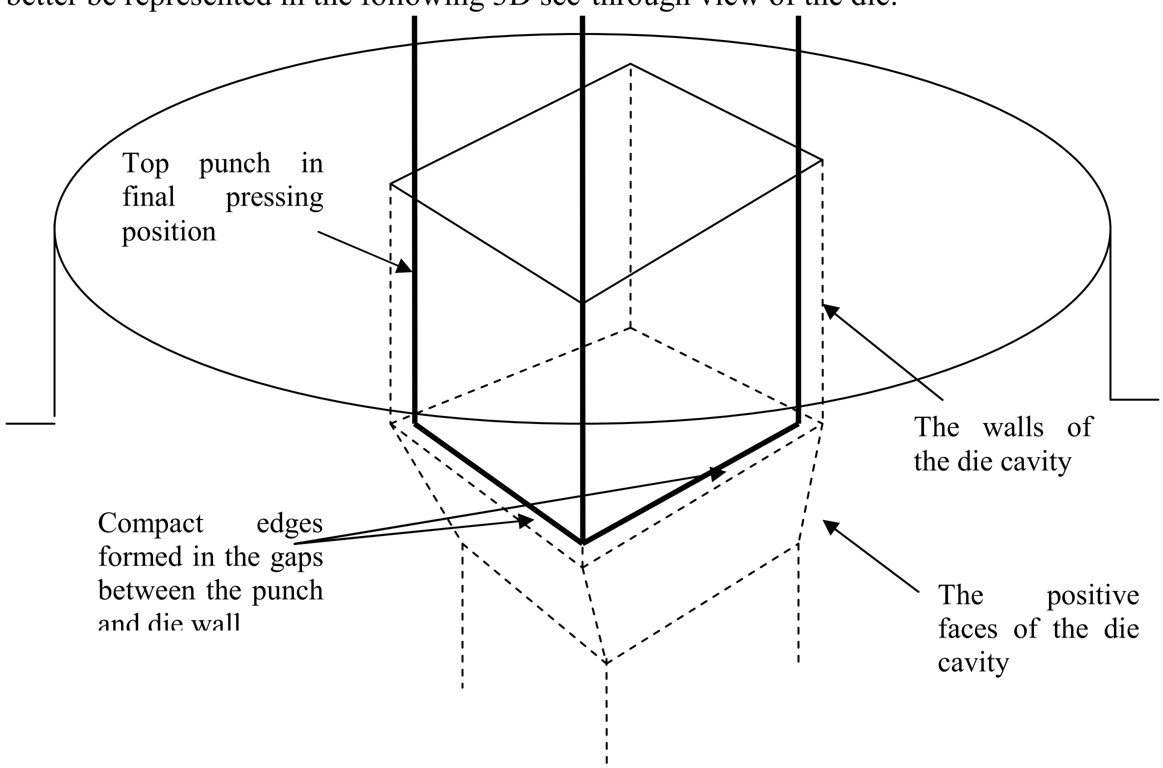

Figure 38: A three dimensional view of the compact edge formation in the square SBA insert.

As seen from the data in Section 6.3 and Tables 12, 18, 79, 85, 91, 97, 103, 109, 115, 121, 127, and 133, the values are as expected generally increasing with increasing pressing force though the individual measurements themselves are not very accurate. The measurements range in value from about 0.020 mm to 0.040 mm indicating that they are slightly larger than one would expect given the final pressing positions of the top punch corresponding to each component pressed. The following calculation for the square compact compacted at a typical pressing force of 26.8 kN, in conjunction with an enlarged section of the above figure helps to clarify this statement (refer to Figure 39).

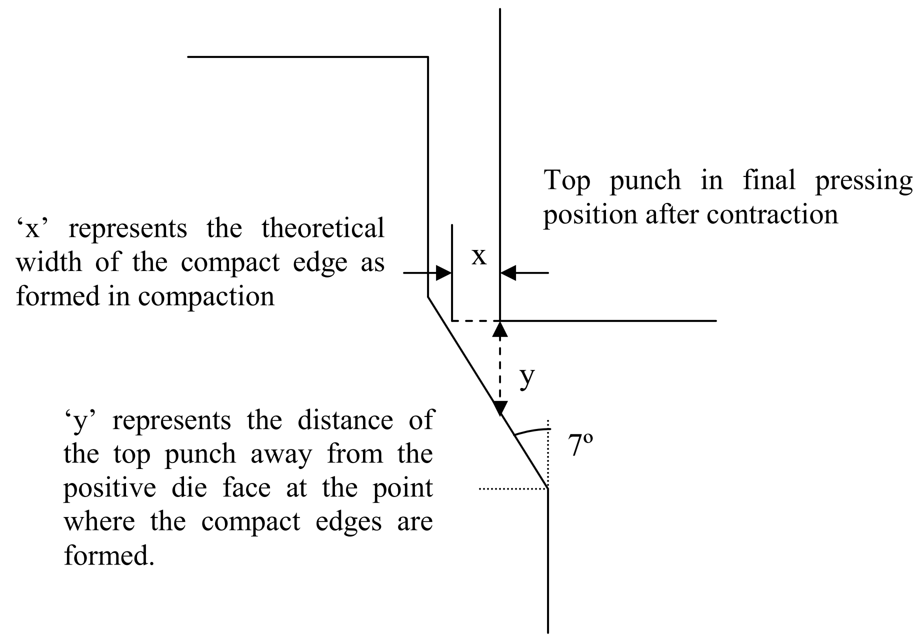

Figure 39: An enlarged section of the edge formation area.

In the experiments 'PD' was chosen so that the theoretical distance 'y' was 0.100 mm before contraction for all the compact geometries tested. At 26.8 kN for the square compact, the upper punch and ram experience approximately 0.052 mm of combined contraction (as calculated based on previously determined contraction constants) making the actual distance 'y' of the upper punch away from the collision point approximately 0.152 mm. Given that the angle of the positive die face as measured from the vertical is 7 degrees for all tools this means that the theoretical edge width 'x' in this example is given by:

$$x = y \tan 7^{o} = 0.152 \tan 7^{o} \approx 0.019 \text{ mm} \qquad \ldots (80)$$

However, the measured edge width on the actual component was 0.024 mm as seen in Table 12. The difference although not large in absolute terms shows that it is difficult to make accurate predictions about the final pressing position of the upper punch through measurements of edge thickness. In some cases, if calculated in the same way to the above, the difference between the calculated values and the measured values as recorded in the tables of Section 6.3 is even greater. There are several reasons for these inconsistencies and they are listed as well as explained below:

1 Burr removal
2 Alignment of the upper punch with respect to the die
3 Springback

In order to make height and diametrical measurements as accurately as possible the burr as shown in Figure 40 has to be removed from the compact. However current deburring techniques involve contact between the deburring medium such as a fine bristle brush and the compact which inevitably leads to some rounding or smudging of the edge which increases the width of the edge and makes it appear larger than it actually is at the time of formation. The following figure aims to help explain the effect of the brushing action on the compact edge.

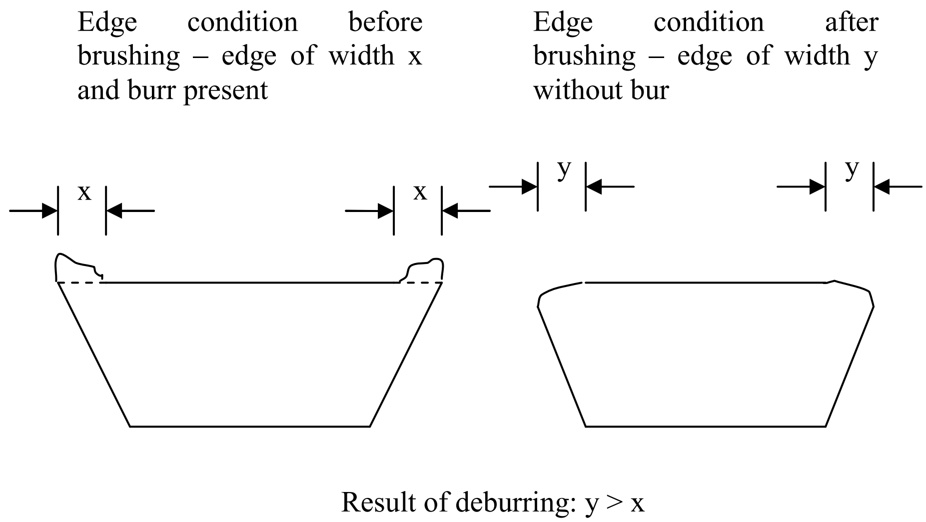

Figure 40: The effect of deburring on the compact edge, particularly the edge width as viewed from the top.

In the course of the experiment it was found that the closer the final pressing position of the upper punch was to the positive die face i.e. at lower pressing forces, the smaller was the width of the formed edge and consequently smaller was the burr that formed above it. The consequence of this was that the underlying edge was stronger and the smaller burr was easier to remove leaving a less rounded edge behind; a result which has significant implications on the general production of light cutting inserts. In a production environment of these types of inserts, a sharp edge is one of the most desirable features to have on the green compact. As a side goal, it was found that when the compact edges after deburring were in the range 0.020 mm to 0.030 mm, the final sintered and blasted insert quality was acceptable. This puts additional demands on the final pressing position of the upper punch that needs to be achieved in production in order to attain such high quality standards. Accurate control over the final pressing positions of the upper punch and therefore accurate knowledge of the amount of punch-ram contraction in pressing is required justifying the need for a project of this kind.

An incorrect alignment of the upper punch with respect to the die can result in different size edges being formed depending on the compact as shown in the below figure. The error in alignment can result either from an incorrect upper ram chuck position i.e. a machine related issue, or badly centralized punch; a result of an inaccuracy in the tool manufacture process (refer to Figure 41).

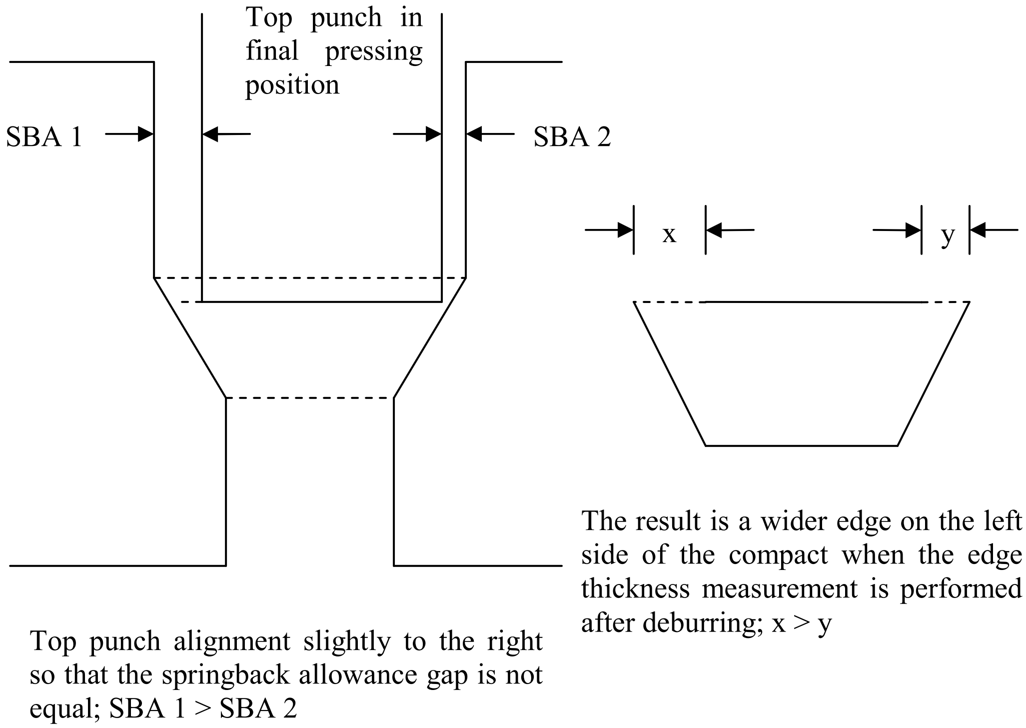

Figure 41: The effect of punch alignment on the compact edge.

A comparison of the compact edges on the square compact geometry revealed that indeed there was some error in the punch alignment as the all four compact edges had slightly different dimensions. This was confirmed by measuring the sides and the periphery of the triangular and round compacts respectively all which had slightly varying dimensions as shown in the below figure (refer to Figure 42).

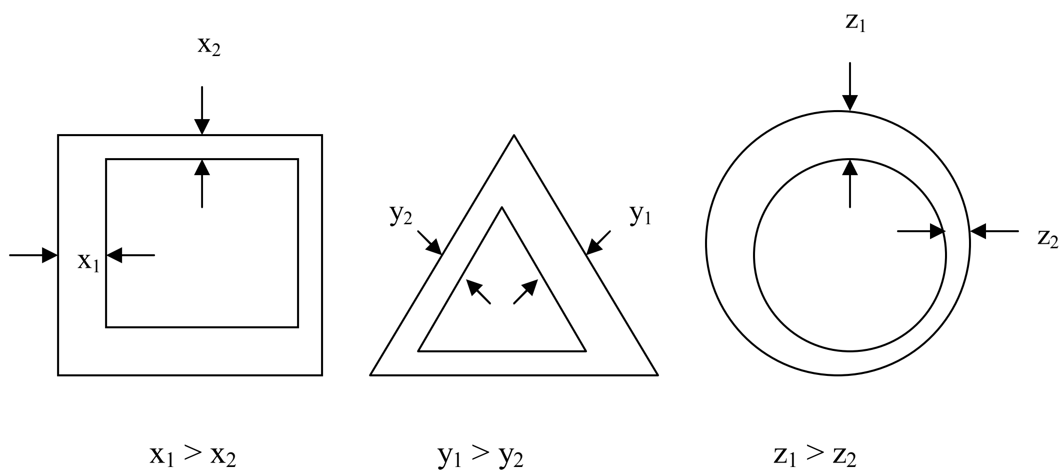

Figure 42: the effect of alignment on the compact edge as view from the top.

Since it was only learnt much later in the course of this work that the edge thickness could be used as an approximate measure of the final pressing position of the upper punch it was too late to correct this error and repeat the experiments in order to check the consistency of the measured results for edge-width against those predicted by the punch contraction values as done in the above calculation (refer to Equation 80). Thus the source of the error, whether it was introduced as a result of poorly manufactured punches or a slightly de-centralized upper ram chuck was not investigated as a part of this experiment. Having said this, the accuracy of the edge width measurements were not of critical importance to this experiment the focus of which, was as explained, primarily the characterization of the effect of springback, punch contraction and tool design on the near-net compact shape.

Finally the effect that springback has on the edge dimension is unknown and was not measured in the course of this experiment. If this effect is similar to the previously determined values which in all cases regardless of whether the axial or radial component was considered, were less than 1.0 % of the starting compact dimension, then it is unlikely that springback would make a considerable contribution to the final measured width of the compact edge. However, it was also previously established that springback is not necessarily uniform and may be greater in certain parts of the compact than other, particularly in the upper regions, and so no definite conclusions can be drawn in regard to this matter.

7.2.14 Lip formation in SBA compacts

From Section 6.3 it can be seen that under certain conditions normally non-lip bearing SBA compacts can develop this feature and therefore become essentially identical in appearance to tight-fitting compacts. Upon a more detailed examination it can be seen that this occurs only at a considerably large pressing force or more specifically at an IC value of the compact diameter that corresponds closely or is larger than the IC of the die which can only occur at very high pressing forces. Furthermore the lip first began to form at the compact corners as seen from the larger corner lip values in Tables 12, 18, 79, 85, 91, 97, 103, 109, 115, 121, 127, and 133.

For example at 124.3 kN of pressing force the radial springback of the square Grade A compact pressed with hold-down resulted in the final compact IC of approximately 11.88 mm (refer to Table 12). The die dimension corresponding to this compact was also 11.88 mm (refer to Tables A2 and A3 in Appendix B). A lip of approximately 0.106 mm was seen on this compact confirming the first statement of the previous paragraph. As established previously, without hold-down the absolute radial springback at the same pressing force is greater than with hold-down. Thus at a much smaller pressing force of 85.7 kN the IC of the square Grade A component was measured at approximately 11.90 mm (refer to Table 18) i.e. slightly larger than the die diameter. An even larger lip of 0.192 mm could be seen on this compact. Similarly, for the round Grade B compact pressed with and without hold-down the measured IC values were approximately 12.49 mm and 12.48 mm respectively (refer to Tables 103 and 109) while the corresponding die diameter was approximately 12.47 mm (refer to Tables A2 and A3 in Appendix B). This resulted in lips on both compacts of 0.268 mm and 0.304 mm respectively.

However, when the measured compact ICs were smaller than the die dimension no lip was seen on the compacts. For example, no lip was seen on the round Grade A compacts pressed with and without hold-down, for which the measured ICs were approximately 12.44 mm (at 109.0 kN) and 12.45 mm (at 91.6 kN) respectively, i.e. slightly smaller than the die dimension. Similarly no lip was seen on the triangular Grade A compacts pressed with and without hold-down, the measured IC dimension of which was approximately 11.87 mm for both compacts, i.e. about 0.010 mm smaller than the die dimension of 11.88 mm.

The following explanation is offered for the emergence of lip seen above:

When the compact IC is more or less equal to or greater than the die diameter then the compact must obviously be in contact with the die at some point during the ejection and since the lip dimension was observed only on those SBA compacts whose ICs were greater than or equal to the corresponding die diameters, that must mean that the formation of the lip in SBA compacts can result purely from contact and scuffing of the otherwise sharp compact edges against the sides of the die.

Thus the two ways that a lip can result from compaction in a die with an SBA clearance is if the final pressing position (i.e. after punch-ram contraction) of the upper punch is above the leadin (refer to Figure 43) – as in tight-fit compaction – or if the final pressing position of the upper punch is well below the leadin, the compact IC after radial springback (which for an SBA die takes place inside the die) is equal to or greater than the die diameter and results in contact between the compact edges and the die during ejection (refer to Figure 44).

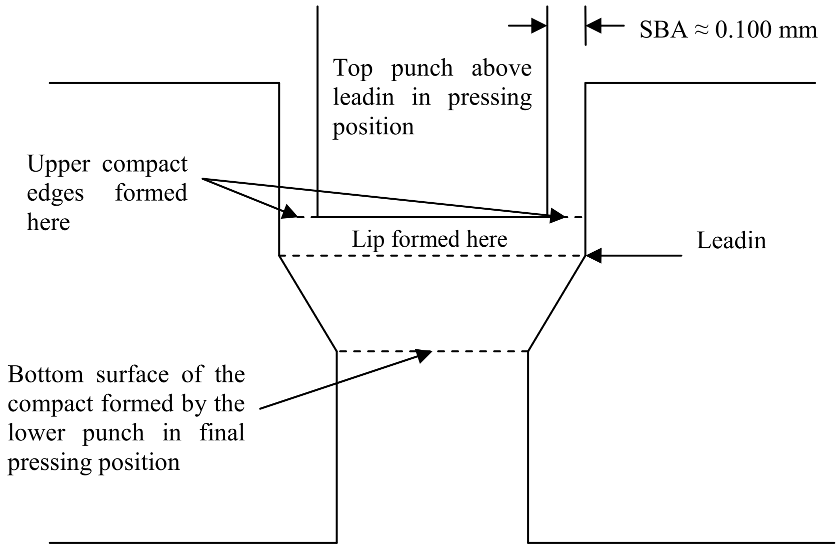

Figure 43: Lip-bearing, tight-fit like SBA compacts can be formed when the final pressing position of the upper punch is above the leadin as shown. Here the compact with the lip is formed naturally in compaction as defined by the shape of the die cavity and the final pressing position of the punches.

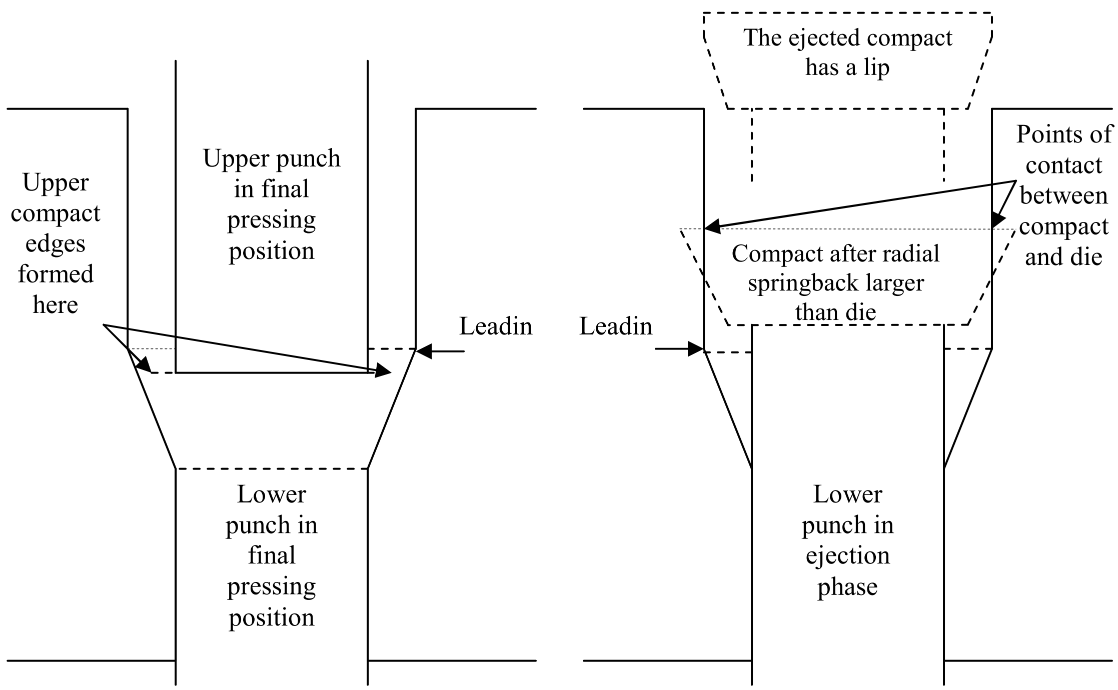

a) Upper punch in final pressing position **b)** Ejecting component after springback

Figure 44: Lip-bearing, tight-fit like SBA compacts can be formed when the final pressing position of the upper punch is below the leadin **a)**, and after radial springback **b)** the compact dimensions exceed the die dimensions leading to contact between the edges and die, and the subsequent formation of the lip.

In the above mentioned case of the triangular Grade A compacts where no lip was seen along the straight edges of the compact, a small corner lip dimension was starting to emerge suggesting that the radial springback and therefore the radial dimensions of the compact extremities are slightly greater, re-enforcing the previously proposed explanation that the corner lip expansion is a result of increased radial springback in compact corners, the concentrators of green density.

8 Conclusions

1 The contraction behaviour of the machine-tool system in the vertical direction along any point of the machine-tool system was found to be slightly quadratic. However the quadratic coefficients were all found to be so small that when the contraction equations were approximated by straight lines with zero intercepts, the difference in the R^2 values was for all practical purposes negligible. An even greater degree of non-elasticity was observed in compact springback particularly in that of tight-fit compacts. The springback behaviour of tight-fit compacts varied also as a quadratic function of the pressing force but with quadratic coefficients of approximately one order of magnitude greater than those observed in the contraction equations. A similar non-straight line springback behaviour with pressing force was observed in SBA compacts, however like those of the contraction results, the quadratic coefficients of the SBA equations turned out to be approximately one order of magnitude smaller than those of tight-fit compacts and the springback behaviour could thus over the same typical range of pressing forces adequately be described by straight line equations (refer to Equations 74 to 79 of section 7.2.2). A closer examination of the SBA compact behaviour revealed that the most significant deviation from straight line behaviour occurred at very high pressing forces when the compact IC approached the diameter of die, i.e. near to or at contact with the die wall, suggesting that although the observed non-elasticity in the contraction and springback behaviour appears to be a natural material property of soft and hard WC-Co, it is significantly more pronounced in the presence of friction or contact with the die wall. This coincides with the formation of a lip on SBA compacts and thus a transformation of geometry from one of sharp compact edges to one with lip bearing edges. This explanation is reinforced by the more spring-like character observed in SBA compacts compared to the tight-fit compacts which over the same range of pressing forces (0 kN to 30 kN) exhibited a significantly greater degree of quadratic behaviour i.e. most likely the result of rubbing and friction due to contact with the die wall.

2 The experimental method chosen for the evaluation of machine-tool contraction enabled the determination of the effect of springback on the compact dimensions. The contraction behaviour was determined by an independent method and subtracted from the change in linear dimensions leaving the effect of springback as the result. In addition, the specific contraction measurements such as the contraction of the upper punch-ram are particularly useful. This quantity for example influences the final pressing position of the upper punch and thus has a direct effect on the quality of the upper cutting edges of the pressed compacts. It was shown that for practical purposes this quantity can be treated as a linearly varying function of force that is independent of tool geometry. The upper punch-ram contraction can be approximated by the following relationship obtained from both tight-fitting and SBA tool results:

$$\Delta L_{\text{Upper Punch-Ram}} = 2.0\times10^{-3}\ \text{mm/kN} \pm 0.7\times10^{-4}\ \text{mm/kN}$$

3 In tight-fit compacts the greatest dimensional change was observed in the lip dimension. For example, the change in the lip dimension was greater than the change in

the total height of the compact suggesting differential springback behaviour of different compact regions. Thus the 'H-L' dimension below the compact lip appeared to be a decreasing function of force. Two theories were proposed to explain this. One possibility was that the nature of decompression in a tight-fitting die favours axial expansion of the upper compact regions i.e. the lip area, and the other that radial force of the compact against the die wall as a result of the radial component of springback, leads to rubbing and subsequent smearing of the lip dimensions which creates an impression of increased springback in this area. Although both effects could be taking place, the enlargement of the lip dimension due to contact with the die wall was almost certainly shown to be true. As seen in the SBA experiments, even when the final pressing position of the upper punch was below the 'leadin' it was possible for the lip to form provided enough radial expansion occurred to result in compact to die-wall contact.

4 A comparison between total axial and radial springback behaviour in tight-fit compacts showed that for Grade A axial springback was in all cases, regardless of the compact geometry, larger than radial springback. However, the same result could not be reproduced with the Grade B tight-fit compacts where in some cases radial springback was greater than axial springback. Three explanations were offered for the inconsistency in this result, namely: the non-linear effect of die-wall friction on the compact springback, an inherent inaccuracy in the experimental method such as the lack of sensitivity of certain measuring techniques (e.g. measurement of radial springback using Vernier callipers), and the possibility of human measuring error. The exact source of the imprecision could not be determined on the basis of the accumulated results however since identical experimental methods and measuring procedures were used in the collection of SBA results which proved to be significantly more consistent, the above inconsistency is most likely the result of non-linear die-wall frictional effects on the compact springback.

The relative axial springback defined as a percentage of the initial or starting axial dimension of the compact before springback, was in all cases found to be greater than the relative radial springback, defined as a percentage of the initial or starting radial dimension of the compact before springback. This result was shown to be true regardless of the compact geometry or material. Thus relative to their respective starting dimensions axial springback was in all cases greater than radial springback for tight-fit compacts. Neither relative axial nor radial springback of any tight-fit compact exceeded 2.0 %, a result similar to Liu and Fu's [27] result for Silicon Carbide powder with PEG below glass transition temperature.

The difference between the axial and radial springback behaviour of SBA compacts appeared to be strongly dependant on the hold-down setting. Unlike tight-fit compaction, SBA compaction allowed for compacts to be formed without the use of the hold-down force during ejection due to the absence of frictional and other effects associated with die-wall contact. Thus both sets of compacts could be compared; those whose decompression behaviour was influenced by the hold-down force and those whose decompression behaviour was natural and unaffected by hold-down. The obtained results were highly unexpected and showed that the application of the hold-down pressure during ejection favoured axial springback while free and natural expansion behaviour as uninfluenced by hold-down, appears to favour radial expansion. This result was non-intuitive since hold-down is applied axially along the vertical axis of the compact and was therefore expected to contain axial expansion and promote radial expansion in the space between the compact and the die wall (springback allowance gap). The result was found to be true regardless of geometry and material used in compaction. An explanation for this behaviour has not as yet been determined.

An examination of the relative axial and radial springback behaviour was in excellent agreement with the above findings. The relative axial springback was greater than the relative radial springback in all cases when the hold-down was present while relative radial springback was greater than the relative axial springback in all cases when the hold-down was not used and the compacts were allowed to expand completely freely. A comparison with the relative springback behaviour of tight-fit compacts reveals one major difference. Although the relative radial springback behaviour between the two types of compacts was found to be relatively similar the relative axial springback of tight-fitting compacts was significantly greater than that of SBA compacts which is further evidence in support of the previously suggested explanation that decompression in tight-fitting dies favours axial expansion. For example, the relative axial springback of tight-fit compacts was in all cases greater than 1.0 % (of the initial compact dimension) while that for the SBA compacts was in all cases less than 1.0 %.

5 Both total axial and radial springback of tight-fit compacts were found to be geometry and material dependant. Thus in addition to varying with force these quantities varied with the type of compact geometry and material used in compaction. These findings were also true of both relative axial and radial springback. This was not a positive result as it implied that linear springback was an essentially unpredictable quantity, varying from one compact geometry to another. However an examination of the axial and radial springback data of SBA compacts revealed that the free springback behaviour as unaffected by friction was in fact for all practical purposes both geometry and material independent and dependant only on the pressing force as well as the programmed hold-down setting. For example, with hold-down, axial springback at a typical pressing force of 25 kN for the range of tested shapes and materials was found to be approximately 0.034 mm. The same value without hold-down was 0.019 mm, a difference of approximately 44 %. Similarly, at a pressing force of 25 kN, an average radial springback of 0.023 mm was observed with hold-down while the same value without hold-down was 0.062 mm, a difference of approximately 63 %.

Similar results were observed for relative axial and radial springback behaviour of SBA compacts; the material and geometric independence being true when initial dimensions were accounted for. At 25 kN a value of 0.71 % was found to be a fairly accurate representation of the average relative axial springback with hold-down for all compact shapes and materials, while 0.39 % was a good estimate of the same quantity without hold-down. In the case of the radial component the same averages were 0.18 % with hold-down and 0.50 % without hold-down.

For instance, a light cutting diamond shaped positive insert compacted using Grade A powder and without hold-down might also be expected to experience radial expansion up to 0.50 % of its original size upon ejection from the die. This is a useful piece of information to have in the tool design stage, when it is necessary to choose the right springback allowance in order to ensure adequate clearance and avoid contact between the insert and the die wall. As shown, contact can lead to the development of lip which in light-cutting inserts is an unwanted feature and can lead to premature failure of the insert in machining operation.

6 In view of the above results similar conclusions were expectedly reached for the behaviour of volumetric springback, a measure of the total compact springback. Absolute volumetric springback of tight-fit compacts was found to be dependent on both geometry and material used in compaction. Similar findings were observed for the relative or fractional volumetric springback except in the case of Grade A compacts, where the relative volumetric springback appeared to be only slightly geometry dependant. Again this was not a positive result since in order to draw general conclusions about springback, which could be applied to other compact geometries in future, it would have been useful to find that springback was dependant on as few parameters as possible, e.g. only the pressing force. However when the SBA data for volumetric springback was analyzed the results were once again more encouraging, as was the case with the above one-dimensional springback behaviours. Although the volumetric springback of SBA compacts was found to be geometry dependant, it was found that the free relative volumetric springback was independent of all these factors and varied only as a function of the pressing force. This meant that when the original compact dimensions were accounted for any of the relationships given by Equations 176, 185, 194, 203, 212, 221, 230, 239, 248, 257, 266, and 275 could be used to approximate the amount of fractional springback any one compact would be expected to experience. The effect of different geometric, material, and press setting factors would be embodied in a single quantity, namely the pressing force.

This result explains why the absolute volumetric springback appeared to be geometry dependant and proportional to the initial size or in-die volume of the compact just before springback. For example the largest absolute volumetric springback was observed in the triangular compacts which were also originally largest in volume. Comparison of SBA results with those of tight-fit compacts showed that the same conclusion could not be extended to this case. This could be due to a marked geometrical difference between the two sets of compacts, namely the presence of a lip in the tight-fitting case as well as the presence of friction which has already been mentioned appears to be highly non-linear and therefore unpredictable in its effect on springback.

Although volumetric springback is not as useful a quantity as the springback of a single axial or radial linear dimension, these results are still significant as they reveal something important and perhaps not so unexpected about the natural behaviour of springback in compacts when observed in its totality through a parameter like volumetric springback, and that is namely that volumetric springback occurs in some kind of proportion to the original or starting size of the compact and that this fact is true regardless of the compact geometry, material, or press setting used in compaction. Thus where one-dimensional springback can be rather sensitive to certain compaction parameters such as the application of hold-down during ejection, relative volumetric springback is not and depends in all cases only one quantity, the pressing force. As mentioned, this is perhaps not so surprising since in the absence of friction, conservation of energy in compaction would ensure that despite different axial and radial compact dimensions, which might have resulted in certain cases from different hold-down or other conditions, volumetric springback is constant and same in both cases. The relative volumetric springback for the range of compact geometries and materials tested in this work was found to be approximately equal to 1.0 % of the initial compact volume.

7 The green density of tight-fit compacts was found to vary logarithmically with compaction pressure. Pressure was chosen as the independent variable instead of force because green density is often plotted as a function of pressure in literature. Logarithmic relationships between these two variables were observed also by other authors van der Voort Maarschalk *et al* [29]. The green density as plotted against pressure was found to be dependent on both geometry and compaction material. Regardless of material type the smallest green densities were observed for the triangular shape while regardless of geometry, Grade B green densities were significantly larger than those of Grade A. These results were compared against those of SBA compacts. The same but slightly more consistent results were also observed with these compacts; the smaller round and square compacts had higher green densities than the triangular compacts regardless of the compaction material, while the green densities of Grade B compacts exceed those of Grade A compacts at the same compaction pressures. The latter statement of the previous sentence meant that in order to achieve the same levels of compaction densities in Grade A as in Grade B, higher pressing forces would have been required.

8 Over the range of pressing forces typically encountered in production, both linear and volumetric springback of tight-fit compacts, was found to vary exponentially with green density upon reaching a certain critical value which was characterized by a sudden decrease or plateauing in the rate of expansion of the compacts. These critical points seemed to occur at approximately the same pressing force regardless of the compact geometry, approximately 20 kN. The critical points were found also in SBA data but at significantly higher pressures. In addition both linear and volumetric springback of all SBA compacts exhibited quadratically increasing behaviour with green density – and not exponential behaviour as seen in the tight-fitting compacts. Thus true springback behaviour when analyzed as function of the green density, over a wide range of densities, is a quadratically increasing function until the breakdown point. In tight-fitting compacts exponential behaviour may have been observed only as a result of a smaller force range having been considered. Indeed an exponential behaviour might have adequately described the SBA data too had it been confined to a smaller pressing force range.

In SBA compact, no clear trend was noticeable in the pressing force values corresponding to the breakdown points while in the tight-fit case these appeared to be geometry independent. Other than being geometry and material dependant, the critical values for the SBA compacts appeared to be highly sensitive to the hold-down condition.

The reasons for the existence of the critical points are not clear to the author except that in SBA compacts they seemed to coincide with the formation of a lip and the resulting sudden increase in, or appearance of friction. As a result of the quadratically varying relationship between springback and green density in compacts a possible explanation for the observed increases in lip size at the corners of tight-fit compacts could be suggested. It was reasoned that the greater expansion of the lip at the compact corners is a result of greater green densities in these areas of the compact. Consequently greater radial pressures due to the radial component of springback can lead to greater scuffing and deformation of the compact corners. This explanation appeared to be consistent with the SBA data findings which showed that lip formation occurred only when the compacts experienced contact with the die wall and first started to appear at the compact corners. These findings were in contrast to those of Nam *et al* [25] who observed that expansions in low density zones of spray dried alumina powder were always larger than in low density zones.

9 A comparison between the effects of contraction and springback on the axial linear dimension of the tight-fit compacts showed that the comparison depended on the type of material used in compaction. For instance the effects of contraction and springback were comparable in the case of Grade A compacts but because axial springback of Grade B geometries was significantly lower than that of Grade A, the effect of contraction on the dimensions of these compacts was greater than that of springback. In the case of SBA compacts where smaller axial expansions to those of tight-fit compacts were observed, the effect of contraction on the axial dimensions of the compacts was about 2.2 times larger than that of axial springback when hold-down was applied in ejection and 3.9 times larger without hold-down.

10 Where as lip formation is a natural phenomenon in tight-fit compaction where the final pressing position of the upper punch is always above the leadin[21], it can also occur in SBA compacts where the final pressing position of the upper punch is below the leadin and normally quite close to the die, but only at unusually high pressing forces, when the compact diameter is sufficiently large that it makes contact with the die wall during ejection, leading to scuffing and associated frictional effects. This result is not expected to raise any practical concerns as far as the production of light-cutting inserts is concerned since the pressing forces encountered in production are typically much smaller than those that were required to produce the lip in the experiments[22]. The large pressing forces were purposefully used in the experiment to determine whether lip can start to form at several points within the die since different pressing forces result in different contractions and therefore different final pressing positions of the upper punch. In all cases the lip was formed only when the diameter of the compact exceeded that of the die

[21] In order to ensure that there is no collision between the upper punch and the die.

[22] The pressing force depends amongst other factors on the tool shrinkage which is normally chosen so that the pressing forces are confined to a relatively narrow and low force range. This is important not only from the point of view of insert quality but also that of tool safety. For example, a 24% - 26% shrinkage range in the compaction tooling of Grade A powder typically results in pressing forces of between 20 and 30kN which is normally a good range for the quality of the insert as well as tool safety.

as mentioned above and was thus a direct result of contact and friction and not of natural formation as in the tight-fitting case.

11 The accuracy of the method proposed for the determination of punch contraction could not be evaluated on the basis of comparison of the compact edge width as predicted by the final pressing position of the punch and as actually measured using a microscope. The established reasons were related to deburring methods, machine-tool alignment, and springback factors. Given perfect deburring methods, perfectly centralized upper ram chuck and punch, and ignoring any springback effects no matter how small they might be the edge width would in all likelihood be an exact representation of the horizontal distance of the upper punch from the positive die face while in the final pressing position of the compaction cycle.

It was however found that the edge dimension can potentially be used as a quantity for gauging the quality of the compact. Compacts whose edges after deburring were in the order of 0.020 mm - 0.030 mm were found to acceptable for production purposes. quality control standards. In order to achieve such tight tolerances in production without incurring tool damage through punch-die collisions means that final punch pressing positions have to be extremely well controlled, which in order to achieve with reasonable safety requires accurate knowledge of the amount of punch contraction that occurs in pressing. This was determined to within an acceptable level of accuracy by the methods and measurements described in this work.

9 References

1. ISO 1832:2004 – Indexible inserts for cutting tools

2. D.A. Stephenson, J.S. Agapiou, *Metal Cutting Theory and Practice*, pg173 (1996).

3. Y.S. Kwon, S.H. Chung, C. Binet, R. Zhang, R.S. Engel, N.J. Salamon, and R. German. Application of optimization technique in the powder compaction and sintering process. In *Advances in Powder Metallurgy and Particulate Materials*, 9:131-14 (2002).

4. Y.S. Kwon, S.H. Chung, H.I. Sanderow, K.T. Kim, and R. German. Numerical analysis and optimization of die compaction process. In *Advances in Powder Metallurgy and Particulate Materials*, 4:37-50 (2003).

5. S.H. Chung, Y.S. Kwon, C.M. Hyun, K.T. Kim, M.J. Kim, and R. German. Analysis and design of a press and sinter process for fabrication of precise tungsten carbide cutting tools. In *Advances in Powder Metallurgy and Particulate Materials*, 8:26-39 (2004).

6. R. German. Powder Metallurgy Science. Metal Powder Industries Foundation second edition, 1989.

7. K. Rodiger, H. van den Berg, K. Dreyer, D. Kassel, S. Orths. Near-net-shaping in the hardmetal industry. In *International Journal of Refractory Metals & Hard Materials*, volume 18:111-120 (2000).

8. Dorst Manual – Introduction to Powder Compacting. Property of Pilot Tool (PTY) Ltd documentation.

9. E. Doege. Static and Dynamic stiffness of presses and some effects on the accuracy of workpieces. In *Annals of the CIRP*, 29/1:167- 171 (1980).

10. E. Doege, G. Silberbach. Influence of various machine tool components on workpiece quality. In *Annals of the CIRP*, Vol 39/1: 209-213 (1990).

11. J.L.A Albaro. Uniaxial Pressing in Ceramic Tile Manufacturing. In *Euroceram News – Edition No. 8.* Instituto de Tecnología Cerámica de la Universidad Jaume I de Castellón.

12. Y. Tien, P. Wu, W. Huang, M. Kuo, C. Chu. Wall friction measurement and compaction characteristics of bentonite powders. In *Powder Technology*, 173: 140–151 (2007).

13. J. Kikuta and N. Kitamuri. Evaluation of the die wall friction during tablet ejection. In *Powder Technology*, 35: 195-200 (1983).

14. M.S. Anuar, B.J. Briscoe. The elastic relaxation of starch tablets during ejection. In *Powder Technology,* 195: 96–104 (2009).

15. A. Weckenmann., K. Nalkntic. Precision Measurement of cutting tools with two matched optical 3D sensors. Chair Quality Management and Manufacturing Metrology, Friedrich-Alexander-University Erlangen - Nuremberg, Erlangen, Germany.

16. M. Arentoft, M. Eriksen, T. Wanheim. Determination of six stiffnesses for a press. In *Journal of Materials Processing Technology*, 105: 246-252 (2000).

17. K. Chodnikiewicz, B. Tomov. A mechanical device for measuring of displacements and rotations of a blanking or forging press. In *Journal of Materials Processing Technology,* 77: 70–72 (1998).

18. H. Ou, C.G. Armstrong. Evaluating the effect of press and die elasticity in forging of aerofoil sections using finite element simulation. In *Finite Elements in Analysis and Design*, 42: 856 – 867 (2006).

19. P.R. Mort, R. Sabia, D.E. Niesz and R.E. Riman. Automated generation and analysis of powder compaction diagrams. In *Powder Technology*, 79: 111-119 (1994).

20. I. Shapiro. In *Mater. Sci. Eng.,* 71: 333 (1985).

21. R.L.K. Matsumoto, J. Am. In *Ceram. Sot.*, 69: C246 (1986).

22. A. Rosochowski, R. Balendra. Effect of secondary yielding on net-shape forming. In *Journal of Materials Processing Technology*, 58:145-152 (1996).

23. O. Antikainen, J. Yliruusi. Determining the compression behaviour of pharmaceutical powders from the force–distance compression profile. In *International Journal of Pharmaceutics,* 252: 253–261(2003).

24. R.D. Carneim, G.L. Messing, Response of granular powders to uniaxial loading and unloading. In *Powder Technology*, 115: 131–138 (2001).

25. J. Nam, W. Li, J.J. Lannutti. Density gradients and springback: environmental influences. In *Powder Technology*, 133: 23– 32 (2003).

26. R.A. Thompson. In *Ceram. Bull*. 60: 244– 247 (1981).

27. D.M Liu, C.T. Fu. Compaction behaviour of Spray-Dried Silicon Carbide Powders. In *Ceramics International*, 22: 61-12 (1996).

28. E. Doelker. Comparative compaction properties of various microcrystalline cellulose types and generic products. In *Drug Dev. Ind. Pharm*.19: 2399- 2471 (1993).

29. K. Van der Voort Maarschalk, K. Zuurman, H. Vromans, G.K. Bolhuis, C.F. Lerk. Stress relaxation of compacts produced from viscoelastic materials. In *International Journal of Pharmaceutics*, 151: 27-34 (1997).

30. W. Duckworth. Discussion of Ryshkewitch paper by Winston Duckworth. In *J. Am. Ceram. Soc.*, 36: 68 (1953).

31. R. Von Mises. Mechanik der Fasten Korper im Plastisch deformablen Zustand – Gottin. Nachr. In *Math. Phys.* 1: 582 – 592.

32. W. Wu, G. Jiang, R.H. Wagoner, G. S. Daehn. Experimental and Numerical investigation of idealized consolidation. In *Acta mater*. 48: 4323–4330 (2000).

33. C.L. Martin. Unloading of powder compacts and their resulting tensile strength. In *Acta Materialia* 51: 4589–4602 (2003).

34. B. Azhdar, B. Stenberg, and L. Kari. Determination of springback gradient in the die on compacted polymer powders during high-velocity compaction. In *Polymer Testing* 25: 114–123 (2006).

35. P. Jonsén. Fracture and Stress in Powder Compacts. Masters Thesis, Lulea University of Technology, Department of Applied Physics and Mechanical Engineering, Division of Solid Mechanics (2006).

36. J.A. Ferreira, P. Sun, J.J. Gracio. Close loop control of a hydraulic press for springback analysis. In *Journal of Materials Processing Technology,* 177: 377–381 (2006).

37. B.J Briscoe, S.L. Rough. The effects of wall friction on the ejection of pressed ceramic parts, In *Powder Technology*, 99: 228-233 (1998).

38. H.S. Huang, Y.C. Lin, K.S. Hwang. Effect of lubricant addition on the powder properties and compacting performance of spray-dried molybdenum powders. In *International Journal of Refractory Metals & Hard Materials*, 20:175–180(2002).

39. V.S. Styskin. Influence of lubricants on green and sintered properties of P/M materials. In *Advances in powder metallurgy and particulate materials*, 1: 2-45–52 (1999).

40. W.V. Knopp. Effect of the lubricant on green strength. In *Advances in powder metallurgy and particulate materials*, 2: 27–33 (1993).

41. R.M. German, K.D.J Christian, R.S. Sacher, L. Hall, J. Reinert. A comparative evaluation of lubricants for ferrous structural alloys. In *Progress in powder metallurgy*, 42: 405–18 (1986).

42. A.I. Lawrence, S.H. Luk, J.A. Hamill. A performance comparison of current P/M lubricants and routes to improvement. In *Advances in powder metallurgy and particulate materials*, 1: 4-3–21 (1997).

43. P.A. Metz, J. Wolfe, R.M. German, A. Griffo, R.T. Steranko. Improved control of lubricant particle size distribution and the effects of particle size on P/M processing. In *Advances in powder metallurgy and particulate materials*, 1: 6-59–71 (1996).

44. Internet resource: http://www.engineeringtoolbox.com/young-modulus-d_417.html (the Wikipedia site on Young's modulus http://en.wikipedia.org/wiki/Young%27s_modulus#cite_note-2.)

45. B. Gale. Determination and optimization of internal density profiles of WC-Co compacts. MSc. Thesis, University of the Witwatersrand, (2009).

Appendix A: Nomenclature

Collision point is the point in the die where the upper punch makes contact with the positive faces of the die and chips or becomes damaged.

Compact refers specifically to the green part i.e. the soft state prior to sintering.

CNC (Computer Numerically Controlled) is a popular type of control system for vertical machining centres, lathes, injection moulding machines, and other tools used to fabricate valves, inserts, and other machining parts.

Die-wall friction refers to the friction experienced by the compact as result of rubbing against the sides of the die during ejection of the part from the die. It is sometimes referred to as ejection friction. It directly influences the cohesiveness ratio and may therefore result in a failure in the green part during ejection. Manufacturing factors such as the type of die design (as shown in this work), the tool shrinkage, and the tool surface finish are thought to play a large role in minimizing the effect of ejection friction. Natural process parameters such as radial springback can also have a large influence on ejection friction as was shown in this work.

Glass transition temperature is that at which a polymer experiences a significant change in properties. Typically a large change in young's modulus is experienced when a polymer structure turns rubbery (soft and pliable) upon heating and glassy (hard and brittle) upon cooling.

Hold-down force is the force with which the upper ram rests on the part during the decompression and ejection phases of the compaction cycle. On the MP250 press the hold-down force is applied pneumatically although this is not always the case on all hydraulic CNC presses. The hold-down force is typically much smaller than the peak pressing force. For example, in the current work the hold-down force not larger than 500N was used to carry out the experiments, while pressing forces of 0 to 100 kN were achieved in some cases.

Insert refers to the sintered compact.

Leadin is the distance from the die or reference level to the point in the die where the positive face begins, as indicated in several figures throughout the main body of the work.

Lip or land or flat as it also sometimes called, refers to the flat area of a positive compact that forms between the upper cutting edges and the positive faces or sides of the part as a result of certain pressing conditions. These conditions have been identified in the current work.

Lip size is the size of the lip as shown in figure 24. It is measured along the straight part of the cutting edge and not at the corners of the insert. The latter measurement is referred to as the corner lip size and is typically a larger quantity.

Negative Insert or compact is one whose wedge angle is = 0 deg.

Penetration Depth is a MP250 press parameter which controls the final pressing position of the upper punch. It is taken as the distance that from die or reference level to the final position of the upper punch assuming a perfectly referenced upper punch and negligible amount of punch contraction.

Positive Insert or compact is one whose wedge angle is > 0 deg. Negative inserts have the advantage of having twice as many cutting edges available as comparable positive inserts because the cutting edges on both top and bottom can be used while only the top cutting edges can be used on positive inserts. However, positive inserts have a distinct advantage when machining long and slender parts, thin-walled parts or other parts that are subject to bending and chatter when the cutting load is applied to them, because the cutting force is significantly lower compared to that for negative inserts.

Punch contraction as explained in the main body of the work, is amount of deformation or strain a punch is subjected to as a result of the evolved pressing force during compaction and the elasticity of the material from which it is manufactured. The pressing frame is subject to similar extensions and upsetting deformations which is why these are collectively referred to as machine-tool deflections.

Sand blasting is a finishing process by which the sintered insert edge is honed to the required radius by blasting of alumina sand or other material at the insert edge. It is essentially a type of controlled wear mechanism.

Secondary yielding is a relatively new or recently recognised phenomenon caused by contracting dies as a result of unloading and involves dimensional changes of the workpiece which should be taken into account when attempting net shape forming. The effect of contracting dies was not examined in this work. Die deformation during pressing was assumed to be negligible.

Setup process on a hydraulic CNC press involves two stages: setting the tools inside the press and making a new press program on the control system of the press that can be used to press a component of required weight, dimension, and quality. Setup time is the duration of time needed to complete this process.

Springback refers to the relaxation or expansion of the compact which occurs during the unloading stage of the pressing cycle. As shown in this work springback can occur inside (in-die) or outside the die (out-of-die) and is typically quantified in terms of two components; axial and radial springback. Understanding of springback is an important step toward near net shaping.

Tools refers to a set of pressing tools: the upper punch, the lower punch, the pin (if present), and the die used to press the powder into shape i.e. into compacts.

Tool geometry in this work refers to the general shape of the tool e.g. square, round or triangular in this work. The surface of a punch has an equal and opposite geometry to the surface of the component which it forms during pressing.

Tool Referencing is a process by which the punch reference positions are established inside the press. The punches are normally referenced with respect to the die level.

Top Pressing is a way of displacing the density distribution to the top of the compact. During pressing, the bottom punch is in final pressing position when the top punch is a programmed distance away from its final pressing position. The final pressing movement is thus executed by the upper punch, by the programmed amount of top pressing.

Travel Ratio is the ratio of distances travelled by the upper and lower punches as they move to their final in-die pressing positions and in doing so displace the powder in certain proportions. The main function of travel ratio in double action pressing is to evenly distribute the powder density inside the pressed component. Typically a 1:1 travel ratio is programmed for equal displacements of powder by top and bottom punches.

Travel Schedule is a collective term for a set of specific press program settings or parameters which determine the size, weight and quality of the pressed compact e.g. pressing speed, ejection speed, hold-down force, travel ratio, etc.

Viscoelastic material is a material which exhibits both viscous and elastic properties when undergoing deformation. Since viscous materials strain linearly with time it is said that they exhibit time-dependant strain.

Appendix B: Tool grade data

Table A1: Tight-fit cross sectional punch areas.

Toolset description	Cross sectional area of the tight-fit top punch (mm^2)
Square	137.9
Round	120.1
Triangle	179.8

Note: cross sectional SBA punch areas were not measured. There was no need for this to be done in the current work. Similarly lower punch surface areas are not reported.

Table A2: Tight-fit tool lengths and other parameters.

Toolset description	Top punch length (mm)	Bottom punch length (mm)	Die height (mm)	Leadin (mm)	Top Punch IC (mm)	Die IC (mm)
Square	63.859	78.855	25.193	3.98	11.876	11.883
Round	63.671	78.750	25.077	3.997	12.459	12.466
Triangle	63.841	78.800	24.894	3.773	11.868	11.878

Table A3: SBA tool lengths and other parameters.

Toolset description	Top punch length (mm)	Bottom punch length (mm)	Die height (mm)	Leadin (mm)	Top Punch IC (mm)	Die IC (mm)	SBA gap (mm)
Square	63.859	78.855	25.193	3.98	11.681	11.883	0.101
Round	63.671	78.750	25.077	3.997	12.266	12.466	0.100
Triangle	63.841	78.800	24.894	3.773	11.674	11.878	0.102

Note: this table is essentially the same as table A2. Top punch IC (mm) values are smaller as a result of the tight-fit punches having been ground down to the required SBA tolerance shown in the last column. These are approximately 0.100mm for each tool.

Table A4: Grade specifications.

Grade	ISO code	WC	Co	TiC	TaC	NbC	Ni	Cr_3C_2
A	M25/M40	89.5	10.0					0.5
B		87.65	6.6	2.30	2.76	0.69		

Appendix C: Contraction measurement data

C.1 Round tight-fit tool

Tables 24 to 27 list the results for the round tight-fit tools. The procedures used to obtain the data are identical to those described in sections 6.1.1 to 6.1.4.

Upper and lower punch-ram system contraction

Table 24: Upper and lower punch-ram system contraction data for the round tight-fit tool.

No.	Upper ram measuring system reading A(mm) ± 0.003mm	Pressing Force F(kN) ± 0.5kN
1	0.000	0.0
2	0.009	2.7
3	0.028	6.9
4	0.048	12.3
5	0.067	18.4
6	0.078	21.6
7	0.087	24.6
8	0.098	27.8
9	0.117	33.9
10	0.136	40.0
11	0.156	46.6
12	0.164	49.7

Upper punch-ram system contraction

Table 25: Upper punch-ram system contraction data for the round tight-fit tool.

No.	Upper ram measuring system reading A(mm) ± 0.003mm	Plate deformation clock reading C(mm) ± 0.002mm	Upper punch- ram system contraction ΔL(mm) ± 0.005mm	Pressing Force F(kN) ± 0.5kN
1	0.000	0.000	0.000	0.0
2	0.010	0.002	0.008	4.0
3	0.022	0.005	0.017	6.9
4	0.032	0.008	0.024	10.1
5	0.054	0.013	0.041	17.1
6	0.066	0.015	0.051	21.5
7	0.076	0.016	0.060	25.5
8	0.098	0.018	0.080	35.0
9	0.119	0.020	0.099	44.5
10	0.141	0.022	0.119	53.8

Upper ram contraction

Table 26: Upper ram contraction data for the round tight-fit tool.

No.	Upper ram measuring system reading A(mm) ± 0.003mm	Chuck position clock reading C(mm) ± 0.002mm	Upper ram system contraction ΔL(mm) ± 0.005mm	Pressing Force F(kN) ± 0.5kN
1	0.000	0.000	0.000	0.0
2	0.010	0.007	0.003	4.1
3	0.020	0.015	0.005	7.4
4	0.033	0.023	0.010	11.8
5	0.043	0.031	0.012	15.7
6	0.054	0.038	0.016	20.2
7	0.065	0.045	0.020	25.1
8	0.079	0.053	0.026	31.0
9	0.090	0.061	0.029	36.5
10	0.105	0.069	0.036	43.6
11	0.119	0.077	0.042	49.8

Contraction of the upper ram and punch base system

Table 27: Upper ram and punch base contraction data for the round tight-fit tool.

No.	Upper ram measuring system reading A(mm) ± 0.003mm	Punch base clock reading C(mm) ± 0.002mm	Upper ram and punch base contraction ΔL(mm) ± 0.005mm	Pressing Force F(kN) ± 0.5kN
1	0.000	0.000	0.000	0.0
2	0.010	0.007	0.003	4.2
3	0.021	0.014	0.007	7.1
4	0.032	0.021	0.011	10.7
5	0.041	0.029	0.012	14.3
6	0.055	0.037	0.018	20.1
7	0.068	0.044	0.024	25.6
8	0.079	0.051	0.028	30.5
9	0.094	0.061	0.033	37.3
10	0.107	0.067	0.040	42.9
11	0.123	0.075	0.048	50.0

C.2 Triangular tight-fit tool

Tables 28 to 31 list the results for the round tight-fit tools. The procedures used to obtain the data are identical to those described in sections 6.1.1 to 6.1.4.

Upper and lower punch-ram system contraction

Table 28: Upper and lower punch-ram system contraction readings for the triangular tight-fit tool.

No.	Upper ram measuring system reading A(mm) ± 0.003mm	Pressing Force F(kN) ± 0.5kN
1	0.000	0.0
2	0.008	3.2
3	0.018	5.9
4	0.037	11.3
5	0.056	17.2
6	0.066	20.5
7	0.076	23.8
8	0.086	26.8
9	0.096	30.6
10	0.115	37.0
11	0.133	43.3
12	0.142	46.5
13	0.153	50.0

Upper punch-ram system contraction

Table 29: Upper punch-ram system contraction data for the triangular tight-fit tool.

No.	Upper ram measuring system reading A(mm) ± 0.003mm	Plate deformation clock reading C(mm) ± 0.002mm	Upper punch- ram system contraction ΔL(mm) ± 0.005mm	Pressing Force F(kN) ± 0.5kN
1	0.000	0.000	0.000	0.0
2	0.007	0.000	0.007	3.2
3	0.017	0.006	0.011	5.8
4	0.028	0.010	0.018	9.3
5	0.038	0.014	0.024	12.8
6	0.048	0.016	0.032	16.8
7	0.068	0.019	0.049	26.0
8	0.078	0.020	0.058	30.9
9	0.100	0.022	0.078	41.7
10	0.109	0.023	0.086	47.0
11	0.120	0.024	0.096	52.9

Upper ram contraction

Table 30: Upper ram contraction data for the triangular tight-fit tool.

No.	Upper ram measuring system reading A(mm) ± 0.003mm	Chuck position clock reading C(mm) ± 0.002mm	Upper ram system contraction ΔL(mm) ± 0.005mm	Pressing Force F(kN) ± 0.5kN
1	0.000	0.000	0.000	0.0
2	0.009	0.007	0.002	3.8
3	0.019	0.015	0.004	6.8
4	0.029	0.024	0.005	10.2
5	0.042	0.033	0.009	15.3
6	0.053	0.039	0.014	19.8
7	0.062	0.047	0.015	24.5
8	0.074	0.055	0.019	30.4
9	0.085	0.061	0.024	36.2
10	0.096	0.067	0.029	41.8
11	0.109	0.075	0.034	48.3

Contraction of the upper ram and punch base system

Table 31: Upper ram and punch base contraction data for the triangular tight-fit tool.

No.	Upper ram measuring system reading A(mm) ± 0.003mm	Punch base clock reading C(mm) ± 0.002mm	Upper ram and punch base contraction ΔL(mm) ± 0.005mm	Pressing Force F(kN) ± 0.5kN
1	0.000	0.000	0.000	0.0
2	0.013	0.010	0.003	4.0
3	0.023	0.018	0.005	7.0
4	0.033	0.024	0.009	10.4
5	0.044	0.030	0.014	14.6
6	0.056	0.038	0.018	19.9
7	0.064	0.042	0.022	24.3
8	0.074	0.046	0.028	28.7
9	0.083	0.051	0.032	33.9
10	0.094	0.056	0.038	39.5
11	0.104	0.060	0.044	44.9
12	0.114	0.065	0.049	50.3

C.3 Square SBA tool contraction measurements

Tables 32 to 35 list the results for the Square SBA tools. The procedures used to obtain the data are identical to those described in sections 6.1.1 to 6.1.4.

Upper and lower punch-ram system contraction

Table 32: Upper and lower punch ram system contraction data for square SBA tool.

No.	Upper ram measuring system reading A(mm) ± 0.003mm	Pressing Force F(kN) ± 0.5kN
1	0.000	0.0
2	0.010	5.9
3	0.020	8.8
4	0.029	11.6
5	0.039	14.6
6	0.049	18.2
7	0.059	21.4
8	0.068	24.5
9	0.078	27.9
10	0.097	34.0
11	0.117	41.0
12	0.137	47.9
13	0.167	58.5
14	0.207	72.6
15	0.235	83.0
16	0.266	93.5
17	0.281	98.6

Upper punch-ram system contraction

Table 33: Upper punch-ram system contraction data for the square SBA tool.

No.	Upper ram measuring system reading A(mm) ± 0.003mm	Plate deformation clock reading C(mm) ± 0.002mm	Upper punch- ram system contraction ΔL(mm) ± 0.005mm	Pressing Force F(kN) ± 0.5kN
1	0.000	0.000	0.000	0.0
2	0.008	0.000	0.008	4.5
3	0.022	0.004	0.018	8.6
4	0.035	0.007	0.028	13.6
5	0.050	0.010	0.040	19.4
6	0.062	0.012	0.050	24.9
7	0.073	0.014	0.059	30.0
8	0.100	0.017	0.083	41.8
9	0.132	0.020	0.112	56.9
10	0.156	0.023	0.133	68.8
11	0.178	0.026	0.152	79.2
12	0.201	0.028	0.173	89.9
13	0.223	0.030	0.193	100.4

Upper ram contraction

Table 34: Upper ram contraction data for the square SBA tool.

No.	Upper ram measuring system reading A(mm) ± 0.003mm	Chuck position clock reading C(mm) ± 0.002mm	Upper ram system contraction ΔL(mm) ± 0.005mm	Pressing Force F(kN) ± 0.5kN
1	0.000	0.000	0.000	0.0
2	0.008	0.003	0.005	4.1
3	0.023	0.014	0.009	8.8
4	0.039	0.023	0.016	15.0
5	0.061	0.037	0.024	23.7
6	0.073	0.045	0.028	29.5
7	0.103	0.063	0.040	43.5
8	0.125	0.075	0.050	53.5
9	0.150	0.090	0.060	65.9
10	0.179	0.107	0.072	79.8
11	0.203	0.121	0.082	90.9
12	0.223	0.134	0.089	101.0

Contraction of the upper ram and punch base system

Table 35: Upper ram and punch base contraction data for the square SBA tool.

No.	Upper ram measuring system reading A(mm) ± 0.003mm	Punch base clock reading C(mm) ± 0.002mm	Upper ram and punch base contraction ΔL(mm) ± 0.005mm	Pressing Force F(kN) ± 0.5kN
1	0.000	0.000	0.000	0.0
2	0.012	0.005	0.007	5.5
3	0.025	0.013	0.012	9.7
4	0.041	0.022	0.019	15.5
5	0.053	0.029	0.024	21.1
6	0.075	0.041	0.034	30.3
7	0.100	0.053	0.047	41.9
8	0.123	0.064	0.059	53.2
9	0.150	0.076	0.074	66.1
10	0.182	0.093	0.089	81.5
11	0.213	0.107	0.106	96.4

C.4 Round SBA tool contraction measurements

Tables 36 to 39 list the results for the round SBA tools. The procedures used to obtain the data are identical to those described in sections 6.1.1 to 6.1.4.

Upper and lower punch-ram system contraction

Table 36: Upper and lower punch-ram system contraction data for the round SBA tool.

No.	Upper ram measuring system reading A(mm) ± 0.003mm	Pressing Force F(kN) ± 0.5kN
1	0.000	0.0
2	0.010	3.8
3	0.028	9.3
4	0.037	12.0
5	0.047	14.7
6	0.057	18.1
7	0.067	21.2
8	0.076	24.2
9	0.086	27.5
10	0.105	34.2
11	0.134	43.9
12	0.164	53.9
13	0.194	63.5
14	0.232	76.6
15	0.261	86.3
16	0.290	95.9

Upper punch-ram system contraction

Table 37: Upper punch-ram system contraction data for the round SBA tool.

No.	Upper ram measuring system reading A(mm) ± 0.003mm	Plate deformation clock reading C(mm) ± 0.002mm	Upper punch- ram system contraction ΔL(mm) ± 0.005mm	Pressing Force F(kN) ± 0.5kN
1	0.000	0.000	0.000	0.0
2	0.021	0.004	0.017	8.5
3	0.033	0.006	0.027	13.8
4	0.055	0.009	0.046	22.8
5	0.069	0.011	0.058	28.9
6	0.090	0.013	0.077	38.7
7	0.115	0.014	0.101	50.3
8	0.146	0.014	0.132	65.1
9	0.179	0.015	0.164	79.9
10	0.222	0.015	0.207	100.0

Upper ram contraction

Table 38: Upper ram contraction data for the round SBA tool.

No.	Upper ram measuring system reading A(mm) ± 0.003mm	Chuck position clock reading C(mm) ± 0.002mm	Upper ram system contraction ΔL(mm) ± 0.005mm	Pressing Force F(kN) ± 0.5kN
1	0.000	0.000	0.000	0.0
2	0.018	0.013	0.005	7.4
3	0.029	0.021	0.008	12.0
4	0.047	0.033	0.014	19.3
5	0.062	0.043	0.019	26.0
6	0.074	0.051	0.023	31.9
7	0.098	0.066	0.032	43.0
8	0.129	0.085	0.044	57.1
9	0.162	0.106	0.056	72.1
10	0.183	0.118	0.065	82.5
11	0.216	0.139	0.077	97.6

Contraction of the upper ram and punch base system

Table 39: Upper ram and punch base system contraction data for the round SBA tool.

No.	Upper ram measuring system reading A(mm) ± 0.003mm	Punch base clock reading C(mm) ± 0.002mm	Upper ram and punch base contraction ΔL(mm) ± 0.005mm	Pressing Force F(kN) ± 0.5kN
1	0.000	0.000	0.000	0.0
2	0.013	0.008	0.005	5.7
3	0.033	0.019	0.014	13.3
4	0.048	0.026	0.022	19.2
5	0.073	0.040	0.033	31.1
6	0.101	0.054	0.047	43.4
7	0.132	0.072	0.060	58.3
8	0.158	0.084	0.074	69.7
9	0.189	0.101	0.088	84.7
10	0.216	0.116	0.100	97.1

C.5 Triangular SBA tool contraction measurements

Tables 40 to 43 list the results for the triangular SBA tools. The procedures used to obtain the data are identical to those described in sections 6.1.1 to 6.1.4.

Upper and lower punch-ram system contraction

Table 40: Upper & lower punch-ram system data for triangular SBA compact.

No.	Upper ram measuring system reading A(mm) ± 0.003mm	Pressing Force F(kN) ± 0.5kN
1	0.000	0.0
2	0.011	4.9
3	0.021	7.8
4	0.031	10.8
5	0.041	14.0
6	0.051	17.2
7	0.060	20.3
8	0.074	24.8
9	0.086	28.7
10	0.106	35.4
11	0.126	42.1
12	0.163	55.2
13	0.192	65.1
14	0.221	74.8
15	0.251	85.3
16	0.280	95.3

Upper punch-ram system contraction

Table 41: Upper punch-ram system contraction data for the triangular SBA tool.

No.	Upper ram measuring system reading A(mm) ± 0.003mm	Plate deformation clock reading C(mm) ± 0.002mm	Upper punch- ram system contraction ΔL(mm) ± 0.005mm	Pressing Force F(kN) ± 0.5kN
1	0.000	0.000	0.000	0.0
2	0.009	0.000	0.009	5.5
3	0.020	0.003	0.017	9.4
4	0.030	0.005	0.025	13.6
5	0.041	0.007	0.034	18.3
6	0.052	0.009	0.043	23.2
7	0.062	0.010	0.052	27.8
8	0.073	0.012	0.061	33.4
9	0.094	0.013	0.081	44.3
10	0.128	0.015	0.113	61.0
11	0.158	0.017	0.141	77.0
12	0.189	0.019	0.170	92.7
13	0.209	0.020	0.189	102.4

Upper ram contraction

Table 42: Upper ram contraction data for the triangular SBA compact.

No.	Upper ram measuring system reading A(mm) ± 0.003mm	Chuck position clock reading C(mm) ± 0.002mm	Upper ram system contraction ΔL(mm) ± 0.005mm	Pressing Force F(kN) ± 0.5kN
1	0.000	0.000	0.000	0.0
2	0.009	0.003	0.006	4.7
3	0.023	0.015	0.008	9.5
4	0.041	0.027	0.014	16.7
5	0.054	0.035	0.019	22.7
6	0.066	0.043	0.023	28.9
7	0.082	0.051	0.031	36.3
8	0.103	0.065	0.038	47.7
9	0.126	0.079	0.047	59.8
10	0.148	0.090	0.058	70.7
11	0.180	0.110	0.070	88.0
12	0.207	0.126	0.081	101.5

Contraction of the upper ram and punch base system

Table 43: Upper ram and punch base contraction data for the triangular SBA compact.

No.	Upper ram measuring system reading A(mm) ± 0.003mm	Punch base clock reading C(mm) ± 0.002mm	Upper ram and punch base contraction ΔL(mm) ± 0.005mm	Pressing Force F(kN) ± 0.5kN
1	0.000	0.000	0.000	0.0
2	0.008	0.002	0.006	4.3
3	0.024	0.013	0.011	9.6
4	0.037	0.021	0.016	15.3
5	0.056	0.032	0.024	24.0
6	0.068	0.037	0.031	29.7
7	0.090	0.048	0.042	40.5
8	0.115	0.062	0.053	53.8
9	0.139	0.073	0.066	66.1
10	0.163	0.084	0.079	78.6
11	0.178	0.092	0.086	86.5
12	0.202	0.104	0.098	99.5

Appendix D: Tight-fit compact measured and calculated data

D.1 Measured and calculated data for Grade B powder

Measured data

As described previously, in order to preserve a 1:1 punch travel ratio, the maximum filling height that could be chosen was 13.19mm. For Grade B powder this filling height corresponded to a pressing force of 42.5kN. However at this filling height the compact mass was also greater; 6.282g compared to 5.594g previously observed with Grade A powder. At approximately the same compact mass the pressing force is much greater with Grade A powder than Grade B powder. From these observations it can be seen that the fill-density of Grade B powder is greater than that of Grade A powder. This is expected given that the apparent density of the former is greater than that of the latter and that Grade B powder "presses softer" than grade A powder. This experiment was limited to a range of pressing forces between 0kN and 42.5kN.

Table 44: Recorded and measured data for the square tight-fit compact using grade B powder.

No.	Filling height F_h(mm)	Pressing Force F(kN) ± 0.1kN	Mass M(g) ± 0.001g	Lip L(mm) ± 0.01mm	Corner Lip L_c(mm) ± 0.01mm	Height H(mm) ± 0.01mm	IC(mm) ± 0.01mm
1	10.50	6.3	5.190	0.222	N/A	5.48	11.90
2	11.00	8.7	5.366	0.229	N/A	5.49	11.90
3	11.50	12.7	5.563	0.264	N/A	5.52	11.90
4	12.00	18.2	5.755	0.301	0.382	5.54	11.91
5	12.50	26.4	5.972	0.329	0.426	5.56	11.92
6	12.75	31.9	6.090	0.370	0.453	5.58	11.92
7	13.00	37.5	6.199	0.384	0.502	5.60	11.92
8	13.19	42.5	6.282	0.414	N/A	5.62	11.92

Calculated data

The data listed in Tables 45 to 50 was calculated using the equations described in section 5.2.

Table 45: Change in lip size with pressing force.

No.	$\Delta L(F)$ $\pm$ 0.01mm	$\Delta L(F)_{contraction}$ $\pm$ 0.005mm	$\Delta L(F)_{springback}$ $\pm$ 0.015mm	$\Delta L(F)_{relative\ springback}$ (%)
1	0.043	0.014	0.029	15.0
2	0.058	0.019	0.039	20.6
3	0.083	0.028	0.055	26.6
4	0.116	0.040	0.076	33.6
5	0.160	0.058	0.102	45.0
6	0.187	0.070	0.117	46.2
7	0.212	0.082	0.130	51.1
8	0.233	0.093	0.139	50.8

Table 46: Change in height with pressing force.

No.	$\Delta H(F)$ $\pm$ 0.01mm	$\Delta H(F)_{contraction}$ $\pm$ 0.005mm	$\Delta H(F)_{springback}$ $\pm$ 0.015mm	$\Delta H(F)_{relative\ springback}$ (%)
1	0.030	0.020	0.010	0.19
2	0.041	0.027	0.014	0.25
3	0.058	0.039	0.019	0.34
4	0.080	0.056	0.024	0.44
5	0.111	0.081	0.030	0.54
6	0.130	0.098	0.032	0.57
7	0.148	0.116	0.032	0.58
8	0.162	0.131	0.031	0.56

Table 47: Change in IC with pressing force.

No.	$\Delta IC(F)$ $\pm$ 0.01mm	$\Delta IC(F)_{springback}$ $\pm$ 0.01mm	$\Delta IC(F)_{relative\ springback}$ (%)
1	0.017	0.017	0.14
2	0.017	0.017	0.14
3	0.017	0.017	0.14
4	0.027	0.027	0.23
5	0.037	0.037	0.31
6	0.037	0.037	0.31
7	0.037	0.037	0.31
8	0.037	0.037	0.31

Table 48: Change in the springback and relative springback ratios with pressing force.

No.	$\Delta H(F)_{springback} / \Delta IC(F)_{springback}$	$\Delta H(F)_{relative\ springback} / \Delta IC(F)_{relative\ springback}$
1	0.60	1.31
2	0.80	1.74
3	1.10	2.37
4	0.90	1.94
5	0.81	1.73
6	0.86	1.84
7	0.87	1.85
8	0.84	1.79

Table 49: Change in volumetric ad relative volumetric springback with pressing force.

No.	$\Delta V(F)$ (cm^3)	$\Delta V(F)_{contraction}$ (cm^3)	$\Delta V(F)_{springback}$ (cm^3)	$\Delta V(F)_{relative\ springback}$ (%)
1	0.005	0.002	0.003	0.34
2	0.007	0.004	0.003	0.46
3	0.010	0.006	0.004	0.63
4	0.014	0.008	0.006	0.83
5	0.019	0.011	0.008	1.05
6	0.021	0.013	0.008	1.14
7	0.024	0.015	0.009	1.18
8	0.026	0.017	0.009	1.19

Table 50: Change in green density with pressure.

No.	Pressure (kN/cm^2)	Green density (g/cm^3)
1	4.57	7.46
2	6.31	7.70
3	9.21	7.93
4	13.2	8.16
5	19.1	8.43
6	23.1	8.56
7	27.2	8.68
8	30.8	8.76

D.2 Measured and calculated data for Grade A powder - round compacts

Measured data

In order to preserve a 1:1 punch travel ratio, the maximum filling height that could be chosen was 13.26mm. This filling height corresponded to a pressing force of 29.6kN. Thus the experiment was limited to a range of pressing forces between 0kN and 29.6kN. Furthermore, no Lc measurements were made for round inserts as round inserts do not have corners.

Table 51: Recorded and measured data for the round tight-fit compact using grade B powder.

No.	Filling height F_h(mm)	Pressing Force F(kN) ± 0.1kN	Mass M(g) ± 0.001g	Lip L(mm) ± 0.01mm	Height H(mm) ± 0.01mm	IC(mm) ± 0.01mm
1	9.50	4.6	3.725	0.109	5.47	12.47
2	10.00	5.7	3.893	0.125	5.48	12.48
3	10.50	7.1	4.060	0.156	5.50	12.49
4	11.00	9.2	4.232	0.176	5.52	12.50
5	11.50	12.0	4.396	0.193	5.53	12.50
6	12.00	15.5	4.556	0.225	5.56	12.51
7	12.25	17.5	4.631	0.238	5.57	12.51
8	12.50	19.8	4.708	0.259	5.58	12.51
9	12.75	22.8	4.790	0.278	5.60	12.51
10	13.00	25.8	4.869	0.300	5.61	12.52
11	13.26	29.6	4.954	0.312	5.63	12.52

Calculated data

The data listed in Tables 52 to 57 was calculated using the equations described in section 4.2.

Table 52: Change in lip size with pressing force.

No.	$\Delta L(F)$ ± 0.01mm	$\Delta L(F)_{contraction}$ ± 0.005mm	$\Delta L(F)_{springback}$ ± 0.015mm	$\Delta L(F)_{relative\ springback}$ (%)
1	0.058	0.010	0.048	77.9
2	0.071	0.013	0.058	87.7
3	0.087	0.016	0.071	83.9
4	0.110	0.021	0.089	101.2
5	0.138	0.028	0.110	133.5
6	0.169	0.035	0.134	146.5
7	0.185	0.040	0.145	156.3
8	0.202	0.045	0.157	153.6
9	0.221	0.051	0.170	156.7
10	0.238	0.059	0.179	148.8
11	0.255	0.067	0.188	150.6

Table 53: Change in height with pressing force.

No.	$\Delta H(F)$ ± 0.01mm	$\Delta H(F)_{contraction}$ ± 0.005mm	$\Delta H(F)_{springback}$ ± 0.015mm	$\Delta H(F)_{relative\ springback}$ (%)
1	0.043	0.016	0.027	0.50
2	0.052	0.019	0.033	0.61
3	0.064	0.024	0.040	0.73
4	0.081	0.031	0.050	0.91
5	0.102	0.041	0.061	1.12
6	0.126	0.053	0.073	1.33
7	0.138	0.060	0.078	1.43
8	0.151	0.067	0.084	1.52
9	0.167	0.078	0.089	1.61
10	0.180	0.088	0.092	1.67
11	0.194	0.101	0.093	1.68

Table 54: Change in IC with pressing force.

No.	$\Delta IC(F)$ ± 0.01mm	$\Delta IC(F)_{springback}$ ± 0.01mm	$\Delta IC(F)_{relative\ springback}$ (%)
1	0.008	0.008	0.06
2	0.010	0.010	0.08
3	0.012	0.012	0.10
4	0.015	0.015	0.12
5	0.020	0.020	0.16
6	0.024	0.024	0.20
7	0.027	0.027	0.22
8	0.030	0.030	0.24
9	0.033	0.033	0.27
10	0.036	0.036	0.29
11	0.040	0.040	0.32

Table 55: Change in the springback and relative springback ratio with pressing force.

No.	$\Delta H(F)_{springback}$ / $\Delta IC(F)_{springback}$	$\Delta H(F)_{relative\ springback}$ / $\Delta IC(F)_{relative\ springback}$
1	3.36	7.70
2	3.33	7.61
3	3.28	7.50
4	3.21	7.33
5	3.11	7.10
6	2.98	6.78
7	2.90	6.59
8	2.80	6.37
9	2.67	6.05
10	2.53	5.73
11	2.33	5.27

Table 56: Change in the volumetric and relative volumetric springback.

No.	$\Delta V(F)$ (cm^3)	$\Delta V(F)_{contraction}$ (cm^3)	$\Delta V(F)_{springback}$ (cm^3)	$\Delta V(F)_{relative\ springback}$ (%)
1	0.006	0.002	0.004	0.68
2	0.008	0.003	0.005	0.82
3	0.009	0.003	0.006	0.99
4	0.012	0.005	0.007	1.24
5	0.015	0.006	0.009	1.53
6	0.018	0.007	0.011	1.83
7	0.020	0.008	0.012	1.98
8	0.022	0.009	0.013	2.13
9	0.024	0.010	0.014	2.27

10	0.026	0.012	0.014	2.37
11	0.028	0.013	0.015	2.44

Table 57: Change in green density with pressure.

No.	Pressure (kN/cm^2)	Green density (g/cm^3)
1	3.83	6.20
2	4.75	6.46
3	5.91	6.70
4	7.66	6.96
5	9.99	7.20
6	12.9	7.42
7	14.6	7.53
8	16.5	7.63
9	19.0	7.74
10	21.5	7.84
11	24.6	7.95

D.3 Measured and calculated data for Grade B powder - round compacts

Measured data

As described previously, in order to preserve a 1:1 punch travel ratio, the maximum filling height that could be chosen was 13.26mm. This filling height corresponded to a pressing force of 35.6kN. Thus the experiment was limited to a range of pressing forces between 0kN and 35.6kN. Again, no Lc measurements were made.

Table 58: Recorded and measured data for the round tight-fit compact using grade B powder.

No.	Filling height F_h(mm)	Pressing Force F(kN) ± 0.1kN	Mass M(g) ± 0.001g	Lip L(mm) ± 0.01mm	Height H(mm) ± 0.01mm	IC(mm) ± 0.01mm
1	11.00	9.3	4.655	0.234	5.50	12.49
2	11.50	12.4	4.823	0.256	5.52	12.49
3	12.00	17.3	5.005	0.270	5.55	12.50
4	12.25	20.1	5.091	0.297	5.56	12.50
5	12.50	23.0	5.160	0.315	5.57	12.51
6	12.75	27.1	5.259	0.350	5.59	12.52
7	13.00	31.5	5.346	0.362	5.61	12.52
8	13.26	35.6	5.423	0.381	5.63	12.52

Calculated data

The data listed in Tables 59 to 64 was calculated using the equations described in section 5.2.

Table 59: Change in lip size with pressing force.

No.	$\Delta L(F)$ ± 0.01mm	$\Delta L(F)_{contraction}$ ± 0.005mm	$\Delta L(F)_{springback}$ ± 0.015mm	$\Delta L(F)_{relative\ springback}$ (%)
1	0.061	0.021	0.040	20.9
2	0.081	0.028	0.053	26.1
3	0.111	0.039	0.072	36.3
4	0.128	0.046	0.082	38.3
5	0.145	0.052	0.093	41.5
6	0.168	0.062	0.106	43.7
7	0.192	0.072	0.120	49.9
8	0.213	0.080	0.133	53.5

Table 60: Change in height with pressing force.

No.	$\Delta H(F)$ ± 0.01mm	$\Delta H(F)_{contraction}$ ± 0.005mm	$\Delta H(F)_{springback}$ ± 0.015mm	$\Delta H(F)_{relative\ springback}$ (%)
1	0.052	0.031	0.021	0.38
2	0.069	0.042	0.027	0.48
3	0.094	0.059	0.035	0.63
4	0.108	0.069	0.039	0.71
5	0.121	0.078	0.043	0.78
6	0.140	0.092	0.048	0.86
7	0.159	0.107	0.052	0.93
8	0.176	0.122	0.054	0.98

Table 61: Change in IC with pressing force.

No.	$\Delta IC(F)$ ± 0.01mm	$\Delta IC(F)_{springback}$ ± 0.01mm	$\Delta IC(F)_{relative\ springback}$ (%)
1	0.020	0.020	0.16
2	0.026	0.026	0.21
3	0.035	0.035	0.28
4	0.039	0.039	0.31
5	0.043	0.043	0.35
6	0.048	0.048	0.39
7	0.053	0.053	0.43
8	0.057	0.057	0.46

Table 62: Change in the springback and relative springback ratios with pressing force.

No.	$\Delta H(F)_{springback} / \Delta IC(F)_{springback}$	$\Delta H(F)_{relative\ springback} / \Delta IC(F)_{relative\ springback}$
1	1.02	2.32
2	1.01	2.30
3	1.00	2.27
4	1.00	2.25
5	0.99	2.24
6	0.98	2.21
7	0.97	2.17
8	0.96	2.14

Table 63: Change in volumetric and relative volumetric springback with pressing force.

No.	$\Delta V(F)$ (cm^3)	$\Delta V(F)_{contraction}$ (cm^3)	$\Delta V(F)_{springback}$ (cm^3)	$\Delta V(F)_{relative\ springback}$ (%)
1	0.008	0.004	0.004	0.65
2	0.010	0.005	0.005	0.83
3	0.014	0.007	0.007	1.10
4	0.016	0.009	0.007	1.24
5	0.018	0.010	0.008	1.36
6	0.020	0.011	0.009	1.52
7	0.023	0.013	0.010	1.67
8	0.025	0.014	0.011	1.77

Table 64: Change in volume with pressing force.

No.	Pressure (kN/cm^2)	Green density (g/cm^3)
1	7.74	7.68
2	10.3	7.91
3	14.4	8.17
4	16.7	8.29
5	19.2	8.37
6	22.6	8.49
7	26.2	8.60
8	29.6	8.69

D.4 Measured and calculated data for Grade A powder – triangular compacts

Measured data

In order to preserve a 1:1 punch travel ratio, the maximum filling height that could be chosen was 12.74mm. This filling height corresponded to a pressing force of 28.9kN. Thus the experiment was limited to a range of pressing forces between 0kN and 28.9kN.

Table 65: Recorded and measured data for the triangular tight-fit compact using grade A powder.

No.	Filling height F_h(mm)	Pressing Force F(kN) ± 0.1kN	Mass M(g) ± 0.001g	Lip L(mm) ± 0.01mm	Corner Lip L_c(mm) ± 0.01mm	Height H(mm) ± 0.01mm	IC(mm) ± 0.01mm
1	10.00	5.9	5.719	0.137	0.263	5.43	11.91
2	10.50	8.0	5.967	0.153	0.286	5.44	11.92
3	11.00	10.3	6.184	0.165	0.306	5.46	11.92
4	11.50	12.7	6.416	0.181	0.339	5.48	11.93
5	11.75	15.2	6.544	0.188	0.384	5.49	11.93
6	12.00	18.8	6.707	0.207	0.400	5.50	11.94
7	12.25	21.7	6.821	0.215	0.432	5.52	11.94
8	12.50	25.6	6.948	0.240	0.434	5.53	11.95
9	12.74	28.9	7.048	0.245	0.471	5.54	11.95

Calculated data

The data listed in Tables 66 to 71 was calculated using the equations described in section 5.2.

Table 66: Change in lip size with pressing force.

No.	$\Delta L(F)$ ± 0.01mm	$\Delta L(F)_{contraction}$ ± 0.005mm	$\Delta L(F)_{springback}$ ± 0.015mm	$\Delta L(F)_{relative\ springback}$ (%)
1	0.038	0.011	0.027	11.4
2	0.050	0.014	0.036	14.2
3	0.063	0.019	0.044	17.0
4	0.076	0.023	0.053	18.5
5	0.089	0.028	0.061	18.9
6	0.106	0.035	0.071	21.7
7	0.119	0.040	0.079	22.2
8	0.134	0.047	0.087	25.0
9	0.145	0.053	0.092	24.3

Table 67: Change in height with pressing force.

No.	$\Delta H(F)$ $\pm$ 0.01mm	$\Delta H(F)_{contraction}$ $\pm$ 0.005mm	$\Delta H(F)_{springback}$ $\pm$ 0.015mm	$\Delta H(F)_{relative\ springback}$ (%)
1	0.047	0.019	0.028	0.53
2	0.062	0.025	0.037	0.68
3	0.077	0.032	0.045	0.82
4	0.091	0.039	0.052	0.95
5	0.105	0.047	0.058	1.07
6	0.123	0.059	0.064	1.18
7	0.135	0.068	0.067	1.24
8	0.148	0.079	0.069	1.26
9	0.157	0.090	0.067	1.23

Table 68: Change in IC with pressing force.

No.	$\Delta IC(F)$ $\pm$ 0.01mm	$\Delta IC(F)_{springback}$ $\pm$ 0.01mm	$\Delta IC(F)_{relative\ springback}$ (%)
1	0.018	0.018	0.15
2	0.024	0.024	0.20
3	0.029	0.029	0.25
4	0.035	0.035	0.29
5	0.040	0.040	0.33
6	0.046	0.046	0.38
7	0.049	0.049	0.42
8	0.053	0.053	0.45
9	0.055	0.055	0.47

Table 69: Change in springback and relative springback ratio with pressing force.

No.	$\Delta H(F)_{springback}$ $/\Delta IC(F)_{springback}$	$\Delta H(F)_{relative\ springback}$ $/\Delta IC(F)_{relative\ springback}$
1	1.57	3.46
2	1.55	3.41
3	1.52	3.35
4	1.50	3.28
5	1.46	3.21
6	1.41	3.09
7	1.37	2.98
8	1.29	2.81
9	1.22	2.64

Table 70: Change in volumetric and relative volumetric springback with pressing force.

No.	$\Delta V(F)$ (cm^3)	$\Delta V(F)_{contraction}$ (cm^3)	$\Delta V(F)_{springback}$ (cm^3)	$\Delta V(F)_{relative\ springback}$ (%)
1	0.006	-0.013	0.019	0.89
2	0.008	-0.013	0.021	1.15
3	0.009	-0.013	0.023	1.41
4	0.011	-0.014	0.025	1.65
5	0.013	-0.018	0.031	1.86
6	0.015	-0.017	0.031	2.10
7	0.016	-0.018	0.034	2.23
8	0.017	-0.014	0.031	2.32
9	0.018	-0.017	0.034	2.33

Table 71: Change in green density with pressure.

No.	Pressure (kN/cm^2)	Green density (g/cm^3)
1	3.28	5.65
2	4.45	5.89
3	5.73	6.09
4	7.06	6.31
5	8.45	6.42
6	10.5	6.57
7	12.1	6.67
8	14.2	6.80
9	16.1	6.88

D.5 Measured and calculated data for Grade B powder - triangular compacts

Measured data

In order to preserve a 1:1 punch travel ratio, the maximum filling height that could be chosen was 12.74mm. This filling height corresponded to a pressing force of 40.2kN. Thus the experiment was limited to a range of pressing forces between 0kN and 40.2kN.

Table 72: Recorded and measured data for the triangular tight-fit compact using grade B powder.

No.	Filling height F_h(mm)	Pressing Force F(kN) ± 0.1kN	Mass M(g) ± 0.001g	Lip L(mm) ± 0.01mm	Corner Lip L_c(mm) ± 0.01mm	Height H(mm) ± 0.01mm	IC(mm) ± 0.01mm
1	10.00	4.7	6.360	0.169	0.310	5.42	11.92
2	10.50	7.3	6.654	0.188	0.315	5.44	11.92
3	11.00	11.0	6.928	0.200	0.354	5.47	11.93
4	11.50	16.1	7.190	0.223	0.399	5.49	11.93
5	11.75	19.6	7.331	0.237	0.427	5.51	11.94
6	12.25	28.8	7.613	0.287	0.486	5.54	11.94
7	12.50	34.2	7.750	0.302	0.516	5.57	11.94
8	12.74	40.2	7.884	0.330	0.561	5.59	11.94

Calculated data

The data listed in Tables 73 to 78 was calculated using the equations described in section 5.2.

Table 73: Change in lip size with pressing force.

No.	$\Delta L(F)$ ± 0.01mm	$\Delta L(F)_{contraction}$ ± 0.005mm	$\Delta L(F)_{springback}$ ± 0.015mm	$\Delta L(F)_{relative\ springback}$ (%)
1	0.022	0.008	0.014	9.91
2	0.035	0.014	0.021	14.3
3	0.052	0.020	0.032	21.3
4	0.076	0.030	0.046	29.5
5	0.092	0.036	0.056	34.8
6	0.133	0.053	0.080	44.3
7	0.157	0.064	0.093	51.8
8	0.182	0.075	0.108	56.5

Table 74: Change in height with pressing force.

No.	$\Delta H(F)$ $\pm$ 0.01mm	$\Delta H(F)_{contraction}$ $\pm$ 0.005mm	$\Delta H(F)_{springback}$ $\pm$ 0.015mm	$\Delta H(F)_{relative\ springback}$ (%)
1	0.032	0.015	0.017	0.32
2	0.048	0.022	0.026	0.48
3	0.071	0.034	0.037	0.68
4	0.100	0.050	0.050	0.92
5	0.118	0.061	0.057	1.05
6	0.160	0.089	0.071	1.30
7	0.181	0.106	0.075	1.36
8	0.201	0.125	0.076	1.38

Table 75: Change in IC with pressing force.

No.	$\Delta IC(F)$ $\pm$ 0.01mm	$\Delta IC(F)_{springback}$ $\pm$ 0.01mm	$\Delta IC(F)_{relative\ springback}$ (%)
1	0.006	0.006	0.05
2	0.010	0.010	0.08
3	0.014	0.014	0.11
4	0.018	0.018	0.15
5	0.021	0.021	0.18
6	0.026	0.026	0.22
7	0.027	0.027	0.23
8	0.027	0.027	0.23

Table 76: Change in springback and relative springback ratio with pressing force.

No.	$\Delta H(F)_{springback}$ $/\Delta IC(F)_{springback}$	$\Delta H(F)_{relative\ springback}$ $/\Delta IC(F)_{relative\ springback}$
1	2.70	5.95
2	2.70	5.95
3	2.71	5.95
4	2.72	5.96
5	2.73	5.97
6	2.76	6.02
7	2.79	6.05
8	2.83	6.11

Table 77: Change in volumetric and relative volumetric springback with force.

No.	$\Delta V(F)$ (cm^3)	$\Delta V(F)_{contraction}$ (cm^3)	$\Delta V(F)_{springback}$ (cm^3)	$\Delta V(F)_{relative\ springback}$ (%)
1	0.006	0.006	0.000	0.19
2	0.009	0.008	0.001	0.28
3	0.013	0.011	0.002	0.38
4	0.016	0.013	0.003	0.48
5	0.017	0.013	0.004	0.51
6	0.016	0.013	0.003	0.50
7	0.013	0.011	0.002	0.41
8	0.007	0.007	0.000	0.25

Table 78: Change in green density with pressure.

No.	Pressure (kN/cm^2)	Green density (g/cm^3)
1	2.61	6.31
2	4.06	6.60
3	6.12	6.83
4	8.95	7.08
5	10.9	7.20
6	16.0	7.48
7	19.0	7.58
8	22.4	7.71

Appendix E: SBA compacts measured and calculated data

E.1 Measured and calculated data for Grade B powder – square compact

Measured data with hold-down activated

A maximum filling height of 13.00mm could be chosen while preserving a 1:1 travel ratio. At this filling height the pressing force was 119.8kN. Thus compacts were pressed in the range of forces between 0kN and 119.8kN. As seen lip and corner lip dimensions appear only at extremely high pressing forces.

Table 79: Recorded and measured data for the square SBA compact using grade B powder with hold-down.

No.	Filling height F_h(mm)	Pressing Force F(kN) ± 0.1kN	Mass M(g) ± 0.001g	Lip L(mm) ± 0.01mm	Corner Lip L_c(mm) ± 0.01mm	Edge width ± 0.01mm	Height H(mm) ± 0.01mm	IC(mm) ± 0.01mm
1	9.00	8.4	4.446	0.000	0.000	0.022	4.68	11.736
2	9.50	13.6	4.661	0.000	0.000	0.023	4.70	11.742
3	10.00	21.0	4.875	0.000	0.000	0.025	4.73	11.753
4	10.50	31.6	5.083	0.000	0.000	0.026	4.77	11.773
5	11.00	44.2	5.286	0.000	0.000	0.027	4.82	11.781
6	12.00	77.7	5.692	0.000	0.000	0.028	4.93	11.817
7	13.00	119.8	6.087	0.000	0.112	0.029	5.06	11.871
8	12.50	98.5	5.895	0.000	0.000	0.026	5.00	11.842
9	10.25	25.8	4.979	0.000	0.000	0.024	4.76	11.759
10	9.75	16.8	4.770	0.000	0.000	0.025	4.72	11.751

Calculated data with hold-down

The data listed in Tables 80 to 84 was calculated using the equations described in section 5.3.

Table 80: Change in height with pressing force.

No.	ΔH(F) ± 0.01mm	$\Delta H(F)_{contraction}$ ± 0.005mm	$\Delta H(F)_{springback}$ ± 0.015mm	$\Delta H(F)_{relative\ springback}$ (%)
1	0.035	0.024	0.011	0.23
2	0.055	0.039	0.017	0.36
3	0.085	0.060	0.025	0.53
4	0.125	0.090	0.036	0.75
5	0.172	0.125	0.046	0.97
6	0.286	0.221	0.065	1.35
7	0.410	0.340	0.070	1.40
8	0.350	0.280	0.070	1.43
9	0.103	0.073	0.030	0.63
10	0.068	0.048	0.020	0.44

Table 81: Change in IC with pressing force.

No.	$\Delta IC(F)$ ± 0.01mm	$\Delta IC(F)_{contraction}$ ± 0.01mm	$\Delta IC(F)_{springback}$ ± 0.02mm	$\Delta IC(F)_{relative\ springback}$ (%)
1	0.012	0.004	0.008	0.06
2	0.018	0.006	0.012	0.10
3	0.028	0.010	0.018	0.15
4	0.042	0.015	0.027	0.23
5	0.057	0.021	0.036	0.31
6	0.094	0.037	0.057	0.49
7	0.134	0.057	0.076	0.65
8	0.115	0.047	0.068	0.57
9	0.034	0.012	0.022	0.19
10	0.023	0.008	0.015	0.13

Table 82: Change in springback and relative springback ratio with pressing force.

No.	$\Delta H(F)_{springback} / \Delta IC(F)_{springback}$	$\Delta H(F)_{relative\ springback} / \Delta IC(F)_{relative\ springback}$
1	1.42	3.57
2	1.40	3.51
3	1.38	3.44
4	1.34	3.32
5	1.29	3.18
6	1.15	2.77
7	0.91	2.16
8	1.04	2.48
9	1.36	3.38
10	1.39	3.48

Table 83: Change in volumetric and relative volumetric springback with pressing force.

No.	$\Delta V(F)$ (cm^3)	$\Delta V(F)_{contraction}$ (cm^3)	$\Delta V(F)_{springback}$ (cm^3)	$\Delta V(F)_{relative\ springback}$ (%)
1	0.005	0.003	0.002	0.30
2	0.008	0.005	0.003	0.47
3	0.012	0.008	0.004	0.70
4	0.018	0.012	0.006	1.00
5	0.024	0.016	0.008	1.30
6	0.041	0.029	0.011	1.88
7	0.059	0.046	0.013	2.11
8	0.050	0.037	0.013	2.06
9	0.014	0.009	0.005	0.84
10	0.009	0.006	0.003	0.57

Table 84: Change in green density with pressure.

No.	Pressure (kN/cm^2)	Green density (g/cm^3)
1	6.19	7.64
2	10.0	7.97
3	15.5	8.27
4	23.3	8.54
5	32.6	8.78
6	57.3	9.21
7	88.3	9.55
8	72.6	9.39
9	19.0	8.39
10	12.4	8.11

Measured data without hold-down

The maximum filling height that could be achieved while preserving the 1:1 travel ratio was 13.0mm. However the compact pressed at this filling height developed defects upon ejection from the die. Therefore maximum filling height that could be achieved while maintaining compact integrity after ejection was 12.50mm corresponding to a pressing force of 98.6kN. Thus compacts were pressed in the range of pressing forces between 0kN and 98.6kN. The lip dimension was visible on the compacts pressed at or near the maximum filling height.

Table 85: Recorded and measured data for the square SBA compact using grade B powder without hold-down.

No.	Filling height F_h(mm)	Pressing Force F(kN) ± 0.1kN	Mass M(g) ± 0.001g	Lip L(mm) ± 0.01mm	Corner Lip L_c(mm) ± 0.01mm	Edge width ± 0.01mm	Height H(mm) ± 0.01mm	IC(mm) ± 0.01mm
1	9.00	8.7	4.470	0.000	0.000	0.024	4.69	11.735
2	9.50	13.8	4.674	0.000	0.000	0.025	4.71	11.749
3	10.00	21.4	4.878	0.000	0.000	0.026	4.74	11.770
4	10.50	31.1	5.081	0.000	0.000	0.030	4.77	11.802
5	10.25	26.1	4.983	0.000	0.000	0.027	4.76	11.780
6	9.75	17.2	4.776	0.000	0.000	0.035	4.73	11.759
7	11.00	44.3	5.284	0.000	0.000	0.031	4.80	11.831
8	12.00	77.6	5.695	0.164	0.295	0.029	4.88	11.875
9	12.50	98.6	5.902	0.315	0.452	0.033	4.93	11.884

Calculated data without hold-down

The data listed in Tables 86 to 90 was calculated using the equations described in section 5.3.

Table 86: Change in height with pressing force.

No.	$\Delta H(F)$ $\pm$ 0.01mm	$\Delta H(F)_{contraction}$ $\pm$ 0.005mm	$\Delta H(F)_{springback}$ $\pm$ 0.015mm	$\Delta H(F)_{relative\ springback}$ (%)
1	0.047	0.025	0.022	0.48
2	0.074	0.039	0.035	0.75
3	0.115	0.061	0.054	1.15
4	0.165	0.088	0.077	1.64
5	0.139	0.074	0.065	1.39
6	0.092	0.049	0.044	0.93
7	0.233	0.126	0.107	2.28
8	0.396	0.220	0.176	3.74
9	0.494	0.280	0.214	4.55

Table 87: Change in IC with pressing force.

No.	$\Delta IC(F)$ $\pm$ 0.01mm	$\Delta IC(F)_{contraction}$ $\pm$ 0.01mm	$\Delta IC(F)_{springback}$ $\pm$ 0.02mm	$\Delta IC(F)_{relative\ springback}$ (%)
1	0.026	0.004	0.022	0.19
2	0.041	0.007	0.034	0.29
3	0.062	0.010	0.052	0.44
4	0.089	0.015	0.074	0.63
5	0.075	0.012	0.063	0.54
6	0.050	0.008	0.042	0.36
7	0.123	0.021	0.102	0.87
8	0.202	0.037	0.165	1.41
9	0.246	0.047	0.199	1.70

Table 88: Change in springback and relative springback ratio with pressing force.

No.	$\Delta H(F)_{springback}$ $/\Delta IC(F)_{springback}$	$\Delta H(F)_{relative\ springback}$ $/\Delta IC(F)_{relative\ springback}$
1	1.03	2.58
2	1.03	2.58
3	1.04	2.59
4	1.04	2.60
5	1.04	2.59
6	1.03	2.58
7	1.05	2.62
8	1.07	2.65
9	1.08	2.68

Table 89: Change in volumetric and relative volumetric springback with pressing force.

No.	$\Delta V(F)$ (cm^3)	$\Delta V(F)_{contraction}$ (cm^3)	$\Delta V(F)_{springback}$ (cm^3)	$\Delta V(F)_{relative\ springback}$ (%)
1	0.007	0.003	0.004	0.68
2	0.010	0.004	0.006	1.07
3	0.015	0.006	0.010	1.64
4	0.021	0.007	0.014	2.33
5	0.018	0.006	0.011	1.98
6	0.013	0.005	0.008	1.32
7	0.026	0.007	0.019	3.24
8	0.031	-0.003	0.033	5.33
9	0.027	-0.015	0.042	6.50

Table 90: Change in green density with pressure.

No.	Pressure (kN/cm^2)	Green density (g/cm^3)
1	6.41	7.66
2	10.2	7.97
3	15.8	8.25
4	22.9	8.51
5	19.2	8.38
6	12.7	8.10
7	32.6	8.77
8	57.2	9.23
9	72.7	9.42

E.2 Measured and calculated data for Grade A powder – round compact

Measured data with hold-down

The maximum filling height that could be chosen while preserving the 1:1 travel ratio and compact integrity was 14.00mm. This corresponded to a pressing force of 109.3kN. Thus compacts were pressed covering a force range of 0kN to 109.3kN. The lip dimension was not visible on the compacts even at very high forces.

Table 91: Recorded and measured data for the round SBA compact using grade A powder with hold-down.

No.	Filling height F_h(mm)	Pressing Force F(kN) ± 0.1kN	Mass M(g) ± 0.001g	Lip L(mm) ± 0.01mm	Edge width ± 0.01mm	Height H(mm) ± 0.01mm	IC(mm) ± 0.01mm
1	10.00	12.8	3.799	0.000	0.025	4.72	12.340
2	10.50	18.6	3.967	0.000	0.024	4.75	12.344
3	11.00	25.9	4.127	0.000	0.028	4.785	12.364
4	11.50	35.4	4.289	0.000	0.030	4.82	12.373
5	12.00	46.2	4.442	0.000	0.033	4.86	12.385
6	12.50	58.7	4.595	0.000	0.029	4.91	12.399
7	13.00	72.6	4.754	0.000	0.043	4.96	12.418
8	13.50	90.3	4.922	0.000	0.040	5.03	12.431
9	14.00	109.3	5.088	0.000	0.038	5.08	12.445

Calculated data with hold-down

The data listed in Tables 92 to 96 was calculated using the equations described in section 4.3.

Table 92: Change in height with pressing force.

No.	ΔH(F) ± 0.01mm	$ΔH(F)_{contraction}$ ± 0.005mm	$ΔH(F)_{springback}$ ± 0.015mm	$ΔH(F)_{relative\ springback}$ (%)
1	0.058	0.039	0.019	0.41
2	0.084	0.057	0.027	0.58
3	0.115	0.078	0.037	0.77
4	0.155	0.108	0.047	0.99
5	0.199	0.141	0.058	1.21
6	0.247	0.179	0.068	1.41
7	0.298	0.221	0.077	1.58
8	0.358	0.274	0.084	1.69
9	0.418	0.332	0.086	1.72

Table 93: Change in IC with pressing force.

No.	$\Delta IC(F)$ $\pm$ 0.01mm	$\Delta IC(F)_{contraction}$ $\pm$ 0.01mm	$\Delta IC(F)_{springback}$ $\pm$ 0.02mm	$\Delta IC(F)_{relative\ springback}$ (%)
1	0.021	0.006	0.015	0.12
2	0.030	0.009	0.021	0.17
3	0.041	0.013	0.028	0.23
4	0.054	0.018	0.037	0.30
5	0.068	0.023	0.045	0.37
6	0.083	0.029	0.054	0.43
7	0.098	0.036	0.061	0.50
8	0.113	0.045	0.068	0.55
9	0.127	0.055	0.072	0.58

Table 94: Change in springback and relative springback ratio with pressing force.

No.	$\Delta H(F)_{springback}$ $/\Delta IC(F)_{springback}$	$\Delta H(F)_{relative\ springback}$ $/\Delta IC(F)_{relative\ springback}$
1	1.32	3.45
2	1.31	3.43
3	1.31	3.40
4	1.30	3.36
5	1.29	3.31
6	1.27	3.25
7	1.26	3.18
8	1.23	3.08
9	1.19	2.96

Table 95: Change in volumetric and relative volumetric springback with pressing force.

No.	$\Delta V(F)$ (cm^3)	$\Delta V(F)_{contraction}$ (cm^3)	$\Delta V(F)_{springback}$ (cm^3)	$\Delta V(F)_{relative\ springback}$ (%)
1	0.007	0.004	0.003	0.54
2	0.010	0.006	0.004	0.76
3	0.014	0.009	0.005	1.02
4	0.019	0.012	0.007	1.32
5	0.025	0.017	0.008	1.61
6	0.031	0.021	0.010	1.89
7	0.037	0.026	0.011	2.12
8	0.044	0.032	0.012	2.30
9	0.051	0.039	0.013	2.36

Table 96: Change in green density with pressure.

No.	Pressure (kN/cm^2)	Green density (g/cm^3)
1	10.8	7.42
2	15.7	7.70
3	21.9	7.94
4	30.0	8.18
5	39.1	8.40
6	49.7	8.59
7	61.4	8.78
8	76.4	8.95
9	92.5	9.15

Measured data without hold-down

The maximum filling height that could be chosen while preserving the 1:1 travel ratio and compact integrity was 13.50mm. This corresponded to a pressing force of 91.6kN. Thus compacts were pressed covering a force range of 0kN to 109.3kN. The compact pressed at 14.00mm broke apart upon ejection from the die. The lip dimension was not visible on the compacts.

Table 97: Recorded and measured data for the round SBA compact using grade A powder without hold-down.

No.	Filling height F_h(mm)	Pressing Force F(kN) ± 0.1kN	Mass M(g) ± 0.001g	Lip L(mm) ± 0.01mm	Edge width ± 0.01mm	Height H(mm) ± 0.01mm	IC(mm) ± 0.01mm
1	10.00	13.1	3.814	0.000	0.029	4.74	12.348
2	10.50	18.8	3.978	0.000	0.030	4.76	12.371
3	11.00	26.5	4.141	0.000	0.030	4.79	12.387
4	11.50	35.8	4.300	0.000	0.031	4.82	12.412
5	12.00	46.9	4.458	0.000	0.028	4.86	12.429
6	12.50	59.5	4.610	0.000	0.032	4.89	12.463
7	13.00	73.5	4.773	0.000	0.034	4.94	12.471
8	13.50	91.6	4.938	0.000	0.035	4.98	12.488

Calculated data without hold-down

The data listed in Tables 98 to 102 was calculated using the equations described in section 5.3.

Table 98: Change in height with pressing force.

No.	$\Delta H(F)$ $\pm$ 0.01mm	$\Delta H(F)_{contraction}$ $\pm$ 0.005mm	$\Delta H(F)_{springback}$ $\pm$ 0.015mm	$\Delta H(F)_{relative\ springback}$ (%)
1	0.051	0.040	0.011	0.23
2	0.072	0.057	0.015	0.31
3	0.100	0.081	0.019	0.40
4	0.132	0.109	0.023	0.48
5	0.168	0.142	0.026	0.53
6	0.207	0.181	0.026	0.53
7	0.247	0.224	0.023	0.47
8	0.293	0.279	0.014	0.28

Table 99: Change in IC with pressing force.

No.	$\Delta IC(F)$ $\pm$ 0.01mm	$\Delta IC(F)_{contraction}$ $\pm$ 0.01mm	$\Delta IC(F)_{springback}$ $\pm$ 0.02mm	$\Delta IC(F)_{relative\ springback}$ (%)
1	0.043	0.007	0.036	0.30
2	0.060	0.010	0.050	0.41
3	0.081	0.013	0.068	0.55
4	0.104	0.018	0.086	0.70
5	0.127	0.023	0.104	0.84
6	0.149	0.030	0.119	0.97
7	0.167	0.037	0.130	1.05
8	0.180	0.046	0.134	1.09

Table 100: Change in springback and relative springback ratio with pressing force.

No.	$\Delta H(F)_{springback}$ $/\Delta IC(F)_{springback}$	$\Delta H(F)_{relative\ springback}$ $/\Delta IC(F)_{relative\ springback}$
1	0.30	0.79
2	0.30	0.77
3	0.28	0.73
4	0.27	0.69
5	0.25	0.63
6	0.22	0.55
7	0.18	0.44
8	0.10	0.26

Table 101: Change in volumetric and relative volumetric springback with pressing force.

No.	$\Delta V(F)$ (cm^3)	$\Delta V(F)_{contraction}$ (cm^3)	$\Delta V(F)_{springback}$ (cm^3)	$\Delta V(F)_{relative\ springback}$ (%)
1	0.007	0.005	0.003	0.56
2	0.011	0.007	0.004	0.76
3	0.015	0.009	0.005	1.00
4	0.019	0.013	0.006	1.24
5	0.024	0.017	0.008	1.44
6	0.029	0.021	0.008	1.58
7	0.034	0.026	0.009	1.61
8	0.040	0.032	0.008	1.47

Table 102: Change in green density with pressure.

No.	Pressure (kN/cm^2)	Green density (g/cm^3)
1	11.1	7.42
2	15.9	7.69
3	22.4	7.94
4	30.3	8.18
5	39.7	8.40
6	50.4	8.60
7	62.2	8.82
8	77.5	9.03

E.3 Measured and calculated data for Grade B powder – round compact

Measured data with hold-down

The maximum filling height that could be chosen while preserving the 1:1 travel ratio and compact integrity was 13.50mm. This corresponded to a pressing force of 129.0kN. Thus compacts were pressed covering a force range of 0kN to 129.0kN. A lip could be seen on the component pressed at maximum filling height.

Table 103: Recorded and measured data for the round SBA compact using grade B powder with hold-down.

No.	Filling height F_h(mm)	Pressing Force F(kN) ± 0.1kN	Mass M(g) ± 0.001g	Lip L(mm) ± 0.01mm	Edge width ± 0.01mm	Height H(mm) ± 0.01mm	IC(mm) ± 0.01mm
1	9.50	12.2	4.088	0.000	0.030	4.74	12.344
2	9.00	7.9	3.903	0.000	0.029	4.72	12.341
3	10.00	18.9	4.274	0.000	0.034	4.78	12.355
4	10.50	27.3	4.448	0.000	0.035	4.80	12.370
5	11.00	38.3	4.625	0.000	0.038	4.85	12.377
6	11.50	51.8	4.802	0.000	0.037	4.90	12.397
7	12.50	87.7	5.178	0.000	0.040	5.03	12.439
8	13.50	129.0	5.530	0.268	0.043	5.13	12.487
9	10.75	32.2	4.536	0.000	0.036	4.83	12.373

Calculated data with hold-down

The data listed in Tables 104 to 108 was calculated using the equations described in section 4.3.

Table 104: Change in height with pressing force.

No.	ΔH(F) ± 0.01mm	$\Delta H(F)_{contraction}$ ± 0.005mm	$\Delta H(F)_{springback}$ ± 0.015mm	$\Delta H(F)_{relative\ springback}$ (%)
1	0.054	0.037	0.017	0.37
2	0.035	0.024	0.011	0.24
3	0.083	0.057	0.026	0.54
4	0.119	0.083	0.036	0.75
5	0.163	0.116	0.047	0.98
6	0.216	0.158	0.059	1.21
7	0.343	0.267	0.076	1.54
8	0.466	0.392	0.074	1.46
9	0.139	0.098	0.041	0.86

Table 105: Change in IC with pressing force.

No.	$\Delta IC(F)$ ± 0.01mm	$\Delta IC(F)_{contraction}$ ± 0.01mm	$\Delta IC(F)_{springback}$ ± 0.02mm	$\Delta IC(F)_{relative\ springback}$ (%)
1	0.017	0.006	0.010	0.09
2	0.011	0.004	0.007	0.06
3	0.026	0.009	0.016	0.13
4	0.037	0.014	0.023	0.19
5	0.051	0.019	0.031	0.25
6	0.067	0.026	0.041	0.34
7	0.109	0.044	0.065	0.53
8	0.153	0.065	0.088	0.71
9	0.043	0.016	0.027	0.22

Table 106: Change in springback and relative springback ratio with pressing force.

No.	$\Delta H(F)_{springback}$ / $\Delta IC(F)_{springback}$	$\Delta H(F)_{relative\ springback}$ / $\Delta IC(F)_{relative\ springback}$
1	1.65	4.30
2	1.67	4.38
3	1.61	4.18
4	1.56	4.05
5	1.50	3.85
6	1.41	3.60
7	1.17	2.92
8	0.84	2.05
9	1.53	3.95

Table 107: Change in volumetric and relative volumetric springback with pressing force.

No.	$\Delta V(F)$ (cm^3)	$\Delta V(F)_{contraction}$ (cm^3)	$\Delta V(F)_{springback}$ (cm^3)	$\Delta V(F)_{relative\ springback}$ (%)
1	0.007	0.004	0.002	0.46
2	0.004	0.003	0.002	0.30
3	0.010	0.007	0.004	0.69
4	0.015	0.010	0.005	0.95
5	0.020	0.013	0.007	1.25
6	0.027	0.018	0.008	1.57
7	0.042	0.031	0.011	2.12
8	0.058	0.042	0.016	2.24
9	0.017	0.011	0.006	1.09

Table 108: Change in green density with pressure.

No.	Pressure (kN/cm^2)	Green density (g/cm^3)
1	10.3	7.95
2	6.7	7.63
3	16.0	8.24
4	23.1	8.52
5	32.4	8.77
6	43.8	8.99
7	74.2	9.41
8	109.2	9.76
9	27.2	8.64

Measured data without hold-down

The maximum filling height that could be chosen while preserving the 1:1 travel ratio and compact integrity was 12.50mm. This corresponded to a pressing force of 85.4kN. Thus compacts were pressed covering a force range of 0kN to 85.4kN. At a filling height of 13.00mm (corresponding to a pressing force of 104.5kN) the compact developed many cracks during ejection.

Table 109: Recorded and measured data for the round SBA compact using grade B powder without hold-down.

No.	Filling height F_h(mm)	Pressing Force F(kN) ± 0.1kN	Mass M(g) ± 0.001g	Lip L(mm) ± 0.01mm	Edge width ± 0.01mm	Height H(mm) ± 0.01mm	IC(mm) ± 0.01mm
1	9.00	8.0	3.915	0.000	0.029	4.73	12.331
2	9.50	12.5	4.096	0.000	0.030	4.76	12.344
3	10.00	18.7	4.274	0.000	0.032	4.78	12.358
4	10.50	27.0	4.445	0.000	0.033	4.80	12.387
5	11.00	37.7	4.619	0.000	0.038	4.84	12.416
6	11.50	50.7	4.792	0.000	0.040	4.88	12.443
7	12.50	85.4	5.157	0.304	0.045	4.96	12.478
8	10.75	32.3	4.538	0.00	0.035	4.82	12.405

Calculated data without hold-down

The data listed in Tables 110 to 114 was calculated using the equations described in section 5.3.

Table 110: Change in height with pressing force.

No.	$\Delta H(F)$ $\pm$ 0.01mm	$\Delta H(F)_{contraction}$ $\pm$ 0.005mm	$\Delta H(F)_{springback}$ $\pm$ 0.015mm	$\Delta H(F)_{relative\ springback}$ (%)
1	0.031	0.024	0.007	0.14
2	0.048	0.038	0.010	0.20
3	0.070	0.057	0.013	0.28
4	0.099	0.082	0.017	0.35
5	0.134	0.115	0.019	0.40
6	0.174	0.154	0.019	0.40
7	0.262	0.260	0.003	0.05
8	0.117	0.098	0.018	0.38

Table 111: Change in IC with pressing force.

No.	$\Delta IC(F)$ $\pm$ 0.01mm	$\Delta IC(F)_{contraction}$ $\pm$ 0.01mm	$\Delta IC(F)_{springback}$ $\pm$ 0.02mm	$\Delta IC(F)_{relative\ springback}$ (%)
1	0.028	0.004	0.024	0.19
2	0.043	0.006	0.037	0.30
3	0.062	0.009	0.053	0.43
4	0.086	0.014	0.073	0.59
5	0.114	0.019	0.095	0.77
6	0.143	0.025	0.118	0.96
7	0.194	0.043	0.152	1.23
8	0.101	0.016	0.084	0.69

Table 112: Change in springback and relative springback ratio with pressing force.

No.	$\Delta H(F)_{springback} / \Delta IC(F)_{springback}$	$\Delta H(F)_{relative\ springback} / \Delta IC(F)_{relative\ springback}$
1	0.27	0.71
2	0.26	0.68
3	0.25	0.64
4	0.23	0.59
5	0.20	0.52
6	0.16	0.42
7	0.02	0.04
8	0.22	0.56

Table 113: Change in volumetric springback and relative volumetric springback with pressing force.

No.	$\Delta V(F)$ (cm^3)	$\Delta V(F)_{contraction}$ (cm^3)	$\Delta V(F)_{springback}$ (cm^3)	$\Delta V(F)_{fractional\ springback}$ (%)
1	0.005	0.003	0.002	0.35
2	0.007	0.004	0.003	0.52
3	0.010	0.007	0.004	0.74
4	0.015	0.009	0.005	0.99
5	0.020	0.013	0.006	1.23
6	0.025	0.018	0.008	1.43
7	0.038	0.026	0.011	1.40
8	0.017	0.011	0.006	1.12

Table 114: Change in green density with pressure.

No.	Pressure (kN/cm^2)	Green density (g/cm^3)
1	6.77	7.64
2	10.6	7.93
3	15.8	8.23
4	22.8	8.51
5	31.9	8.74
6	42.9	8.98
7	72.3	9.41
8	27.3	8.63

E.5 Measured and calculated data for Grade A powder – triangular compact

Measured data with hold-down

The maximum filling height that could be chosen while preserving the 1:1 travel ratio and compact integrity was 13.00mm. This corresponded to a pressing force of 106.4kN. Thus compacts were pressed covering a force range of 0kN to 106.4kN. The lip and corner lip dimensions were visible on the compact pressed at maximum filling height and pressing force.

Table 115: Recorded and measured data for the triangular SBA compact using grade A powder with hold-down.

No.	Filling height F_h(mm)	Pressing Force F(kN) ± 0.1kN	Mass M(g) ± 0.001g	Lip L(mm) ± 0.01mm	Corner Lip L_c (mm) ± 0.01mm	Edge width ± 0.01mm	Height H(mm) ± 0.01mm	IC(mm) ± 0.01mm
1	9.00	9.7	5.159	0.000	0.000	0.023	4.63	11.735
2	9.25	11.9	5.278	0.000	0.000	0.025	4.64	11.740
3	9.50	13.4	5.396	0.000	0.000	0.026	4.65	11.745
4	9.75	16.7	5.520	0.000	0.000	0.024	4.66	11.750
5	10.00	20.2	5.643	0.000	0.000	0.028	4.68	11.755
6	10.25	23.8	5.756	0.000	0.000	0.030	4.69	11.760
7	10.50	28.3	5.876	0.000	0.000	0.030	4.71	11.765
8	10.75	33.2	5.987	0.000	0.000	0.029	4.73	11.770
9	11.50	53.0	6.353	0.000	0.000	0.032	4.80	11.790
10	12.25	76.6	6.704	0.000	0.000	0.035	4.87	11.840
11	13.00	106.4	7.063	0.000	0.234	0.037	4.96	11.865

Calculated data with hold-down

The data listed in Tables 116 to 120 was calculated using the equations described in section 5.3.

Table 116: Change in height with pressing force.

No.	ΔH(F) ± 0.01mm	$\Delta H(F)_{contraction}$ ± 0.005mm	$\Delta H(F)_{springback}$ ± 0.015mm	$\Delta H(F)_{relative\ springback}$ (%)
1	0.044	0.029	0.016	0.34
2	0.054	0.035	0.019	0.41
3	0.060	0.040	0.021	0.45
4	0.075	0.049	0.025	0.55
5	0.089	0.060	0.030	0.64
6	0.104	0.070	0.034	0.73
7	0.122	0.084	0.039	0.83
8	0.141	0.098	0.044	0.93
9	0.213	0.156	0.056	1.19
10	0.284	0.226	0.058	1.21
11	0.355	0.314	0.041	0.84

Table 117: Change in IC with pressing force.

No.	$\Delta IC(F)$ ± 0.01mm	$\Delta IC(F)_{contraction}$ ± 0.01mm	$\Delta IC(F)_{springback}$ ± 0.02mm	$\Delta IC(F)_{relative\ springback}$ (%)
1	0.020	0.004	0.015	0.13
2	0.024	0.005	0.019	0.16
3	0.027	0.006	0.021	0.18
4	0.034	0.008	0.026	0.22
5	0.041	0.009	0.032	0.27
6	0.048	0.011	0.037	0.32
7	0.057	0.013	0.044	0.38
8	0.066	0.015	0.051	0.44
9	0.105	0.024	0.081	0.69
10	0.149	0.035	0.114	0.97
11	0.203	0.048	0.154	1.32

Table 118: Change in springback and relative springback ratio with pressing force.

No.	$\Delta H(F)_{springback}$ / $\Delta IC(F)_{springback}$	$\Delta H(F)_{relative\ springback}$ / $\Delta IC(F)_{relative\ springback}$
1	1.02	2.59
2	1.00	2.55
3	0.99	2.51
4	0.97	2.45
5	0.94	2.38
6	0.92	2.31
7	0.88	2.22
8	0.85	2.12
9	0.70	1.72
10	0.51	1.25
11	0.27	0.63

Table 119: Change in volumetric and relative volumetric springback with pressing force.

No.	$\Delta V(F)$ (cm^3)	$\Delta V(F)_{contraction}$ (cm^3)	$\Delta V(F)_{springback}$ (cm^3)	$\Delta V(F)_{relative\ springback}$ (%)
1	0.009	0.005	0.004	0.37
2	0.011	0.006	0.005	0.45
3	0.012	0.007	0.006	0.50
4	0.015	0.009	0.007	0.61
5	0.018	0.010	0.008	0.73
6	0.022	0.012	0.009	0.84
7	0.025	0.015	0.011	0.97
8	0.030	0.017	0.012	1.11
9	0.045	0.028	0.017	1.56
10	0.062	0.042	0.020	1.90
11	0.080	0.059	0.021	2.03

Table 120: Change in green density with pressing force.

No.	Pressure (kN/cm^2)	Green density (g/cm^3)
1	5.49	5.97
2	6.74	6.10
3	7.59	6.22
4	9.45	6.34
5	11.4	6.46
6	13.5	6.56
7	16.0	6.67
8	18.8	6.77
9	30.0	7.07
10	43.4	7.31
11	60.2	7.54

Measured data without hold-down

The maximum filling height that could be chosen while preserving the 1:1 travel ratio and compact integrity was 12.00mm. This corresponded to a pressing force of 68.7kN. The edges of a compact pressed at 12.5mm (87.1kN) were cracked. Thus compacts were pressed covering a force range of 0kN to 68.7kN. A corner lip was visible at lower pressing forces than expected (68.7kN).

Table 121: Recorded and measured data for the triangular SBA compact using grade A powder without hold-down.

No.	Filling height F_h(mm)	Pressing Force F(kN) ± 0.1kN	Mass M(g) ± 0.001g	Lip L(mm) ± 0.01mm	Corner Lip L_c(mm) ± 0.01mm	Edge width ± 0.01mm	Height H(mm) ± 0.01mm	IC(mm) ± 0.01mm
1	9.00	9.6	5.181	0.000	0.000	0.024	4.64	11.735
2	9.50	14.0	5.424	0.000	0.000	0.025	4.66	11.755
3	9.75	16.9	5.547	0.000	0.000	0.027	4.67	11.765
4	10.00	20.5	5.667	0.000	0.000	0.030	4.69	11.770
5	10.25	24.4	5.776	0.000	0.000	0.029	4.70	11.775
6	10.50	29.2	5.900	0.000	0.000	0.033	4.71	11.790
7	10.75	34.6	6.021	0.000	0.000	0.032	4.73	11.800
8	11.50	53.5	6.369	0.000	0.168	0.034	4.78	11.840
9	12.00	68.7	6.599	0.000	0.254	0.035	4.83	11.865

Calculated data without hold-down

The data listed in Tables 122 to 126 was calculated using the equations described in section 5.3.

Table 122: Change in height with pressing force.

No.	$\Delta H(F)$ $\pm$ 0.01mm	$\Delta H(F)_{contraction}$ $\pm$ 0.005mm	$\Delta H(F)_{springback}$ $\pm$ 0.015mm	$\Delta H(F)_{relative\ springback}$ (%)
1	0.037	0.028	0.009	0.20
2	0.054	0.041	0.013	0.27
3	0.064	0.050	0.015	0.31
4	0.077	0.060	0.017	0.36
5	0.091	0.072	0.019	0.40
6	0.107	0.086	0.021	0.44
7	0.124	0.102	0.022	0.47
8	0.180	0.158	0.022	0.47
9	0.218	0.203	0.016	0.33

Table 123: Change in IC with pressing force.

No.	$\Delta IC(F)$ $\pm$ 0.01mm	$\Delta IC(F)_{contraction}$ $\pm$ 0.01mm	$\Delta IC(F)_{springback}$ $\pm$ 0.02mm	$\Delta IC(F)_{fractional\ springback}$ (%)
1	0.027	0.004	0.023	0.20
2	0.039	0.006	0.033	0.28
3	0.047	0.008	0.039	0.33
4	0.056	0.009	0.046	0.40
5	0.065	0.011	0.054	0.46
6	0.077	0.013	0.063	0.54
7	0.089	0.016	0.073	0.62
8	0.127	0.024	0.103	0.87
9	0.152	0.031	0.121	1.03

Table 124: Change springback and relative springback ratio with pressing force.

No.	$\Delta H(F)_{springback}$ $/\Delta IC(F)_{springback}$	$\Delta H(F)_{relative\ springback}$ $/\Delta IC(F)_{relative\ springback}$
1	0.40	1.01
2	0.38	0.97
3	0.37	0.94
4	0.36	0.91
5	0.35	0.87
6	0.33	0.82
7	0.30	0.76
8	0.22	0.53
9	0.13	0.32

Table 125: Change in volumetric and relative volumetric springback with pressing force.

No.	$\Delta V(F)$ (cm^3)	$\Delta V(F)_{contraction}$ (cm^3)	$\Delta V(F)_{springback}$ (cm^3)	$\Delta V(F)_{relative\ springback}$ (%)
1	0.009	0.006	0.003	0.41
2	0.013	0.008	0.005	0.57
3	0.016	0.010	0.006	0.67
4	0.019	0.012	0.007	0.79
5	0.022	0.014	0.008	0.90
6	0.026	0.017	0.009	1.03
7	0.030	0.020	0.010	1.15
8	0.044	0.031	0.013	1.41
9	0.053	0.040	0.013	1.44

Table 126: Change in green density with pressure.

No.	Pressure (kN/cm^2)	Green density (g/cm^3)
1	5.43	5.99
2	7.92	6.23
3	9.57	6.35
4	11.6	6.46
5	13.8	6.56
6	16.5	6.68
7	19.6	6.79
8	30.3	7.08
9	38.9	7.25

E.6 Measured and calculated data for Grade B powder – triangular compact

Measured data with hold-down

The maximum filling height that could be chosen while preserving the 1:1 travel ratio and compact integrity was 12.25mm. This corresponded to a pressing force of 102.5kN. Thus compacts were pressed covering a force range of 0kN to 102.5kN. No lip or corner lip dimensions were observed on any of the compacts.

Table 127: Recorded and measured data for the triangular SBA compact using grade B powder with hold-down.

No.	Filling height F_h(mm)	Pressing Force F(kN) ± 0.1kN	Mass M(g) ± 0.001g	Lip L(mm) ± 0.01mm	Corner Lip L_c(mm) ± 0.01mm	Edge width ± 0.01mm	Height H(mm) ± 0.01mm	IC(mm) ± 0.01mm
1	8.75	8.7	5.619	0.000	0.000	0.023	4.63	11.750
2	9.25	13.9	5.887	0.000	0.000	0.025	4.66	11.755
3	9.75	21.6	6.152	0.000	0.000	0.027	4.69	11.765
4	10.25	31.9	6.414	0.000	0.000	0.030	4.73	11.780
5	10.75	45.9	6.674	0.000	0.000	0.032	4.78	11.795
6	11.25	62.6	6.934	0.000	0.000	0.035	4.83	11.810
7	12.00	93.4	7.326	0.000	0.000	0.039	4.93	11.850
8	11.75	82.8	7.193	0.000	0.000	0.037	4.88	11.830
9	12.25	102.5	7.452	0.000	0.000	0.040	4.94	11.880

Calculated data with hold-down

The data listed in Tables 128 to 132 was calculated using the equations described in section 5.3.

Table 128: Change in height with pressing force.

No.	$\Delta H(F)$ ± 0.01mm	$\Delta H(F)_{contraction}$ ± 0.005mm	$\Delta H(F)_{springback}$ ± 0.015mm	$\Delta H(F)_{relative\ springback}$ (%)
1	0.041	0.026	0.015	0.32
2	0.064	0.041	0.023	0.49
3	0.096	0.064	0.033	0.70
4	0.137	0.094	0.043	0.92
5	0.187	0.135	0.052	1.10
6	0.239	0.185	0.054	1.14
7	0.312	0.276	0.036	0.73
8	0.290	0.244	0.046	0.94
9	0.327	0.302	0.025	0.50

Table 129: Change in IC with pressing force.

No.	$\Delta IC(F)$ $\pm$ 0.01mm	$\Delta IC(F)_{contraction}$ $\pm$ 0.01mm	$\Delta IC(F)_{springback}$ $\pm$ 0.02mm	$\Delta IC(F)_{relative\ springback}$ (%)
1	0.012	0.004	0.008	0.07
2	0.019	0.006	0.013	0.11
3	0.029	0.010	0.019	0.16
4	0.041	0.014	0.027	0.23
5	0.057	0.021	0.036	0.31
6	0.074	0.028	0.046	0.39
7	0.101	0.042	0.058	0.49
8	0.092	0.038	0.055	0.47
9	0.107	0.046	0.061	0.51

Table 130: Change in springback and relative springback ratio with pressing force.

No.	$\Delta H(F)_{springback}$ $/\Delta IC(F)_{springback}$	$\Delta H(F)_{relative\ springback}$ $/\Delta IC(F)_{relative\ springback}$
1	1.86	4.73
2	1.81	4.58
3	1.72	4.35
4	1.61	4.03
5	1.43	3.56
6	1.18	2.92
7	0.62	1.49
8	0.83	2.03
9	0.41	0.98

Table 131: Change in volumetric and relative volumetric springback with pressing force.

No.	$\Delta V(F)$ (cm^3)	$\Delta V(F)_{contraction}$ (cm^3)	$\Delta V(F)_{springback}$ (cm^3)	$\Delta V(F)_{relative\ springback}$ (%)
1	0.009	0.005	0.003	0.40
2	0.013	0.008	0.005	0.61
3	0.020	0.013	0.008	0.88
4	0.029	0.019	0.010	1.17
5	0.040	0.027	0.013	1.43
6	0.051	0.037	0.014	1.56
7	0.066	0.055	0.012	1.28
8	0.062	0.049	0.013	1.45
9	0.070	0.060	0.010	1.07

Table 132: Change in green density with pressure.

No.	Pressure (kN/cm^2)	Green density (g/cm^3)
1	4.92	6.50
2	7.87	6.77
3	12.2	7.02
4	18.1	7.24
5	26.0	7.45
6	35.4	7.64
7	52.9	7.89
8	46.9	7.83
9	58.0	7.98

Measured data without hold-down

The maximum filling height that could be chosen while preserving the 1:1 travel ratio and compact integrity was 11.75mm. This corresponded to a pressing force of 82.3kN. Thus compacts were pressed covering a force range of 0kN to 82.3kN. At a filling height of 12.25mm (corresponding to a pressing force of 102.3kN) the compact corners appeared to be cracked and damaged.

Table 133: Recorded and measured data for the triangular SBA compact using grade B powder with hold-down.

No.	Filling height F_h(mm)	Pressing Force F(kN) ± 0.1kN	Mass M(g) ± 0.001g	Lip L(mm) ± 0.01mm	Corner Lip L_c(mm) ± 0.01mm	Edge width ± 0.01mm	Height H(mm) ± 0.01mm	IC(mm) ± 0.01mm
1	8.75	9.2	5.619	0.000	0.000	0.024	4.64	11.750
2	9.25	14.1	5.887	0.000	0.000	0.027	4.66	11.760
3	9.75	22.6	6.153	0.000	0.000	0.037	4.69	11.775
4	10.25	33.3	6.410	0.000	0.000	0.033	4.72	11.805
5	10.75	46.8	6.677	0.000	0.000	0.032	4.76	11.835
6	11.25	63.9	6.939	0.000	0.207	0.030	4.80	11.870
7	11.75	82.3	7.197	0.172	0.427	0.045	4.84	11.895

Calculated data without hold-down

The data listed in Tables 134 to 138 was calculated using the equations described in section 4.3.

Table 134: Change in height with pressing force.

No.	$\Delta H(F)$ $\pm$ 0.01mm	$\Delta H(F)_{contraction}$ $\pm$ 0.005mm	$\Delta H(F)_{springback}$ $\pm$ 0.015mm	$\Delta H(F)_{relative\ springback}$ (%)
1	0.036	0.027	0.009	0.19
2	0.054	0.042	0.012	0.26
3	0.083	0.067	0.016	0.35
4	0.117	0.098	0.018	0.39
5	0.154	0.138	0.016	0.34
6	0.193	0.189	0.004	0.09
7	0.225	0.243	-0.018	-0.38

Table 135: Change in IC with pressing force.

No.	$\Delta IC(F)$ $\pm$ 0.01mm	$\Delta IC(F)_{contraction}$ $\pm$ 0.01mm	$\Delta IC(F)_{springback}$ $\pm$ 0.02mm	$\Delta IC(F)_{relative\ springback}$ (%)
1	0.025	0.004	0.021	0.18
2	0.038	0.006	0.032	0.27
3	0.060	0.010	0.049	0.42
4	0.085	0.015	0.070	0.59
5	0.114	0.021	0.093	0.79
6	0.147	0.029	0.118	1.01
7	0.177	0.037	0.140	1.19

Table 136: Change in springback and relative springback ratio with pressing force.

No.	$\Delta H(F)_{springback}$ / $\Delta IC(F)_{springback}$	$\Delta H(F)_{relative\ springback}$ / $\Delta IC(F)_{relative\ springback}$
1	0.41	1.04
2	0.38	0.96
3	0.33	0.83
4	0.26	0.66
5	0.17	0.42
6	0.04	0.09
7	-0.13	-0.32

Table 137: Change in volumetric springback and relative volumetric springback with pressing force.

No.	$\Delta V(F)$ (cm^3)	$\Delta V(F)_{contraction}$ (cm^3)	$\Delta V(F)_{springback}$ (cm^3)	$\Delta V(F)_{relative\ springback}$ (%)
1	0.008	0.005	0.003	0.38
2	0.012	0.007	0.005	0.55
3	0.019	0.012	0.007	0.80
4	0.027	0.018	0.009	1.03
5	0.037	0.027	0.011	1.19
6	0.048	0.038	0.011	1.18
7	0.059	0.071	-0.012	0.92

Table 138: Change in green density with pressure.

No.	Pressure (kN/cm^2)	Green density (g/cm^3)
1	5.21	6.49
2	7.98	6.76
3	12.8	7.00
4	18.8	7.23
5	26.5	7.45
6	36.2	7.66
7	46.6	8.04

Appendix F: Contraction results

F.1 Round tight-fit tool

Upper and lower punch-ram system contraction

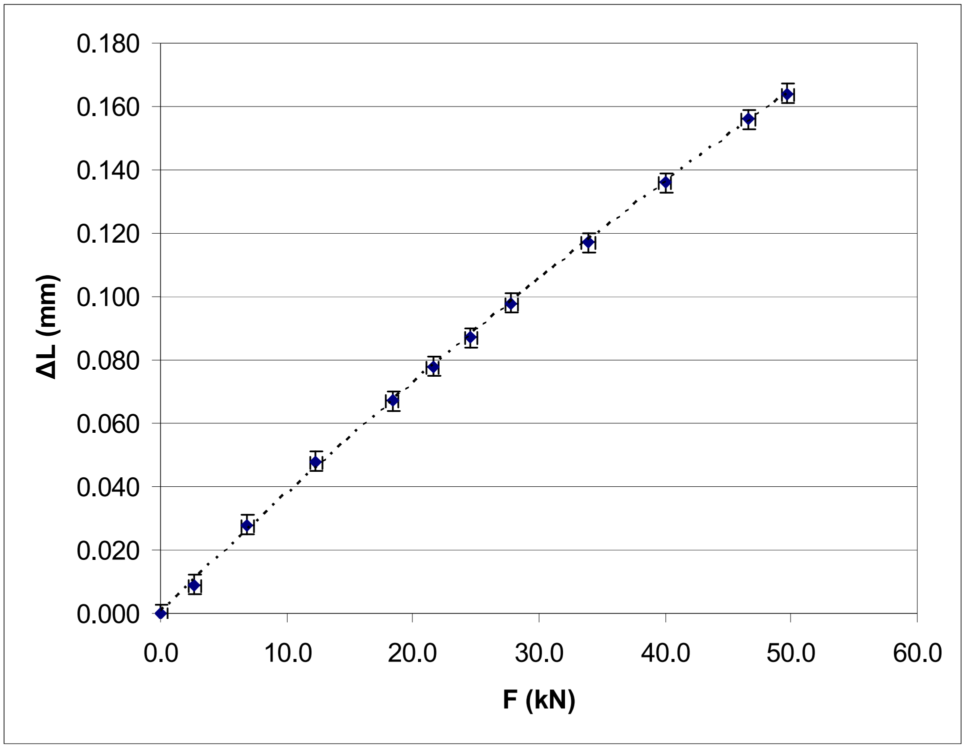

Figure 45: Change in upper and lower punch-ram system contraction with pressing force.

Best fit equation:

$$\Delta L_{\text{Upper-Lower Punch-Ram}} = -1.066\times10^{-5}\,F^2 + 3.819\times10^{-3}\,F - 4.783\times10^{-4}\;(R^2 = 9.996\times10^{-1}) \qquad \ldots (81)$$

Best fit straight line with zero intercept:

$$\Delta L_{\text{Upper-Lower Punch-Ram}} = 3.417\times10^{-3}\,F\;(R^2 = 9.953\times10^{-1}) \qquad \ldots (82)$$

Maximum difference between equations 81 and 82, at a typical pressing force of 25kN, is approximately 0.003mm thus equation 82 is an excellent approximation of equation 81.

Upper punch-ram system contraction

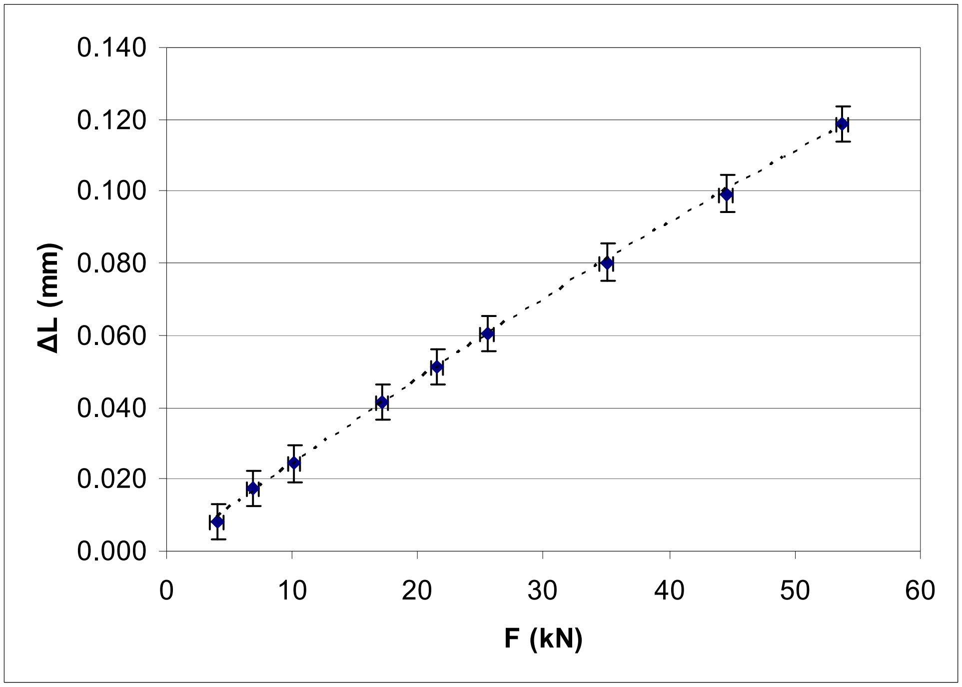

Figure 46: Change in upper punch-ram system contraction with pressing force.

Best fit equation:

$\Delta L_{\text{Upper Punch-Ram}} = -6.203\times10^{-6}\, F^2 + 2.545\times10^{-3}\, F - 7.331\times10^{-4}\ (R^2 = 9.997\times10^{-1})$ . . . (83)

Best fit straight line with zero intercept:

$\Delta L_{\text{Upper Punch-Ram}} = 2.265\times10^{-3}\, F\ (R^2 = 9.966\times10^{-1})$ . . . (84)

Maximum difference between equations 83 and 84, at a typical pressing force of 25kN, is approximately 0.002mm thus equation 84 is an excellent approximation of equation 83.

Upper ram contraction

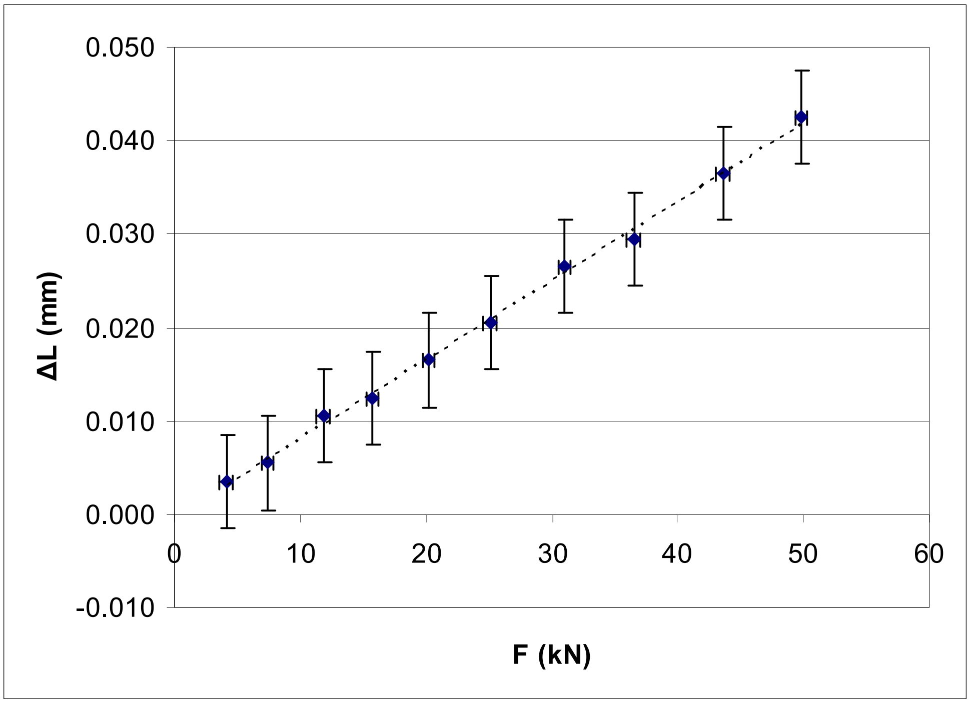

Figure 47: Change in upper ram contraction with pressing force.

Best fit equation:

$$\Delta L_{\text{Upper Ram}} = 8.228 \times 10^{-4}\, F \ (R^2 = 9.960 \times 10^{-1}) \qquad \ldots (85)$$

In this case the data were better interpolated by a straight line rather than a quadratic equation.

Contraction of the upper ram and punch base system

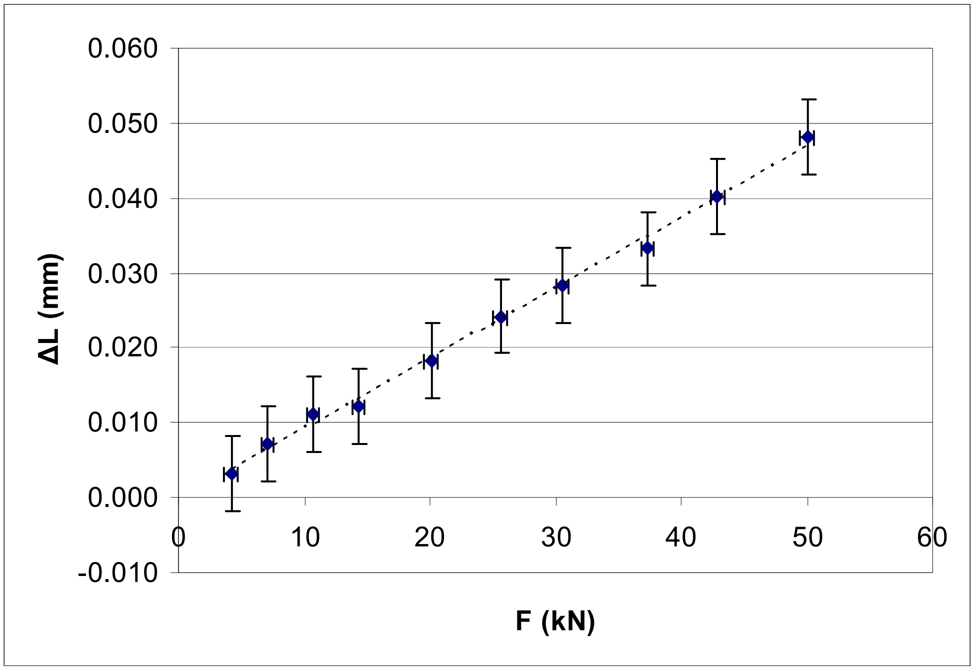

Figure 48: Change in the upper ram and punch base system contraction.

Best fit equation:

$$\Delta L_{\text{Upper Ram and Punch Base}} = 9.344 \times 10^{-4} F \ (R^2 = 9.933 \times 10^{-1}) \qquad \ldots (86)$$

Again a straight line rather than a quadratic equation forms the best fit equation.

F.2 Triangular tight-fit tool

Upper and lower punch-ram system contraction

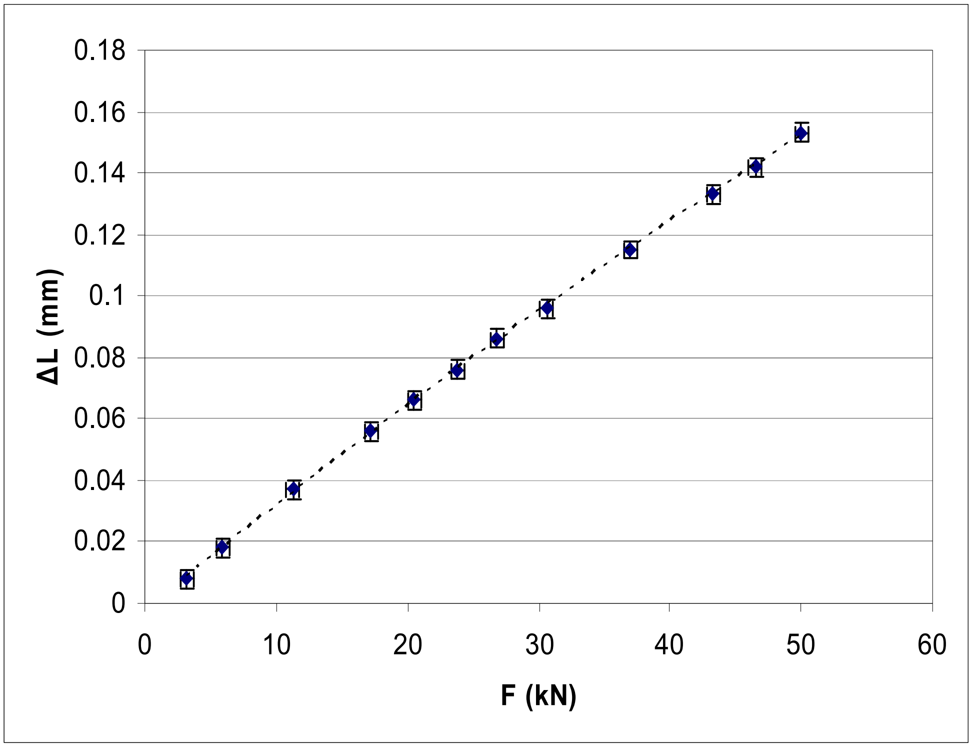

Figure 49: Change in upper and lower punch-ram system contraction with pressing force.

Best fit equation:

$$\Delta L_{\text{Upper-Lower Punch-Ram}} = -8.016\times10^{-6} F^2 + 3.482\times10^{-3} F - 2.204\times10^{-4} \; (R^2 = 9.998\times10^{-1}) \quad \ldots (87)$$

Best fit straight line with zero intercept:

$$\Delta L_{\text{Upper-Lower Punch-Ram}} = 3.103\times10^{-3} F \; (R^2 = 9.982\times10^{-1}) \quad \ldots (88)$$

Maximum difference between equations 87 and 88, at a typical pressing force of 25kN, is approximately 0.004mm thus equation 88 is an excellent approximation of the actual behaviour.

Upper punch-ram system contraction

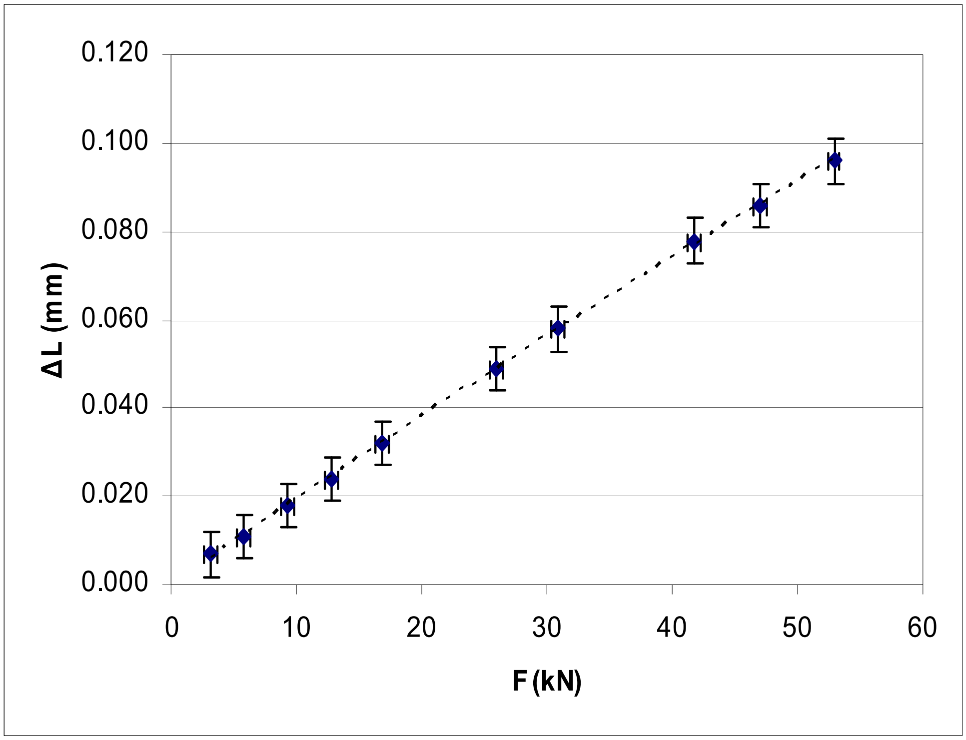

Figure 50: Change in upper punch-ram system contraction with pressing force.

Best fit equation:

$\Delta L_{\text{Upper Punch-Ram}} = -2.393\times10^{-6}\,F^2 + 1.946\times10^{-3}\,F - 2.075\times10^{-6}\ (R^2 = 9.998\times10^{-1})$ . . . (89)

Best fit straight line with zero intercept:

$\Delta L_{\text{Upper Punch-Ram}} = 1.844\times10^{-3}\,F\ (R^2 = 9.991\times10^{-1})$ . . . (90)

Maximum difference between equations 89 and 90, at a typical pressing force of 25kN, is approximately 0.001mm thus equation 90 is an excellent approximation of the actual behaviour.

Upper ram contraction

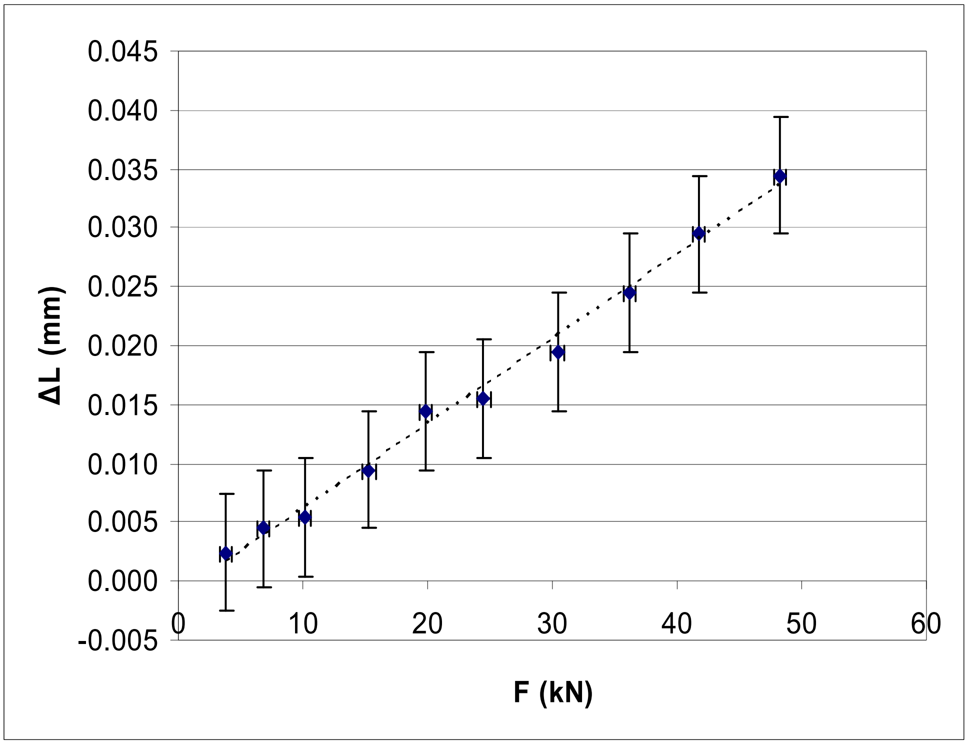

Figure 51: Change in contraction of the upper ram with pressing force.

Best fit equation:

$\Delta L_{\text{Upper Ram}} = 6.849 \times 10^{-4} F \ (R^2 = 9.902 \times 10^{-1})$ . . . (91)

Again, the case where the best fit equation is a straight line function.

Contraction of the upper ram and punch base system

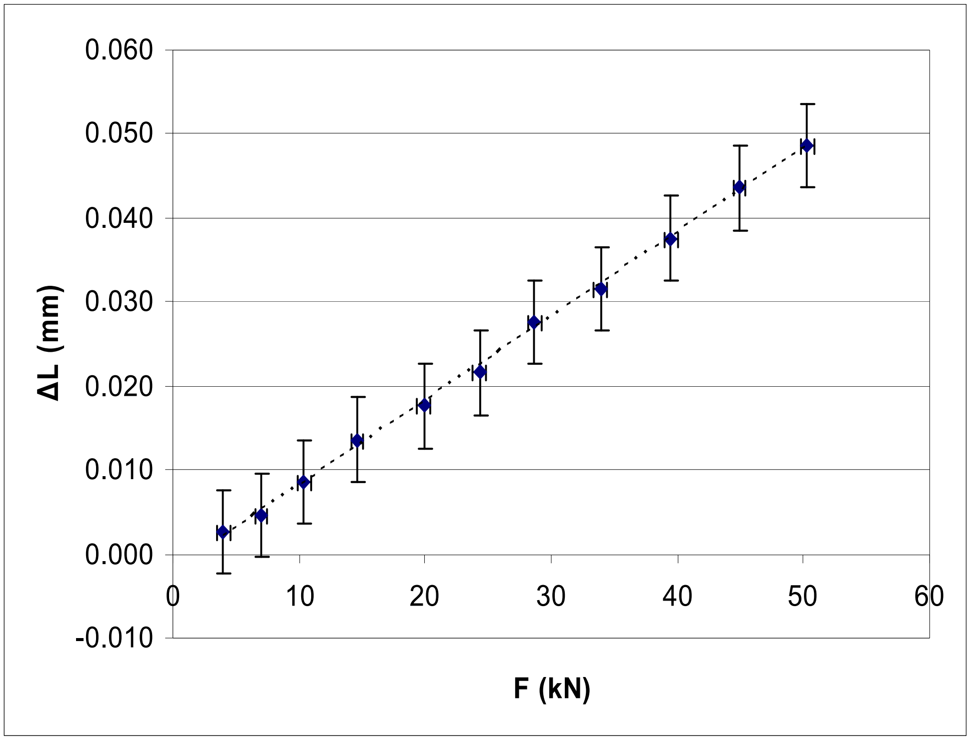

Figure 52: Change in upper ram and punch base contraction with pressing force.

Best fit equation:

$$\Delta L_{\text{Upper Ram and Punch Base}} = 1.003 \times 10^{-3} F \; (R^2 = 9.987 \times 10^{-1}) \qquad \ldots (92)$$

Again a straight line best describes the data above.

F.3 Square SBA tool

Upper and lower punch-ram system contraction

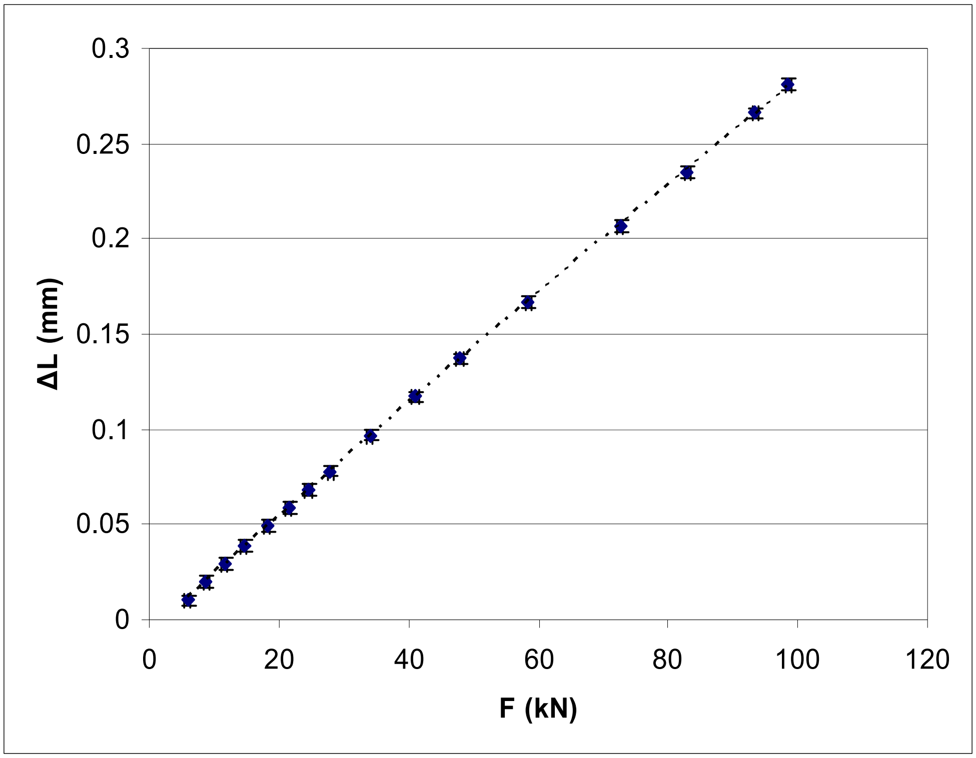

Figure 53: Change in upper and lower punch-ram system contraction with pressing force.

Best fit equation:

$$\Delta L_{\text{Upper-Lower Punch-Ram}} = -1.811\times10^{-6}\,F^2 + 3.082\times10^{-3}\,F - 6.615\times10^{-3}\ (R^2 = 9.999\times10^{-1}) \quad \ldots (93)$$

Best fit straight line with zero intercept:

$$\Delta L_{\text{Upper-Lower Punch-Ram}} = 2.839\times10^{-3}\,F\ (R^2 = 9.991\times10^{-1}) \quad \ldots (94)$$

Maximum difference between equations 93 and 94, at a typical pressing force of 25kN, is approximately 0.001mm thus equation 94 is an excellent approximation of equation 93.

Upper punch-ram system contraction

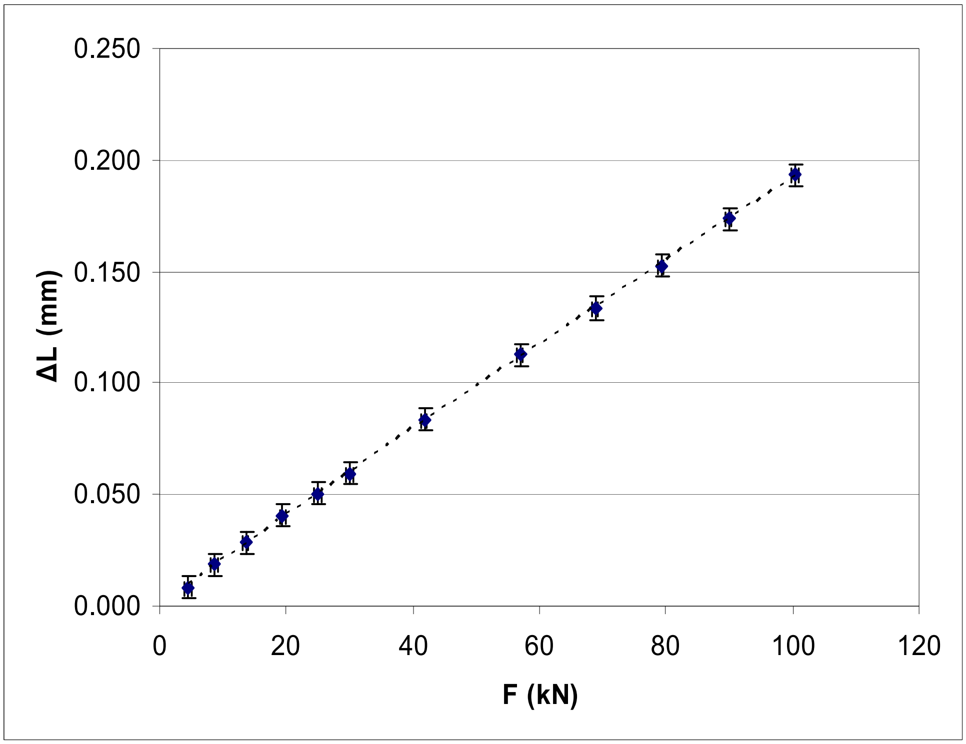

Figure 54: Change in punch-ram system contraction with pressing force.

Best fit equation:

$\Delta L_{\text{Upper Punch-Ram}} = -9.030\times10^{-7} F^2 + 2.000\times10^{-3} F - 9.469\times10^{-4} (R^2 = 9.998\times10^{-1})$ . . . (95)

Best fit straight line with zero intercept:

$\Delta L_{\text{Upper Punch-Ram}} = 1.943 \times10^{-3} F (R^2 = 9.992\times10^{-1})$ . . . (96)

Maximum difference between equations 95 and 96, at a typical pressing force of 25kN, is less than a micron thus equation 96 is an excellent approximation of equation 95.

Upper ram contraction

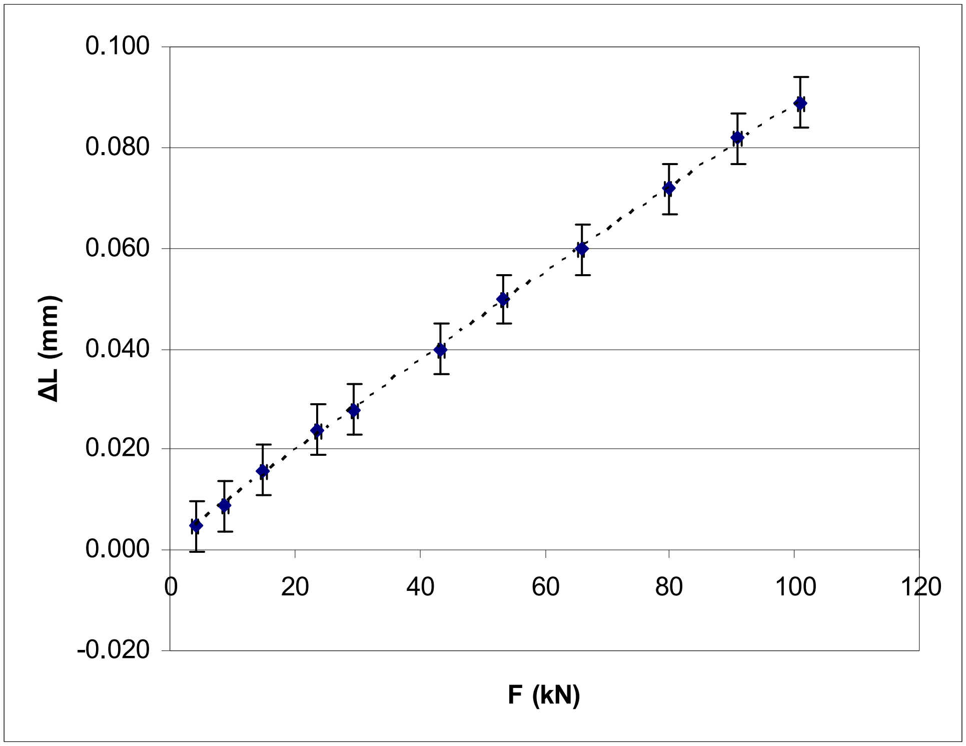

Figure 55: Change in upper ram contraction with pressing force.

Best fit equation:

$\Delta L_{\text{Upper Ram}} = -6.218\times10^{-7}\, F^2 + 9.352\times10^{-4}\, F - 1.175\times10^{-3}\ (R^2 = 9.996\times10^{-1})$ . . . (97)

Best fit straight line with zero intercept:

$\Delta L_{\text{Upper Ram}} = 9.024\times10^{-4}\, F\ (R^2 = 9.974\times10^{-1})$ . . . (98)

Maximum difference between equations 97 and 98, at a typical pressing force of 25kN, is less than 0.001mm thus equation 98 is an excellent approximation of equation 97.

Contraction of the upper ram and punch base system

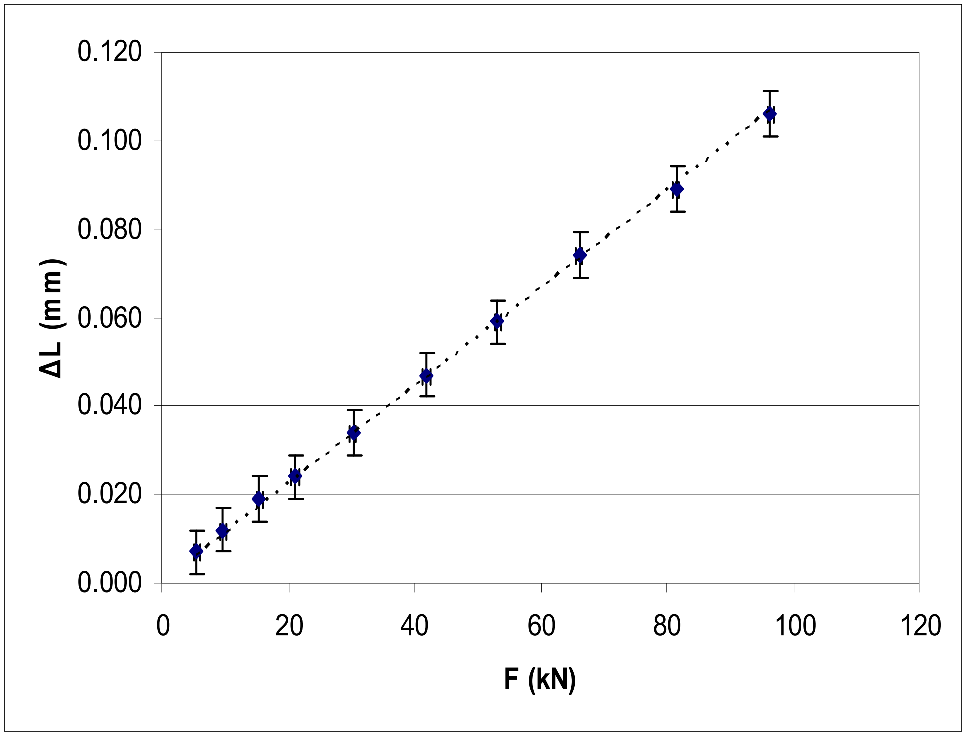

Figure 56: Change in upper ram and punch base contraction with pressing force.

Best fit equation:

$$\Delta L_{\text{Upper Ram and Punch Base}} = -1.135\times10^{-7}\, F^2 + 1.095\times10^{-3}\, F - 1.367\times10^{-3}\ (R^2 = 9.998\times10^{-1}) \quad \text{. . . (99)}$$

Best fit straight line with zero intercept:

$$\Delta L_{\text{Upper Ram and Punch Base}} = 1.108\times10^{-3}\, F\ (R^2 = 9.990\times10^{-1}) \quad \text{. . . (100)}$$

Maximum difference between equations 99 and 100, at a typical pressing force of 25kN, is approximately 0.002mm thus equation 100 is an excellent approximation of equation 99.

F.4 Round SBA tool

Upper and lower punch-ram system contraction

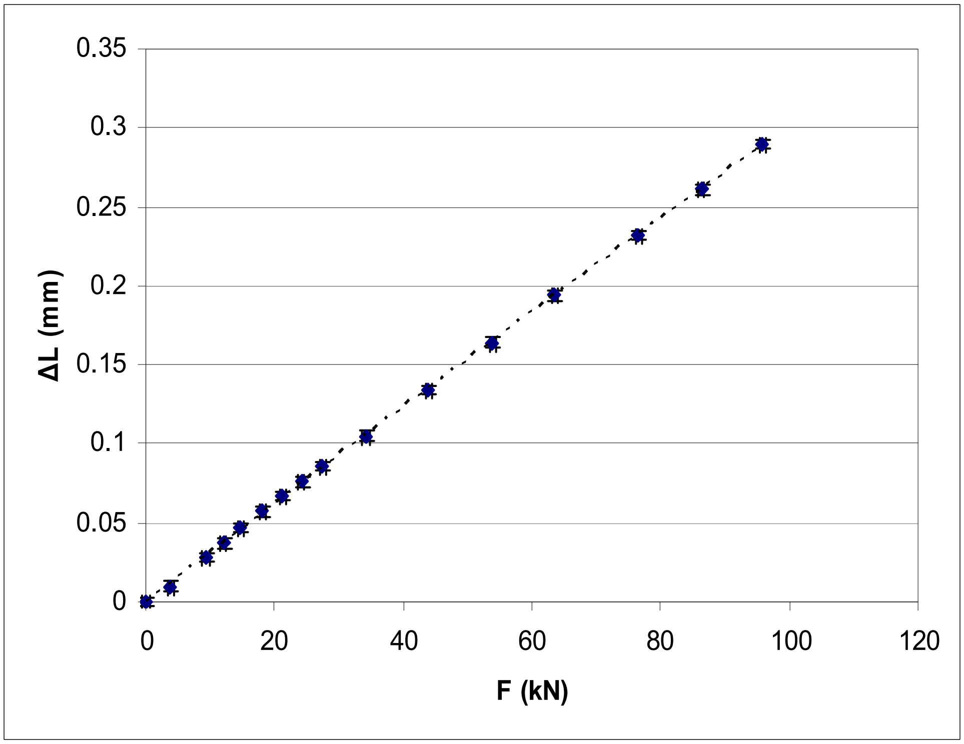

Figure 57: Change in upper and lower punch-ram system contraction with pressing force.

Best fit equation:

$$\Delta L_{\text{Upper-Lower Punch-Ram}} = -1.164\times10^{-6}\,F^2 + 3.127\times10^{-3}\,F - 5.332\times10^{-5}\ (R^2 = 9.999\times10^{-1}) \quad \ldots (101)$$

Best fit straight line with zero intercept:

$$\Delta L_{\text{Upper-Lower Punch-Ram}} = 3.041\times10^{-3}\,F\ (R^2 = 9.997\times10^{-1}) \quad \ldots (102)$$

Maximum difference between equations 101 and 102, at a typical pressing force of 25kN, is approximately 0.001mm thus equation 102 is an excellent approximation of equation 101.

Upper punch-ram system contraction

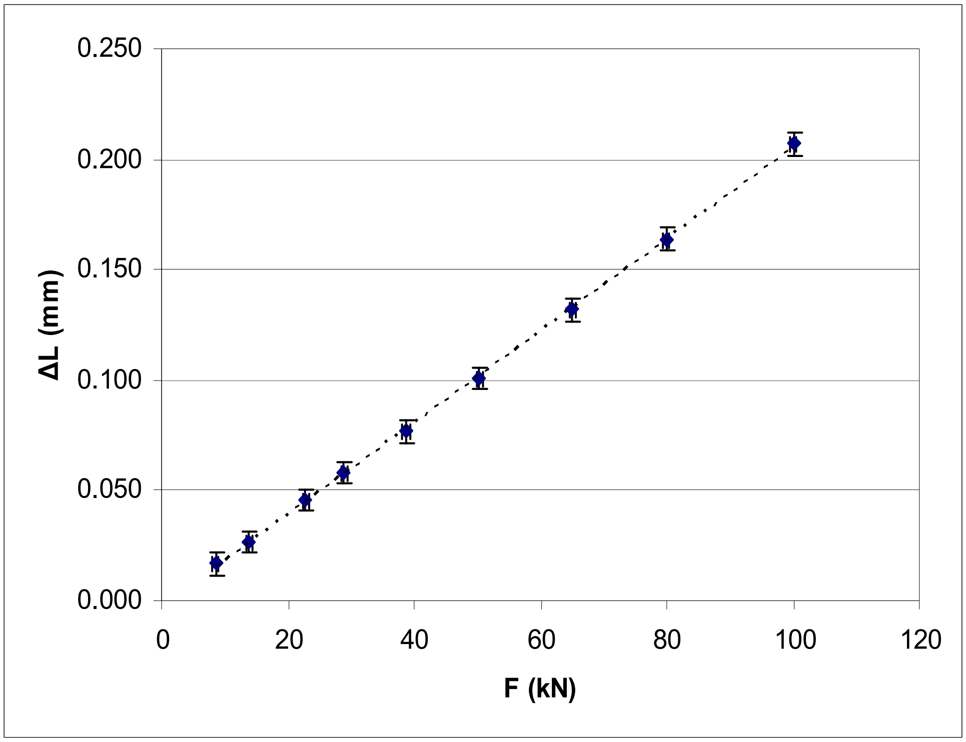

Figure 58: Change in upper punch-ram system contraction with pressing force.

Best fit equation:

$\Delta L_{\text{Upper Punch-Ram}} = 2.041\times10^{-3}\,F\;(R^2 = 9.994\times10^{-1})$ . . . (103)

Best fit equation is a straight line rather than a quadratic.

Upper ram contraction

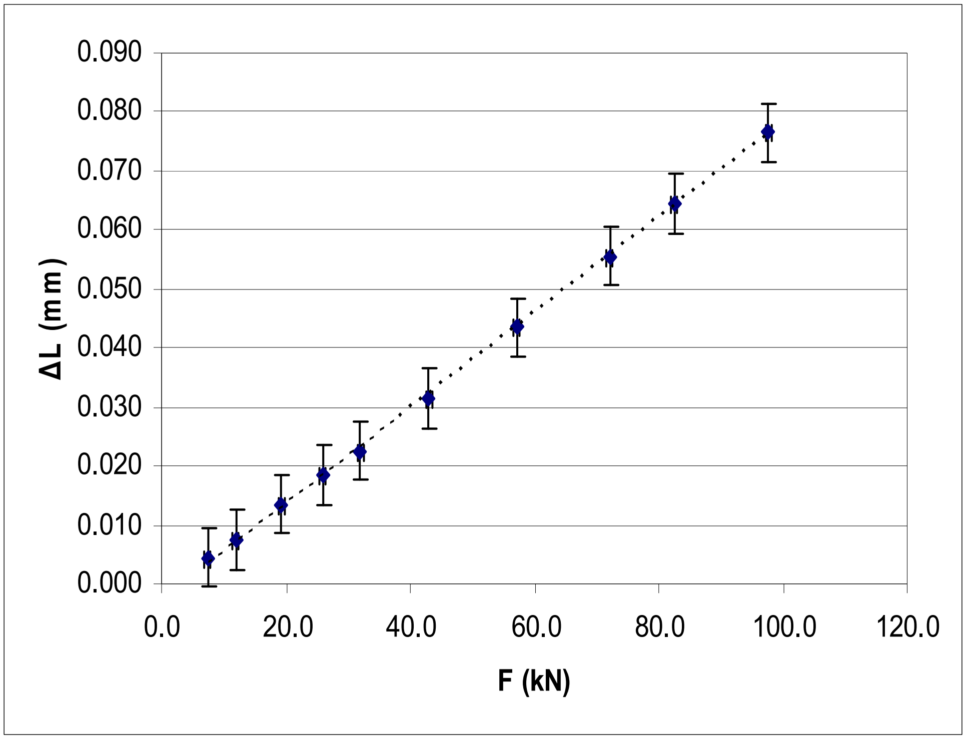

Figure 59: Change in upper ram contraction with pressing force.

Best fit equation:

$$\Delta L_{\text{Upper Ram}} = 7.686\times10^{-4}\,F \;(R^2 = 9.968\times10^{-1}) \qquad \ldots (104)$$

Best fit equation is a straight line rather than a quadratic.

Contraction of the upper ram and punch base system

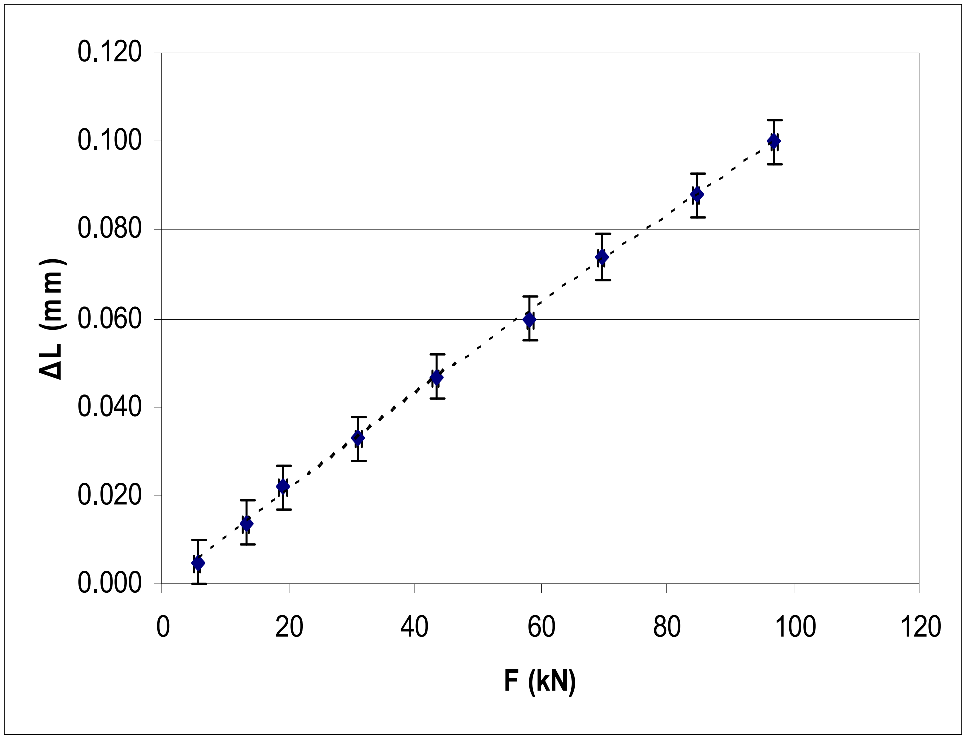

Figure 60: Change in upper ram and punch base system contraction with pressing force.

Best fit equation:

$$\Delta L_{\text{Upper Ram and Punch Base}} = -8.703\times10^{-7}\,F^2 + 1.120\times10^{-3}\,F - 7.539\times10^{-4}\ (R^2 = 9.993\times10^{-1}) \quad \ldots (105)$$

Best fit straight line with zero intercept:

$$\Delta L_{\text{Upper Ram and Punch Base}} = 1.042\times10^{-3}\,F\ (R^2 = 9.987\times10^{-1}) \quad \ldots (106)$$

Maximum difference between equations 105 and 106, at a typical pressing force of 25kN, is less than 0.001mm thus equation 106 is an excellent approximation of equation 105.

F.5 Triangular SBA tool

Upper and lower punch-ram system contraction

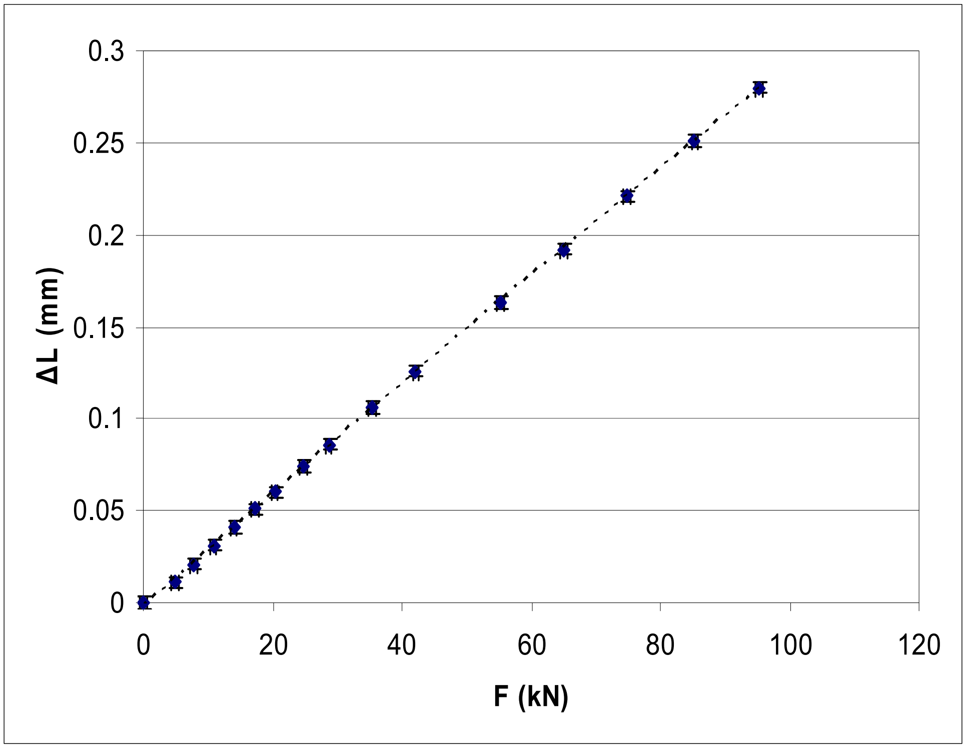

Figure 61: Change in upper and lower punch-ram system contraction with pressing force.

Best fit equation:

$$\Delta L_{\text{Upper-Lower Punch-Ram}} = -1.265\times10^{-6}\,F^2 + 3.073\times10^{-3}\,F - 1.863\times10^{-3}\ (R^2 = 9.999\times10^{-1}) \quad \ldots (107)$$

Best fit straight line with zero intercept:

$$\Delta L_{\text{Upper-Lower Punch-Ram}} = 2.951\times10^{-3}\,F\ (R^2 = 9.998\times10^{-1}) \quad \ldots (108)$$

Maximum difference between equations 107 and 108, at a typical pressing force of 25kN, is less than 0.001mm thus equation 108 is an excellent approximation of equation 107.

Upper punch-ram system contraction

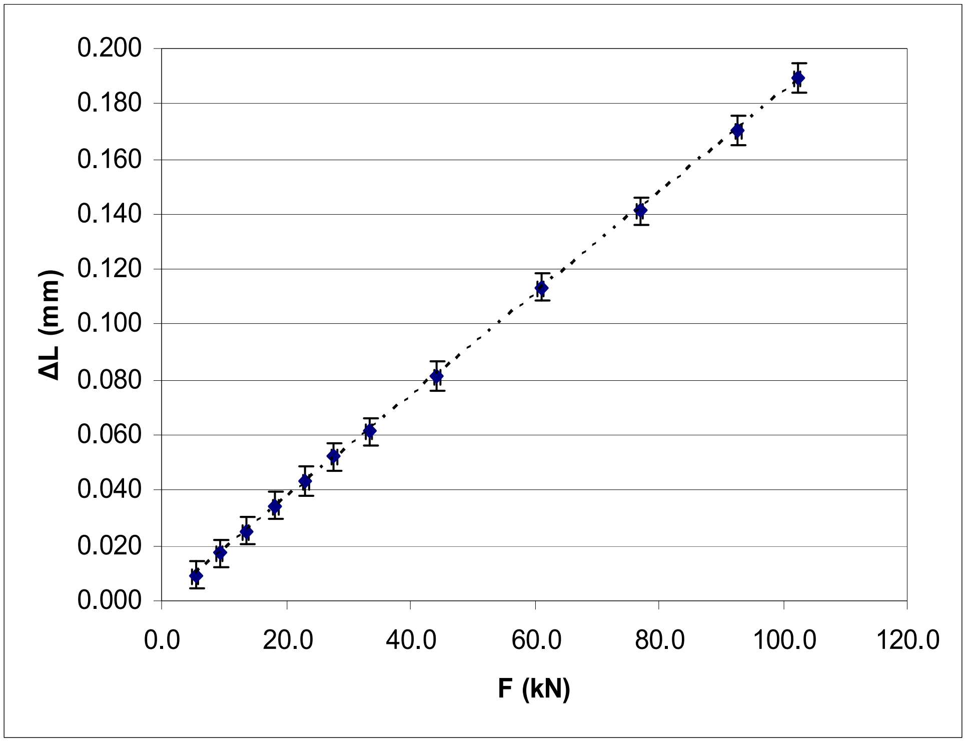

Figure 62: Change in upper punch-ram system contraction with pressing force.

Best fit equation:

$$\Delta L_{\text{Upper Punch-Ram}} = -1.366\times10^{-7} F^2 + 1.857\times10^{-3} F - 3.905\times10^{-8} \ (R^2 = 9.999\times10^{-1}) \quad \text{. . (109)}$$

Best fit straight line with zero intercept:

$$\Delta L_{\text{Upper Punch-Ram}} = 1.846 \times10^{-3} F \ (R^2 = 9.999\times10^{-1}) \quad \text{. . . (110)}$$

Maximum difference between equations 109 and 110, at a typical pressing force of 25kN, is less than 0.001mm thus equation 110 is thus an excellent approximation of equation 109.

Upper ram contraction

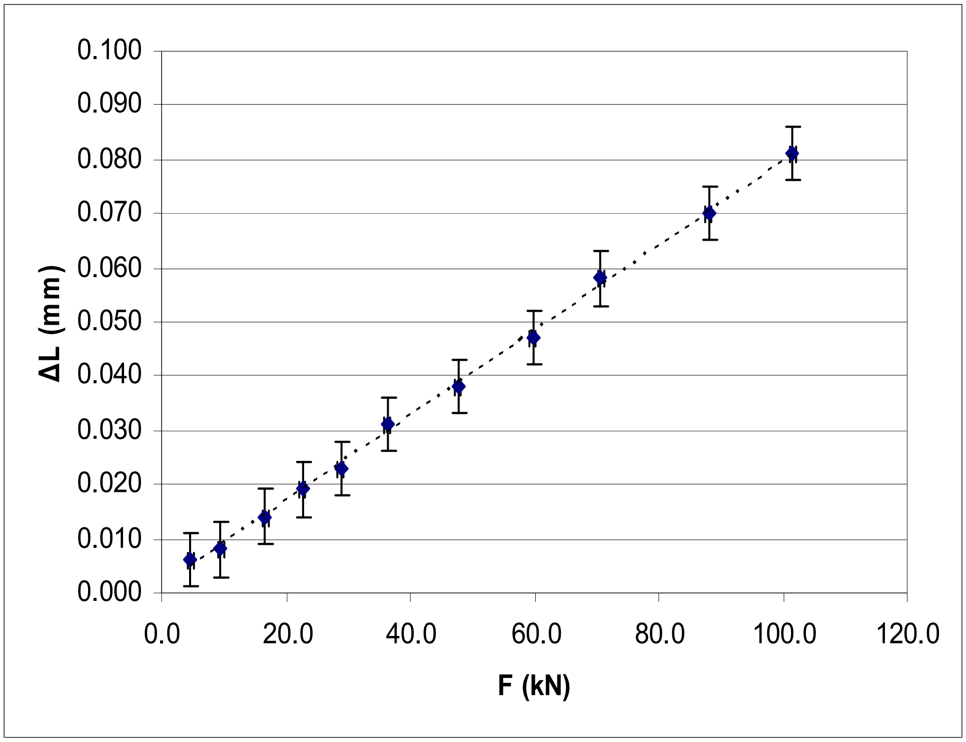

Figure 63: Change in upper ram contraction with pressing force.

Best fit equation:

$$\Delta L_{\text{Upper Ram}} = 8.042 \times 10^{-4} F \ (R^2 = 9.979 \times 10^{-1}) \qquad \ldots (111)$$

Best fit equation is a straight line rather than a quadratic.

Contraction of the upper ram and punch base system

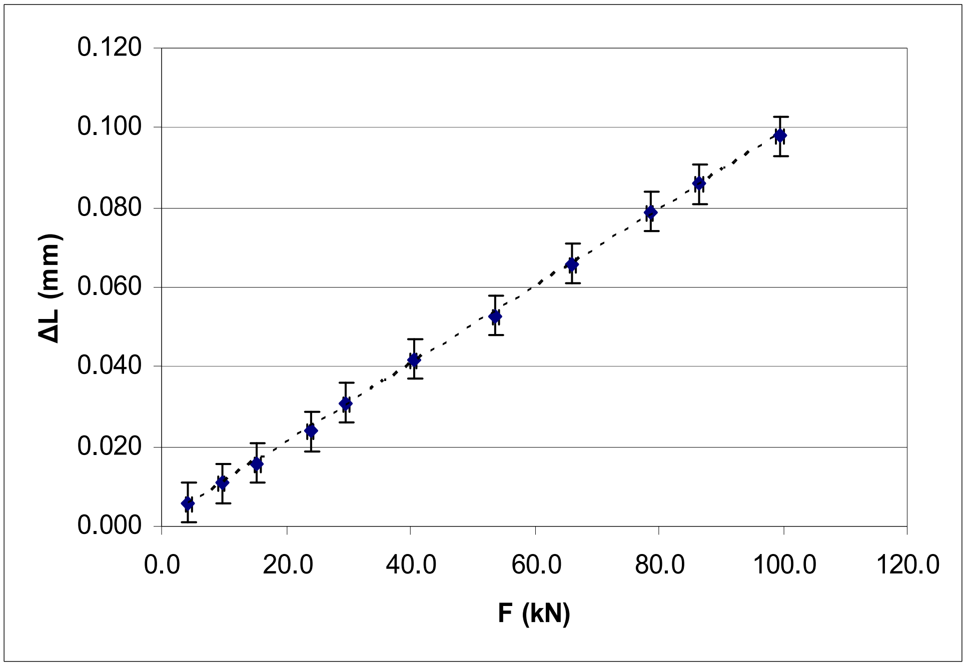

Figure 64: Change in upper ram and punch base contraction with pressing force.

Best fit equation:

$$\Delta L_{\text{Upper Ram and Punch Base}} = -8.355\times10^{-8}\,F^2 + 9.835\times10^{-4}\,F - 1.271\times10^{-3}\ (R^2 = 9.996\times10^{-1}) \quad \ldots (112)$$

Best fit straight line with zero intercept:

$$\Delta L_{\text{Upper Ram and Punch base}} = 9.959\times10^{-4}\,F\ (R^2 = 9.989\times10^{-1}) \quad \ldots (113)$$

Maximum difference between equations 112 and 113, at a typical pressing force of 25kN, is less than 0.002mm thus equation 113 is an excellent approximation of equation 112.

Appendix G: Springback results

G.1 Springback results for tight-fit compacts

The following best fit equations are derived from the measured and calculated data shown in tables of section 6.2.

Results for Grade B powder – square compact

$\Delta L(F)_{springback} = -3.621\times10^{-5}F^2 + 4.818\times10^{-3}F\ (R^2 = 9.928\times10^{-1})$ . . . (114)
$\Delta L(F)_{relative\ springback} = -2.569\times10^{-2}F^2 + 2.241F + 2.285\ (R^2 = 9.954\times10^{-1})$ . . . (115)
$\Delta H(F)_{springback} = -2.469\times10^{-5}F^2 + 1.782\times10^{-3}F\ (R^2 = 9.892\times10^{-1})$ . . . (116)
$\Delta H(F)_{relative\ springback} = -4.530\times10^{-4}F^2 + 3.232\times10^{-2}F - 1.793\times10^{-3}\ (R^2 = 1.000)$ . . . (117)
$\Delta IC(F)_{springback} = -2.868\times10^{-5}F^2 + 2.075\times10^{-3}F\ (R^2 = 9.067\times10^{-1})$ . . . (118)
$\Delta IC(F)_{relative\ springback} = -1.727\times10^{-4}F^2 + 1.396\times10^{-2}F - 3.581\times10^{-2}\ (R^2 = 9.314\times10^{-1})$ . . . (119)
$\Delta H(F)_{springback} / \Delta IC(F)_{springback} = 0.85 \pm 0.24$ . . . (120)
$\Delta H(F)_{relative\ springback} / \Delta IC(F)_{fractional\ springback} = 1.82 \pm 0.29$ . . . (121)
$\Delta V(F)_{springback} = -5.009\times10^{-6}F^2 + 4.107\times10^{-4}F\ (R^2 = 9.949\times10^{-1})$ . . . (122)
$\Delta V(F)_{relative\ springback} = -7.304\times10^{-4}F^2 + 5.887\times10^{-2}F + 3.052\times10^{-3}\ (R^2 = 1.000)$ . . . (123)
$\rho_g(P) = 6.736\times10^{-1}\mathrm{Ln}(P) + 6.443 (R^2 = 9.996\times10^{-1})$ . . . (124)

Results for Grade A powder – round compact

$\Delta L(F)_{springback} = -1.624\times10^{-4}F^2 + 1.115\times10^{-2}F\ (R^2 = 9.936\times10^{-1})$ . . . (125)
$\Delta L(F)_{relative\ springback} = -2.547\times10^{-1}F^2 + 1.171\times10^{1}F + 2.400\times10^{1}\ (R^2 = 9.648\times10^{-1})$. . (126)
$\Delta H(F)_{springback} = -1.108\times10^{-4}F^2 + 6.419\times10^{-3}F\ (R^2 = 9.959\times10^{-1})$ . . . (127)
$\Delta H(F)_{relative\ springback} = -2.052\times10^{-3}F^2 + 1.174\times10^{-1}F - 3.241\times10^{-3}\ (R^2 = 1.000)$ . . . (128)
$\Delta IC(F)_{springback} = -1.657\times10^{-5}F^2 + 1.835\times10^{-3}F\ (R^2 = 9.796\times10^{-1})$ . . . (129)
$\Delta IC(F)_{relative\ springback} = -1.326\times10^{-4}F^2 + 1.470\times10^{-2}F - 8.994\times10^{-5}\ (R^2 = 1.000)$ . . . (130)
$\Delta H(F)_{springback}/\Delta IC(F)_{springback} = -4.375\times10^{-4}F^2 - 2.585\times10^{-2}F + 3.486\ (R^2 = 1.000)$ . . . (131)
$\Delta H(F)_{relative\ springback} / \Delta IC(F)_{relative\ springback} = -9.600\times10^{-4}F^2 - 6.386\times10^{-2}F + 8.006\ (R^2 = 1.000)$ . .(132)
$\Delta V(F)_{springback} = -1.503\times10^{-5}F^2 + 9.460\times10^{-4}F\ (R^2 = 1.000)$ . . .(133)
$\Delta V(F)_{relative\ springback} = -2.540\times10^{-3}F^2 + 1.574\times10^{-1}F + 5.203\times10^{-3}\ (R^2 = 1.000)$ . . .(134)
$\rho_g(P) = 9.240\times10^{-1}\mathrm{Ln}(P) + 5.033\ (R^2 = 9.958\times10^{-1})$ . . .(135)

Results for Grade B powder – round compact

$\Delta L(F)_{springback} = -2.347\times10^{-5}F^2 + 4.563\times10^{-3}F\ (R^2 = 9.851\times10^{-1})$ . . . (136)
$\Delta L(F)_{relative\ springback} = -2.192\times10^{-2}F^2 + 2.178F + 3.018\ (R^2 = 9.877\times10^{-1})$ . . . (137)
$\Delta H(F)_{springback} = -2.660\times10^{-5}F^2 + 2.475\times10^{-3}F\ (R^2 = 9.943\times10^{-1})$ . . . (138)
$\Delta H(F)_{relative\ springback} = -4.968\times10^{-4}F^2 + 4.506\times10^{-2}F + 2.052\times10^{-3}\ (R^2 = 1.000)$ . . . (139)
$\Delta IC(F)_{springback} = -2.235\times10^{-5}F^2 + 2.394\times10^{-3}F\ (R^2 = 9.650\times10^{-1})$ . . . (140)
$\Delta IC(F)_{relative\ springback} = -1.792\times10^{-4}F^2 + 1.920\times10^{-2}F - 5.120\times10^{-5}\ (R^2 = 1.000)$ . . . (141)
$\Delta H(F)_{springback}/\Delta IC(F)_{springback} = -2.821\times10^{-5}F^2 - 1.114\times10^{-3}F + 1.032\ (R^2 = 9.990\times10^{-1})$ . . . (142)
$\Delta H(F)_{relative\ springback} / \Delta IC(F)_{relative\ springback} = -5.903\times10^{-5}F^2 - 4.101\times10^{-3}F + 2.361\ (R^2 = 9.990\times10^{-1})$ ..(143)
$\Delta V(F)_{springback} = -4.335\times10^{-6}F^2 + 4.602\times10^{-4}F\ (R^2 = 1.000)$ . . . (144)

$\Delta V(F)_{relative\ springback} = -7.426\times10^{-4}\,F^2 + 7.620\times10^{-2}\,F + 3.546\times10^{-3}\ (R^2 = 1.000)$ . . . (145)
$\rho_g(P) = 7.469\times10^{-1}Ln(P) + 6.165\ (R^2 = 9.991\times10^{-1})$ . . . (146)

Results for Grade A powder – triangular compact

$\Delta L(F)_{springback} = -6.034\times10^{-5}\,F^2 + 4.927\times10^{-3}F\ (R^2 = 9.927\times10^{-1})$ . . . (147)
$\Delta L(F)_{relative\ springback} = -2.041\times10^{-2}\,F^2 + 1.253F + 5.361\ (R^2 = 9.787\times10^{-1})$ . . . (148)
$\Delta H(F)_{springback} = -1.079\times10^{-4}\,F^2 + 5.448\times10^{-3}\,F\ (R^2 = 9.953\times10^{-1})$ . . . (149)
$\Delta H(F)_{relative\ springback} = -2.009\times10^{-3}\,F^2 + 1.005\times10^{-1}\,F + 3.196\times10^{-3}\ (R^2 = 1.000)$ . . . (150)
$\Delta IC(F)_{springback} = -5.013\times10^{-5}\,F^2 + 3.363\times10^{-3}\,F\ (R^2 = 9.942\times10^{-1})$ . . . (151)
$\Delta IC(F)_{relative\ springback} = -4.218\times10^{-4}\,F^2 + 2.829\times10^{-2}\,F - 8.964\times10^{-5}\ (R^2 = 1.000)$ . . . (152)
$\Delta H(F)_{springback}\ /\Delta IC(F)_{springback} = -3.068\times10^{-4}F^2 - 4.399\times10^{-3}\,F + 1.603\ (R^2 = 9.997\times10^{-1})$ . . (153)
$\Delta H(F)_{relative\ springback}/\Delta IC(F)_{relative\ springback} = -6.458\times10^{-4}\,F^2 - 1.231\times10^{-2}\,F + 3.546\ (R^2 = 9.996\times10^{-1})$ . . (154)
$\Delta V(F)_{springback} = -3.020\times10^{-5}\,F^2 + 1.672\times10^{-3}\,F\ (R^2 = 9.462\times10^{-1})$ . . . (155)
$\Delta V(F)_{relative\ springback} = -3.079\times10^{-3}\,F^2 + 1.700\times10^{-1}\,F + 1.074\times10^{-2}\ (R^2 = 1.000)$ . . . (156)
$\rho_g(P) = 7.789\times10^{-1}Ln(P) + 4.738\ (R^2 = 9.976\times10^{-1})$ . . . (157)

Results for Grade B powder – triangular compact

$\Delta L(F)_{springback} = -6.793\times10^{-6}\,F^2 + 2.966\times10^{-3}F\ (R^2 = 9.952\times10^{-1})$ . . . (158)
$\Delta L(F)_{relative\ springback} = -1.554\times10^{-2}\,F^2 + 2.003F + 9.077\times10^{-1}\ (R^2 = 9.985\times10^{-1})$ . . . (159)
$\Delta H(F)_{springback} = -5.006\times10^{-5}\,F^2 + 3.901\times10^{-3}\,F\ (R^2 = 9.951\times10^{-1})$ . . . (160)
$\Delta H(F)_{relative\ springback} = -9.352\times10^{-4}\,F^2 + 7.176\times10^{-2}\,F + 2.807\times10^{-3}\ (R^2 = 1.000)$ . . . (161)
$\Delta IC(F)_{springback} = -1.949\times10^{-5}\,F^2 + 1.451\times10^{-3}\,F\ (R^2 = 9.430\times10^{-1})$ . . . (162)
$\Delta IC(F)_{fractional\ springback} = -1.637\times10^{-4}\,F^2 + 1.218\times10^{-2}\,F - 2.581\times10^{-5}\ (R^2 = 1.000)$ . . . (163)
$\Delta H(F)_{springback}\ /\Delta IC(F)_{springback} = 7.133\times10^{-5}F^2 + 4.304\times10^{-4}F + 2.695\ (R^2 = 9.986\times10^{-1})$ . . . (164)
$\Delta H(F)_{relative\ springback}/\Delta IC(F)_{relative\ springback} = 1.542\times10^{-4}\,F^2 - 2.427\times10^{-2}\,F + 5.958\ (R^2 = 9.971\times10^{-1})$ . . . (165)
$\Delta V(F)_{springback} = -9.866\times10^{-6}\,F^2 + 4.592\times10^{-4}\,F\ (R^2 = 9.996\times10^{-1})$ . . . (166)
$\Delta V(F)_{relative\ springback} = -9.712\times10^{-4}\,F^2 + 4.513\times10^{-2}\,F + 2.588\times10^{-3}\ (R^2 = 1.000)$ . . . (167)
$\rho_g(P) = 6.257\times10^{-1}Ln(P) + 5.355\ (R^2 = 9.989\times10^{-1})$ . . . (168)

G.2 Springback results for SBA compacts

The following best fit equations are derived from the measured and calculated data shown in tables of section 6.3.

Results for Grade A powder with hold-down – square compact

$\Delta H(F)_{springback} = -7.340\times10^{-6}\,F^2 + 1.510\times10^{-3}\,F\ (R^2 = 9.971\times10^{-1})$ . . . (169)
$\Delta H(F)_{relative\ springback} = -1.645\times10^{-4}\,F^2 + 3.210\times10^{-2}\,F + 3.889\times10^{-3}\ (R^2 = 1.000)$ . . . (170)
$\Delta IC(F)_{springback} = -7.305\times10^{-7}\,F^2 + 8.662\times10^{-4}\,F\ (R^2 = 9.927\times10^{-1})$ . . . (171)
$\Delta IC(F)_{relative\ springback} = -6.515\times10^{-6}\,F^2 + 7.388\times10^{-3}\,F - 1.563\times10^{-5}\ (R^2 = 1.000)$ . . . (172)
$\Delta H(F)_{springback}/\Delta IC(F)_{springback} = -6.656\times10^{-6}F^2 - 6.975\times10^{-3}F + 1.743\ (R^2 = 1.000)$. . (173)
$\Delta H(F)_{relative\ springback}/\Delta IC(F)_{relative\ springback} = -4.463\times10^{-6}\,F^2 - 2.020\times10^{-2}\,F + 4.407\ (R^2 = 9.999\times10^{-1})$ . . . (174)
$\Delta V(F)_{springback} = -9.156\times10^{-7}\,F^2 + 2.338\times10^{-4}\,F\ (R^2 = 9.974\times10^{-1})$ . . . (175)
$\Delta V(F)_{relative\ springback} = -1.705\times10^{-4}\,F^2 + 4.007\times10^{-2}F + 4.030\times10^{-3}(R^2 = 1.000)$ . . . (176)

$\rho_g(P) = 7.350\times10^{-1}\,Ln(P) + 5.689\ (R^2 = 9.984\times10^{-1})$ . . . (177)

Results for Grade A powder without hold-down – square compact

$\Delta H(F)_{springback} = -1.674\times10^{-5}\,F^2 + 1.436\times10^{-3}\,F\ (R^2 = 9.984\times10^{-1})$ . . . (178)
$\Delta H(F)_{relative\ springback} = -3.640\times10^{-4}\,F^2 + 3.056\times10^{-2}\,F + 1.508\times10^{-3}\ (R^2 = 1.000)$ . . . (179)
$\Delta IC(F)_{springback} = -2.236\times10^{-5}\,F^2 + 3.161\times10^{-3}\,F\ (R^2 = 9.904\times10^{-1})$ . . . (180)
$\Delta IC(F)_{relative\ springback} = -1.913\times10^{-4}\,F^2 + 2.697\times10^{-2}\,F + 1.942\times10^{-4}\ (R^2 = 1.000)$ . . . (181)
$\Delta H(F)_{springback}/\Delta IC(F)_{springback} = -3.151\times10^{-5}F^2 - 1.608\times10^{-3}F + 4.509\times10^{-1}\ (R^2 = 9.999\times10^{-1})$ . . (182)
$\Delta H(F)_{relative\ springback}/\Delta IC(F)_{relative\ springback} = -3.073\times10^{-5}\,F^2 - 7.498\times10^{-3}\,F + 1.149\ (R^2 = 9.998\times10^{-1})$. . . (183)
$\Delta V(F)_{springback} = -3.229\times10^{-6}\,F^2 + 3.485\times10^{-4}\,F\ (R^2 = 9.995\times10^{-1})$ . . . (184)
$\Delta V(F)_{relative\ springback} = -5.643\times10^{-4}\,F^2 + 5.947\times10^{-2}F + 5.402\times10^{-3}\ (R^2 = 1.000)$ . . . (185)
$\rho_g(P) = 7.248\times10^{-1}\,Ln(P) + 5.696\ (R^2 = 9.982\times10^{-1})$ . . . (186)

Results for Grade B powder with hold-down – square compact

$\Delta H(F)_{springback} = -6.176\times10^{-6}\,F^2 + 1.323\times10^{-3}\,F\ (R^2 = 9.984\times10^{-1})$ . . . (187)
$\Delta H(F)_{relative\ springback} = -1.379\times10^{-4}\,F^2 + 2.795\times10^{-2}\,F + 4.878\times10^{-3}\ (R^2 = 1.000)$ . . . (188)
$\Delta IC(F)_{springback} = -2.303\times10^{-6}\,F^2 + 9.141\times10^{-4}\,F\ (R^2 = 9.941\times10^{-1})$ . . . (189)
$\Delta IC(F)_{relative\ springback} = -1.986\times10^{-5}\,F^2 + 7.793\times10^{-3}\,F + 9.264\times10^{-7}\ (R^2 = 1.000)$ . . . (190)
$\Delta H(F)_{springback}/\Delta IC(F)_{springback} = -1.211\times10^{-5}\,F^2 - 2.917\times10^{-3}\,F + 1.445\ (R^2 = 1.000)$. . . (191)
$\Delta H(F)_{relative\ springback}/\Delta IC(F)_{relative\ springback} = -2.287\times10^{-5}\,F^2 - 9.540\times10^{-3}\,F + 3.646\ (R^2 = 9.999\times10^{-1})$ . . (192)
$\Delta V(F)_{springback} = -8.649\times10^{-7}\,F^2 + 2.136\times10^{-4}\,F\ (R^2 = 9.987\times10^{-1})$ . . . (193)
$\Delta V(F)_{relative\ springback} = -1.581\times10^{-4}\,F^2 + 3.638\times10^{-2}F + 5.712\times10^{-3}\ (R^2 = 1.000)$ . . . (194)
$\rho_g(P) = 7.105\times10^{-1}\,Ln(P) + 6.322\ (R^2 = 9.991\times10^{-1})$ . . . (195)

Results for Grade B powder without hold-down – square compact

$\Delta H(F)_{springback} = -4.471\times10^{-6}\,F^2 + 2.616\times10^{-3}\,F\ (R^2 = 9.959\times10^{-1})$ . . . (196)
$\Delta H(F)_{relative\ springback} = -9.160\times10^{-5}\,F^2 + 5.546\times10^{-2}\,F + 5.355\times10^{-3}\ (R^2 = 1.000)$ . . . (197)
$\Delta IC(F)_{springback} = -5.443\times10^{-6}\,F^2 + 2.552\times10^{-3}\,F\ (R^2 = 9.942\times10^{-1})$ . . . (198)
$\Delta IC(F)_{relative\ springback} = -4.711\times10^{-5}\,F^2 + 2.178\times10^{-2}\,F + 8.970\times10^{-5}\ (R^2 = 1.000)$ . . . (199)
$\Delta H(F)_{springback}/\Delta IC(F)_{springback} = 1.105\times10^{-6}\,F^2 + 4.307\times10^{-4}\,F + 1.025\ (R^2 = 1.000)$. . (200)
$\Delta H(F)_{relative\ springback}/\Delta IC(F)_{relative\ springback} = 2.495\times10^{-5}\,F^2 - 3.833\times10^{-4}\,F + 2.584\ (R^2 = 9.809\times10^{-1})$ . . . (201)
$\Delta V(F)_{springback} = -7.788\times10^{-7}\,F^2 + 4.617\times10^{-4}\,F\ (R^2 = 9.983\times10^{-1})$ . . . (202)
$\Delta V(F)_{relative\ springback} = -1.310\times10^{-4}\,F^2 + 7.883\times10^{-2}F + 7.952\times10^{-3}\ (R^2 = 1.000)$ . . . (203)
$\rho_g(P) = 6.779\times10^{-1}\,Ln(P) + 6.389\ (R^2 = 9.987\times10^{-1})$ . . . (204)

Results for Grade A powder with hold-down – round compact

$\Delta H(F)_{springback} = -7.536\times10^{-6}\,F^2 + 1.608\times10^{-3}\,F\ (R^2 = 9.991\times10^{-1})$ . . . (205)
$\Delta H(F)_{relative\ springback} = -1.640\times10^{-4}\,F^2 + 3.348\times10^{-2}\,F + 1.246\times10^{-2}\ (R^2 = 1.000)$ . . . (206)
$\Delta IC(F)_{springback} = -5.020\times10^{-6}\,F^2 + 1.207\times10^{-3}\,F\ (R^2 = 9.928\times10^{-1})$ . . . (207)
$\Delta IC(F)_{relative\ springback} = -4.085\times10^{-5}\,F^2 + 9.781\times10^{-3}\,F + 1.886\times10^{-4}\ (R^2 = 1.000)$ . . . (208)
$\Delta H(F)_{springback}/\Delta IC(F)_{springback} = -7.556\times10^{-6}\,F^2 - 4.164\times10^{-4}\,F + 1.328\ (R^2 = 9.995\times10^{-1})$ . . . (209)
$\Delta H(F)_{relative\ springback}/\Delta IC(F)_{relative\ springback} = -1.607\times10^{-5}\,F^2 - 3.334\times10^{-3}\,F + 3.509\ (R^2 = 9.997\times10^{-1})$ . . (210)

$$\Delta V(F)_{springback} = -1.027\times10^{-6} F^2 + 2.294\times10^{-4} F \ (R^2 = 9.992\times10^{-1}) \quad \ldots (211)$$
$$\Delta V(F)_{relative\ springback} = -2.081\times10^{-4} F^2 + 4.411\times10^{-2} F + 1.682\times10^{-2} \ (R^2 = 1.000) \quad \ldots (212)$$
$$\rho_g(P) = 8.004\times10^{-1} \mathrm{Ln}(P) + 5.485 \ (R^2 = 9.982\times10^{-1}) \quad \ldots (213)$$

Results for Grade A powder without hold-down – round compact

$$\Delta H(F)_{springback} = -8.781\times10^{-6} F^2 + 9.582\times10^{-4} F \ (R^2 = 9.993\times10^{-1}) \quad \ldots (214)$$
$$\Delta H(F)_{relative\ springback} = -1.883\times10^{-4} F^2 + 2.008\times10^{-2} F + 3.233\times10^{-3} \ (R^2 = 1.000) \quad \ldots (215)$$
$$\Delta IC(F)_{springback} = -1.671\times10^{-5} F^2 + 2.998\times10^{-3} F \ (R^2 = 9.939\times10^{-1}) \quad \ldots (216)$$
$$\Delta IC(F)_{relative\ springback} = -1.359\times10^{-4} F^2 + 2.432\times10^{-2} F + 4.479\times10^{-4} \ (R^2 = 1.000) \quad \ldots (217)$$
$$\Delta H(F)_{springback} / \Delta IC(F)_{springback} = -1.996\times10^{-5} F^2 - 3.881\times10^{-4} F + 3.099\times10^{-1} \ (R^2 = 9.991\times10^{-1}) \quad \ldots (218)$$
$$\Delta H(F)_{relative\ springback} / \Delta IC(F)_{relative\ springback} = -4.677\times10^{-5} F^2 - 1.727\times10^{-3} F + 8.162\times10^{-1} \ (R^2 = 9.993\times10^{-1}) \quad \ldots (219)$$
$$\Delta V(F)_{springback} = -1.667\times10^{-6} F^2 + 2.392\times10^{-4} F \ (R^2 = 9.995\times10^{-1}) \quad \ldots (220)$$
$$\Delta V(F)_{relative\ springback} = -3.312\times10^{-4} F^2 + 4.609\times10^{-2} F + 1.127\times10^{-2} \ (R^2 = 1.000) \quad \ldots (221)$$
$$\rho_g(P) = 8.216\times10^{-1} \mathrm{Ln}(P) + 5.408 \ (R^2 = 9.967\times10^{-1}) \quad \ldots (222)$$

Results for Grade B powder with hold-down – round compact

$$\Delta H(F)_{springback} = -7.240\times10^{-6} F^2 + 1.505\times10^{-3} F \ (R^2 = 9.988\times10^{-1}) \quad \ldots (223)$$
$$\Delta H(F)_{relative\ springback} = -1.608\times10^{-4} F^2 + 3.161\times10^{-2} F + 4.166\times10^{-3} \ (R^2 = 1.000) \quad \ldots (224)$$
$$\Delta IC(F)_{springback} = -1.524\times10^{-6} F^2 + 8.788\times10^{-4} F \ (R^2 = 9.957\times10^{-1}) \quad \ldots (225)$$
$$\Delta IC(F)_{relative\ springback} = -1.259\times10^{-5} F^2 + 7.125\times10^{-3} F + 1.265\times10^{-5} \ (R^2 = 1.000) \quad \ldots (226)$$
$$\Delta H(F)_{springback} / \Delta IC(F)_{springback} = -1.180\times10^{-5} F^2 - 5.168\times10^{-3} F + 1.712 \ (R^2 = 1.000) \quad \ldots (227)$$
$$\Delta H(F)_{relative\ springback} / \Delta IC(F)_{relative\ springback} = -1.927\times10^{-5} F^2 - 1.640\times10^{-2} F + 4.504 \ (R^2 = 1.000) \quad \ldots (228)$$
$$\Delta V(F)_{springback} = -8.252\times10^{-7} F^2 + 2.023\times10^{-4} F \ (R^2 = 9.991\times10^{-1}) \quad \ldots (229)$$
$$\Delta V(F)_{relative\ springback} = -1.735\times10^{-4} F^2 + 3.928\times10^{-2} F + 4.697\times10^{-3} \ (R^2 = 1.000) \quad \ldots (230)$$
$$\rho_g(P) = 7.361\times10^{-1} \mathrm{Ln}(P) + 6.218 \ (R^2 = 9.993\times10^{-1}) \quad \ldots (231)$$

Results for Grade B powder without hold-down – round compact

$$\Delta H(F)_{springback} = -1.010\times10^{-5} F^2 + 8.942\times10^{-4} F \ (R^2 = 9.914\times10^{-1}) \quad \ldots (232)$$
$$\Delta H(F)_{relative\ springback} = -2.170\times10^{-4} F^2 + 1.880\times10^{-2} F + 1.097\times10^{-3} \ (R^2 = 1.000) \quad \ldots (233)$$
$$\Delta IC(F)_{springback} = -1.580\times10^{-5} F^2 + 3.125\times10^{-3} F \ (R^2 = 9.955\times10^{-1}) \quad \ldots (234)$$
$$\Delta IC(F)_{relative\ springback} = -1.288\times10^{-4} F^2 + 2.538\times10^{-2} F + 1.890\times10^{-4} \ (R^2 = 1.000) \quad \ldots (235)$$
$$\Delta H(F)_{springback} / \Delta IC(F)_{springback} = -1.496\times10^{-5} F^2 - 1.617\times10^{-3} F + 2.850\times10^{-1} \ (R^2 = 1.000) \quad \ldots (236)$$
$$\Delta H(F)_{relative\ springback} / \Delta IC(F)_{relative\ springback} = -3.412\times10^{-5} F^2 - 4.742\times10^{-3} F + 7.454\times10^{-1} \ (R^2 = 9.999\times10^{-1}) \quad \ldots (237)$$
$$\Delta V(F)_{springback} = -1.734\times10^{-6} F^2 + 2.362\times10^{-4} F \ (R^2 = 9.962\times10^{-1}) \quad \ldots (238)$$
$$\Delta V(F)_{relative\ springback} = -3.518\times10^{-4} F^2 + 4.594\times10^{-2} F + 3.261\times10^{-3} \ (R^2 = 1.000) \quad \ldots (239)$$
$$\rho_g(P) = 7.257\times10^{-1} \mathrm{Ln}(P) + 6.236 \ (R^2 = 9.995\times10^{-1}) \quad \ldots (240)$$

Results for Grade A powder with hold-down – triangular compact

$$\Delta H(F)_{springback} = -1.263\times10^{-5} F^2 + 1.731\times10^{-3} F \ (R^2 = 9.994\times10^{-1}) \quad \ldots (241)$$
$$\Delta H(F)_{relative\ springback} = -2.819\times10^{-4} F^2 + 3.726\times10^{-2} F + 3.701\times10^{-3} \ (R^2 = 1.000) \quad \ldots (242)$$
$$\Delta IC(F)_{springback} = -1.312\times10^{-6} F^2 + 1.592\times10^{-3} F \ (R^2 = 9.946\times10^{-1}) \quad \ldots (243)$$
$$\Delta IC(F)_{relative\ springback} = -1.061\times10^{-5} F^2 + 1.356\times10^{-2} F + 1.914\times10^{-4} \ (R^2 = 1.000) \quad \ldots (244)$$

$$\Delta H(F)_{springback}/\Delta IC(F)_{springback} = -6.302\times10^{-6} F^2 - 7.020\times10^{-3}F + 1.087 \ (R^2 = 1.000) \quad ...(245)$$
$$\Delta H(F)_{relative\ springback}/\Delta IC(F)_{relative\ springback} = -2.556\times10^{-6}F^2 - 1.982\times10^{-2}F + 2.780 \ (R^2=1.000) \quad ...(246)$$
$$\Delta V(F)_{springback} = -2.383\times10^{-6} F^2 + 4.483\times10^{-4} F \ (R^2 = 9.991\times10^{-1}) \quad ...(247)$$
$$\Delta V(F)_{relative\ springback} = -2.916\times10^{-4} F^2 + 5.188\times10^{-2}F + 4.666\times10^{-3} \ (R^2 = 1.000) \quad ...(248)$$
$$\rho_g(P) = 6.389\times10^{-1} Ln(P) + 4.900 \ (R^2 = 9.986\times10^{-1}) \quad ...(249)$$

Results for Grade A powder without hold-down – triangular compact

$$\Delta H(F)_{springback} = -1.220\times10^{-5} F^2 + 1.067\times10^{-3} F \ (R^2 = 9.957\times10^{-1}) \quad ...(250)$$
$$\Delta H(F)_{relative\ springback} = -2.643\times10^{-4} F^2 + 2.278\times10^{-2} F + 2.950\times10^{-3} \ (R^2 = 1.000) \quad ...(251)$$
$$\Delta IC(F)_{springback} = -1.059\times10^{-5} F^2 + 2.483\times10^{-3} F \ (R^2 = 9.940\times10^{-1}) \quad ...(252)$$
$$\Delta IC(F)_{relative\ springback} = -9.087\times10^{-5} F^2 + 2.119\times10^{-2} F + 3.601\times10^{-5} \ (R^2 = 1.000) \quad ...(253)$$
$$\Delta H(F)_{springback} / \Delta IC(F)_{springback} = -2.287\times10^{-5} F^2 - 2.728\times10^{-3}F + 4.265\times10^{-1} \ (R^2 = 1.000) \quad ...(254)$$
$$\Delta H(F)_{relative\ springback}/\Delta IC(F)_{relative\ springback} = -4.972\times10^{-5}F^2 - 7.734\times10^{-3}F + 1.087 \ (R^2=9.999\times10^{-1}) \quad ...(255)$$
$$\Delta V(F)_{springback} = -3.040\times10^{-6} F^2 + 3.968\times10^{-4} F \ (R^2 = 9.964\times10^{-1}) \quad ...(256)$$
$$\Delta V(F)_{fractional\ springback} = -3.587\times10^{-4} F^2 + 4.548\times10^{-2}F + 6.676\times10^{-3} \ (R^2 = 1.000) \quad ..(257)$$
$$\rho_g(P) = 6.336\times10^{-1} Ln(P) + 4.913 \ (R^2 = 9.996\times10^{-1}) \quad ...(258)$$

Results for Grade B powder with hold-down – triangular compact

$$\Delta H(F)_{springback} = -1.569\times10^{-5} F^2 + 1.850\times10^{-3} F \ (R^2 = 9.997\times10^{-1}) \quad ...(259)$$
$$\Delta H(F)_{relative\ springback} = -3.438\times10^{-4} F^2 + 3.960\times10^{-2} F + 5.246\times10^{-3} \ (R^2 = 1.000) \quad ...(260)$$
$$\Delta IC(F)_{springback} = -3.509\times10^{-6} F^2 + 9.519\times10^{-4} F \ (R^2 = 9.985\times10^{-1}) \quad ...(261)$$
$$\Delta IC(F)_{relative\ springback} = -3.005\times10^{-5} F^2 + 8.105\times10^{-3} F + 4.841\times10^{-5} \ (R^2 = 1.000) \quad ...(262)$$
$$\Delta H(F)_{springback} / \Delta IC(F)_{springback} = -7.106\times10^{-5} F^2 - 7.388\times10^{-3}F + 1.922 \ (R^2 = 1.000) \quad ..(263)$$
$$\Delta H(F)_{relative\ springback}/\Delta IC(F)_{relative\ springback} = -1.314\times10^{-4}F^2 - 2.428\times10^{-2}F + 4.944 \ (R^2=1.000) \quad ..(264)$$
$$\Delta V(F)_{springback} = -3.171\times10^{-6} F^2 + 4.214\times10^{-4} F \ (R^2 = 9.995\times10^{-1}) \quad ...(265)$$
$$\Delta V(F)_{relative\ springback} = -3.759\times10^{-4} F^2 + 4.838\times10^{-2}F + 6.273\times10^{-3} \ (R^2 = 1.000) \quad ...(266)$$
$$\rho_g(P) = 5.875\times10^{-1} Ln(P) + 5.553 \ (R^2 = 9.993\times10^{-1}) \quad ...(267)$$

Results for Grade B powder without hold-down – triangular compact

$$\Delta H(F)_{springback} = -1.584\times10^{-5} F^2 + 1.082\times10^{-3} F \ (R^2 = 9.990\times10^{-1}) \quad ...(268)$$
$$\Delta H(F)_{relative\ springback} = -3.432\times10^{-4} F^2 + 2.316\times10^{-2} F + 1.985\times10^{-3} \ (R^2 = 1.000) \quad ...(269)$$
$$\Delta IC(F)_{springback} = -8.033\times10^{-6} F^2 + 2.363\times10^{-3} F \ (R^2 = 9.995\times10^{-1}) \quad ...(270)$$
$$\Delta IC(F)_{relative\ springback} = -6.914\times10^{-5} F^2 + 2.016\times10^{-2} F + 8.441\times10^{-6} \ (R^2 = 1.000) \quad ...(271)$$
$$\Delta H(F)_{springback} / \Delta IC(F)_{springback} = -2.376\times10^{-5} F^2 - 4.985\times10^{-3}F + 4.567\times10^{-1} \ (R^2 = 1.000) \quad ...(272)$$
$$\Delta H(F)_{relative\ springback}/\Delta IC(F)_{relative\ springback} = -4.960\times10^{-5}F^2 - 1.346\times10^{-2}F + 1.163 \ (R^2=1.000) \quad ..(273)$$
$$\Delta V(F)_{springback} = -3.495\times10^{-6} F^2 + 3.888\times10^{-4} F \ (R^2 = 9.992\times10^{-1}) \quad ...(274)$$
$$\Delta V(F)_{relative\ springback} = -4.147\times10^{-4} F^2 + 4.477\times10^{-2}F + 3.562\times10^{-3} \ (R^2 = 1.000) \quad ...(275)$$
$$\rho_g(P) = 5.848\times10^{-1} Ln(P) + 5.526 \ (R^2 = 9.989\times10^{-1}) \quad ...(276)$$

-end-